Advances in Mechanical Engineering

Drag Reduction of Turbulent Flow by Additives

Guest Editors: Jinjia Wei, Yasuo Kawaguchi, and Bo Yu

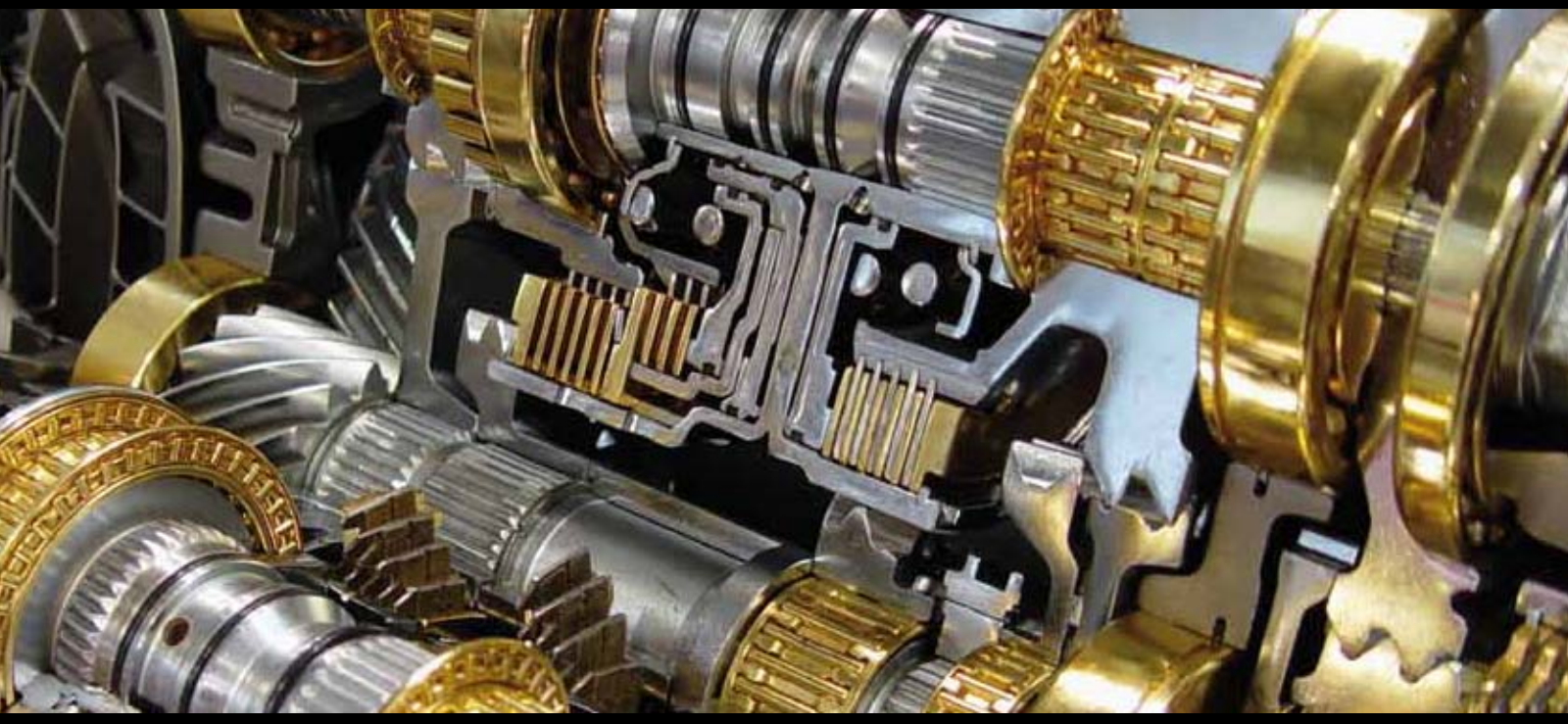

Drag Reduction of Turbulent Flow by Additives

Advances in Mechanical Engineering

Drag Reduction of Turbulent Flow by Additives

Guest Editors: Jinjia Wei, Yasuo Kawaguchi, and Bo Yu

Editorial Board

Contents

Drag Reduction of Turbulent Flow by Additives, Jinjia Wei, Yasuo Kawaguchi, and Bo Yu
Volume 2011, Article ID 952659, 2 pages

Review on Drag Reduction and Its Heat Transfer by Additives, Yi Wang, Bo Yu, Jacques L. Zakin, and Haifeng Shi
Volume 2011, Article ID 478749, 17 pages

The Combination of Polymer, Compliant Wall, and Microbubble Drag Reduction Schemes, Boris N. Semenov
Volume 2011, Article ID 743975, 10 pages

Drag Reduction of Bacterial Cellulose Suspensions, Satoshi Ogata, Tetsuya Numakawa, and Takuya Kubo
Volume 2011, Article ID 528373, 6 pages

Combined Effects of Temperature and Reynolds Number on Heat Transfer Characteristics of a Cationic Surfactant Solution, Ning Ma, Jianfeng Wang, and Jinjia Wei
Volume 2011, Article ID 879615, 8 pages

Flow Drag and Heat Transfer Reduction Characteristics of Organic Brine (Potassium Acetate) and Inorganic Brine (Calcium Chloride) Solutions with Nonionic Surfactant, Naoto Haruki and Akihiko Horibe
Volume 2011, Article ID 206219, 10 pages

Enhancing Heat Transfer of Drag-Reducing Surfactant Solution by an HEV Static Mixer with Low Pressure Drop, Haifeng Shi, Yi Wang, Wu Ge, Bo Fang, Jacob T. Huggins, Thaddaus R. Huber, and Jacques L. Zakin
Volume 2011, Article ID 315943, 10 pages

On Relationships among the Aggregation Number, Rheological Property, and Turbulent Drag-Reducing Effect of Surfactant Solutions, Ying-Bo Zhou, Na Xu, Ning Ma, Feng-Chen Li, Jin-Jia Wei, and Bo Yu
Volume 2011, Article ID 345328, 5 pages

Experimental Investigation on Zonal Structure in Drag-Reducing Channel Flow with Surfactant Additives, Masaaki Motozawa, Takahiro Watanabe, Weiguo Gu, and Yasuo Kawaguchi
Volume 2011, Article ID 120438, 12 pages

Analysis of Zero Reynolds Shear Stress Appearing in Dilute Surfactant Drag-Reducing Flow, Weiguo Gu, Dezhong Wang, and Yasuo Kawaguchi
Volume 2011, Article ID 367042, 9 pages

Evaluation of Surfactant Drag Reduction Effect in a District Heating System, Ning Ma, Jinjia Wei, and Jianfeng Wang
Volume 2011, Article ID 947179, 7 pages

Hindawi Publishing Corporation
Advances in Mechanical Engineering
Volume 2011, Article ID 952659, 2 pages
doi:10.1155/2011/952659

Editorial

Drag Reduction of Turbulent Flow by Additives

Jinjia Wei,[1] Yasuo Kawaguchi,[2] and Bo Yu[3]

[1] *State Key laboratory of Multiphase Flow in Power Engineering, Xi'an Jiaotong University, Xi'an 710049, China*
[2] *Department of Mechanical Engineering, Tokyo University of Science, Chiba 278-8510, Japan*
[3] *Beijing Key Laboratory of Urban Oil and Gas Distribution Technology, China University of Petroleum-Beijing, Beijing 102249, China*

Correspondence should be addressed to Jinjia Wei, jjwei@mail.xjtu.edu.cn

Received 9 August 2011; Accepted 9 August 2011

Turbulent drag reduction by additives is a striking phenomenon in which the presence of small quantities of additives in a carrier fluid can reduce turbulent friction greatly compared with the pure fluid at the same flow rate. There are several kinds of drag reducers including surfactants, polymers, bubbles, and fibers, which are promising for saving pumping energy in fluid transportation of pipelines. The key issues related to the drag-reducing flow by additives are the complicated microstructure, rheological properties, turbulence structure, drag reduction and heat transfer characteristics, and heat transfer enhancement. The purpose of this special issue is to collect a series of papers to show the recent advancement of these aspects. We received active submissions from America, Australia, China, Japan, and Russia, and finally 10 papers were accepted to publish in the special issue after peer reviews.

The first two papers of this special issue review the advancement of turbulent drag reduction by additives from two different respects. The first paper gives a full review on the main advancements of drag reduction of fibers, polymers, and surfactants during these 60 years, including background, application, development, theory, and research methods of the three different drag reducers and discusses future directions of development. The second paper summarizes the turbulence drag reduction methods by joint use of compliant coatings with other drag reduction means and shows fine outlooks of turbulence management by joint use of compliant coatings, riblets, polymer additives, and microbubbles.

Drag reduction and heat transfer characteristics of drag-reducing flow are investigated experimentally by four papers in this issue. The third paper investigates the drag reduction performance of bacterial cellulose suspensions and observes a maximum drag reduction ratio of 11%. Suspensions of nata de coco, which is a layered form of bacterial cellulose, show a higher drag reduction at lower concentrations. The fourth paper studies the combined effects of temperature and Reynolds number on heat transfer characteristics of a cationic surfactant solution with different concentrations. The results show that the heat transfer performance of cationic surfactant solution is largely deteriorated and is greatly affected by concentration, temperature, and Reynolds number. It is supposed that temperature and shear stress are two kinds of energy applied on the surfactant microstructure, which can be helpful to the surfactant network formation or dissociation depending on their values. The fifth paper describes the flow drag and heat transfer reduction characteristics of organic (potassium acetate) and inorganic (calcium chloride) brine solutions. The nonionic surfactant oleyl dihydroxyethyl amine oxide (ODEAO) is used as a drag-reducing additive. It is found that the formation of rod-like micelles in a non-ionic surfactant is related to the ionic strength of the brine solution. The sixth paper uses two methods, high-efficiency vortex (HEV) static mixer, and Helix static mixer, to enhance heat transfer performance of drag-reducing flow of Ethoquad O/12 with sodium salicylate. It is found that the Nusselt numbers by using the HEV are three to five times those of normal drag-reducing flow without mixer with only modest energy penalty.

The microstructure and rheology, and turbulence characteristics of drag-reducing fluid flow are investigated by three papers to reveal drag reduction mechanisms. The seventh paper aims at gaining insights of interrelationships among turbulent drag reduction rate, rheological properties and micelle microstructures of drag-reducing surfactant solution by measuring the aggregation number, turbulent drag reduction and shear-rate-dependent shear viscosity of

sodium dodecyl sulfate (SDS), and CTAC aided with sodium salicylate. The eighth paper investigates zonal structures in surfactant drag reducing flow. It is found that there appears an area where the root mean square of streamwise velocity fluctuation and the vorticity fluctuation sharply decrease toward the center of the channel, indicating that two layers with different turbulent structure coexist on the boundary of this area. The layer in the near-wall region has a striped structure, and the layer in the center of the channel has a grained structure. The ninth paper mainly analyzes the Reynolds shear stress in drag-reducing flow. The results show that when drag reduction reaches the maximum value, Reynolds shear stress disappears and reaches zero although the RMS of the velocity fluctuations is not zero.

The final paper of this special issue evaluates surfactant drag-reduction effect in a district heating system based on the experimental data from laboratory. The results show that the reduction of the pressure drop in the system reaches 23.28% by the addition of surfactants, indicating a very good energy saving effect and application prospective.

Jinjia Wei
Yasuo Kawaguchi
Bo Yu

Hindawi Publishing Corporation
Advances in Mechanical Engineering
Volume 2011, Article ID 478749, 17 pages
doi:10.1155/2011/478749

Review Article

Review on Drag Reduction and Its Heat Transfer by Additives

Yi Wang,[1] Bo Yu,[1] Jacques L. Zakin,[2] and Haifeng Shi[2]

[1] *Beijing Key Laboratory of Urban Oil and Gas Distribution Technology, China University of Petroleum-Beijing, Beijing 102249, China*
[2] *Department of Chemical and Biomolecular Engineering, The Ohio State University, 140 West 19th Avenue, Columbus, OH 43210, USA*

Correspondence should be addressed to Bo Yu, yubobox@cup.edu.cn

Received 7 May 2011; Accepted 22 July 2011

Academic Editor: Jinjia Wei

Since its discovery more than 60 years ago, the drag reduction phenomenon has achieved many notable energy saving effects. These achievements have encouraged researchers to study drag reduction further and further so that it can be utilized better. But due to the complex characteristics of turbulent flow, recent theories cannot explain all the phenomena of drag reduction. To give an overview of drag reduction and corresponding heat transfer for further understanding, this paper summarizes the main advancements of drag reduction during these 60 years, including background, application, development, theory, and research methods of different drag reducers. Future directions of development are also discussed.

1. Introduction

1.1. Background of Drag Reduction. Forrest and Grierson [1] were the first to report a reduction in energy loss in the turbulent pipe flow of wood pulp fiber suspensions in water. This first report of drag reduction was unnoticed. Later, Mysels [2] found that the skin friction for gasoline in pipe flow was significantly reduced by the addition of an aluminum disoap (an anionic surfactant). This was the first drag reduction result which was recognized. While doing polymer degradation research, Toms observed that the addition of a long chain polymer (polymethyl methacrylate) in monochlorobenzene dramatically reduced the turbulent skin friction drag by up to 80% [3]. At the First International Rheological Congress, Toms [3] reported these results, the first that identified polymers as effective drag reducers. He observed that at constant pressure gradient, the flow rate could be increased by the addition of the polymer. Therefore, it is usually referred to as the "Toms Effect." Later, Savins [4] first used the term "Drag Reduction." His drag ratio (D_R) is the ratio of the pressure gradient of the drag reducing solution to that of the solvent at the same flow rate in the same pipe:

$$D_R = \frac{\Delta p}{\Delta p_s}, \tag{1}$$

where Δp and Δp_s are the pressure gradients for the drag reducing solution and the solvent, respectively. Any fluid whose drag ratio is less than one is a drag reducing fluid. Thus, drag reduction can be defined by

$$\mathrm{DR}\% = (1 - D_R) \times 100\%. \tag{2}$$

The first commercial application for high polymer drag reduction was its use in the 48-inch diameter 800 mile long Alaska pipeline carrying crude oil from the North slope in Alaska to Valdez in the south of Alaska [5, 6]. Due to the very slow recovery (days) after high shear through a pump, aluminum disoaps were not practical as a drag reducer [7]. Later, drag reduction in aqueous systems using surfactant additives were found to be effective and because of rapid recovery after shear were of interest for recirculation systems. Savins found anionic surfactants were good at drag reducing and stable mechanically [8], but they had precipitation and foam problems [9]. Zakin and Lui [10] found that the effective drag reducing temperature range of nonionic surfactants was very narrow which restricted their application. Chou noted that cationic surfactants had much broader effective drag reducing temperature ranges, recovered rapidly after shear in a pump, and had fewer foam problems, and thus they were more useful [11].

A large number of publications has appeared since the first research paper in 1931. Nadolink and Haigh collected and summarized more than 2,500 references relating the concept of "Skin Friction Reduction" [12]. Ge [13] analyzed 3,800 publications concerning "Drag Reduction" from 1950 to 2007 and found drag reduction research gained much attention from the early 1960s, when polymer drag reduction researches were focused. Drag reduction publications continued to rise and reached a peak around 1977, after the first oil crisis in 1973-1974. By the 1980s, high polymers in both aqueous and hydrocarbon systems [14] were the main research interests. From the 1980s, district heating and cooling (DHC) systems and other potential applications were being developed for energy saving. Correspondingly, research on surfactant drag reduction began to increase. Around 2000, the number of publications each year recovered to the 1977 peak and continued to increase. From 2000 to 2007, publication numbers had the largest increase probably due to rising energy costs. Ge also pointed out that research journal articles made up the majority of the publications, 69%. Patents (12%) have been the second largest contributor, since drag reduction has important practical applications. About 10% of the publications have been reviews, reports, theses, and books.

Since drag reduction has a close relation to energy conservation. It will receive more and more attention as more and more potential applications become practical.

1.2. Applications of Drag Reduction. The application of drag reducing additives (DRAs) is greatly decreasing system energy requirements, reducing pipe diameter, or increasing flow rate, etc. The first famous application of DRAs was in transport of crude oil in the trans-Alaska (TAPS or Alyeska) Pipeline in 1979. The pipeline is 800 miles long with 48-inch diameter. After injecting a concentrated solution of a high molecular weight polymer downstream of pumping stations at homogeneous concentrations as low as 1 ppm [6], crude throughput was increased by up to 30%. Polymer DRAs were also successfully applied in other crude oil pipelines such as Iraq-Turkey, Bass Strait in Australia, Mumbai Offshore [15] and North Sea Offshore [16], and in finished hydrocarbon product lines [17]. In each case, the polymer composition had to be designed for the particular hydrocarbon to be transported.

Polymer DRAs have also been proposed for the following applications: oil field operations [18, 19], slurry or hydraulic capsule pipeline transportation [20, 21], suppression of atherosclerosis [22, 23], prevention of lethality from hemorrhagic shock [24], increased water flow and water jet focusing in firefighting equipment [25, 26], prevention of overflows of water in sewage systems after heavy rains [27], increase of volumetric flow rate of water in hydropower and irrigation systems [28], and as antimisting agents in jet fuel [29].

Drag reducing surfactants (DRAs) can be used in district heating or cooling systems (DHC). These systems provide or remove heat in buildings or a district by a recirculation of water heated or chilled at a central station. The water recirculation energy requirements make up about 15% of the total energy for a DHC. In order to decrease this large proportion of the energy requirements, it is desirable to reduce friction in the water recirculation system. Thus, drag reduction by surfactants is an alternative choice to meet this purpose. Surfactant DRAs can reduce pumping energy requirements by 50–70%. The effectiveness depends on the kinds of additives used and the layout of the primary system. The savings by DRAs are greater if the pipeline has fewer branches or the pipelines are longer or the number of fittings (e.g., valves, elbows, etc.) is relatively small [30].

Surfactant DRAs field tests have been carried out successfully in large-scale district heating systems and reduced pipe flow energy significantly. The representative applications are Herning, Denmark [31], Volklingen, Germany [32], and Prague, Czech Republic [33]. Surfactants have been tested in district cooling systems at the University of California at Santa Barbara [34] and in Japan. Takeuchi et al. [35] applied surfactant drag reduction to the central heating/cooling system of the building of the Sapporo City Hall. Saeki reported using cationic surfactant DRAs in practical air conditioning systems for energy saving using ice slurries [36]. Surfactant DRAs were also used to prevent the agglomeration of ice slurries which was also investigated [37]. The combination of the ice-dispersion ability and drag reduction effectiveness improved the performance of ice slurry systems in advanced cold heat storage, transportation, and heat exchange systems [38]. Recently, Saeki reported that cationic surfactants in aqueous systems have bed used in over 130 buildings throughout Japan and reduced pumping energy by 20% ~ 60% [39].

Besides DHC applications, a novel application of surfactant DRAs is preventing flow-induced localized corrosion (FILC) [40, 41]. Surfactants can not only reduce wall shear stresses at a constant Reynolds number, but also suppress turbulent eddies near the wall, whose repeated impacts cause intermittent stresses on the wall, leading to mechanical damage to the surface material. Another promising novel application of drag reducing surfactant systems is in hydraulic fracturing fluids.

As mentioned above, there are three main kinds of drag reducers: fibers, polymers, and surfactants. Drag reduction by each of these types of drag reducers is reviewed in Sections 2 to 4.

2. Drag Reduction in Fiber Suspensions

Solutions with fibers of aspect ratio (l/d) of 25 ~ 35 showed drag reduction with high concentration of fibers [42, 43]. With increasing aspect ratio and decreasing fiber diameter, the effectiveness of fibers increases [42–44]. Systems of fibers mixed with polymers achieved up to 95% drag reduction [45, 46]. This drag reduction level is higher than that for polymers or for fibers alone. The polymer in this kind of system was also more resistant to degradation.

Fibers are chemically and mechanically stable in an aqueous environment. Since they are insensitive to water chemistry, piping materials, and temperature, they can be effective over a wide temperature range [42, 47]. Lee and Duffy [44]

suggested that fiber drag reduction might be caused by suppression of turbulent eddies in the turbulent core region.

However, use of fibers is limited by the drawback that they can cause plugging problems in pipelines due to the high concentration (as high as a few percent [42]) required for drag reduction.

3. Drag Reduction in Polymer Solutions

Polymer solution drag reduction has been studied extensively in both aqueous and hydrocarbon media by many researchers [48–51]. Some important characteristics of polymer drag reduction are summarized below.

3.1. Drag Reduction Types. Early work proposed two types of drag reduction in dilute polymer solutions [52]. Very dilute solutions display onset drag reduction that is in the fully developed turbulence region, drag reduction only occurs above an onset Reynolds number, where the friction factor decreases below that for ordinary Newtonian turbulent flow. At Reynolds numbers less than the onset value, no drag reduction occurs. Thus, there is an onset shear stress and an onset shear rate.

For more concentrated polymer solutions, drag reduction occurs by extension of the laminar region. In this case, onset conditions are reached at low Reynolds numbers, that is, the laminar-turbulent transition is not observed and laminar-like behavior is extended to an extended laminar region, in which the friction factor is lower than that of ordinary Newtonian turbulent flow at the same Reynolds number. Drag reduction here and also in onset drag reduction increases with flow rate until a critical wall shear stress is reached [49, 53], at which the rate of polymer degradation in the wall region exceeds the rate at which polymer is replenished in this region and drag reduction diminishes.

The main difference between these two kinds of drag reduction is the region where drag reduction occurs. The former begins in the fully developed turbulent region. The latter is observed in the extended laminar region. They were later labeled Type A and Type B drag reduction by Virk and Wagger [54].

The onset phenomenon in drag reduction is discussed below. Some important effects, which affect drag reduction, will also be discussed.

3.2. The Onset Phenomenon. For randomly coiled polymer solutions, drag reduction does not occur until a certain wall shear stress [50, 55] or shear rate [56, 57] is exceeded. This is the onset phenomenon. Its mechanisms are presumably stretching of the polymer molecules in the extensional flow regions or the entanglement of many molecules reaching the size of turbulent eddies [56, 58]. White [59], Virk [50] and Hershey [60] found the onset shear stress was not dependent on pipe diameter. The onset Reynolds number is proportional to the 8/7th power of the pipe diameter. So the same polymer solution has different onset Reynolds numbers in different pipe diameters, reflecting the onset shear stress or shear rate. Therefore, it is more appropriate to define the onset phenomenon using the onset shear stress or shear rate rather than the onset Reynolds numbers which are a function of polymer parameters. It decreases with increase of molecular weight and radius of gyration of the polymer molecules [50].

In predicting the onset phenomenon, researchers proposed three different hypotheses, namely, length scale, time scale, and strain energy storage models. The length scale model was proposed by Virk and Merrill [61] who proposed that onset occurs when the ratio of the polymer length scale (radius of gyration) to the turbulent length scale reaches a certain value. In the time scale model, the onset occurs when the time ratio (or Deborah number) is around unity. The time ratio is defined as the ratio of polymer relaxation time and the turbulent time scale. Most researchers preferred the time scale model because polymer size is several orders of magnitude smaller than the turbulent eddy size at onset, while the polymer relaxation time is about the same order as the turbulent time scale [51, 56, 57, 61]. In the strain energy storage model based on Gaussian bead-spring theory, Kohn [62] proposed that the polymer molecules stored energy when they are strained by high shear stress near the wall, and released it by relaxation when transported to the low shear region at the core. The onset of drag reduction occurs when strain energy convection is comparable to energy diffusion. This model as well as the time scale model predicts a decrease in onset Deborah number as polymer concentration increases which was confirmed by experiment [63]. The length scale model does not.

3.3. Maximum Drag Reduction Asymptote. Early researchers reported the existence of a maximum drag reduction asymptote for dilute polymer solutions. Usually, the maximum drag reduction can be achieved when concentration is tens or hundreds of ppm [53]. Castro and Squire [64] studied two different molecular weights of polyethylene oxide and reported the following equation in power-law form as a maximum drag reduction asymptote:

$$C_f = 1.4\mathrm{Re}^{-2/3}, \tag{3}$$

where C_f is the Fanning friction factor, $\mathrm{Re}(=\rho U_m D/\mu)$ the Reynolds number, ρ the solvent density, μ the dynamic viscosity of the solvent, U_m the mean velocity, and D the inner diameter of the pipe. Giles and Pettit [65] proposed another asymptote, also from correlating drag reduction data for polyethylene oxide aqueous solutions:

$$C_f^{-1} = 34.8\log_{10}\left(\mathrm{Re}\,C_f^{1/2}\right) - 53.9. \tag{4}$$

Virk et al. [66, 67] obtained an equation for the maximum drag reduction asymptote (MDRA) by correlating the flow data for different polymer solutions from a number of sources. This MDRA has been most commonly cited by drag reduction researchers and is called Virk's maximum drag reducing asymptote. Different polymer-solvent systems require

different polymer concentrations to reach the asymptote. The equation is:

$$C_f^{-1/2} = 19\log_{10}\left(\mathrm{Re}\, C_f^{1/2}\right) - 32.4, \tag{5a}$$

or

$$C_f \approx 0.58\mathrm{Re}^{-0.58} (4000 \le \mathrm{Re} \le 40000). \tag{5b}$$

Moreover, Virk et al. [66] derived an ultimate mean velocity profile from (5a). They proposed a model for drag reducing fluids in the turbulent region, analogous to those of Newtonian fluids. It can be summarized in the dimensionless form:

(a) viscous sublayer ($0 < y^+ < 11.6$)

$$u^+ = y^+, \tag{6}$$

(b) core region ($y_e^+ < y^+$)

$$u^+ = 2.5 \ln y^+ + 5.5 + \Delta B, \tag{7}$$

where u^+ is the dimensionless velocity, y^+ the dimensionless distance from the wall, y_e^+ the joint point of the elastic sublayer and the core region, and ΔB the velocity increment from Newtonian flow. u^+ is defined as

$$u^+ = \frac{u}{u_\tau}, \tag{8}$$

where u is the time averaged mean flow velocity in the axial direction at a distance y from the wall, $u_\tau = \sqrt{\tau_w/\rho}$ is the friction velocity (or shear velocity) where τ_w is the shear stress at the wall.

y^+ is defined as

$$y^+ = \frac{u_\tau}{\nu} y, \tag{9}$$

where ν is the kinematic viscosity of the fluid.

One can easily compare the velocity profile of a drag reducing fluid to the model and to a Newtonian fluid at any Reynolds number. Virk et al. also proposed a velocity profile asymptote of the ultimate elastic sublayer asymptote ($11.6 < y^+ < y_e^+$) for polymer solutions at the MDRA condition [66]:

$$u^+ = 11.7 \ln y^+ - 17. \tag{10}$$

For most polymer solutions, drag reduction curves (both friction factors and mean velocities) are located in a domain bounded by the Newtonian line and by Virk's line. It is interesting to note that some systems other than polymer solutions have reported drag reduction which exceeds this asymptote [45, 68, 69]. The reason for that is the polymer equation was empirically derived from polymer drag reduction data [66]. Zakin et al. [70] proposed an alternate drag reduction asymptote for surfactant systems:

$$C_f = 0.32\mathrm{Re}^{-0.55}. \tag{11}$$

The limiting equation for the elastic sublayer (they found the elastic sublayer expanded to $y^+ = 15$ for surfactant solutions) corresponding to (11) is

$$u^+ = 53.9 \log_{10} y^+ - 65. \tag{12}$$

3.4. Concentration Effect. Generally speaking, drag reduction at a fixed velocity increases as polymer concentration increases until a certain concentration is reached. This concentration is usually called the saturation concentration. Above this concentration, drag reduction falls off [71, 72]. The initial increase in drag reduction with concentration increase is probably due to the increasing number of polymer molecules which cause the damping of more turbulent eddies. The decrease in drag reduction after the saturation concentration is caused by increase in solution viscosity.

Concentration is quantitatively related to drag reduction effectiveness of randomly coiled polymer solutions. It has a relation to the slope increment, which has been defined as the slope difference between a drag reducing solution and the solvent in a von Karman plot. Virk [73] suggested the slope increment is proportional to the 1/2 power of polymer concentration. Berman and Yuen [74] observed a 2/3 power relation when the polymer concentration is very low (less than 1 ppm).

Many studies on the inhomogeneous drag reduction have been performed. Hou et al. obtained inhomogeneous drag reduction by polymer injection from the slot [75]. White et al. [76] observed that the concentration of polymer is not uniform in the streaks and the spatial distribution of the polymer is related to the turbulent structure.

3.5. Molecular Weight Effect. When molecular weight is less than 10^5, polymers are generally ineffective for drag reduction [53]. For a given concentration and Reynolds number, drag reduction increases with increasing average molecular weight. Virk [50] concluded that for the same polymer species an increase in molecular weight resulted in a decrease in onset shear stress and in the amount of polymer required to obtain the same level of drag reduction. Paterson and Abernathy [77] pointed out that the highest molecular weight species in the distribution mainly determined drag reducing effectiveness. Berman [78] and Jacobs et al. [79] further studied the molecular weight effect, using modern gel permeation chromatography technique, which allows separation of the high molecular weight portions of the polymer. Their results confirmed the conclusion reached by Paterson and Abernathy [77]. Hunston and Reischman [80] found that the highest molecular weight fraction of polymer primarily determined the onset shear stress. They confirmed this conclusion quantitatively by observing that, when 2.5 ppm of a high molecular weight polystyrene (7.1 million) and 25 ppm of a low molecular weight polystyrene (1.8 million) were mixed, the drag reduction was almost identical to that using the high molecular weight sample alone. However, when the amount of low molecular weight polymer was increased to 100 ppm, low molecular weight polymer made a significant contribution to the drag reducing effectiveness of the mixture. McCormick et al. [81] also suggested that good drag reduction can be achieved by low molecular weight polymers if their concentrations are high enough. However, they also pointed out that there might be a low molecular weight limit for effective drag reduction.

Liaw et al. [82] defined a critical concentration, which separates dilute drag reducing polymer solutions (Type A) and concentrated drag reducing polymer solutions (Type B). When polymer concentration exceeded this critical concentration, a laminar-to-turbulent transition was not observed in their experiments. They also proposed that the ratio of polymer molecular weight to critical molecular weight for entanglements to occur [82, 83] is a useful measure of molecular weight for predicting drag reducing efficiency. According to Liaw et al. [82], good drag reduction was always obtained if the ratio was greater than 50.

3.6. Molecular Conformation and Solvent Effect. Sellin et al. [84] and Hoyt [53] found that linear polymers without branches are more effective drag reducers than other polymers. Polyoxyethylene and polydimethylsiloxane, the two most flexible polymers, are the most effective polymer drag reducers. The effectiveness of polymer solutions depends on the stretching of individual molecules by the stresses in the flow.

The molecular conformation can lead to different types of drag reduction. For dilute less flexible randomly coiled polymers, a transition from laminar to turbulent flow is usually observed and onset occurs in the turbulent region. On the other hand, flexible polymers usually do not show a clear transition. Drag reduction occurs in the extended laminar region. This is probably because the onset shear rate or shear stress has already been reached in the laminar or transition zone [52, 58].

Many workers studied the effect of molecular conformation on drag reduction by changing the interactions between polymer molecules and solvent. Hershey and Zakin [52] found the drag reducing ability of polyisobutylene was better in a good solvent-cyclohexane than in a poor solvent-benzene. They indicated that drag reduction in good solvents, which allow polymer molecules to expand more freely in the solution, is greater than in poor solvents, where the molecule's volume is smaller. Later, Hunston and Zakin [63] reported that the onset phenomenon occurred earlier when polymer molecules were dissolved in a better solvent. Poor solvents also affect the mechanical degradation of polymers. They found that in a poor solvent, mechanical degradation is more rapid than in a good solvent [85].

Virk [54, 86] and Rochefort and Middleman [87] demonstrated that molecular conformation can also be altered by changing the salinity of an aqueous polyelectrolyte solution. They found that polyacrylamide in low salt aqueous medium produced more drag reduction than in high salt solutions in which molecules coiled. The polymer molecules expanded in the former solution due to charge repulsions and coiled in the latter solutions in which charges were neutralized. The molecular conformation of polyacrylic acid can be varied by changing the pH value of the solution. At low pH the polymer molecules collapse due to protonation, while at high pH the molecules expand due to charge re-pulsions. The pH value reflects the concentration of the hydrogen ion. Parker and Hedley [88] and Banijamali et al. [89] reported greater drag reduction in high pH than in low pH solutions, while Hand and Williams [90] found maximum drag reduction at low PH in PAA-water solutions.

3.7. Diameter Effect. For Newtonian fluids in the turbulent region, the von Karman equation describes flow behavior well. Each Reynolds number corresponds to a specific friction factor. However, for viscoelastic fluids at a given Reynolds number, the same polymer solution in different diameter pipes gave different values of the friction factor. In general, the drag reduction observed in large pipes is smaller than that obtained in small pipe systems [4, 58] because of lower wall shear stresses and shear rates.

Viscoelastic theories predict a 1.1-power dependency of critical solvent Reynolds number on diameter in apparently Newtonian solutions [91]. Hershey and Zakin [52] noted in their experiments that the critical solvent Reynolds number varies with about the first power of diameter, in good agreement with the predictions. Thus, for a solution which has a critical solvent Reynolds number for drag reduction of 100,000 in a 2-centimeter diameter tube, the critical solvent Reynolds number for an 8-centimeter tube would be about 400,000. Thus the larger the diameter, the higher the critical Reynolds number needed to initiate drag reduction.

3.8. Stability of Drag Reduction in Polymer Solutions. Polymers as drag reducers have a serious drawback in that they degrade permanently when subjected to high shear or extensional stress. High molecular weight polymers are particularly sensitive to degradation [49], and the rate of mechanical degradation increases with increasing molecular weight [49, 85]. This disadvantage prevents the application of polymers in recirculation systems where high shear stresses in pumps irreversibly degrade the high molecular weight molecules.

4. Drag Reduction in Surfactant Solutions

In addition to fibers and polymers, surfactants are also effective drag reducers. Their advantage over high polymers is that their nanostructures can self-assemble after breakup by high shear.

4.1. Characteristics of Surfactant Solutions. Surfactants are characterized by amphiphilic structures that consist of a hydrophobic group (nonpolar end) and a hydrophilic group (polar end). In aqueous systems, when the concentration exceeds a certain value, surfactant molecules gather into assemblies with their polar ends headed towards water and the nonpolar ends headed to the center based on the rule "like dissolves like". The assemblies are called micelles. The critical concentration is called the critical micelle concentration (CMC). Surfactants form micelles in order to minimize the hydrocarbon-water interface.

When surfactant concentration is the same as or slightly above the CMC, the shape of micelles is spherical or ellipsoidal. As the concentration increases, micelles are forced to move closer to each other. This increases the system energy due to electronic repulsions. To keep the system stable at

a lower energy level, micelles tend to form nonspherical shapes when the concentration reaches a second critical value (CMC_{II}). While they may form vesicles or disklike shapes in some cases, they may also form long cylindrical shapes, usually called rodlike or wormlike micelles. In the presence of electrolytes, cosurfactants or organic counterions, the charges on cationic surfactant head groups can be partly neutralized or diluted and the micelles can be packed more closely into a rodlike or wormlike shape. Examples of these three materials are sodium halides, alcohols with intermediate chain length, and salicylate, respectively [92–96]. The rodlike shape of micelles is generally considered a necessity for drag reduction [97, 98].

The forces, which hold the surfactant molecules together in micelles, are much weaker than the primary chemical bonds of polymer molecules. But these forces persist even if the micelles encounter strong shear and break up. They reform or self-assemble when the strong shear disappears, while polymer molecules cannot reform after mechanical degradation. Thus surfactants can be used in recirculation systems containing high shear pumps as they self-repair. The characteristics of surfactant solutions are affected by several factors which are reviewed below.

4.1.1. Effects on the CMC and CMC_{II}. The main factors which affect the CMC in aqueous medium are the nature of the surfactant and the presence of added salts, that is, hydrophobic characteristics, hydrophilic group species, and counterion effect. They will be discussed in detail below.

First, the CMC usually decreases with increase in the hydrophobic character of the surfactant. In aqueous solution, the CMC decreases as the length of the surfactant hydrocarbon chains increases up to 16 carbon atoms. The CMC decreases slowly above 16 carbon atoms and may stop at 18 carbon atoms. The CMC for surfactants with double bonds in the hydrocarbon chain is higher than the corresponding saturated chain [99]. For ionic surfactants with alkyl chains and a common hydrophilic group, the CMC decreases by half for each addition of a methylene group to the hydrophobic chain [99, 100]. A relation between the CMC for straight chain ionic surfactants and the number of carbon atoms (N) in the hydrophobic chain was established by Klevens [101]:

$$\log \mathrm{CMC} = A - BN, \tag{13}$$

where A and B are two positive constants for a particular ionic head group and given temperature. They are tabulated by Rosen [99] based on many results. The value of B (≈ 0.3) is close to $\log 2$ at 35°C. This is consistent with Rosen's conclusion that the CMC is halved for each increase in N.

Second, the CMC is also affected by the hydrophilic group species. Stigter [102] examined the CMCs of five surfactants each having a different type of head group, and proposed that the CMC was higher when the ionic charge on the head group was closer to the α-carbon of the alkyl chain. Head groups with the same charge will generate electrical repulsion, which may be the reason that the CMCs of ionic surfactants are higher than those of nonionic surfactants [99].

Third, the CMC is affected by the counterions, including inorganic salts, aliphatic salts, and aromatic salts. It decreases due to their dispersion of the charge of the ionic head groups thus diminishing their repulsion in the micelle [99]. Underwood and Anacker [103] found CMC had good correlation with the hydration enthalpy and hydration size of the inorganic counterions. They suggested that the most effective anions in promoting micellization are those which interact the least with water. For cationic surfactants, it has been shown that increase in hydrophobicity of the aliphatic counterion resulted in a decrease in CMC [104, 105]. Aromatic acid counterions (such as benzoates, benzenesulfonates, p-methyl-benzoates and p-methyl-benzenesulfonates) can reduce CMC to an order lower than inorganic and aliphatic counterions [104–106].

The CMC_{II} increases very rapidly with temperature [98, 107]. It is reduced at high salt concentrations [108–110]. For example, the CMC_{II} for cetyltrimethylammonium bromide (CTAB) in aqueous medium is approximately 0.3 M (10% by weight) [111, 112]. However, it is reduced to 0.004 M if 0.2 M sodium bromide is added. Rodlike micelles several hundred nanometers long in the 0.004 M CTAB/0.2 M NaBr solution were detected by dynamic light scattering measurements [113].

4.1.2. Effects on Micelle Shape. The major types of micelles are spherical, rodlike, lamellar, and vesicles [99]. The radii of the spherical micelles are approximately equal to the fully extended lengths of the hydrophobic chains [114]. Micellar shape is spherical at the CMC, and the spherical shape is retained even at low concentrations of inorganic salts [113, 115–121]. High salt concentrations can result in micellar-shape transformation from sphere to rod [108–110]. A number of investigators used different experimental techniques to show that the micelles in solutions of high ionic strength are rodlike in shape. Debye and Anacker [108], using static light scattering measurements, found the data for the CTAB/KBr system were well fitted to a rodlike shape rather than a spherical or a disklike shape. Young et al. [122] concluded that the micelles in high concentration salt solutions were rodlike by results from both static and dynamic light scattering techniques. The rodlike shape of micelles was also supported by results from nuclear magnetic resonance [123] and magnetic birefringence [124]. Israelachvili et al. [125] developed a theory of micellar structure. They considered geometry and energy and proposed that the micelle shape was determined by the dimensionless parameter, called the packing parameter, $V/(A_0L_0)$, where V and L_0 are the volume and length of the surfactant hydrophobic chain, and A_0 is the optimal surface area occupied by each surfactant head group. According to Israelachvili et al., micelles were spherical for $0 < V/(A_0L_0) < 1/3$, rodlike for $1/3 < V/(A_0L_0) < 1/2$, disklike for $1/2 < V/(A_0L_0) < 1$, and $V/(A_0L_0) > 1$ gave reversed micelles in nonpolar media. A shape transformation from sphere to rod can be induced by the addition of salt because the salt can reduce A_0 by partially screening the electrostatic head group repulsion.

4.1.3. Effects on Micelle Size. Micelle size is affected by many factors, such as the chain structure of the surfactant, the head group of the surfactant, counterions, and temperature, etc. It can be characterized by aggregation number, which is the number of surfactant monomers aggregating to form a micelle. The classical method for determining the aggregation number is elastic light scattering [126]. It has been observed that the aggregation number increases rapidly with increase of hydrocarbon chain length and decreases with increasing head group size [127].

The length of the rodlike micelles increases with decreasing temperature and with increasing concentration of surfactant and salt [109, 113, 128]. Missel et al. [109, 110] observed rapid increases of the aggregation number and the hydrodynamic radius of micelles with increasing surfactant concentration. With an increase in surfactant monomer chain length, micelle length becomes more sensitive to the variations of temperature and salt concentration [110, 113].

For surfactants with a common hydrophobic chain, micelle size decreases with increasing head group size [129]. Geer et al. studied the effect by a light scattering technique. In their study, they sequentially replaced the protons on the decylammonium head group with methyl or ethyl groups. They proposed that the larger head groups tended to make it more difficult for the counterions to approach the charge center and disfavored micelle growth leading to micelle size decrease. Other researchers attributed this effect to the increased difficulty in packing the head groups on the micelle surface [130]. Rehage and Hoffman [131] explained the effects of head groups on micelle shape using geometry. If the area of the hydrophilic head group is larger than that of the hydrocarbon chain, the system will tend to form aggregates with convex curvatures. If both areas are the same, planar structures will be formed. If the head group has an area less than that of the hydrocarbon chain, inverse micelles will be formed.

Salts play an important role in micellar growth. Certain types of salts can strongly affect micelle size. In general, the effect of salt on the aggregation number of rodlike micelles increases with increasing lyotropic number of the anion. Thus, those anions which can more effectively reduce surfactant CMC are usually more efficient in inducing micelle growth. This is because the formation of both the spherical and the long rodlike micelles is strongly controlled by the charges on the surfactant head groups. Salts with greater ability to neutralize these charges are useful for both micelle formation and size [99].

Aromatic acid anions are known to greatly promote micellar growth. The influence of salicylate ions on the properties of cetylpyridinium micelles has been extensively studied by Hoffmann et al. [94, 95, 132–134] using electric birefringence, static and dynamic light scattering, and small angle neutron scattering. They found that, at a concentration of a few millimoles of surfactant per liter, micelles grew to be several hundred angstroms long with a few millimoles per liter of salicylate [97].

4.1.4. Shear Effects. Surfactant solutions are very sensitive to shear. Shear can induce reversible structural transformations in the solution [135]. Shear effects appear as shear thinning, shear-induced structures (SIS), shear-induced phase transitions (in shear bands), gelation, and flow instabilities [136, 137]. The mechanisms of these phenomena are not fully understood. However, these behaviors have both theoretical and practical scientific importance [138, 139].

At low shear rates, surfactant solutions with rodlike or threadlike micelles usually act as Newtonian fluids because micelles rotate freely in the solution. At higher shear rates, micelles start to align in the shearing direction causing shear thinning [139, 140]. A particular phenomenon may occur for some solutions at a critical shear rate at which the shear viscosity and elasticity have a sudden increase. This phenomenon is called shear-induced structure (SIS). The SIS structure is orders of magnitude larger than the individual rodlike micelles [141–146] and the solution is like a viscoelastic gel [147]. However, as shear rate increases, the SIS is no longer stable and viscosity begins to decrease with shear rate. At the viscosity peak, it is believed that micelles are fully aligned in the flow direction. This opinion was confirmed by flow birefringence [140] and small angle neutron scattering experiments [148–151]. The critical shear rate for SIS depends on the surfactant concentration/chemical structure, counterion concentration/chemical structure, temperature, and also on the geometry of the rheological measuring devices [152].

Several authors proposed that SIS may relate to the drag reduction phenomenon in turbulent flow [138, 141, 142, 153]. SIS and phase separation were detected by Koch [154]. He hypothesized that the monomer surfactant concentration increases rapidly with shear causing a coacervate phase to form. Fischer [136] observed oscillations in the first normal stress difference and shear stress indicating that elastic structures were formed and destroyed with SIS and the induced new phase was more elastic than the initial one. Butler [137] observed a new phase generated from the solution at SIS and used the concept of shear banding to distinguish the two phases. Shear banding is usually observed at high micelle concentrations and is characterized by a stress plateau at a critical shear rate. The shear stress becomes independent of shear rate while a second phase appears. As shear rate further increases, shear thinning occurs [98, 155]. In some systems, the proportions of old and new phases change with shear when a second critical shear rate ($\dot{\gamma}_2$) is reached. Above $\dot{\gamma}_2$, the stress once again begins to increase with shear rate. Transient behavior from $\dot{\gamma}_1$ to $\dot{\gamma}_2$ includes huge stress overshoots [137]. Hu et al. [156] proposed that the growth of SIS is associated with shear thickening. They also found strongly aligned structures with shear flow by strong flow birefringence and highly anisotropic neutron and light scattering [157]. According to their results, the SIS forms, grows, and interconnects to form a network at a particular stress. The viscosity is much higher than the original micelle solution. Oda et al. [158] used cryo-TEM to directly observe micelle aggregates and branches. They concluded that SIS is not a phase transition caused by the micellar alignment or elongation, but rather a shear-induced inhomogeneity and phase separation.

Despite the many studies made on the subject, the nature of SIS is not well understood. Its relation to drag reduction needs to be further investigated. It is still unclear whether a universal shear-induced structure indeed exists for different surfactant solutions [153, 157] because there are some surfactant systems that do not show any SIS in the ranges of shear rate studied. However, it appears that in surfactant solutions, SIS is only stable when shear conditions can induce viscoelastic behavior in the solution [145].

4.2. Main Classes of Surfactants in Drag Reduction. There are two broad classes of surfactants, namely, nonionic and ionic surfactants. Ionic surfactants include anionic, cationic, and zwitterionic surfactants.

4.2.1. Drag Reduction of Nonionic Surfactants. Nonionic surfactants do not carry charges. So they are less affected by other ions. This property is an advantage for nonionic surfactants compared to anionic surfactants. But nonionic surfactants only show drag reduction in a narrow temperature range around their coacervation temperature or cloud point. This characteristic limits the usefulness of nonionic surfactants.

Zakin and Chang observed that nonionic surfactants with straight chain alkyl groups were effective. They discovered that some mixtures of nonionic surfactants at 1% concentration were effective drag reducers at temperatures around their cloud point. The mixtures had the chemical structure of $C_{18}H_{35}$-$(OCH_2$-$CH_2)_n$-OH. The cloud point could be lowered by lowering the value of n or by the addition of a multivalent salt such as sodium sulfate. Therefore, the drag reduction temperature range can be lowered to temperatures below the cloud point [159]. Deroussel [160] measured drag reduction on nonionic surfactants containing saturated and unsaturated 12-carbons to 18-carbons alkyl groups with 4 to 23 ethylene oxide groups at 1% concentration. His conclusion was that the temperature of maximum drag reduction is close to the cloud point of the surfactant solution. With increasing length of the alkyl group and decreasing number of ethylene oxides, the cloud point and the effective temperature range for drag reduction could be lowered. The drag reducing effective temperature is also affected by the length of alkyl chain, the number of ethylene oxide groups, and the concentration ratios in mixed surfactant systems. Hellsten and Harwigsson [161] tested two groups of ethoxylated fatty acid ethanolamides, RMA-m and OMA-m. They found the RMA was effective at high temperature and OMA was effective at low temperature. This kind of surfactant is rapidly biodegradable and has low toxicity against marine organisms. They suggested that OMA would be a good candidate for use in district cooling systems ($5 \sim 15^{\circ}$C).

4.2.2. Drag Reduction of Anionic Surfactants. Since the early observations by Mysels et al. [2] of drag reduction by aluminum disoap thickened gasoline, many researchers investigated drag reduction of anionic surfactants in nonaqueous media, primarily lithium, sodium, or aluminum salts of disoaps. They are presently the only known effective surfactant drag reducers in hydrocarbon media. To obtain good drag reduction for this kind of surfactant, the concentration usually needs to be very high (about a few thousands ppm) [162, 163]. This leads to large costs and environmental problems. In aqueous solutions, anionic surfactants form foams with air. Due to their sensitivity to calcium and magnesium ions present in most tap water which cause precipitation, anionic surfactants are not practical for most aqueous applications [47]. Thus they have limited applicability. Savins [8, 164] found that a critical shear stress exists for anionic surfactants in water above which drag reduction was rapidly lost. When the shear stress was reduced below the critical value, drag reduction was completely regained without any delay, different than the permanent degradation of polymer drag reducers under high shear stress.

4.2.3. Drag Reduction of Cationic Surfactants. Cationic surfactants with appropriate counterions are insensitive to cations and show much broader effective temperature ranges. Thus, they have more potential applications. So a great deal of research on cationic surfactants has been carried out since the 1980s. Drag reduction in cationic surfactant solutions is affected by surfactant structure, counterion, and concentration, temperature, which will be reviewed below.

(a) Surfactant Structure Effect. In the family of cationic surfactants, quaternary ammonium surfactants and those with related structure (cetyl pyridinium salicylate) are excellent drag reducers. The first cationic surfactant studied in drag reduction was cetyl trimethyl ammonium bromide (CTAB). White [165] and Zakin et al. [9] tested CTAB with 1-naphthol at different concentrations and found drag reduction increased until a critical wall shear stress was reached and beyond which drag reduction decreased. This is similar to Savins' conclusion for anionic surfactants. Chou et al. [166, 167] studied three cationic surfactants (Arquad 16-50, Arquad 18-50, and Kemamine Q-2983C) and concluded that the upper temperature limit for effective drag reduction is dependent on the alkyl chain length. When temperature is reduced below the upper critical temperature, drag reduction effectiveness can be regained. Rose and Foster [168] and Chou et al. [169] found the lower temperature limit depends on solubility of the surfactant. Surfactants containing alkyl bishydroxyethyl methyl can provide drag reduction down to lower temperatures compared to those with alkyl trimethyl because the former are more hydrophilic. Unsaturation of the alkyl chain also improves the solubility of long chain surfactants and thus can give drag reduction at low temperature [168, 170, 171]. Chou and Zakin and Lu et al. also studied the drag reduction effectiveness of mixed cationic surfactant systems. They noted that the effective drag reduction temperature range for long hydrocarbon chain cationic surfactants extends to higher temperatures than that for short chains which are effective at lower temperatures. The temperature range can be extended when a long chain surfactant and a short chain surfactant are mixed. The lower temperature limit of the long chain surfactant can

be greatly decreased by adding a small amount of short chain surfactant, while the upper temperature limit is only slightly reduced. Thus, cationic surfactants can have wide temperature ranges suitable for both district heating and cooling systems. The effects of mixed counterions were similar but less dramatic [11, 172, 176].

(b) Counterion Effect. Counterions are added to cationic surfactant solutions useful for drag reduction because cationic surfactants would not form long rodlike micelles without counterions to disperse the head group charges. 1-naphthol was the first counterion to receive wide attention. Elson and Garside [173] investigated the counterion concentration effect of 1-naphthol and concluded that the optimum molar ratio of counterion to surfactant was 1 : 1 for high concentrations of surfactant and more than 1 : 1 for low concentrations of surfactant. Sodium salicylate is the most widely studied counterion. Chou et al. [171, 174] found that an Ethoquad O-12/sodium salicylate solution at a molar ratio of 1.5 : 1 showed most effective drag reduction at 2°C. Excess quantities of sodium salicylate (0.2 wt.%) in the cetyl trimethyl ammonium salicylate (CTASal) system (0.2 wt.%) were observed by Rose et al. [168, 170] to increase the critical Reynolds number (from about 20000 to about 50000) and the critical temperature (from 50°C to 70°C). The effectiveness of drag reduction systems can be promoted by hydrophobic substitute groups on benzoate compounds if the hydrophobic substitute groups are widely separated from hydrophilic substitute groups on the same carbon ring. The orientation of counterion molecules at the micelle-water interface is affected by the position of the substituent groups on the benzoate ring. This was confirmed by Smith et al. [175]. Chou [174] and Ge et al. [13, 176] observed increased drag reduction temperature ranges with certain mixtures of counterions. Chou et al. [169, 174] proposed a number of counterions that may be very effective at temperatures between 40°C and 90°C.

4.2.4. Drag Reduction of Zwitterionic Surfactants. Because cationic surfactants are not easily biodegradable, zwitterionic surfactant or combinations of zwitterionic with anionic surfactants have been studied as drag reducers. Zwitterionic molecules have both positive and negative charges on different locations of the molecules. Zwitterionic/anionic mixtures containing up to 20% anionic are most effective drag reducers [177]. However, despite their potential as drag reducing agents, only limited studies of them have been carried out. Hellsten and Harwigsson [178] reported on a mixture of 2.5 mM alkylbetaine/0.5 mM SDBS which was effective as a drag reducer from 6 to 60°C for C16 and from 20 to 100°C for C18. Zhang et al. [179] determined that an Akzo Nobel alkyl ammonium carboxylate (zwitterionic)/SDBS at molar ratio 4 : 1 was effective as a drag reducer in both water and ethylene glycol/water systems. At low temperatures, they reported that surfactant containing the oleyl group was even more effective because of better low temperature solubility.

4.3. Diameter Effect. It is important to study scale-up to predict drag reduction performance in large pipes from small diameter measurements because most practical flow systems use larger pipes than those in the laboratory. However, while the friction factor for Newtonian fluids can be predicted from the Reynolds number, the friction factor for drag reducing fluids is a function of both Reynolds number and pipe diameter. Some research relating polymer drag reduction scale-up was noted in Section 3.7. A few scale-up studies on surfactant drag reducers are reviewed below.

White [165] observed that the critical wall shear stress was independent of pipe diameter. Gasljevic et al. [180] found that drag reduction of Ethoquad T 13/27 (2000 ppm)/NaSal (91740 ppm)+3.75 mMol/L of $Cu(OH)_2$ in pipes with five diameters (2 mm, 5 mm, 10 mm, 20 mm, and 52 mm) was independent of tube diameter when plotted against bulk (mean) velocity up to the wall shear stress corresponding to maximum drag reduction. They also suggested that surfactant drag reduction scales even better with solvent shear viscosity.

4.4. Stability of Drag Reduction in Surfactant Solutions. Savins noted that drag reduction for anionic surfactants was regained when the shear stress was lowered [8]. The loss of drag reduction was presumably caused by breaking up of the micelle nanostructure due to high shear stresses. No permanent degradation was found after 88 hours of continuous shear above the critical wall shear stress. Zakin and Lui [10] found mechanically degraded nonionic surfactant solutions quickly regained their drag reducing ability after passing through a pump. White [165] and Zakin et al. [9] found cationic surfactants that showed no permanent mechanical degradation. These findings are important for surfactant drag reduction applications and make surfactants good agents for recirculation systems in which the fluid is repeatedly passed through pump.

5. Heat Transfer of Drag Reducing Surfactant Solutions

Along with drag reduction, the heat transfer ability of surfactant solutions is also reduced significantly [84, 170, 181–189]. Aguilar et al. [183] showed that the reduction of heat transfer is always a little larger than drag reduction. In a tube-in-tube heat exchanger, Christensen and Zakin [188] found that the heat transfer reduction of a Kemamine Q-2983C/NaSal (2000 ppm/2200 ppm) drag reducing surfactant solution could reach as high as 90%. Heat transfer reduction of drag reducing solutions is beneficial in transporting crude oils that need to be heated to keep them flowing. It reduces the need for heat insulation materials on long distant pipelines. However, for DHC systems, the heat transfer reduction is a major problem since heat exchange in DHC is very important. Thus, techniques for enhancing heat transfer of drag reducing surfactant solutions must be developed for DHC systems.

5.1. Reasons for Heat Transfer Reduction. The mechanism of heat transfer reduction of drag reducing surfactant solutions is still not totally understood. However, it may be attributed

to two characteristics observed in turbulent drag reduction flows.

As mentioned in Section 3.3, the viscous sublayer of drag reducing solutions is extended compared to Newtonian fluids. Sellin et al. [84] suggested that this extended viscous sublayer increases the thermal resistance between wall and bulk fluid and therefore decreases the heat transfer ability of the solution.

Another characteristic is that velocity fluctuations of drag reducing surfactant solutions in turbulent flow in the radial and tangential directions are greatly suppressed compared with Newtonian fluids [190–195]. It is postulated that velocity fluctuations in the radial direction are strongly related to the heat transfer ability of the fluid. Thus, heat transfer in the radial direction is greatly reduced because of the decrease of radial velocity fluctuations.

5.2. Methods for Enhancing Heat Transfer Ability. There are two methods to enhance the heat transfer ability of drag reducing surfactant solutions by overcoming one or both of the two possible reasons for heat transfer reduction in Section 5.1. One is to modify the inner surface of heat exchangers to cause disturbances to the viscous sublayer of drag reducing flows. Another is to temporarily destroy or alter the surfactant nanostructure by mechanical or other means at the entrance to the heat exchanger to obtain Newtonian, water-like flow behavior in the heat exchanger. Self-assembly of the micelle nanostructure downstream of the heat exchanger would restore drag-reducing behavior in the pipeline flow.

5.2.1. Modify Inner Surface of Heat Exchanger. Plate heat exchangers and fluted tube-in-tube heat exchangers can enhance the heat transfer ability of drag reducing solutions very effectively. Plate exchangers generate high shear stress and their convoluted paths can cause extensional flows both of which can cause micelles to break up. The special inner surface of fluted tubes enhances the heat transfer ability of surfactant solutions by altering the viscous sublayer [181, 188]. In the fluted tube-in-tube heat exchanger [181], the spiral wall generates a swirling motion and extra shear stress on the fluid. Both the high shear stress in the fluted tube and the swirling motion increase the heat transfer ability of the solutions.

Kishimoto et al. [196] and Sato et al. [197] investigated heat transfer of drag reducing surfactant solutions using a spiral grooved rough inner tube, a two-dimensional fence plate, a saw-toothed plate, and a porous plate. They found heat transfer enhancement can be achieved by changing the geometry of these heat transfer exchangers. Investigators at the UMSICHT Institute in Germany tried to enhance heat transfer by inserting spring coils inside the inner tube of the heat exchanger. But this method was not effective [198].

While some of these methods enhanced heat transfer, the pressure drops of drag reducing surfactant solutions passing through these exchangers are higher than straight tube-in-tube heat exchangers due to their tortuous paths. This is the price that must be paid. However, compared with other heat transfer enhancement methods, the pressure drop penalty in fluted tube-in-tube heat exchangers is small [181]. Thus the fluted tube method is most applicable for heat exchangers in new DHC systems. The economic viability of these methods depends on the ratio of capital costs to operation costs and the ratio of heat transfer ability to pressure drop penalty. All of these depend on DHC design and user requirements.

5.2.2. Destruction of Nanostructure in Heat Exchanger. Five different methods have been proposed to break up the micelle nanostructure in drag-reducing surfactant solutions before a heat exchanger.

The first method is to position a pump at the entrance of the heat exchanger. The pump provides high shear which would temporarily destroy the surfactant nanostructure and enhance heat transfer in the heat exchanger. This is the most convenient method but may not be possible for existing DHC systems or for many newly designed systems.

The second method is to use ultrasonic energy to destroy the surfactant nanostructure at the heat exchanger entrance. While this method does not impart additional pressure drop penalties to the flow as it does not change the flow field, however, it does take a great deal of energy to breakdown the micelle nanostructure and it is difficult to transmit ultrasonic energy effectively to a large-scale flowing system [199, 200].

The third method is by insertion of small destructive devices such as static mixers, honeycombs, or meshes at the entrance to the heat exchanger [184, 201–203]. This method is similar to the first method. The destructive devices can generate large shear and extensional stresses on the surfactant solution to destroy the micelle nanostructure. This method is easy to install and uninstall in existing systems and should be inexpensive. However, it may cause large pressure drop penalties. In a similar approach, Li et al. [204] studied the effectiveness of three types of wire meshes. Heat transfer enhancement largely depended on the Reynolds number and concentration of surfactant.

Drag reduction recovery times for these methods depend on the temperature, chemical structure, and concentration of the surfactant [182] as well as the counterion. The self-repair time of surfactant nanostructures can be estimated from measurements of pressure gradients of the flowing solution downstream from the destructive devices.

The fourth method is to increase wall shear stress in the heat exchanger above the critical wall shear stress for surfactant micelle break up. Pollert et al. [205] noted that when the flow velocity of the solution through a heat exchanger reaches a certain level, heat transfer enhancement is observed. Thus increasing the flow velocity of surfactant solutions at the entrance of or inside the heat exchangers so that the critical shear stress is exceeded will also destroy the micelle nanostructure.

Wollerstrand and Frederiksen [198] tested this method by installing small diameter tubes or orifices. Kishimoto et al. [206] also tested it by increasing the flow velocity at the entrance of the heat exchanger by decreasing the tube diameter (from $D_i = 14$ mm to 10 mm and 8 mm, resp.). Heat transfer enhancement was observed for an Ethoquad

O/12/NaSal solution at a flow velocity above 1.5 m/s in the small tube but a large pressure drop penalty was incurred. Moreover, this approach is probably not practical for existing DHC systems because of the difficulty of tube replacement.

The fifth method is to use photorheological (PR) surfactants as drag reducers. All of the methods above require large energy input and major changes in the flow field. The ideal result would be to reduce drag reduction ability in the heat exchanger to enhance heat transfer and then regain their drag reduction ability at the outlet of the heat exchanger without large energy input. Recently, Raghavan's group has developed new photorheological counterions which are commercially available and relatively inexpensive [207–209]. One of their new PR counterions is the sodium salt of trans-O-Methyl-o-coumaric Acid (trans-OMCA). They found the trans-OMCA/CTAB system is viscoelastic but, when the trans-OMCA is photoisomerized to cis-OMCA by irradiation with ultraviolet (UV) light, the fluid viscosity is largely reduced and viscoelasticity is lost. This is because the change in the counterion from trans to cis configuration causes micelles to rearrange into much smaller ones. Shi et al. [210] found cationic surfactant solutions with trans-OMCA have good drag reduction, while the solutions with cis-OMCA are not drag reducing. Thus irradiating trans-OMCA or a similar functional chemical counterion can enhance heat transfer but it is necessary to convert the cis-OMCA back to trans-OMCA to regain drag reduction behavior downstream from the heat exchanger. They are exploring other PR systems.

This method requires a balance of heat exchanger length, UV dosage, with low energy requirements surfactant nanostructure recovery time and control of the surfactant solution flow rate to achieve high heat transfer enhancement.

Determination of which heat transfer enhancement method is most practical for drag reducing surfactant solutions in a DHC system depends on the nature of surfactant solution, the temperature range, and the size of the DHC system, and so forth. Minimum additional equipment and energy penalty costs and maximum heat transfer enhancement effects are the targets of future studies.

6. Concluding Remarks

From the summary above, further drag reduction research on mechanism and application covering fields, such as fluid mechanics, heat transfer, turbulence, rheology, and chemistry, is needed to develop surfactant systems useful for DHC and other applications. Advanced experimental methods (such as particle image velocimetry) combined with advanced numerical methods (direct numerical simulation, large eddy simulation, proper orthogonal decomposition, etc.) are among the future directions for research. Field tests of drag reduction and heat transfer are also needed to evaluate the economy and efficiency in practical applications.

References

[1] F. Forrest and G. A. Grierson, "Friction losses in cast iron pipe carrying paper stock," *Paper Trade Journal*, vol. 92, no. 22, pp. 39–41, 1931.

[2] K. J. Mysels, "Early experiences with viscous drag reduction," *AIChE Chemical Engineering Progress Symposium Series III*, vol. 67, pp. 45–49, 1971.

[3] B. A. Toms, "Some observations on the flow of linear polymer solutions through straight tubes at large Reynolds numbers," in *Proceedings of the 1st International Congress on Rheology*, vol. 2, pp. 135–141, North Holland, 1949.

[4] J. G. Savins, "Drag reductions characteristics of solutions of macromolecules in turbulent pipe flow," *Society of Petroleum Engineers Journal*, vol. 4, p. 203, 1964.

[5] E. D. Burger, W. R. Munk, and H. A. Wahl, "Flow increase in the Trans Alaska Pipeline through use of a polymeric drag-reducing additive," *Journal of Petroleum Technology*, vol. 34, no. 2, pp. 377–386, 1982.

[6] J. F. Motier, L. C. Chou, and N. S. Kommareddi, "Commercial drag reduction: past, present, and future," in *Proceedings of the ASME Fluids Engineering Division Summer Meeting*, ASME, San Diego, Calif, USA, 1996.

[7] K. C. Lee and J. L. Zakin, "Drag reduction in hydrocarbon-aluminum soap polymer systems," in *Proceedings of the 72nd National Meeting of the American Institute of Chemical Engineers, Symposium on Drag Reduction in Polymer Solutions*, St. Louis, Mo, USA, paper 14a, May 1972; *AIChE Symposium Series* no. 130, N. D. Sylvester, Ed., vol. 69, pp. 45–51, 1973.

[8] J. G. Savins, "A stress controlled drag reduction phenomenon," *Rheologica Acta*, vol. 6, no. 4, pp. 323–330, 1967.

[9] J. L. Zakin, M. Poreh, A. Brosh, and M. Warshavsky, "Exploratory study of friction reduction in slurry flows," *Chemical Engineering Progress Symposium Series*, vol. 67, pp. 85–89, 1971.

[10] J. L. Zakin and H. L. Lui, "Variables affecting drag reduction by nonionic surfactant additives," *Chemical Engineering Communications*, vol. 23, pp. 77–80, 1983.

[11] L. C. Chou, *Drag reducing cationic surfactant solutions for district heating and cooling systems*, Ph.D. thesis, The Ohio State University, 1991.

[12] R. H. Nadolink and W. W. Haigh, "Bibliography on skin friction reduction with polymers and other boundary-layer additives," *Applied Mechanics Reviews*, vol. 48, no. 7, pp. 351–460, 1995.

[13] W. Ge, *Studies on the nanostructure, rheology and drag reduction characteristics of drag reducing cationic surfactant solutions*, Ph.D. thesis, The Ohio State University, 2008.

[14] P. D. Manfield, C. J. Lawrence, and G. F. Hewitt, "Drag reduction with additives in multiphase flow: a literature survey," *Multiphase Science and Technology*, vol. 11, no. 3, pp. 197–221, 1999.

[15] L. Nijs, "New generation drag reducer," in *Proceedings of the 2nd International Pipeline Technology Conference*, Elsevier, Ostend, Belgium, 1995.

[16] T. Dujmovich and A. Gallegos, "Drag reducers improve throughput, cut costs," *Offshore*, vol. 65, no. 12, pp. 1–4, 2005.

[17] J. F. Motier and A. M. Carreir, "Recent studies on polymer drag reduction in commercial pipelines," in *Drag Reduction in Fluid Flows: Techniques for Friction Control*, R. Sellin and R. Moses, Eds., pp. 197–204, Ellis Horwood, West Sussex, UK, 1989.

[18] M. Hellsten and H. Oskarsson, "A drag-reducing agent for use in injection water at oil recovery," application: WO/2004/007630 (patent), 2004.

[19] P. Sullivan, E. B. Nelson, V. Anderson, and T. Hughes, "Oilfield applications of giant micelles," in *Giant Micelles: Properties and Applications*, R. Zana and E. W. Kaler, Eds.,

vol. 140 of *Surfactant Science Series*, pp. 453–472, CRC Press, Boca Raton, Fla, USA, 2007.

[20] J. Golda, "Hydraulic transport of coal in pipes with drag reducing additives," *Chemical Engineering Communications*, vol. 43, no. 1–3, pp. 53–67, 1986.

[21] G. Wul, J. Xu, and J. Miles, "Polymer drag reduction in large diameter coal log pipeline," in *Proceedings of the International Technical Conference on Coal Utilization & Fuel Systems*, vol. 23, pp. 889–900, 1998.

[22] R. A. Mostardi, L. C. Thomas, H. L. Greene, F. VanEssen, and R. F. Nokes, "Suppression of atherosclerosis in rabbits using drag reducing polymers," *Biorheology*, vol. 15, no. 1, pp. 1–14, 1978.

[23] J. L. Unthank, S. G. Lalka, J. C. Nixon, and A. P. Sawchuk, "Improvement of flow through arterial stenoses by drag reducing agents," *Journal of Surgical Research*, vol. 53, no. 6, pp. 625–630, 1992.

[24] M. V. Kameneva, Z. J. Wu, A. Uraysh et al., "Blood soluble drag-reducing polymers prevent lethality from hemorrhagic shock in acute animal experiments," *Biorheology*, vol. 41, no. 1, pp. 53–64, 2003.

[25] A. G. Fabula, "Fire-fighting benefits of polymeric friction reduction," *Journal of Basic Engineering*, vol. 93, no. 3, pp. 453–455, 1971.

[26] R. C. R. Figueredo and E. Sabadini, "Firefighting foam stability: the effect of the drag reducer poly(ethylene) oxide," *Colloids and Surfaces A*, vol. 215, no. 1–3, pp. 77–86, 2003.

[27] G. Dembek and H. W. Bewersdorff, "Short-time increase of sewer capacity by addition of water-soluble polymers," *GWF, Wasser/Abwasser*, vol. 122, no. 9, pp. 392–395, 1981.

[28] R. P. Singh, J. Singh, S. R. Deshmukh, and A. Kumar, "The effect of grafted and ungrafted guar gum on turbulent flow of water and on hydraulic conductivity of soil," in *Proceedings of the IUTAM Symposium on the Influence of Polymer Additives on Velocity and Temperature Fields*, pp. 131–139, 1985.

[29] J. L. Zakin, Y. Zhang, and W. Ge, "Drag reduction by surfactant giant micelles," in *Giant Micelles: Properties and Applications*, R. Zana and E. W. Kaler, Eds., Surfactant Science Series, pp. 140–489, CRC Press, Boca Raton, Fla, USA, 2007.

[30] J. L. Zakin, B. Lu, and H. W. Bewersdorff, "Surfactant drag reduction," *Reviews in Chemical Engineering*, vol. 14, no. 4-5, pp. 253–320, 1998.

[31] F. Hammer, "Demonstration of smooth water in the district heating system of herning, Denmark," in *Proceedings of the International Symposium on Fluids for District Heating*, Copenhagen, Denmark, 1991.

[32] H. H. Kleuker, W. Althaus, A. Steiff, and P. M. Weinspach, "Results of the EC-demonstration-project in Volklingen (Germany)," in *Proceedings of the International Symposium on Fluids for District Heating*, Copenhagen, Denmark, 1991.

[33] J. Pollert, J. L. Zakin, J. Myska, and P. Kratochvil, "Use of friction reducing additives in district heating system field test at Kladno-Krocehlavy, Czech Republic," in *Proceedings of the 85th International District Heating and Cooling Association (IDHCA '94)*, Seattle, Wash, USA, 1994.

[34] K. Gasljevic and E. F. Matthys, "Field test of a drag-reducing surfactant additive in a hydronic cooling system," in *Proceedings of the ASME Fluids Engineering Division Summer Meeting (FEDSM '96)*, vol. 2, pp. 249–260, 1996.

[35] H. Takeuchi, Y. Kawaguchi, K. Tokuhara, and Y. Fujiwara, "Actual proof test of energy conservation in central heating/cooling system adapting surfactant drag reduction," in *Proceedings of the 8th International Conference on Sustainable Energy Technologies*, Aachen, Germany, 2009.

[36] T. Saeki, K. Tokuhara, T. Matsumura, and S. Yamamoto, "Application of surfactant drag reduction for practical air conditioning systems," *Nippon Kikai Gakkai Ronbunshu, B Hen*, vol. 68, no. 669, pp. 1482–1488, 2002.

[37] P. R. Modak, H. Usui, and H. Suzuki, "Agglomeration control of ice particles in ice-water slurry system using surfactant additives," *HVAC & R Research*, vol. 8, no. 4, pp. 453–466, 2002.

[38] H. Inaba, T. Inada, A. Horibe, H. Suzuki, and H. Usui, "Preventing agglomeration and growth of ice particles in water with suitable additives," *International Journal of Refrigeration*, vol. 28, no. 1, pp. 20–26, 2005.

[39] T. Saeki, "Application of drag reduction with cationic surfactant solutions," in *Proceedings of the 5th Pacific Rim Conference on Rheology (PRCR '10)*, Hokkaido University, Sapporo, Japan, August 2010.

[40] G. Schmitt, "Drag reduction—a widely neglected property of corrosion inhibitors," in *Proceedings of the 9th European Symposium on Corrosion Inhibitors*, vol. 2, pp. 1089–1123, Annali dell'Universita di Ferrara, Sezione 5: Chimica Pura ed Applicata, Supplemento 11, 2000.

[41] C. Deslouis, "Microscopic aspects of surfactants action on flow induced corrosion," *Electrochimica Acta*, vol. 48, no. 20–22, pp. 3279–3288, 2003.

[42] I. Radin, *Solid-fluid drag reduction*, Ph.D. thesis, University of Missouri-Rolla, 1974.

[43] I. Radin, J. L. Zakin, and G. K. Patterson, "Drag reduction in solid-fluid systems," *AIChE Journal*, vol. 21, no. 2, pp. 358–371, 1975.

[44] P. F. W. Lee and G. G. Duffy, "Relationships between velocity profiles and drag reduction in turbulent fiber suspension flow," *AIChE Journal*, vol. 22, no. 4, pp. 750–753, 1976.

[45] W. K. Lee, R. C. Vaseleski, and G. B. Metzner, "Turbulent drag reduction in polymeric solutions containing suspended fibers," *AIChE Journal*, vol. 20, no. 1, pp. 128–133, 1974.

[46] D. D. Kale and A. B. Metzner, "Turbulent drag reduction in fiber polymer systems: specificity considerations," *AIChE Journal*, vol. 20, no. 6, pp. 1218–1219, 1974.

[47] A. V. Shenoy, "A review on drag reduction with special reference to micellar systems," *Colloid & Polymer Science*, vol. 262, no. 4, pp. 319–337, 1984.

[48] J. L. Lumley, "Drag reduction by additives," *Annual Review of Fluid Mechanics*, vol. 1, pp. 367–384, 1969.

[49] G. K. Patterson, J. L. Zakin, and J. M. Rodriguez, "Drag reduction ," *Industrial & Engineering Chemistry*, vol. 61, pp. 22–30, 1969.

[50] P. S. Virk, "Drag reduction fundamentals," *AIChE Journal*, vol. 21, no. 4, pp. 625–656, 1975.

[51] A. White and J. A. G. Hemmings, *Drag Reduction by Additives—Review and Bibliography*, BHRA Fluid Engineering, Cranfield, UK, 1976.

[52] H. C. Hershey and J. L. Zakin, "Existence of two types of drag reduction in pipe flow of dilute polymer solutions," *Industrial and Engineering Chemistry Fundamentals*, vol. 6, no. 3, pp. 381–387, 1967.

[53] J. W. Hoyt, "Drag reduction," in *Encyclopedia of Polymer Science and Engineering*, vol. 5, pp. 129–151, John Wiley & Sons, New York, NY, USA, 2nd edition, 1986.

[54] P. S. Virk and D. L. Wagger, "Aspects of mechanism in type B drag reduction," in *Proceedings of the 2nd IUTAM*

Symposium on Structure of Turbulence and Drag Reduction, Zurich, Switzerland, 1989.

[55] P. I. Gold, P. K. Amar, and B. E. Swaidan, "Friction Reduction Degradation in Dilute Poly(ethy1ene Oxide) Solutions," *Journal of Applied Polymer Science*, vol. 17, p. 333, 1973.

[56] S. Eskinazi, *Modern Developments in the Mechanics of Continua*, Academic Press, New York, NY, USA, 1966.

[57] H. C. Hershey and J. L. Zakin, "A molecular approach to predicting the onset of drag reduction in the turbulent flow of dilute polymer solutions," *Chemical Engineering Science*, vol. 22, no. 12, pp. 1847–1857, 1967.

[58] N. S. Berman, "Drag reduction by polymers," *Annual Review of Fluid Mechanics*, vol. 10, pp. 47–64, 1978.

[59] A. White, "Turbulent drag reduction with polymer additives," *Journal of Mechanical Engineering Science*, vol. 8, pp. 452–455, 1966.

[60] H. C. Hershey, *Drag reduction in Newtonian polymer solutions*, Ph.D. thesis, University of Missouri-Rolla, 1965.

[61] P. S. Virk and E. W. Merrill, "Onset of dilute polymer solution phenomena," in *Proceedings of the Symposium on Viscous Drag Reduction*, pp. 107–130, 1969.

[62] M. C. Kohn, "Criteria for the onset of drag reduction," *AIChE Journal*, vol. 20, p. 185, 1974.

[63] D. L. Hunston and J. L. Zakin, "Effect of molecular parameters on the flow rate dependence of drag reduction and similar phenomena," *Progress in Astronautics and Aeronautics*, vol. 72, pp. 373–385, 1980.

[64] W. Castro and W. Squire, "The effect of polymer additives on transition in pipe flow," *Applied Scientific Research*, vol. 18, no. 1, pp. 81–96, 1967.

[65] W. B. Giles and W. T. Pettit, "Stability of dilute viscoelastic flows," *Nature*, vol. 216, no. 5114, pp. 470–472, 1967.

[66] P. S. Virk, H. S. Mickley, and K. A. Smith, "The ultimate asymptote and mean flow structure in Toms' phenomenon," *Journal of Applied Mechanics*, vol. 37, no. 2, pp. 488–493, 1970.

[67] P. S. Virk, "An elastic sublayer model for drag reduction by dilute solutions of linear macromolecules," *The Journal of Fluid Mechanics*, vol. 45, pp. 417–440, 1971.

[68] H. C. Hershey, J. T. Kuo, and M. L. McMillan, "Drag reduction of straight and branched chain aluminum disoaps," *Industrial and Engineering Chemistry Product Research and Development*, vol. 14, no. 3, pp. 192–199, 1975.

[69] Y. I. Cho and J. P. Hartnett, "Non-Newtonian fluids in circular pipe flow," *Advances in Heat Transfer*, vol. 15, pp. 59–141, 1982.

[70] J. L. Zakin, J. Myska, and Z. Chara, "New limiting drag reduction and velocity profile asymptotes for nonpolymeric additives systems," *AIChE Journal*, vol. 42, no. 12, pp. 3544–3546, 1996.

[71] Y. Goren and J. F. Norbury, "Turbulent flow in dilute aqueous polymer solutions," *Journal of Basic Engineering*, vol. 814, 1967.

[72] P. R. Kenis, "Turbulent flow friction reduction effectiveness and hydrodynamic degradation of polysaccharides and synthetic polymers," *Journal of Applied Polymer Science*, vol. 15, no. 3, pp. 607–618, 1971.

[73] P. S. Virk, "The effect of polymer concentration on drag reduction," *Chemical Engineering Science*, vol. 25, no. 7, pp. 1183–1189, 1970.

[74] N. S. Berman and J. Yuen, "The study of drag reduction using narrow fractions of polyox," in *Proceedings of the 2nd International Conference on Drag Reduction*, H. S. Stephens and J. A. Clarke, Eds., BHRA Fluid Engineering, Cranfield, UK, paper C1, 1977.

[75] Y. X. Hou, V. S. R. Somandepalli, and M. G. Mungal, "Streamwise development of turbulent boundary-layer drag reduction with polymer injection," *The Journal of Fluid Mechanics*, vol. 597, pp. 31–66, 2008.

[76] C. M. White, V. S. R. Somandepalli, and M. G. Mungal, "The turbulence structure of drag-reduced boundary layer flow," *Experiments in Fluids*, vol. 36, no. 1, pp. 62–69, 2004.

[77] R. W. Paterson and F. H. Abernathy, "Turbulent drag reduction and degradation with dilute polymer solutions," *The Journal of Fluid Mechanics*, vol. 43, p. 689, 1970.

[78] N. S. Berman, "Drag reduction of the highest molecular weight fractions of polyethylene oxide," *Physics of Fluids*, vol. 20, no. 5, pp. 715–718, 1977.

[79] E. W. Jacobs, G. W. Anderson, C. A. Smith, J. S. Schroeder, and J. J. Rohr, "Drag reduction using high molecular weight fractions of polyethylene oxide," in *Drag Reduction in Fluid Flows*, R. H. SeIlin and R. T. Moses, Eds., p. 53, Ellis Horwood, Chichester, UK, 1989.

[80] D. L. Hunston and M. M. Reischman, "The role of polydispersity in the mechanism of drag reduction," *Physics of Fluids*, vol. 18, no. 12, pp. 1626–1629, 1975.

[81] C. L. McCormick, R. D. Hester, S. E. Morgan, and A. M. Safieddine, "Water-soluble copolymers. Effects of molecular parameters, solvation, and polymer associations on drag reduction performance," *Macromolecules*, vol. 23, no. 8, pp. 2132–2139, 1990.

[82] G. C. Liaw, J. L. Zakin, and G. K. Patterson, "Effects of molecular characteristics of polymers on drag reduction," *AIChE Journal*, vol. 17, pp. 391–397, 1971.

[83] G. C. Liaw, *The effect of polymer structure on drag reduction in nonpolar solvents*, Ph.D. thesis, University of Missouri-Rolla, 1968.

[84] R. H. J. Sellin, J. W. Hoyt, and O. Scrivener, "The effect of drag-reducing additives on fluid flows and their industrial applications, part 1: basic aspects," *Journal of Hydraulic Research*, vol. 20, no. 1, pp. 29–68, 1982.

[85] J. L. Zakin and D. J. Hunston, "Mechanical degradation and drag reducing efficiency of dilute solutions of polystyrene," in *Proceedings of the 2nd International Conference on Drag Reduction*, H. S. Stephens and J. A. Clarke, Eds., Cambridge, UK, paper C5, 1977.

[86] P. S. Virk, "Drag reduction by collapsed and extended polyelectrolytes," *Nature*, vol. 253, no. 5487, pp. 109–110, 1975.

[87] W. E. Rochefort and S. Middleman, "Relationship between rheological behavior and drag reduction for dilute xanthan gum solutions," in *Drag Reduction Fluid Flows*, R. H. Sellin and R. T. Moses, Eds., p. 69, Ellis Horwood, Chichester, UK, 1989.

[88] C. A. Parker and A. H. Hedley, "Drag reduction and molecular structure," *Nature Physical Science*, vol. 236, p. 61, 1972.

[89] S. H. Banijamali, E. W. Merrill, K. A. Smith, and L. H. PeebIes, "Turbulent drag reduction by polyacrylic acid," *AIChE Journal*, vol. 20, pp. 824–826, 1974.

[90] J. H. Hand and M. C. Williams, "Effect of secondary polymer structure on the drag-reducing phenomenon," *Journal of Applied Polymer Science*, vol. 13, no. 11, pp. 2499–2503, 1969.

[91] A. G. Fabula, J. L. Lumley, and W. D. Taylor, "Some interpretations of the Toms effect," in *Proceedings of the*

Syracuse University Rheology Conference, Saranac Lake, NY, USA, August 1965.

[92] S. Ikeda, S. Ozeki, and M. A. Tsunoda, "Micelle molecular weight of dodecyldimethylammonium chloride in aqueous solutions, and the transition of micelle shape in concentrated NaCl solutions," *Journal of Colloid and Interface Science*, vol. 73, no. 1, pp. 27–37, 1980.

[93] N. A. Mazer, G. B. Benedek, and M. C. Carey, "An investigation of the micellar phase of sodium dodecyl sulfate in aqueous sodium chloride solutions using quasielastic light scattering spectroscopy," *The Journal of Physical Chemistry*, vol. 80, no. 10, pp. 1075–1085, 1976.

[94] H. Hoffmann, G. Platz, H. Rehage, and W. Schorr, "The influence of the salt concentration on the aggregation behavior of viscoelastic detergents," *Advances in Colloid and Interface Science*, vol. 17, no. 1, pp. 275–298, 1982.

[95] H. Hoffmann, G. Platz, H. Rehage, and W. Schorr, "The influence of counter-ion concentration on the aggregation behaviour of viscoelastic detergents," *Berichte der Bunsengesellschaft für Physikalische Chemie*, vol. 85, no. 10, pp. 877–882, 1981.

[96] H. W. Bewersdorff and D. Ohlendorf, "The behaviour of drag-reducing cationic surfactant solutions," *Colloid & Polymer Science*, vol. 266, no. 10, pp. 941–953, 1988.

[97] D. Ohlendorf, W. Interthal, and H. Hoffmann, "Drag reducing surfactant systems: concentration and temperature effects, flow characteristics," in *Proceedings of the 9th International Congress on Rheology*, B. Mena, A. Carcia-Rejon, and C. Rungel-Nafaile, Eds., vol. 2, p. 41, Independent University of Mexico, Acapulco, Mexico, 1984.

[98] D. Ohlendorf, W. Interthal, and H. Hoffmann, "Surfactant systems for drag reduction: physico-chemical properties and rheological behaviour," *Rheologica Acta*, vol. 25, no. 5, pp. 468–486, 1986.

[99] M. J. Rosen, *Surfactants and Interfacial Phenomena*, John Wiley & Sons, New York, NY, USA, 2nd edition, 1989.

[100] M. J. Rosen, *Surfactants and Interfacial Phenomena*, John Wiley & Sons, New York, NY, USA, 1978.

[101] H. B. Klevens, "Structure and aggregation in dilate solution of surface active agents," *Journal of the American Oil Chemists Society*, vol. 30, no. 2, pp. 74–80, 1953.

[102] D. Stigter, "Micelle formation by ionic surfactants. II. Specificity of head groups, micelle structure," *The Journal of Physical Chemistry*, vol. 78, no. 24, pp. 2480–2485, 1974.

[103] A. L. Underwood and E. W. Anacker, "Counterion lyotropy and micelle formation," *Journal of Colloid and Interface Science*, vol. 117, no. 1, pp. 242–250, 1987.

[104] A. L. Underwood and E. W. Anacker, "Organic counterions and micellar parameters: unusual effects of hydroxy and chlorobenzoates," *Journal of Colloid and Interface Science*, vol. 106, no. 1, pp. 86–93, 1985.

[105] A. L. Underwood and E. W. Anacker, "Organic counterions as probes of the micellar surface," *Journal of Colloid and Interface Science*, vol. 117, no. 1, pp. 296–298, 1987.

[106] S. Gravsholt, "Viscoelasticity in highly dilute aqueous solutions of pure cationic detergents," *Journal of Colloid and Interface Science*, vol. 57, no. 3, pp. 575–577, 1976.

[107] D. Ohlendorf, W. Interthal, and H. Hoffmann, "Drag reduction in aqueous solution of hexadecyltrimethylammonium-salicylate," in *Surfactants in Soultion*, K. L. Mittal and P. Bothorel, Eds., vol. 6, pp. 1589–1598, 1986.

[108] P. Debye and E. W. Anacker, "Micelle shape from dissymmetry measurements," *The Journal of Physical and Colloid Chemistry*, vol. 55, no. 5, pp. 644–655, 1951.

[109] P. J. Missel, N. A. Mazer, G. B. Benedek, C. Y. Young, and M. C. Carey, "Thermodynamic analysis of the growth of sodium dodecyl sulfate micelles," *The Journal of Physical Chemistry*, vol. 84, no. 9, pp. 1044–1057, 1980.

[110] P. J. Missel, N. A. Mazer, G. B. Benedek, and M. C. Carey, "Influence of chain length on the sphere-to-rod transition in alkyl sulfate micelles," *The Journal of Physical Chemistry*, vol. 87, no. 7, pp. 1264–1277, 1983.

[111] P. Ekwall, L. Mandell, and P. Solyom, "The aqueous cetyl trimethylammonium bromide solutions," *Journal of Colloid and Interface Science*, vol. 35, no. 4, pp. 519–528, 1971.

[112] K. G. Götz and K. Heckmann, "The shape of soap micelles and other polyions as obtained from anisotropy of electrical conductivity," *Journal of Colloid Science*, vol. 13, no. 3, pp. 266–272, 1958.

[113] D. F. Nicoli, R. Ciccolello, J. Briggs et al., "Micellar size as a function of pressure, temperature and salt concentration for a series of cationic surfactants," in *Scattering Techniques Applied to Supramolecular and Non-Equilibrium Systems*, S. H. Chen, B. Chu, and R. Nossal, Eds., p. 363, Plenum Press, New York, NY, USA, 1981.

[114] H. V. Tartar, "A theory of the structure of the micelles of normal paraffin chain salts in aqueous solution," *The Journal of Physical Chemistry*, vol. 59, no. 12, pp. 1195–1199, 1955.

[115] D. F. Nicoli, R. B. Dorshow, and C. A. Bunton, "The effect of intermicellar interactions on interpretations of micellar diffusivities by dynamic light scattering," in *Surfactants in Solution*, K. L. Mittal and B. Lindman, Eds., vol. 1, p. 455, Plenum Press, New York, NY, USA, 1984.

[116] D. F. Nicoli and R. B. Dorshow, "The role of intermicellar interactions in interpretations of micellar diffusion coefficients," in *Physics of Amphiphiles: Micelles, Vesicles, Microemulsions*, V. Degiorgio and M. Corti, Eds., p. 429, North Holland, Amsterdam, The Netherlands, 1985.

[117] J. Briggs, R. B. Dorshow, C. A. Bunton, and D. F. Nicoli, "Diffusion of interacting micelles: a general treatment at low salt concentrations," *The Journal of Chemical Physics*, vol. 76, no. 2, pp. 775–779, 1982.

[118] R. B. Dorshow, J. Briggs, C. A. Bunton, and D. F. Nicoli, "Dynamic light scattering from cetyltrimet hylammonium bromide micelles: intermicellar interactions at low ionic strengths," *The Journal of Physical Chemistry*, vol. 86, pp. 2388–2395, 1982.

[119] R. B. Dorshow, C. A. Bunton, and D. F. Nicoli, "Comparative study of intermicellar interactions using dynamic light scattering," *The Journal of Physical Chemistry*, vol. 87, no. 8, pp. 1409–1416, 1983.

[120] M. Corti and V. Degiorgio, "Investigation of micelle formation in aqueous solution by laser-light scattering," *Chemical Physics Letters*, vol. 53, no. 2, pp. 237–241, 1978.

[121] M. Corti and V. Degiorgio, "Quasi-elastic light scattering study of intermicellar interactions in aqueous sodium dodecyl sulfate solutions," *The Journal of Physical Chemistry*, vol. 85, no. 6, pp. 711–717, 1981.

[122] C. Y. Young, P. J. Missel, N. A. Mazer, G. B. Benedek, and M. C. Carey, "Deduction of micellar shape from angular dissymmetry measurements of light scattered from aqueous sodium dodecyl sulfate solutions at high sodium chloride concentrations," *The Journal of Physical Chemistry*, vol. 82, no. 12, pp. 1375–1378, 1978.

[123] E. J. Staples and G. J. T. Tiddy, "Nuclear magnetic resonance technique to distinguish between micelle size changes and secondary aggregation in anionic and nonionic surfactant

solutions," *Journal of the Chemical Society, Faraday Transactions I*, vol. 74, pp. 2530–2541, 1978.

[124] G. Porte, J. Appell, and Y. Poggi, "Experimental investigations on the flexibility of elongated cetylpyridinium bromide micelles," *The Journal of Physical Chemistry*, vol. 84, no. 23, pp. 3105–3110, 1980.

[125] J. N. Israelachvili, D. J. Mitchell, and B. W. Ninham, "Theory of self-assembly of hydrocarbon amphiphiles into micelles and bilayers," *Journal of the Chemical Society, Faraday Transactions II*, vol. 72, pp. 1525–1568, 1976.

[126] D. Myers, *Surfactant Science and Technology*, John Wiley & Sons, New York, NY, USA, 3rd edition, 2006.

[127] H. Wennerström and B. Lindman, "Micelles. Physical chemistry of surfactant association," *Physics Reports*, vol. 52, no. 1, pp. 1–86, 1979.

[128] G. Porte and J. Appell, "Growth and size distributions of cetylpyridinium bromide micelles in high ionic strength aqueous solutions," *The Journal of Physical Chemistry*, vol. 85, no. 17, pp. 2511–2519, 1981.

[129] R. D. Geer, E. H. Eylar, and E. W. Anacker, "Dependence of micelle aggregation number on polar head structure. I. Light scattering by aqueous solutions of decylammonium salts and related surfactants," *The Journal of Physical Chemistry*, vol. 75, no. 3, pp. 369–374, 1971.

[130] R. L. Venable and R. V. Nauman, "Micellar weights of and solubilization of benzene by a series of tetradecylammonium bromides. The effect of the size of the charged head," *The Journal of Physical Chemistry*, vol. 68, no. 12, pp. 3498–3503, 1964.

[131] H. Rehage and H. Hoffmann, "Viscoelastic surfactant solutions: model for rheological research," *Molecular Physics*, vol. 74, no. 5, pp. 933–973, 1991.

[132] H. Hoffmann, G. Platz, H. Rehage, W. Schorr, and W. Ulbricht, "Viskoelastische tensidlosungen," *Berichte der Bunsengesellschaft für Physikalische Chemie*, vol. 85, no. 4, pp. 255–266, 1981 (German).

[133] H. Hoffmann, H. Rehage, H. Thurn, and D. Ohlendorf, "Drag reducing surfactant systems: characterization of the systems," in *Proceedings of the 9th International Congress on Rheology*, B. Mena, A. Carcia-Rejon, and C. Rungel-Nafaile, Eds., vol. 2, p. 31, Independent University of Mexico, Acapulco, Mexico, 1984.

[134] H. Hoffmann, M. Lobl, and H. Rehage, "Flow birefringence and rheological measurements on viscoelastic detergent solutions," in *Physics of Amphiphiles: Micelles, Vesicles, Microemulsions*, V. Degiorgio and M. Corti, Eds., p. 237, North Holland, Amsterdam, The Netherlands, 1985.

[135] H. Rehage, I. Wunderlich, and H. Hoffmann, "Shear induced phase transitions in dilute aqueous surfactant solutions," *Progress in Colloid & Polymer Science*, vol. 72, pp. 51–59, 1986.

[136] P. Fischer, "Time dependent flow in equimolar micellar solutions: transient behaviour of the shear stress and first normal stress difference in shear induced structures coupled with flow instabilities," *Rheologica Acta*, vol. 39, no. 3, pp. 234–240, 2000.

[137] P. D. Butler, "Shear induced structures and transformations in complex fluids," *Current Opinion in Colloid & Interface Science*, vol. 4, no. 3, pp. 214–221, 1999.

[138] S. Hofmann and H. Hoffmann, "Shear-induced micellar structures in ternary surfactant mixtures: the influence of the structure of the micellar interface," *The Journal of Physical Chemistry B*, vol. 102, no. 29, pp. 5614–5624, 1998.

[139] V. Hartmann and R. Cressely, "Shear thickening of an aqueous micellar solution of cetyltrimethylammonium bromide and sodium tosylate," *Journal de Physique II*, vol. 7, no. 8, pp. 1087–1098, 1997.

[140] J. Myska and P. Stern, "Significance of sheer induced structure in surfactants for drag reduction," *Colloid and Polymer Science*, vol. 276, no. 9, pp. 816–823, 1998.

[141] S. Koch, "New aspects of shear induced phase transition in dilute cationic surfactant solutions," in *Proceedings of the 12th International Congress on Rheology*, pp. 229–230, Quebec City, Canada, August 1996.

[142] C.-H. Liu and D. J. Pine, "Shear-induced gelation and fracture in micellar solutions," *Physical Review Letters*, vol. 77, no. 10, pp. 2121–2124, 1996.

[143] H. W. Bewersdorff, "Rheology of drag reducing surfactant solutions," in *Proceedings of the ASME Fluids Engineering Division Summer Meeting (FEDSM '96)*, vol. 2, pp. 25–29, 1996.

[144] P. Boltenhagen, Y. Hu, E. F. Matthys, and D. J. Pine, "Inhomogeneous structure formation and shear-thickening in worm-like micellar solutions," *Europhysics Letters*, vol. 38, no. 5, pp. 389–394, 1997.

[145] Y. Hu and E. F. Matthys, "Rheological and rheo-optical characterization of shear-induced structure formation in a nonionic drag-reducing surfactant solution," *Journal of Rheology*, vol. 41, no. 1, pp. 151–165, 1997.

[146] W. J. Kim and S. M. Yang, "Effects of sodium salicylate on the microstructure of an aqueous micellar solution and its rheological responses," *Journal of Colloid and Interface Science*, vol. 232, no. 2, pp. 225–234, 2000.

[147] I. Wunderlich, H. Hoffmann, and H. Rehage, "Flow birefringence and rheological measurements on shear induced micellar structures," *Rheologica Acta*, vol. 26, no. 6, pp. 532–542, 1987.

[148] W. Richtering, G. Schmidt, and P. Lindner, "Small-angle neutron scattering from a hexagonal phase under shear," *Colloid and Polymer Science*, vol. 274, no. 1, pp. 85–88, 1996.

[149] E. Mendes, R. Oda, C. Manohar, and J. Narayanan, "A small-angle neutron scattering study of a shear-induced vesicle to micelle transition in surfactant mixtures," *The Journal of Physical Chemistry B*, vol. 102, no. 2, pp. 338–343, 1998.

[150] R. Linemann, J. Läuger, G. Schmidt, K. Kratzat, and W. Richtering, "Linear and nonlinear rheology of micellar solutions in the isotropic, cubic and hexagonal phase probed by rheo-small-angle light scattering," *Rheologica Acta*, vol. 34, no. 5, pp. 440–449, 1995.

[151] P. D. Butler, L. J. Magid, W. A. Hamilton, J. B. Hayter, B. Hammouda, and P. J. Kreke, "Kinetics of alignment and decay in a highly entangled transient threadlike micellar network studied by small-angle neutron scattering," *The Journal of Physical Chemistry*, vol. 100, no. 2, pp. 442–445, 1996.

[152] Y. Qi, *Investigation of relationships among microstructure, rheology, drag reduction and heat transfer of drag reducing surfactant solutions*, Ph.D. thesis, The Ohio State University, 2003.

[153] R. Cressely and V. Hartmann, "Rheological behaviour and shear thickening exhibited by aqueous CTAB micellar solutions," *The European Physical Journal B*, vol. 6, no. 1, pp. 57–62, 1998.

[154] S. Koch, "Formation of the shear-induced state in dilute cationic surfactant solutions," *Rheologica Acta*, vol. 36, no. 6, pp. 639–645, 1997.

[155] H. Rehage and H. Hoffmann, "Rheological properties of viscoelastic surfactant systems," *The Journal of Physical Chemistry*, vol. 92, no. 16, pp. 4712–4719, 1988.

[156] Y. T. Hu, P. Boltenhagen, and D. J. Pine, "Shear thickening in low-concentration solutions of wormlike micelles. I. Direct visualization of transient behavior and phase transitions," *Journal of Rheology*, vol. 42, no. 5, pp. 1185–1208, 1998.

[157] Y. T. Hu, P. Boltenhagen, E. Matthys, and D. J. Pine, "Shear thickening in low-concentration solutions of wormlike micelles. II. Slip, fracture, and stability t of the shear-induced phase," *Journal of Rheology*, vol. 42, no. 5, pp. 1209–1226, 1998.

[158] R. Oda, P. Panizza, M. Schmutz, and F. Lequeux, "Direct evidence of the shear-induced structure of wormlike micelles: gemini surfactant 12-2-12," *Langmuir*, vol. 13, no. 24, pp. 6407–6412, 1997.

[159] R. C. Chang and J. L. Zakin, "Drag reduction of non-ionic surfactant mixtures," in *Proceedings of the IUTAM Symposium on Influence of Polymer Additives on Velocity and Temperature Fields, Essen*, B. Gampert, Ed., pp. 61–70, Springer, Berlin, Germany, 1985.

[160] P. Deroussel, *Nonionic surfactant drag reduction*, B. S. Honors Thesis, The Ohio State University, Columbus, Ohio, USA, 1993.

[161] M. Hellsten and I. Harwigsson, "A new biodegradable friction reducing additive (FRA) for district cooling networks," in *Proceedings of the 85th International District Heating and Cooling Association (IDHCA '94)*, pp. 281–299, Seattle, Wash, USA, 1994.

[162] I. Radin, J. L. Zakin, and G. K. Patterson, "Exploratory drag reduction studies in non-polar soap systems," in *Viscous Drag Reduction*, C. S. Wells, Ed., p. 213, Plenum Press, New York, NY, USA, 1969.

[163] M. L. McMillan, H. C. Hershey, and R. A. Baxter, "Effects of aging, concentration, temperature, method of preparation, and other variables on the drag reduction of aluminum disoaps in toluene," *Chemical Engineering Progress Symposium Series*, vol. 67, no. 111, pp. 27–44, 1971.

[164] J. G. Savins, "Contrasts in the solution drag reduction characteristics of polymeric solutions and micellar systems," in *Viscous Drag Reduction*, C. S. Wells, Ed., p. 183, Plenum Press, New York, NY, USA, 1969.

[165] A. White, "Flow characteristics of complex soap systems," *Nature*, vol. 214, no. 5088, pp. 585–586, 1967.

[166] L. C. Chou, R. N. Christensen, and J. L. Zakin, "The use of cationic surfactant additives to reduce transmission pumping costs in district heating systems," in *Proceedings of the 78th International District Heating and Cooling Association (IDHCA '87)*, pp. 284–299, Baltimore, Md, USA, 1987.

[167] L. C. Chou, R. N. Christensen, and J. L. Zakin, "Effectiveness of drag reducing surfactant additives in district heating systems," in *Proceedings of the 79th International District Heating and Cooling Association (IDHCA '88)*, pp. 530–548, Chautauqua, NY, USA, 1988.

[168] G. D. Rose and K. L. Foster, "Drag reduction and rheological properties of cationic viscoelastic surfactant formulations," *Journal of Non-Newtonian Fluid Mechanics*, vol. 31, no. 1, pp. 59–85, 1989.

[169] L. C. Chou, R. N. Christensen, and J. L. Zakin, "The influence of chemical composition of quaternary ammonium salt cationic surfactants on their drag reducing effectiveness," in *Drag Reduction in Fluid Flows*, R. H. J. Sellin and R. T. Moses, Eds., pp. 141–148, Ellis Horwood, Chichester, UK, 1989.

[170] G. D. Rose, K. L. Foster, V. L. Slocum, and J. G. Lenhart, "Drag reduction and heat transfer characteristics of viscoelastic surfactant formulations," in *Proceedings of the 3rd International Congress on Drag Reduction*, R. H. J. Sellin and R. T. Moses, Eds., pp. 6–7, paper D, University of Bristol, Bristol, UK, 1984.

[171] L. C. Chou, R. N. Christensen, and J. L. Zakin, "Drag reducing additives for district cooling systems," in *Proceedings of the 80th International District Heating and Cooling Association (IDHCA '89)*, pp. 352–367, Virginia Beach, Va, USA, 1989.

[172] W. Ge, *Studies on the nanostructure, rheology and drag reduction characteristics of drag reducing cationic surfactant solutions*, Ph.D. thesis, The Ohio State University, 2008.

[173] T. P. Elson and J. Garside, "Drag reduction in aqueous cationic soap solutions," *Journal of Non-Newtonian Fluid Mechanics*, vol. 12, no. 2, pp. 121–133, 1983.

[174] L. C. Chou, *Drag Reducing Cationic Surfactant Solutions for District Heating and Cooling Systems*, Ph.D. thesis, The Ohio State University, Columbus, Ohio, USA, 1991.

[175] B. C. Smith, L. C. Chou, and J. L. Zakin, "Measurement of the orientational binding of counterions by nuclear magnetic resonance measurements to predict drag reduction in cationic surfactant micelle solutions," *Journal of Rheology*, vol. 38, no. 1, pp. 73–83, 1994.

[176] W. Ge, H. F. Shi, Y. Talmon, D. J. Hart, and J. L. Zakin, "Synergistic effects of mixed aromatic counterions on nanostructures and drag reducing effectiveness of aqueous cationic surfactant solutions," *The Journal of Physical Chemistry B*, vol. 115, no. 19, pp. 5939–5946, 2011.

[177] S. Hofmann, P. Stern, and J. Myska, "Rheological behavior and birefringence investigations on drag-reducing surfactant solutions of tallow-(tris-hydroxyethyl)-ammonium acetate/sodiumsalicylate mixtures," *Rheologica Acta*, vol. 33, no. 5, pp. 419–430, 1994.

[178] M. Hellsten and I. Harwigsson, "Use of a betaine surfactant together with an anionic surfactant as a drag-reducing agent," WO patent application, 96-EP950, 9628527, 1996.

[179] Y. Zhang, J. Schmidt, Y. Talmon, and J. L. Zakin, "Co-solvent effects on drag reduction, rheological properties and micelle microstructures of cationic surfactants," *Journal of Colloid and Interface Science*, vol. 286, no. 2, pp. 696–709, 2005.

[180] K. Gasljevic, E. F. Matthys, and G. Aguilar, "On two distinct types of drag-reducing fluids, diameter scaling, and turbulent profiles," *Journal of Non-Newtonian Fluid Mechanics*, vol. 96, no. 3, pp. 405–425, 2001.

[181] Y. Qi, Y. Kawaguchi, Z. Lin, M. Ewing, R. N. Christensen, and J. L. Zakin, "Enhanced heat transfer of drag reducing surfactant solutions with fluted tube-in-tube heat exchanger," *International Journal of Heat and Mass Transfer*, vol. 44, no. 8, pp. 1495–1505, 2001.

[182] H. Usui, H. Suzuki, T. Okunishi, H. Sugawara, and M. Yamaguchi, "Optimization of molecular structure of cationic surfactants to prevent the heat transfer reduction in a drag-reducing system," in *Proceedings of the 13th International Congress on Rheology*, vol. 2, pp. 294–296, Cambridge, UK, 2000.

[183] G. Aguilar, K. Gasljevic, and E. F. Matthys, "Coupling between heat and momentum transfer mechanisms for drag-reducing polymer and surfactant solutions," *Journal of Heat Transfer*, vol. 121, no. 4, pp. 796–802, 1999.

[184] P. W. Li, H. Daisaka, Y. Kawaguchi, A. Yabe, K. Hishida, and M. Maeda, "Turbulence structure of drag-reducing surfactant solution in two-dimensional channel with additional

heat transfer enhancement method," in *Proceedings of the 5th ASME/JSME Joint Thermal Engineering Conference*, San Diego, Calif, USA, March 1999.

[185] J. W. Hoyt, "Drag reduction by polymers and surfactants," in *Viscous Drag Reduction in Boundary Layers*, vol. 123 of *Progress in Astronautics and Aeronautics*, pp. 413–432, 1990.

[186] M. Kostic, "On turbulent drag and heat transfer reduction phenomena and laminar heat transfer enhancement in non-circular duct flow of certain non-Newtonian fluids," *International Journal of Heat and Mass Transfer*, vol. 37, no. 1, pp. 133–147, 1994.

[187] K. Gasljevic, X. Nan, and E. F. Matthys, "Effect of drag-reducing surfactant additives on heat exchangers," in *Developments in Non-Newtonian Flows*, D. A. Siginer, W. W. Van Arsdale, M. C. Altan, and A. N. Alexandrou, Eds., vol. ASME-AMD-175, pp. 101–108, ASME, 1993.

[188] R. N. Christensen and J. L. Zakin, "Drag and heat transfer reduction in circular tubes and plate fin heat exchangers," in *Proceedings of the International District Heating and Cooling Association (IDHCA '91)*, vol. 81, pp. 189–202, 1991.

[189] Y. Dimant and M. Poreh, "Heat transfer in flows with drag reduction," *Advances in Heat Transfer*, vol. 12, pp. 77–113, 1976.

[190] I. Gampert and A. Rensch, "Polymer concentration and near wall turbulence structure of chemical flow of polymer solutions," *Turbulence Modification and Drag Reduction*, vol. 237, no. 2, pp. 129–136, 1996.

[191] Z. Chara, J. L. Zakin, M. Severa, and J. Myska, "Turbulence measurements of drag reducing surfactant systems," *Experiments in Fluids*, vol. 16, no. 1, pp. 36–41, 1993.

[192] Y. Kawaguchi, Y. Tawaraya, A. Yabe, K. Hishida, and M. Maeda, "Active control of turbulent drag reduction in surfactant solutions by wall heating," in *Proceedings of the ASME Fluids Engineering Division Summer Meeting*, vol. 2, pp. 47–52, 1996.

[193] J. Myska, J. L. Zakin, and Z. Chara, "Viscoelasticity of a surfactant and its drag-reducing ability," *Applied Scientific Research*, vol. 55, no. 4, pp. 297–310, 1996.

[194] G. Schmidt, *Surfactant induced drag reduction in a channel flow facility*, B.S. thesis, University of Illinois at Urbana-Champaign, Urbana, Ill, USA, 1997.

[195] M. D. Warholic, H. Massah, and T. J. Hanratty, "Influence of drag-reducing polymers on turbulence: effects of Reynolds number, concentration and mixing," *Experiments in Fluids*, vol. 27, no. 5, pp. 461–472, 1999.

[196] A. Kishimoto, H. Usui, and H. Suzuki, "Influences of the inner-surface conditions of circular tubes on the heat transfer in a surfactant drag-reducing system," in *Proceedings of the AIChE Annual Meeting*, Dallas, Tex, USA, November 1999.

[197] K. Sato, J. Mimatsu, and M. Kumada, "Drag reduction and heat transfer augmentation of surfactant additives in two-dimensional channel flow," in *Proceedings of the 5th ASME/JSME Joint Thermal Engineering Conference*, San Diego, Calif, USA, March 1999.

[198] J. Wollerstrand and S. Frederiksen, "Enhancement of heat transfer in tubes of heat exchangers with friction reducing additive fluids-district heating steam condenser applications," in *Proceedings of the 12th European Drag Reduction Meeting*, Herning, Denmark, April 2002.

[199] Y. Qi, *Investigation of relationships among microstructure, rheology, drag reduction and heat transfer of drag reducing surfactant solutions*, Ph.D. thesis, The Ohio State University, 2003.

[200] Y. Qi, Y. Kawaguchi, R. N. Christensen, and J. L. Zakin, "Enhancing heat transfer ability of drag reducing surfactant solutions with static mixers and honeycombs," *International Journal of Heat and Mass Transfer*, vol. 46, no. 26, pp. 5161–5173, 2003.

[201] C. Blais, I. Harwigsson, M. Hellsten, and J. Wollerstrand, "Drag reduction in district heating and cooling circuits-temporary disruption of micelles to preserve the heat exchanger capacity," in *Proceedings of the 4th World Surfactants Congress*, vol. 2, pp. 424–438, 1996.

[202] H. Inaba and K. Ozaki, "Heat transfer enhancement and flow-drag reduction of forced convection in circular tubes by means of wire coil insert," in *Proceedings of the International Conference on Compact Heat Exchangers*, pp. 445–452, 1997.

[203] K. Gasljevic and E. F. Matthys, "Experimental investigation of thermal and hydrodynamic development regions for drag-reducing surfactant solutions," *Journal of Heat Transfer*, vol. 119, no. 1, pp. 80–88, 1997.

[204] P. W. Li, Y. Kawaguchi, H. Daisaka, A. Yabe, K. Hishida, and M. Maeda, "Heat transfer enhancement to the drag-reducing flow of surfactant solution in two-dimensional channel with mesh-screen inserts at the inlet," *Journal of Heat Transfer*, vol. 123, no. 4, pp. 779–789, 2001.

[205] J. Pollert, P. Komrzy, K. Svejkovsky, J. Pollert Jr., B. Lu, and J. L. Zakin, "Drag reduction and heat transfer of cationic surfactant solutions," in *Proceedings of the ASME Fluids Engineering Division Summer Meeting*, vol. 237, no. 2, pp. 31–36, 1996.

[206] A. Kishimoto, T. Okunishi, H. Suzuki, and H. Usui, "Heat transfer augmentation in a surfactant solution flow with an insertion of a micelle squeezer," in *Proceedings of the 4th JSME-KSME Thermal Engineering Conference*, Kobe, Japan, October 2000.

[207] A. M. Ketner, R. Kumar, T. S. Davies, P. W. Elder, and S. R. Raghavan, "A simple class of photorheological fluids: surfactant solutions with viscosity tunable by light," *Journal of the American Chemical Society*, vol. 129, no. 6, pp. 1553–1559, 2007.

[208] R. Kumar and S. R. Raghavan, "Photogelling fluids based on light-activated growth of zwitterionic wormlike micelles," *Soft Matter*, vol. 5, no. 4, pp. 797–803, 2009.

[209] S. R. Raghavan, A. M. Ketner, and R. Kumar, "Photorheological fluids made easy: light-sensitive wormlike micelles based on common, inexpensive surfactants," in *Proceedings of the 15th International Congress on Rheology*, Monterrey, Calif, USA, 2008.

[210] H. Shi, Y. Wang, B. Fang et al., "Light-responsive threadlike micelles as drag reducing fluids with enhanced heat-transfer capabilities," *Langmuir*, vol. 27, no. 10, pp. 5806–5813, 2011.

Hindawi Publishing Corporation
Advances in Mechanical Engineering
Volume 2011, Article ID 743975, 10 pages
doi:10.1155/2011/743975

Review Article

The Combination of Polymer, Compliant Wall, and Microbubble Drag Reduction Schemes

Boris N. Semenov

Institute of Thermophysics, Siberian Branch of Russian Academy of Sciences, Prospekt Ac. Lavrentyev, 1, Novosibirsk 630090, Russia

Correspondence should be addressed to Boris N. Semenov, boris_n_semenov@mail.ru

Received 9 March 2011; Accepted 30 April 2011

Academic Editor: Jinjia Wei

The promising study of turbulence management by joint use of compliant coatings with other drag reduction means is proposed. Its outlooks are conditioned by different considered factors and confirmed by the first experimental and theoretical results.

1. Introduction

The combined use of different means is one of the main principles of nature development. The study of hydrodynamic problems of bionics (Aleyev [1], Bushnell and Moore [2]) also convinces us of the correctness of this statement. Bionics is the way from observations and astonishment at making the first estimations (the conclusion about the paradox existence) to the explanation for the phenomenon.

The characteristic "nature" example of the study of bodies with low drag is the investigation of dolphins, the search of reasons of well-known paradox of Gray [3]. These investigations showed that in consequence of long evolution dolphins possess different variants of adaptation to different, rapidly changing conditions of their inhabitation in sea (Woodcock [4], Focke [5], Semenov [6], Alekseeva and Semenov [7], Wu and Chwang [8]). Here, excellent variants of economical swimming of dolphins were discovered and described. For example, Woodcock [4] described the "motionless" swimming of dolphins near the ship nosing. Focke [5] investigated this fact. He showed by calculations that dolphins (using pressure distribution near the ship nosing) can swim with any ship velocity and without essential energy losses (as "external passengers of ship-travellers without tickets"). The other example: Wu and Chwang [8] show by theoretical calculations that dolphins can obtain an energy for their swimming from a wavy stream. So, they can swim in sea waves with minimum energy losses (quoted work permits to explain the physical essence of surf boards too). Above-mentioned results requested to introduce new, additional conditions for selection of dolphin speed observations (used for analysis of Gray's paradox). But note: they cannot explain Gray's paradox for observations of high-speed swimming of dolphins under conditions of the absolute calm, far from ships. And here, the other conclusion is important. As the result of long evolution, dolphins enjoyed different variants of adaption to very different and often changed residing conditions in sea. So, our aim is to search and study many dolphins "secrets". Here, the analysis of the dolphin body shape (Young [9], Hertel [10]) was the important step to explain the observed low drag. The other important step was made by Kramer [11–13], who simulated the dolphin skin compliance in delaying the transition to turbulence. Semenov [14] gave the additional explanation for low drag (of dolphin *Tursiops Tursio Ponticus*) taking into account also the possibilities of joint use of compliant dolphin skin, water-soluble secretions decreasing drag, and gas microbubbles observed in experiments.

Technical progress is connected with this main principle of nature development (the combined use of different means) too. There are a lot of possible variants of the combined use of different (and numerous) methods of drag reduction for different hydrodynamic conditions. Two passive means (compliant coatings and riblets) and two active means (polymeric additives and gas microbubbles) are considered here in order to estimate outlooks for their joint action investigations.

2. Some Notes on Investigation Outlooks

These notes can be interesting to both research of near-wall turbulence and representatives of industry who use scientific successes. So, first of all, it is important to note that all considered methods of turbulence management (compliant coatings, riblets, air microbubbles, and PEO additives) satisfy the ecology requirements.

Motivations of fine outlooks on joint use of the considered methods of drag reduction can be divided into four groups.

2.1. Initial Approach. The initial approach to joint use of different drag reducing means took into account only the simplified dependence of possible drag reduction efficiency Ψ for their joint action on their individual efficiencies Ψ_i

$$\Psi = 1 - (1 - \Psi_1)(1 - \Psi_2) \cdots (1 - \Psi_n). \tag{1}$$

This expression is correct if all considered drag reducing means act independently and do not change the action conditions for the others (here and further, drag reduction efficiency is considered concerning turbulent friction coefficient c_{f0} for smooth hard surface: $\Psi = 1 - c_f/c_{f0}$).

In this case, the possible drag reduction efficiency for joint action of different drag reducing means must be less than the sum of their individual drag reducing possibilities

$$\Psi < \sum_{i=0}^{n} \Psi_i \quad \text{for } \Psi_i > 0. \tag{2}$$

The prognosticated negative deviation from the sum of individual efficiencies $\operatorname{dev}\Psi \equiv \Psi - \sum_{i=0}^{n} \Psi_i$ depends on their values and number n of means used jointly for turbulence management.

These dependences can be analysed at ease for the variant of equal individual efficiencies: $\Psi_1 = \Psi_2 = \cdots = \Psi_n$. So, the deviation from the sum of individual efficiencies is calculated as

$$\operatorname{dev}\Psi = 1 - \sum_{i=0}^{n} \Psi_i - \left(1 - \frac{\sum_{i=0}^{n} \Psi_i}{n}\right)^n. \tag{3}$$

This deviation increases for increasing n.

And for $n \gg 1$, it has the limit

$$\lim(\operatorname{dev}\Psi) = 1 - \sum_{i=0}^{n} \Psi_i - \exp\left(\sum_{i=0}^{n} \Psi_i\right). \tag{4}$$

Results of this prognosis are shown in Figure 1. The prognosticated negative deviations are small when the sum of individual efficiencies is less than 20%. But they are very considerable for 80% sum: for example, $\operatorname{dev}\Psi = -0.16$ for two combined drag reducing means and $\operatorname{dev}\Psi = -0.25$ for $n \gg 1$.

This approach was used for our initial estimations. Viscoelastic coatings, riblets, gas bubbles, and polymer additives are four well-known means for the action on near-wall turbulence. Their actions for the decrease of the turbulence production are very different.

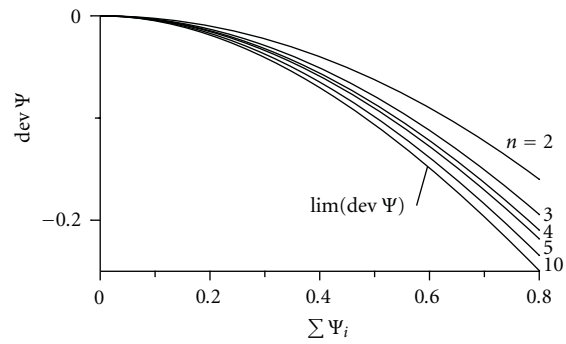

Figure 1: The deviation of drag reduction for joint use of different drag reducing means from the sum of their individual efficiency values: prognosis according to (3) and (4).

Compliant surface reacts on long-wave disturbances. According to the estimation of the interference theory of Semenov [15] and experimental data of Kulik et al. [16] the real viscoelastic coating is deformed by the pressure wave with length more than one thousand viscous scales. Viscous scale is ν/v_d, where friction velocity is $v_d = (\tau_w/\rho)^{0.5}$, ρ and ν are density and viscosity of flow, and τ_w is friction stress on a wall (Hinze [17]). Small additives in a flow put out the microeddy turbulence for the turbulence linear scales less than one hundred viscous scales (Greshilov et al. [18]). Riblets manage microeddy structures too (Choi [19]). The flowing screen of gas bubbles can destroy long-wave powerful fluctuations going to the wall from the turbulent core and background flow (Bogdevich et al. [20]).

It is known (Hinze [17], Cantwell [21]) that in the main both microeddies of viscous sublayer and long waves of turbulent core generate a new turbulence. So, the joint use of considered methods of drag reduction gives possibility to wait for new qualities of turbulence production decrease. Therefore, the combined use of these four methods permits to obtain the best results in turbulent drag reduction as compared with above described prognosis.

2.2. Association of Useful Qualities. A study of joint use of different methods of drag reduction is promising because of a number of other reasons too. It is attractive as a possible origin of other useful properties (in addition to drag reduction possibility) which are inherent in separate methods.

For example, drag reducing compliant coatings can have high anticorrosion properties. One-layer coatings created in Institute of Thermophysics of Russian Academy of Sciences (Kulik et al. [22]) have the excellent immunity to a damage by acids and alkalis.

Another example: tests carried out by Russian and Bulgarian scientists (Malyuga et al. [23]) show that creation of an air-bubble layer in a near-wall region is a sufficiently effective method for reducing the amplitudes of the propelled-induced pressures and the plate vibrations for ships.

And thirdly, for joint use of compliant coatings, air microbubbles, and polymeric additives, it is possible to

suppress turbulent wall-pressure fluctuations in the very wide frequency band that is impossible for any method used separately. So, it is possible to believe that these combinations will lead to the strong decrease of the hydrodynamic noise in the very wide frequency band too.

2.3. Here, It Is Important to Take into Account the Economic Factor. The turbulence management by compliant coatings and riblets is particularly useful due to their passive nature. As a result, additional energy is not required for the turbulence control. The injection of gas microbubbles and polymer additives is connected with consumption of some energy and materials. Although drag reduction by the high-molecular polymer additive use is realized for its very small concentration in a flow, expenses for its use may be higher than the economy (for example) of expenses for fuel. Therefore, Berman [24] suggested to estimate the specific efficiency Ψ_P/c_P, determining the expediency of drag reduction. He showed for a flow in a pipe that Ψ_P/c_P decreased as the concentration c_P increased (for a flow with constant concentration of polymer additives) and was significantly less at the friction minimization than the specific efficiency at moderate values of drag reduction Ψ_P. It is connected with nonlinear form of dependence of Ψ_P on c_P and asymptotic achievement of maximum value of drag reduction. Semenov [25, 26] carried out analogous analysis for a flow with variable concentration of polymer additives in a flow (for turbulent boundary layer on a plate) and showed that from the point of view of profit, it is worthwhile not to tend to the drag minimization but to restrict drag reduction nearly twice ($\Psi_P < 50\%$). So, the combined investigations must be carried out for variants of small consumptions of PEO too. And only the joint use of the considered methods can permit to achieve maximum and profitable efficiency of drag reduction.

The similar situation is realized for drag reduction using gas bubbles. However, in this case, it is possible even to achieve drag reduction "free of charge" by the use of engine exhaust.

2.4. "Mutual Aid" of Different Drag Reducing Means. And after all, here, it is necessary to enumerate to some other factors of an interaction between jointly used methods of turbulence management. They are subject to a study as proposed factors of "a mutual aid" promoting to an appearance of new qualities.

The flowing screen of gas bubbles destroys powerful fluctuations going to a wall from the turbulent core and background flow. So, the bubble screen defends polymer additives acting with high efficiency just in a near-wall region. It decreases their ousting from this region.

The drag reducing polymers (polyethylene oxide, polyacril amide, etc.) are surface-active substances which decrease the surface tension and so the separation diameter of a bubble at its generation on the porous injecting insert. Besides, polymer additives in flow prevent the bubble coalescence and also impede bubble rising. Note that it is very important for drag reduction to have microbubbles with diameter less than 0.2 mm. The decrease of microbubble diameter leads to an improvement of screening properties of a bubble layer, to a displacement of the peak concentration of gas bubbles in a water flow to a wall, and to a decrease of the bubble buoyancy velocity. Hence, one can expect that the flow of high-polymer solutions aerated by gas bubbles will result in mutual increase of effects of drag reduction on a streamlined surface (Malyuga et al. [27, 28]).

Waves and eddies are responsible for the near-wall turbulence production near a smooth surface. The wave action role is decreased as a result of the surface roughness increase. Compliant coatings respond to the pressure fluctuation waves. So, the viscoelastic boundary action losses a physical sense as a result of high roughness of a surface (Semenov and Semenova [29, 30]). The increase of the viscous sublayer thickness by polymer additives increases the permissible roughness of a compliant surface that simplifies and cheapens the coatings preparation technology.

Semenov and Semenova [29–31] have carried out the first calculations for joint action of compliant boundary and polymer additives in the turbulent boundary layer in order to explain the obtained experimental results (Semenov et al. [32, 33] and Kulik et al. [34, 35]). One of possible factors of an interaction between two considered methods of turbulence management is the action of compliant boundary on mass transfer in a near-wall region. Carried-out calculations show that the decrease (increase) of mass transfer, achieved by the use of a viscoelastic coating, decreases (increases) the polymer consumption a little. The other factor is the influence of polymer additives in a flow on the interference action of viscoelastic boundary on near-wall turbulence. The calculations show that injected polymer additives extend the phase-frequency region of positive action of compliant boundary; that is, they extend possibilities of drag (and noise) reduction by compliant coatings. These two problems are described in Section 4 in details.

Semenov and Semenova [29, 30] considered the action of drag reducing riblets for joint use with compliant coating and concluded that it extends the phase-frequency region of positive action of compliant boundary too.

The viscoelastic coating for drag reduction is the mechanical vibrational system with amplitude-phase-frequency characteristic chosen for action on the near-wall turbulence spectrum band responsible for the main production of new turbulence. And, of course, this choice must take into account the existence of natural turbulence background conditions. However, both for different usual experimental hydrodynamic installations and for practical objects (ships and pipe-lines) the existence of additional strong pressure fluctuations in a flow is quite possible. These additional pressure fluctuations can swing the compliant coating in the frequency region of its negative action very essentially. So, the total production of new turbulence (for all frequency regions) can be even increased. The important factor of the gas bubble layer action is the defence of a near-wall region of the turbulent boundary layer. So, the injection of gas bubbles into a near-wall flow will ensure the stable drag reduction action of viscoelastic coating for different exploitation conditions.

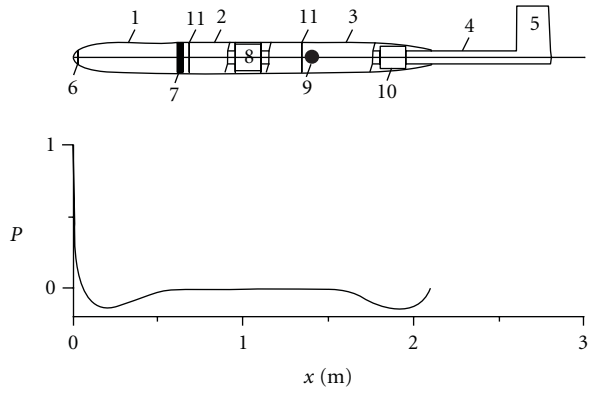

Figure 2: Scheme of the model with the dimensionless hydrodynamic pressure distribution. 1 nosing, 2 floating cylindrical element, 3 stern part, 4 thrust tube, 5 knife strut, 6 ringed slot, 7 porous insert, 8 floating-drag balance, 9 piezoresistive pressure transducer, 10 three-component balance, and 11 ringed slit.

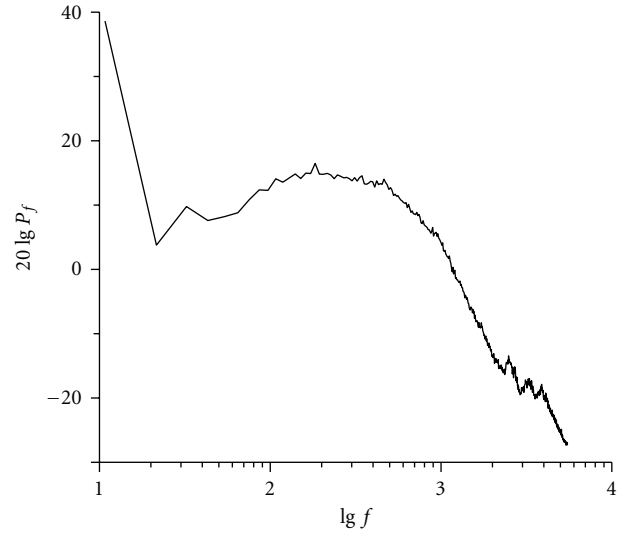

Figure 3: The dimensionless spectra of wall-pressure fluctuations measured behind floating element with hard surface. $U_0 = 9$ m/s.

Further, the following indexes are used for meaning: compliant surface—C, polymer additives—P, air microbubbles—A, riblets—r, and joint use—their combinations.

3. Experimental Investigations

The quantity of experimental investigations is small still. Only some variants of joint use of different drag reducing means were considered.

Already the first experiments (carried out at the Institute of Thermophysics RAS) for joint use of compliant coatings and polymer additives (Semenov et al. [32, 33]) showed fine outlooks of this study. There was obtained that the total effectiveness of turbulent drag reduction is equal to the algebraic sum of individual small efficiencies of these methods of turbulence management. These successes initiated new investigations.

3.1. Experimental Conditions. The experiments were carried out in the saline lake Issyk-Kool, where 2.1 m—long, 0.175 m—diameter streamline body of revolution was towed by the tow boat with speed $U_0 = 6$–15 m/s.

This model (see Figure 2) was described in details formerly by Kulik et al. [16, 36]. It was equipped (in the middle of its length) with 0.66 m—long "floating" surface element for measuring the skin-friction drag. There were tested different variants of these cylindrical elements. One had a solid smooth surface, and the others were mounted with compliant coatings. Careful measurement of friction coefficient for the case of hard polished surface in water flow c_{f_0} was used for comparison as a standard.

The model nosing had a ring slot for polymeric solution injection. The model was equipped with the 35-mm long insert made from porous metal for air injection. Sizes of injected microbubbles varied from 0.07 mm to 0.2 mm.

All experiments were carried out for low background turbulence conditions. The spectrum analysis of measured wall-pressure fluctuations (see the example in Figure 3) in frequency band from 10 Hz to 10 kHz revealed strong peaked deviation from smooth distribution in frequency only for low frequencies (below 20 Hz), that is inessential for these investigations.

All experimental conditions were described in details by Semenov et al. [37].

3.2. Joint Action of Compliant Coatings and Polymer Additives. New results of these investigations were described by Kulik et al. [34, 35] and Semenov et al. [37]. There the mass consumption q of polyethylene oxide (PEO of different molecular mass M) was varied. The corresponding dimensionless parameter is $q_\delta = q/(\rho_P \pi D \delta U_0)$, where D is diameter of the measured "floating" element, ρ_P: density of PEO, δ: thickness of turbulent boundary layer calculated for water flow (with temperature T) without polymer additives for the middle abscissa of the "floating" element (with solid smooth surface). According to Kutateladze and Leontyev [38], the thicknesses of diffusion and dynamic turbulent layers near this "floating" element are approximately equal. So, q_δ is like to the near-wall concentration of PEO for the middle abscissa of the "floating" element.

The first experimental results of Semenov et al. [32, 33] showed that $\Psi_{CP}(q_\delta)$ is shifted concerning $\Psi_P(q_\delta)$ so as $\Psi_{CP}(q_\delta) \approx \Psi_C + \Psi_P(q_\delta)$; that is, the summarizing property was discovered for the joint of compliant coating and polymer additives that confirmed our initial prognosis for small individual effectivenesses. However, contrary to initial estimations, it was noted that for the case of the increase of separate effects the magnitude of combined drag reduction exceeded their sum. So, further, it is considered the deviation of the drag reduction efficiency for joint action from the sum of the drag reduction efficiencies for separate actions in order to investigate this summarizing property.

Shown in Figure 4 are data (from Semenov et al. [37]) for the joint use of different compliant coatings (both decreasing and increasing the turbulent friction) and polymer additives

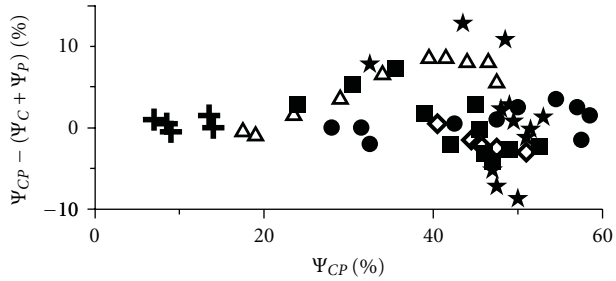

Figure 4: Deviation of friction reduction for joint use of compliant coating and polymer additives from the sum of their individual efficiencies as a function of efficiency of joint action. For U_0 = 9 m/s: Δ: coating N6 (from compound N1, H = 2 mm), $T = 16 \cdots 17^\circ$C $\Psi_C = -11.5\%$, M(PEO) = 3.5 mln., $2.1 \cdot 10^{-6} \le q_\delta \le 1.2 \cdot 10^{-5}$; +: coating A, $T = 8.5 \cdots 10.5^\circ$C, $\Psi_C = +2.6\%$, M(PEO)= 4.5 mln., $6.0 \cdot 10^{-8} \le q_\delta \le 5 \cdot 10^{-7}$; •: coating N10 (from compound N2, H = 7 mm), $T = 17^\circ$C, $\Psi_C = +6\%$, M(PEO) = 3.5 mln, $1.6 \cdot 10^{-6} \le q_\delta \le 1 \cdot 10^{-5}$; ◊: coating N10, $T = 10.5^\circ$C, $\Psi_C = +12\%$, M(PEO) = 3.5 mln., $3.5 \cdot 10^{-6} \le q_\delta \le 5.5 \cdot 10^{-6}$; For U_0 = 7 m/s: $T = 6.5 \cdots 8.5^\circ$C, M(PEO) = 4.7 mln, ■: coating N10, $\Psi_C = +5\%$, $4 \cdot 10^{-7} \le q_\delta \le 3.5 \cdot 10^{-6}$; ⋆: coating N7 (from compound N2, H = 2.5 mm), $\Psi_C = +9\%$, $4 \cdot 10^{-7} \le q_\delta \le 3.5 \cdot 10^{-6}$.

(for the great variation of polymer consumption and, accordingly, Ψ_P). These results witness the existence of three zones:

(1) the zone of the exact sum of individual efficiencies ($\Psi_{CP}(q_\delta) \approx \Psi_C + \Psi_P(q_\delta)$);

(2) the zone of positive deviation ($\Psi_{CP}(q_\delta) > \Psi_C + \Psi_P(q_\delta)$);

(3) the zone of negative deviation ($\Psi_{CP}(q_\delta) < \Psi_C + \Psi_P(q_\delta)$).

Here, the zone of the exact sum is observed for all tested variants till $\Psi_{CP} < 20\%$. Zones of positive and negative deviations follow the zone of the exact sum when polymer consumption increases. But here, we see considerable differences for different tested variants.

Experimental results from Figure 4 are shown in Figure 5 again for their comparison with initial prognosis. Here, these results are considered in dependence on drag reduction of hard surface by polymer additives, that is, on individual efficiency of polymer additives Ψ_P.

According to (1), $\Psi_{CP} = 1 - (1 - \Psi_C)(1 - \Psi_P)$. The prognosticated deviation must be

$$\text{dev}\,\Psi \equiv \Psi_{CP} - (\Psi_C + \Psi_P) = -\Psi_C \Psi_P. \tag{5}$$

So, in this case, the deviation must be negative for a "positive coating" ($\Psi_C > 0$) and positive for a "negative coating" ($\Psi_C < 0$).

The deviations prognosticated according to (5) (shown in Figure 5 by lines) are contrary to experimental data for the second and third zones. Thus, these results show the presence of an interaction of compliant coating and polymeric

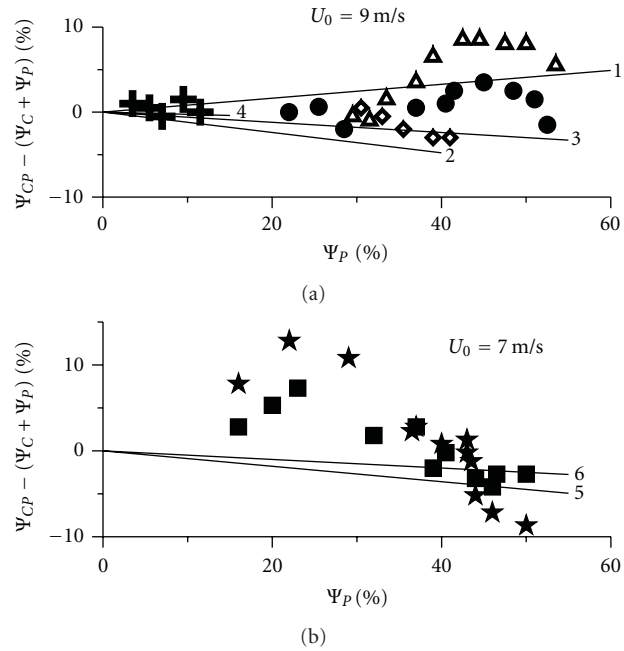

Figure 5: The comparison of drag reduction deviations calculated according to (5) (lines) with measured deviations (signs). Δ: $\Psi_C = -11.5\%$, line 1; ◊: $\Psi_C = +12\%$, line 2; •: $\Psi_C = +6\%$, line 3; +: $\Psi_C = +2.6\%$, line 4; ⋆: $\Psi_C = +9\%$, line 5; ■: $\Psi_C = +5\%$, line 6.

additives. So, above-mentioned zones can be termed as

(2) the zone of positive interaction of two considered methods of drag reduction (with $\Psi_{CP}(q_\delta) > \Psi_C + \Psi_P(q_\delta)$),

(3) the zone of negative interaction of two considered methods of drag reduction (with $\Psi_{CP}(q_\delta) < \Psi_C + \Psi_P(q_\delta)$).

3.3. Joint Action of Air-Microbubbles and Polymer Additives. Malyuga et al. [27, 28] carried out first experiments on drag reduction using the injection of PEO (WSR-301)—solutions aerated by air bubbles. They measured the friction in 3 points of the hard flat plate from distance 0.25 m (N1), 0.99 m (N2) and 2.23 m (N3) behind the slot for U_0 = 5–10 m/s. They determined that an aeration of injected PEO solutions can lead to an increase of their efficiency of drag reduction. The maximum additional increase of their efficiency was measured: 36% in point N2 and 16% in point N3 but in point N2 were measured both an increase and a decrease of drag reduction efficiency. And here, the results were worse for an increase of PEO consumption. It is important to note that highly large consumption of injected air and polymer was used in this experiment. The corresponding dimensionless parameters were

$$1.3 \cdot 10^{-3} \le C_A = \frac{Q}{(U_0 \cdot S)} \le 1.7 \cdot 10^{-3};$$
$$1.05 \cdot 10^{-6} \le q_\delta \le 7.8 \cdot 10^{-6}. \tag{6}$$

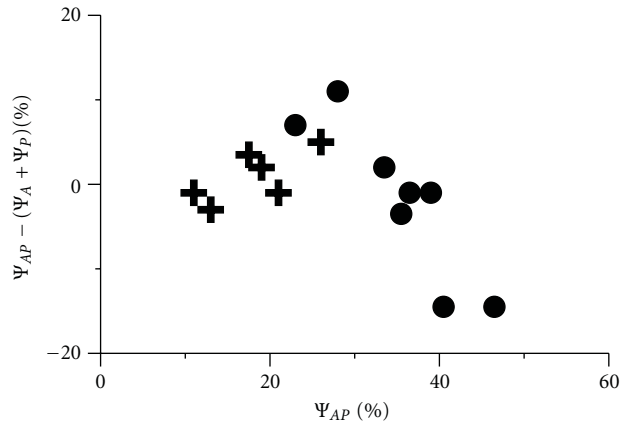

Figure 6: Deviation of friction reduction on hard surface for the joint use of polymer additives and air microbubbles from the sum of their individual efficiencies as a function of efficiency of joint action. +: $U_0 = 9$ m/s, M(PEO) = 4.5 mln., $1.0 \cdot 10^{-7} \le q_\delta \le 4.6 \cdot 10^{-7}$, $2.3 \cdot 10^{-4} \le C_A \le 3.2 \cdot 10^{-4}$; •: $U_0 = 7$ m/s, WSR-301, $1.0 \cdot 10^{-6} \le q_\delta \le 2.7 \cdot 10^{-6}$, $1.36 \cdot 10^{-3} \le C_A \le 1.73 \cdot 10^{-3}$.

Here, S is the surface of studied plate part, and Q is the volumetric consumption of injected air.

Some above-mentioned results and new data (Semenov et al. [37]) obtained in experiments (described in Section "Experimental conditions") for very small consumption of air and polymer are shown in Figure 6. Here, we can see the same three zones: the zone of the exact sum, zones of positive and negative interaction.

Note that the negative interaction zone corresponds to very high consumption of PEO and air.

3.4. Joint Action of Compliant Coating and Air Microbubbles. The first experiment is described by Semenov et al. [37]. One compliant coating was tested for very small consumption of injected air $2.1 \cdot 10^{-4} \le C_A \le 3.7 \cdot 10^{-4}$. $U_0 = 9$ m/s, $T = 8.5 \cdots 10.5$°C. Drag reduction of hard surface by air-microbubbles Ψ_A varied from 7% to 14%. There was obtained that the total efficiency of turbulent drag reduction is equal to the sum of individual efficiencies $\Psi_{CA} = \Psi_C + \Psi_A$.

3.5. Joint Action of Riblets and Surface Compliance. According to theoretical estimations of Semenov and Semenova [29], this combination must be the fine variant of passive (without energy expenditure) methods of turbulent drag reduction.

But experimental data are still absent.

3.6. Joint Action of Riblets and Polymer Additives. The first experimental results were described by Reidy and Anderson [39] and Choi et al. [40]. They found out that individual efficiencies of two methods of drag reduction are summed up for their joint use. Note that they considered very small consumption of polymers.

Koury and Virk [41] and Virk and Koury [42] investigated this problem in detail: for two polyethyleneoxides ($M = 5.3 \cdot 10^6$ and $M = 7.9 \cdot 10^6$) and one polyacrylamide ($M = 7.4 \cdot 10^6$), in two hydraulically smooth pipes of 7.82 mm and 10.2 mm i.d. and in four riblets pipes formed by, respectively, lining each of the smooth pipes with 0.11 mm and 0.15 mm V—groove riblets of equal height and spacing. Within the polymeric regime, at moderate drag reductions of order 50%, drag reduction in the riblet walled pipe significantly exceeded that in the smooth pipe, by as much as 15%. But the greatest drag reduction by riblets in water was measured ~10%. So, the positive deviation from the exact sum of individual efficiencies is observed here. At conditions of asymptotic maximum drag reduction, of order 80%, friction factors in the present riblet-walled pipe were identical to smooth for $h^+ < 10$ but departed off the smooth asymptote in the direction of lesser drag reduction for $h^+ > 10$. And here, the negative interaction is observed.

3.7. Joint Action of Riblets and Air Microbubbles. The opinion about the promising study of this combination is based on an expectation that riblets and air microbubbles manage with very differed structures of turbulence. But both experimental and theoretical investigations were not carried out still.

3.8. Joint Action of Compliant Coating, Air Microbubbles, and Polymeric Additives. The first experiment is described by Semenov et al. [37]. Russian scientists measured the friction of a floating cylindrical element (see "Experimental Conditions" here). They carried out tests for very small consumption of air and PEO. They used the one-layer compliant coating tested also by Choi et al. [43] after this experiment. Results are shown in Figure 7. Here, the positive deviation increases monotonously with increasing consumption of air and PEO. It shows the presence of an interaction of compliant coating, air microbubbles, and polymer additives in the whole region of this investigation.

Note that the effectiveness of drag reduction for joint use of compliant coating, air microbubbles, and PEO additives exceeded the sum of individual efficiencies by as much as 11% (for $\Psi_{CAP} = 35\%$).

4. Theoretical Analysis of Interaction between Compliant Boundary and Polymer Additives

The discovered peculiarities of drag reduction using a complex of different methods of turbulence management require theoretical explanations.

Compliant coatings and polymer additives manage with very differed structures of near-wall turbulence. So, both methods of drag reduction are independent according to this point of view.

But the other factor of an interaction between compliant boundary and polymer additives is a possible reason of observed contradictions between experimental data and initial prognosis: a change of action conditions of one method by other method of drag reduction.

4.1. The Considered Influence of the Viscoelastic Boundary on the Turbulent Diffusion of Polymer Additives. One possible

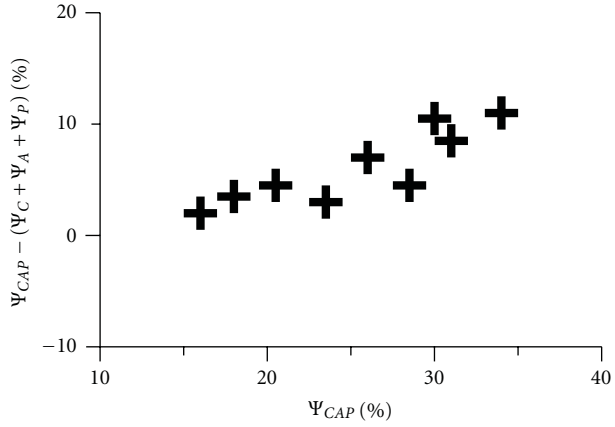

Figure 7: Deviation of friction reduction for joint use of compliant coating A, air microbubbles and polymer additives from the sum of their individual efficiencies as a function of efficiency of joint action. $T = 8.5 \cdots 10.5°\text{C}$, $U_0 = 9$ m/s, $M(\text{PEO}) = 4.5$ mln, $1.5 \cdot 10^{-7} \le q_\delta \le 4.5 \cdot 10^{-7}$, $2.0 \cdot 10^{-4} \le C_A \le 3.7 \cdot 10^{-4}$.

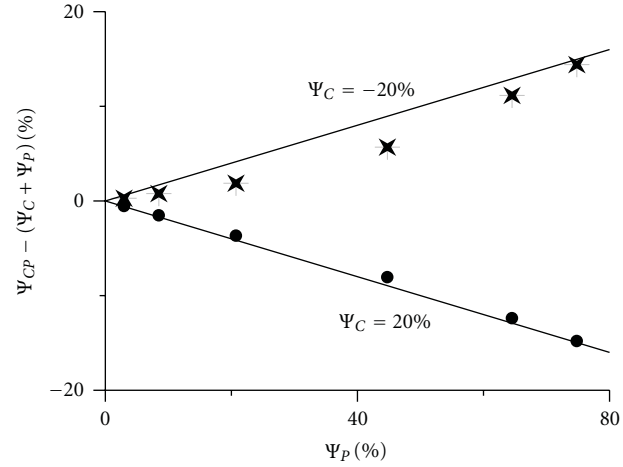

Figure 8: The estimation of the mass transfer change influence by the viscoelastic boundary on drag reduction deviation (points). Lines correspond to the initial prognosis according to (5).

factor of an interaction between two considered methods of turbulence management is the action of compliant boundary on mass transfer in a near-wall region. Here, the integral approach was used. The calculation analysis was carried out on the base of approximate model [26] for a flat plate analogous to the construction scheme tested in quoted experiments [32–35] described here in Section "Experimental Conditions".

It is supposed that the slot injection of PEO solutions at x_i satisfies the conditions of pulseless injection of polymeric additives into a near-wall flow [25]. Here, the constant efficiency of drag variation using compliant coating Ψ_C (independent on polymer additives in flow) is considered from $x_1 = 0.35L$ to $x_2 = 0.65L$. L is the body length. For this part of the body, it was calculated

$$\Psi_{CP} = \frac{\int_{x_1}^{x_2} (\Psi_C + \Psi_\tau - \Psi_C \Psi_\tau) c_{f0} dx}{\int_{x_1}^{x_2} c_{f0} dx}. \tag{7}$$

The local friction reduction by PEO additives is determined according to the formula grounded in [26]

$$\Psi_\tau = 0.51 \operatorname{arc} tg(3 c_W M^{0.85}). \tag{8}$$

The near-wall concentration of PEO may be determined according to the experimental data of Fabula and Burns [44] as

$$c_W = \frac{2\overline{q}L}{\delta_\Psi}. \tag{9}$$

The thickness of turbulent boundary layer δ_Ψ is determined as

$$\delta_\Psi = \frac{9.441 x_i}{\sqrt{\text{Re}_i}} + \int_{x_i}^{x} \frac{(1 - \Psi_\tau)(1 - \Psi_C)}{0.141} c_{f0}\, dx, \tag{10}$$

where $\text{Re}_i = U_0 x_i / \nu$, ν is the kinematic coefficient of water viscosity, $\Psi_C = 0$ for $x < x_1$ and $x > x_2$. Here, the existence of laminar boundary layer from $x = 0$ to x_i is proposed. In the point of transition from laminar form a flow to a turbulent one (at $x = x_i$) the condition of continuity of momentum thickness is written. On its base, the initial thickness of turbulent boundary layer at $x = x_i$ is determined. Here, the power form of the velocity profile with index 1/11 was taken.

So, the friction coefficient (without polymer injection) is calculated according to the Falkner's formula [45]

$$c_{f0} = 0.0256 \left(\frac{x U_0}{\nu} \right)^{-1/7}. \tag{11}$$

The system of (8), (9), (10) is solved for given molecular M, dimensionless coefficient of PEO consumption $\overline{q} = q/\rho U_0 S$, Reynolds number $\text{Re} = U_0 L/\nu$. After its solution, the drag variation Ψ_{CP} (for $\Psi_C \neq 0$) and drag reduction Ψ_P (for $\Psi_C = 0$) are calculated according to (7). On the base of these calculations, the deviation of drag reduction for joint use of compliant surface and polymer additives from the sum of efficiencies for separate actions is determined.

Carried out calculations show that the mass transfer decrease (increase) by the use of viscoelastic coating decreases (increases) the polymer consumption a little. So, it is unlikely that it is the main factor of the interaction between these two methods of turbulence management. However, this approach can and must be taken into account for future investigations and accurate analysis.

One example is shown in Figure 8. We see that in both considered cases ($\Psi_C = 20\%$ and $\Psi_C = -20\%$), the calculated deviations (points) differ from the initial prognosis (lines) inessentially.

4.2. The Interference Action of Viscoelastic Boundary on Near-Wall Turbulence in Flow with Polymer Additives. Here, the other factor of interaction between two methods of drag reduction (the influence of polymer additives in a flow on the interference action of viscoelastic boundary on near-wall turbulence) is considered.

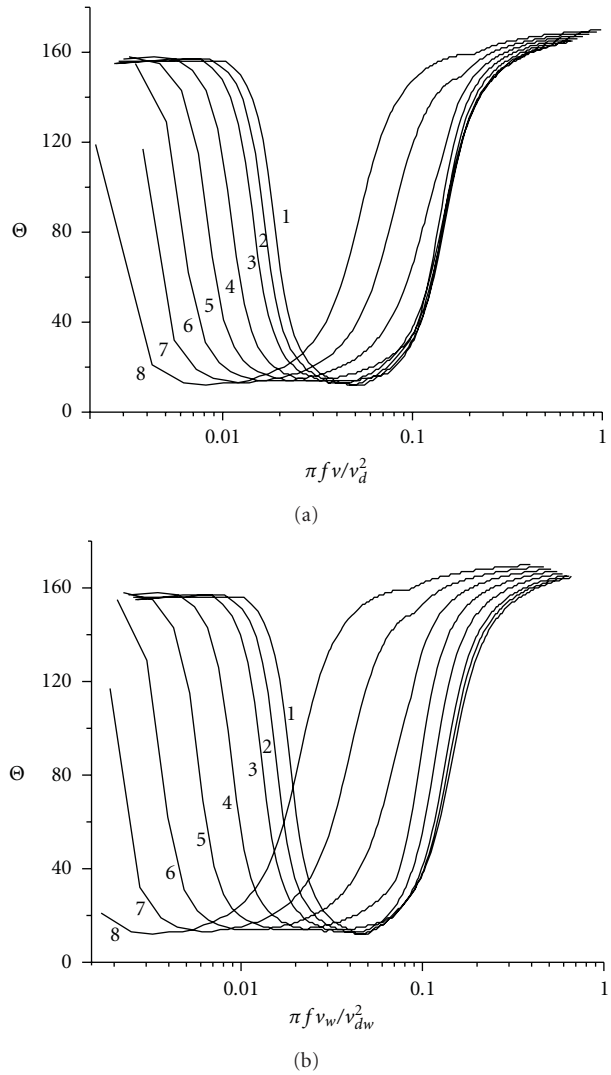

Figure 9: Dependence of PFRPA of smooth compliant surface on drag reduction using polymer additives: (1) $\Psi_P = 0$, (2) $\Psi_P = 5\%$, (3) $\Psi_P = 10\%$, (4) $\Psi_P = 20\%$, (5) $\Psi_P = 30\%$, (6) $\Psi_P = 40\%$, (7) $\Psi_P = 50\%$, (8) $\Psi_P = 60\%$; $\mathrm{Re}_0 = 6.2 \cdot 10^6$; $k_z/k_x = 1.0$.

Formerly, the interference form of a compliant boundary action was analysed by Semenov [15, 46] for a turbulent near-wall flow of Newtonian fluids. He used the near-wall turbulence model of Sternberg [47]. The main modeling parameter (written by Semenov for solution of the problem [46]) is the complex dimensionless compliance of a boundary. He determined the region of this parameter values for drag reduction [48–50]. This theoretical model was used for modeling and choice of one-layer compliant drag reducing coatings. These coatings provided up to 20% drag reduction in experiments [16, 36]. They were used in above-written experimental combined investigations of different methods of turbulence management too.

Here, the interference approach is used for a compliant boundary of a water flow with PEO additives. In this case is suitable the former solution [46] of the problem on an interaction between a viscoelastic boundary and the viscous sublayer of a turbulent boundary layer. Here, we take into account that PEO additives in a flow do not change long-wave structures, the ratio of wave numbers for transverse (k_z) and main (k_x) directions.

Drag reduction by polymer additives, a change of the velocity profile $U(y)$, viscosity and wave velocity are taken into account in calculations. It is important to note that the increase of the viscous sublayer thickness by polymer additives increases the region of permissible use of the linear theory near a wall.

The complex compliance of the boundary (the modeling parameter) is characterised by amplitude and phase of the boundary displacement relative to the turbulent pressure fluctuation. This parameter must be determined for the frequency band of the main production of turbulence. The increase of permissible amplitudes of viscoelastic boundary oscillations follows the increase of thickness of a viscous sublayer.

The obtained solution [46] shows the restriction of the phase region $\Theta(\omega)$ for positive action of a viscoelastic boundary (for drag reduction). This positive action is connected with the decrease of near-wall turbulence production. For fixed frequency ω ($\omega = 2\pi f$, where f is cyclic frequency) the production change of the turbulence energy should be

$$-\int_0^l \left[\langle uv \rangle \left(\frac{dU}{dy} \right) - \langle uv \rangle_C \left(\frac{dU}{dy} \right)_C \right] dy \geq 0. \tag{12}$$

Index "C" corresponds to a compliant boundary. The interference action of a compliant boundary for fixed frequency ω is neutral if this integral is equal to zero. According to the near-wall turbulence model of Sternberg [47], the calculated viscous sublayer thickness l is connected with the fluctuation frequency as $l \approx 5/(\omega/2\nu)^{1/2}$.

For the neutral action variant, the mean velocity profile $U(y)$ is written according to the experimental data for a hard wall.

The improved interference theory (presented by Semenov and Semenova [29]) was used for first calculations of joint action of a compliant boundary and polymer additives.

Neutral phase-frequency lines (calculated according to condition (12)) restrict (from below) a region of Θ for positive action of compliant boundary ($\Psi_C > 0$). One example for $\mathrm{Re}_0 = 6.2 \cdot 10^6$ is shown in Figure 9 (for two variants of the abscissa). The phase shift Θ of the compliant boundary displacement relative to acting fluctuating pressure is on the ordinate. The dimensionless frequency is on the abscissa. In Figure 9(a), it is made dimensionless by the use of real flow viscosity ν near a wall and real friction velocity v_d. In Figure 9(b), it is made dimensionless by the use of kinematic viscosity of water ν_w and friction velocity without drag reduction v_{dw} in order to compare the different influences of drag reducing polymer additives for identical conditions of a water flow.

We see that injected polymer additives extend the phase-frequency region of positive action (PFRPA) of compliant boundary. This extension of PFRPA is maximum at $\Psi_P \approx 40\%$.

The injection of drag reducing polymeric additives into a flow leads to a displacement of PFRPA to the left that can lead

even to the change of the action sign of compliant boundary (from "+" to "−" and on the contrary).

We see that from $\Psi_P \approx 30\%$ the right branch of the neutral line is displaced distinctly to the left. So, minimum velocity of possible drag reduction using compliant coating must increase with the increasing individual efficiency of drag reducing polymeric additives. For example, it must increase to two times at $\Psi_P \approx 50\%$.

It leads to explanation of reasons of drag reduction peculiarities discovered in experiments [32–35, 37] on joint use of compliant coating and polymer additives.

The used theoretical approach does not permit still to carry out a quantitative comparison. It is a problem for future investigations.

5. Conclusion

So, this exposition shows fine outlooks of further study of turbulence management by joint use of compliant coatings, riblets, polymer additives, and microbubbles.

References

[1] Y. G. Aleyev, *Nekton*, The Hague, 1977.

[2] D. M. Bushnell and K. J. Moore, "Drag reduction in nature," *Annual Review of Fluid Mechanics*, vol. 23, no. 1, pp. 65–79, 1991.

[3] J. Gray, "Studies in animal locomotion. The propulsive powers of the Dolphin," *The Journal of Experimental Biology*, vol. 13, pp. 192–199, 1936.

[4] A. H. Woodcock, "The swimming of dolphins," *Nature*, vol. 161, no. 4094, p. 602, 1948.

[5] H. Focke, "Ueber die ursachen der hohen schwimmgeschwindigkeiten der delphine," *Zeitschrift für Flugwissenschaften und Weltraumforschung*, vol. 13, no. 2, pp. 54–61, 1965.

[6] B. N. Semenov, "On the existence of the hydrodynamic phenomenon of Dolphins (*Tursiops Tursio Ponticus*)," *Bionika*, no. 3, pp. 54–61, 1969.

[7] T. E. Alekseeva and B. N. Semenov, "On the determination of the hydrodynamic drag of Dolphins," *Journal of Applied Mechanics and Technical Physics*, no. 2, pp. 160–164, 1971.

[8] T. Y. Wu and A. T. Chwang, "Extraction of flow energy by fish and birds in a wavy stream," in *Swimming and Flying in Nature*, pp. 687–702, Plenum Press, New York, NY, USA, 1975.

[9] A. D. Young, "The calculation of the total and skin friction drags of bodies of revolution at 0^0 Incidence," Tech. Rep. RM 1947, ARC, 1939.

[10] H. Hertel, *Structur—Form—Bewegung*, Krauskopf, Mainz, Germany, 1963.

[11] M. O. Kramer, "The Dolphin's secret," *New Scientist*, vol. 7, pp. 1118–1120, 1960.

[12] M. O. Kramer, "Boundary layer stabilization by distributed damping," *Journal of the American Society of Naval Engineers*, vol. 72, no. 1, pp. 25–33, 1960.

[13] M. O. Kramer, "Boundary layer stabilization by distributed damping," *Naval Engineers Journal*, vol. 74, no. 2, pp. 341–348, 1962.

[14] B. N. Semenov, "The study of Dolphins as low-drag bodies (e.g., Tursiops Tursio Ponticus)," in *Proceedings of the 4th International Congress of the Society for Technical Biology and Bionics*, Munich, Germany, 1998.

[15] B. N. Semenov, "On conditions of modelling and choice of viscoelastic coatings for drag reduction," in *Recent Developments in Turbulence Management*, pp. 241–262, Kluwer Academic Publishers, 1991.

[16] V. M. Kulik, I. S. Poguda, and B. N. Semenov, "Experimental investigation of one-layer viscoelastic coating action on turbulent friction and wall pressure pulsations," in *Recent Developments in Turbulence Management*, pp. 236–289, Kluwer Academic Publishers, 1991.

[17] J. O. Hinze, *Turbulence*, McGraw-Hill, 1959.

[18] E. M. Greshilov, A. M. Evtushenko, L. M. Lyamshev, and N. L. Shirokova, "Some peculiarities of an action of polymeric on near-wall turbulence," *Journal of Engineering Physics*, vol. 25, pp. 999–1004, 1973.

[19] K.-S. Choi, "Turbulent drag reduction strategies," in *Emerging Techniques in Drag Reduction*, pp. 77–98, MEP, London, UK, 1996.

[20] V. G. Bogdevich, N. V. Malykh, A. G. Malyuga, and I. A. Ogorodnikov, "Acoustic properties of wall bubble layer in water of great void fraction," in *Hydrodynamics and Acoustics of Near-Wall and Free Flows*, pp. 77–107, Institute of Thermophysics, Novosibirsk, Russia, 1981.

[21] B. J. Cantwell, "Organized motion in turbulent flow," *Annual Review of Fluid Mechanics*, pp. 457–515, 1981.

[22] V. M. Kulik, I. S. Poguda, and B. N. Semenov, "The action of viscoelastic coatings on the friction reduction for flows of water and polymeric solutions," in *Proceedings of the 12th Short Course for Pipe-Line Problems*, pp. 42–43, Upha, 1989.

[23] A. G. Malyuga, V. I. Mikuta, and G. Gerchev, "The influence of near-wall bubble layer on screw propeller-induced effects on the wall," in *Proceedings of the 17th Session of BSHC*, vol. 2, pp. 42/1–42/12, Varna, Bulgaria, 1988.

[24] N. S. Berman, "Drag reduction by polymers," *Annual Review of Fluid Mechanics*, vol. 10, pp. 47–64, 1978.

[25] B. N. Semenov, "The polymeric solution injection into flow for drag reduction," *Siberian Physical-Technical Journal*, no. 4, pp. 99–108, 1991.

[26] B. N. Semenov, "The pulseless injection of polymeric additives into near-wall flow and perspectives of drag deduction," in *Recent Developments in Turbulence Management*, pp. 293–308, Kluwer Academic Publisher, 1991.

[27] A. G. Malyuga, V. I. Mikuta, and O. I. Stoyanovsky, "Turbulent drag reduction at flow of polymer solutions aerated by air bubbles," in *Near-Wall and Free Turbulent Flows*, pp. 121–130, Institute of Thermophysics, Novosibirsk, Russia, 1988.

[28] A. Malyuga, V. Mikuta, A. Nenashev, S. Kravchenko, and O. Stoyanovsky, "Local drag reduction at flow of polymer solutions aerated by air bubbles," in *Proceedings of the 6th National Congress*, pp. 74/1–74/6, Varna, Bulgaria, 1989.

[29] B. N. Semenov and A. V. Semenova, "Recent developments in interference analysis of compliant boundary action on near-wall turbulence," in *Proceedings of the International Symposium on Sea Water Drag Reduction*, pp. 189–195, Newport, UK, 1998.

[30] B. N. Semenov and A. V. Semenova, "On interference action of a compliant boundary on near-wall turbulence," *Thermophysics and Aeromechanics*, vol. 9, no. 3, pp. 393–403, 2002.

[31] B. N. Semenov and A. V. Semenova, "Joint effect of a compliant boundary and polymer additives on the near-wall turbulent flow," *Thermophysics and Aeromechanics*, vol. 7, no. 7, pp. 187–195, 2000.

[32] B. N. Semenov, V. M. Kulik, V. A. Lopyrev, B. P. Mironov, I. S. Poguda, and T. I. Yushmanova, "The combined effect of small

quantities of polymeric additives and pliability of the wall on friction in turbulent flow," *Fluid Mechanics. Soviet Research*, vol. 14, no. 1, pp. 143–149, 1985.

[33] B. N. Semenov, V. M. Kulik, V. A. Lopyrev, B. P. Mironov, I. S. Poguda, and T. I. Yushmanova, "Towards the influence of flow polymer additives and surface compliance on wall-turbulence," in *Proceedings of the 5th International Congress on Theoretical and Applied Mechanics*, vol. 2, pp. 371–376, Varna, Bulgaria, 1985.

[34] V. M. Kulik, I. S. Poguda, B. N. Semenov, and T. I. Yushmanova, "Influence of flow velocity in combined effect of a compliant surface and polymer additives on turbulent friction," *Izvestia Sibirskogo Otdelenia Akademii nauk SSSR*, no. 15, pp. 42–46, 1987.

[35] V. M. Kulik, I. S. Poguda, B. N. Semenov, and T. I. Yushmanova, "Effect of flow velocity on the synergistic decrease of turbulent friction by a compliant wall and a polymeric additive," *Soviet Journal of Applied Physics*, no. 1, pp. 49–54, 1988.

[36] V. M. Kulik, I. S. Poguda, and B. N. Semenov, "Experimental study of the effect of single-layer viscoelastic coatings on turbulent friction and pressure pulsation on a wall," *Journal of Engineering Physics*, vol. 47, no. 2, pp. 878–883, 1984.

[37] B. N. Semenov, A. I. Amirov, V. M. Kulik, A. G. Malyuga, and I. S. Poguda, "Turbulent drag reduction by a combined use of compliant coatings, gas microbubbles and polymer additives," *Thermophysics and Aeromechanics*, vol. 6, no. 2, pp. 211–219, 1999.

[38] S. S. Kutateladze and A. I. Leontyev, *Heat and Mass Transfer and Friction in Turbulent Boundary Layers*, Energiya, Moscow, Russia, 1972.

[39] L. W. Reidy and G. W. Anderson, "Drag reduction for external and internal boundary layer using riblets and polymers," *AIAA Paper*, 1988, N138.

[40] K. S. Choi, G. E. Gadd, H. H. Pearcey, A. M. Savill, and S. Svensson, "Tests of drag-reducing polymer coated on a riblet surface," *Applied Scientific Research*, vol. 46, no. 3, pp. 209–216, 1989.

[41] E. Koury and P. S. Virk, "Drag reduction by polymer solutions in riblet-lined pipes," in *Proceedings of the 8th European Drag Reduction Working Meeting*, Lausanne, Switzerland, 1993.

[42] E. Koury and P. S. Virk, "Maximum drag reduction by polymer solutions in riblet-lined pipes," in *Proceedings of the 9th European Drag Reduction Meeting*, Napoly, Italy, 1995.

[43] K. S. Choi, X. Yang, B. R. Clayton et al., "Turbulent drag reduction using compliant surfaces," *Proceedings of the Royal Society A*, vol. 453, no. 1965, pp. 2229–2240, 1997.

[44] A. G. Fabula and T. G. Burns, *Dilution in a Turbulent Boundary Layer with Polymeric Friction Reduction*, Naval Undersea Research and Development Center, Pasadena, Calif, USA, 1970.

[45] Y. I. Voitkunsky, R. Y. Pershitz, and I. A. Titov, *Handbook on Theory of a Ship*, Sudpromgiz, Leningrad, 1960.

[46] B. N. Semenov, "Interaction of an elastic boundary with a viscous sublayer of a turbulent boundary layer," *Journal of Applied Mechanics and Technical Physics*, no. 3, pp. 58–62, 1971.

[47] J. Sternberg, "A theory for viscous sublayer of a turbulent flow," *The Journal of Fluid Mechanics*, vol. 13, no. 2, pp. 241–271, 1962.

[48] B. N. Semenov, "Analysis of deformation characteristics of viscoelastic coatings," in *Hydrodynamics and Acoustics of Near-Wall and Free Flows*, pp. 57–76, Nauka, Novosibirsk, Russia, 1981.

[49] B. N. Semenov, "On the properties of viscoelastic boundary for turbulent friction reduction," *Siberian Physics-Technical Journal*, no. 1, pp. 63–73, 1993.

[50] B. N. Semenov, "Analysis of four types of viscoelastic coating for turbulent drag reduction," in *Emerging Techniques in Drag Reduction*, pp. 187–206, MEP, London, UK, 1996.

Hindawi Publishing Corporation
Advances in Mechanical Engineering
Volume 2011, Article ID 528373, 6 pages
doi:10.1155/2011/528373

Research Article

Drag Reduction of Bacterial Cellulose Suspensions

Satoshi Ogata, Tetsuya Numakawa, and Takuya Kubo

Department of Science and Engineering, Tokyo Metropolitan University, 1-1 Minamiosawa, Hachiojishi, Tokyo 192-0397, Japan

Correspondence should be addressed to Satoshi Ogata, ogata-satoshi@tmu.ac.jp

Received 31 March 2011; Accepted 1 June 2011

Academic Editor: Bo Yu

Drag reduction due to bacterial cellulose suspensions with small environmental loading was investigated. Experiments were carried out by measuring the pressure drop in pipe flow. It was found that bacterial cellulose suspensions give rise to drag reduction in the turbulent flow range. We observed a maximum drag reduction ratio of 11% and found that it increased with the concentration of the bacterial cellulose suspension. However, the drag reduction effect decreased in the presence of mechanical shear.

1. Introduction

In order to resolve various environmental issues, numerous investigations are currently focusing on energy conservation techniques. One topic of particular interest is drag reduction in heat transport systems. The addition of drag reducing agents leads to reduced frictional loss, and a corresponding reduction in pumping power, and results in effective energy conservation [1].

Additives such as polymers, surfactants, and fibers are well-known drag reducing agents and offer a simple means of reducing drag. Since Toms [2] observed drag reduction with the addition of polymers in 1949, numerous investigations into drag reducing agents under various conditions have been carried out. Among these, surfactants [3–5] have been researched intensively due to their effectiveness and low mechanical degradation. However, as most of these additives are synthetic chemicals, they contaminate rivers and soil when solutions are drained directly, and therefore require careful disposal. Although biopolymers [6–8] are not subject to such disposal issues, they are not practical due to their significant mechanical degradation. On the other hand, fibers [9–11] such as asbestos or nylon are resistant to mechanical degradation but have a disadvantage with regard to environmental load, while pulp, which is a plant-based fiber, requires high concentrations to achieve drag reduction effects.

Bacterial cellulose, a type of fiber, is considered to have a low environmental load, as it is a naturally derived cellulose produced by acetic bacteria. In addition, nanometer-scale fibers of bacterial cellulose produce large networks as a result of complex interactions. Such networks are closely related to the drag reduction effects induced by polymers and surfactants. Therefore, drag reduction can also be expected with bacterial cellulose solutions if their networks behave similarly.

In the present study, the drag reduction effects of such bacterial cellulose solutions are empirically evaluated.

2. Experimental Setup and Procedure

The syringe pump experimental setup is shown in Figure 1. The piston operates in a range from 10 to 15 mm/s, and the volume of the syringe is 200 mL. The velocity of the piston is controlled by a personal computer. The range of Reynolds numbers based on the viscosity of the solvent solution is about 500∼8,000. The test pipe is made of aluminum, having an inner diameter of 2.00 mm and a smooth internal wall. The inner diameter of the pipe was measured in cross-section using an optical microscope. Pressure taps with diameters of 0.2 mm were placed 50 mm and 150 mm from the outlet of the pipe. The length of the test section was 100 mm. The pressure taps were connected to a Validyne differential pressure transducer (DP15, ±0.25% F. S. accuracy) using clear vinyl tubing. The entrance length was 150 mm. The suspension was first taken up by the syringe and was then pushed into the test section by the piston, after which the pressure drop was measured. The reported value of the

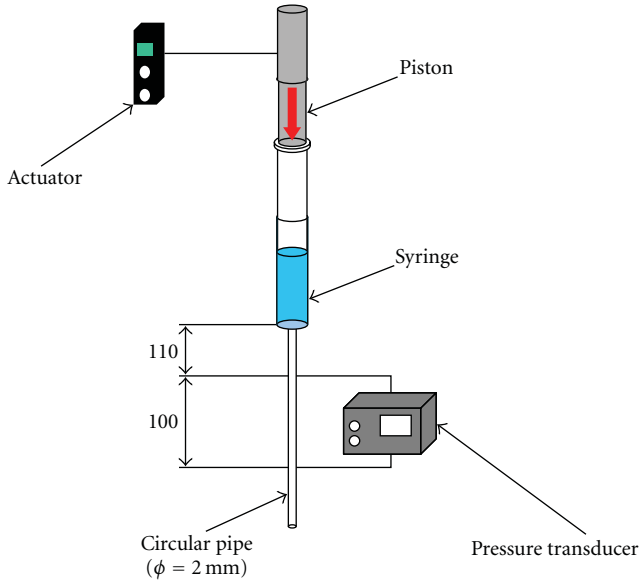

Figure 1: Experimental apparatus.

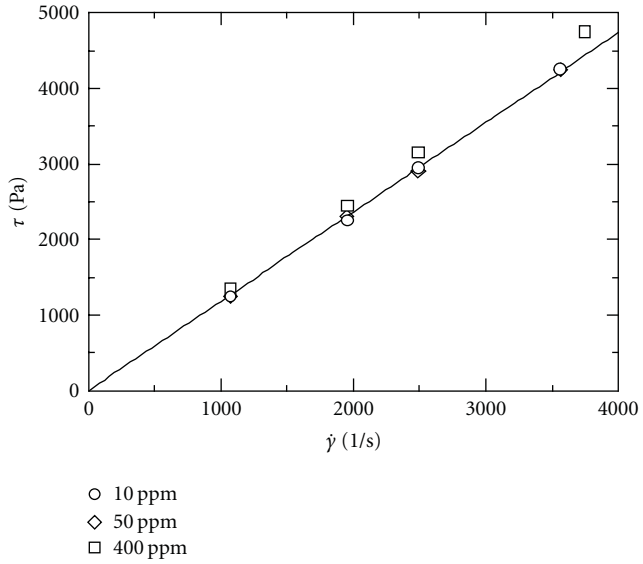

Figure 2: Flow curves for test fluids.

friction factor in the laminar flow range is the best estimate of the result, and with a 95% confidence limit, the value is believed to lie within ±0.89% of it.

The bacterial cellulose additive was made from commercial nata de coco. Since this is preserved in syrup, that is, contains sugar, it was soaked in tap water for over 24 hours in order to dilute the sugar before preparation of the suspension. The desugared nata de coco was then compressed under a load of ~1 ton in order to extract the water (a block of nata de coco contains 99% water and less than 1% bacterial cellulose by volume) and to obtain dried bacterial cellulose. Following compression, the mass of the nata de coco was found to be 0.25% of the original mass. The additive was then mixed with tap water and agitated with

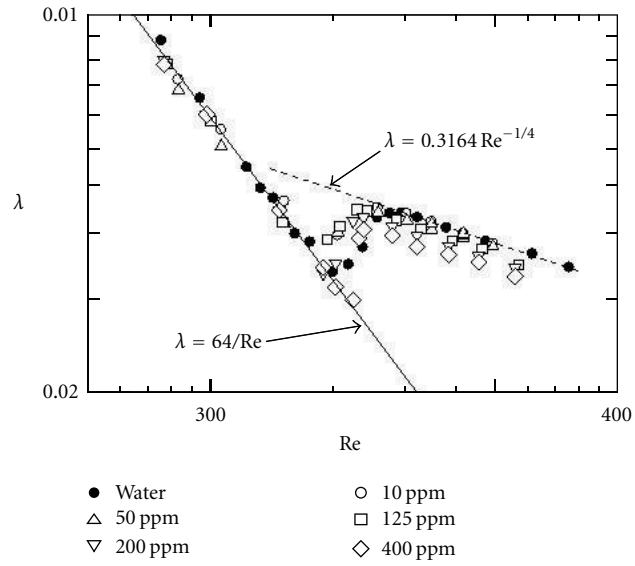

Figure 3: Frictional coefficient of bacterial cellulose suspensions.

a mixer. The weight concentration of the suspension, C_w, was determined based on the mass ratio of compressed nata de coco and tap water. Concentrations of 10, 50, 125, 200, and 400 ppm were examined. In addition, solutions made using the additive before compression were prepared and examined for comparison. Their concentrations were 5, 7.5, and 10 ppm, based on the mass after compression.

Figure 2 shows the flow curves for the tested bacterial cellulose suspensions. The wall shear stress τ and shear rate $\dot{\gamma}$ were calculated from the experimental data in the laminar flow region. The solid line in Figure 2 indicates the value obtained by the viscosity of water. The viscosity is seen to increase with concentration, and the test tested bacterial cellulose suspensions are considered to be Newtonian. The values in Figure 2 were used to calculate the Reynolds number.

3. Results and Discussion

Figure 3 shows the relationship between the Reynolds number Re and the friction factor λ, based on the measured pressure drops for 5 suspensions (10, 50, 125, 200, and 400 ppm). The data show that λ in the region of Re >2500 for the suspension decreases in comparison to the value for water. On the other hand, the critical Reynolds numbers for suspensions with concentrations less than 200 ppm are smaller than that of water.

For biopolymers, the results may be affected by the solvent. As the solution used in this experiment was also of plant origin, experiments with different solvents (distilled water and tap water) were performed, and the results are shown in Figure 4. It can be seen that the experimental results with the two solvents are very similar, and thus the influence of the solvent is negligible.

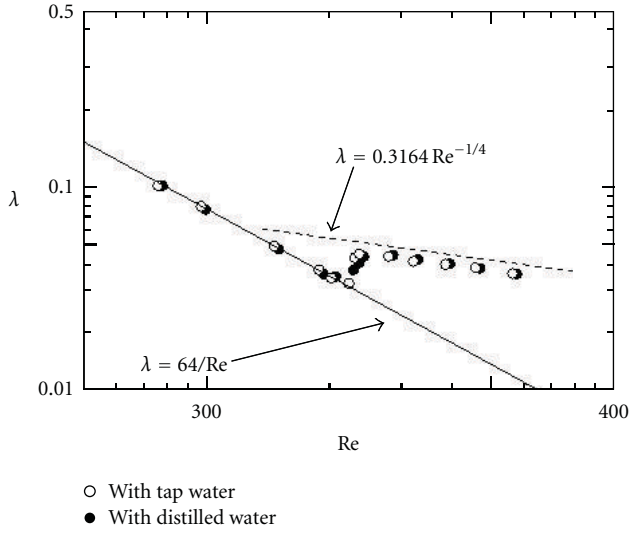

Figure 4: Effects of solvent on frictional coefficient.

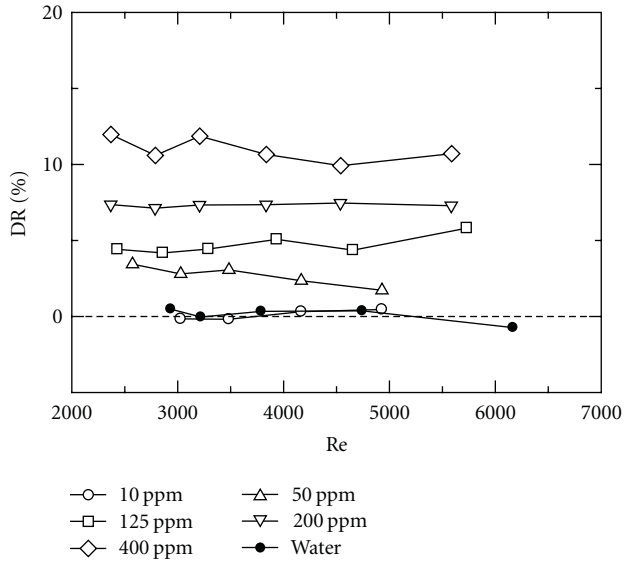

Figure 5: Drag reduction of bacterial cellulose suspensions.

The relationship between the drag reduction DR, which is defined by (1), and the Reynolds number Re is shown in Figure 5:

$$\mathrm{DR}\ (\%) = \frac{\lambda_{\mathrm{water}} - \lambda_{\mathrm{suspension}}}{\lambda_{\mathrm{water}}} \times 100. \tag{1}$$

In (1), λ_{water} and $\lambda_{\mathrm{suspension}}$ denote the friction factor for the water and suspension, respectively. From Figure 5, it can be seen that DR is almost constant against Re and its maximum value is 11%. Figure 6 shows the relationship between DR and the concentration of the suspension, C_w. DR is seen to increase significantly with C_w under these experimental conditions.

The relationship between $f^{-1/2}$ and $\mathrm{Re}\cdot f^{1/2}$, where f denotes the Fanning friction factor, is shown in Figure 7. It can be seen that in the laminar flow regime, where $\mathrm{Re}\cdot f^{1/2}$

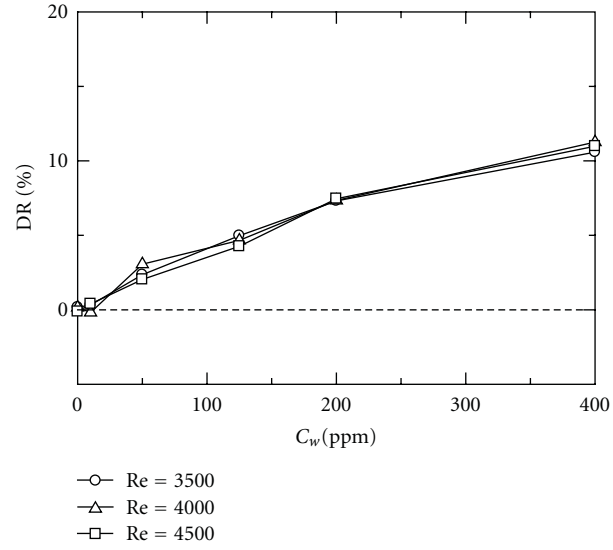

Figure 6: Effects of concentration of bacterial cellulose suspensions on DR.

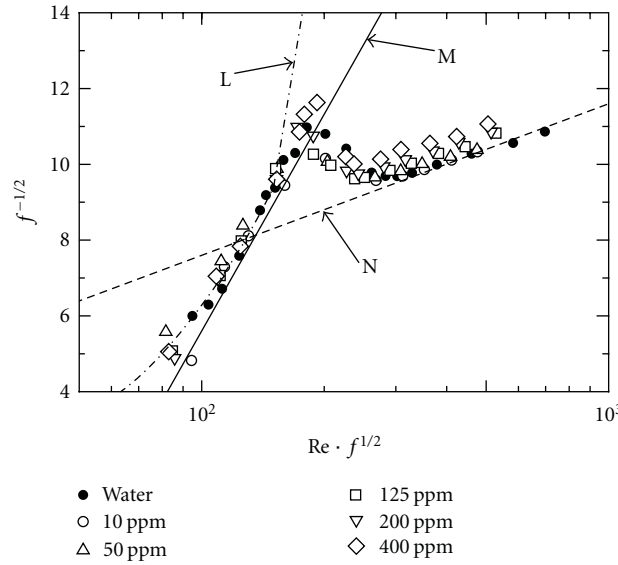

Figure 7: $1/\sqrt{f}$ versus $\mathrm{Re}\sqrt{f}$.

is small, the data is well fitted by a Newtonian laminar flow curve (L). In contrast, in the turbulent regime, the data is aligned parallel to the curve (N) in order of concentration (higher concentrations are located higher in the graph). This indicates a type B drag reduction, which can be seen in fiber suspensions and polymer solutions. Generally, a type B drag-reducing mechanism is associated with suppression of vortices. For fiber suspensions, it is thought that flocs produced in the flow field influence the fluid resistance, and the fibers suppress vortices when they are uniformly distributed in the flow direction, thus resulting in drag reduction.

A micrograph of a bacterial cellulose suspension is shown in Figure 8(a). The bacterial cellulose is in fiber form, and

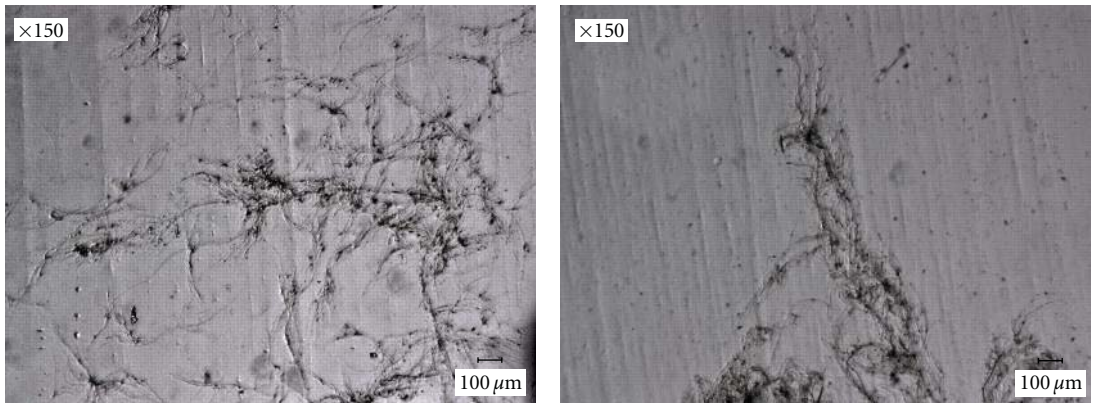

(a) Bacterial cellulose suspension ($N = 0$) (b) Nata de coco ($N = 0$)

Figure 8: Micrographs of test fluids (before experiment).

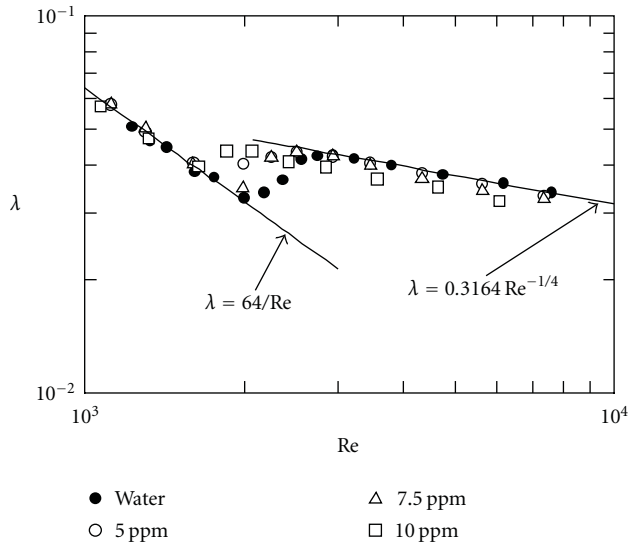

Figure 9: Frictional coefficient of nata de coco suspensions.

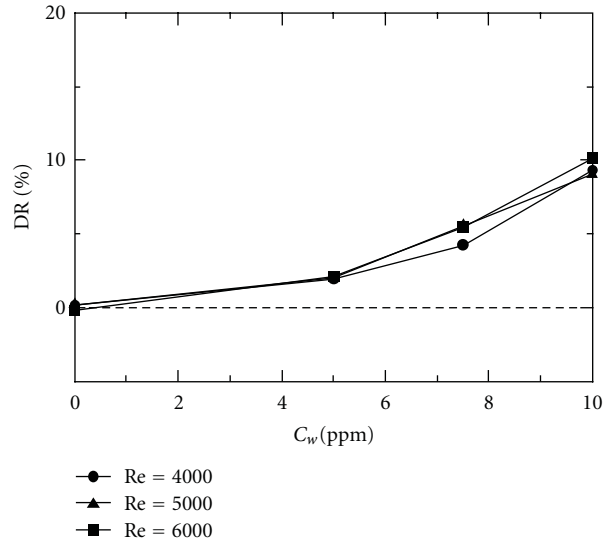

Figure 10: Effects of concentration of nata de coco suspensions on DR.

similar suspensions made from synthetic fibers, such as nylon or rayon with aspect ratios of 40–100, show up to 20% drag reduction at high concentrations (5000–20000 ppm). On the other hand, asbestos fiber, which has an aspect ratio of 10^5, shows a high DR (20–85%) at low concentrations (25–500 ppm). In the case of bacterial cellulose, although drag reduction has been observed in the low concentration region, similar to that for asbestos, its DR value is similar to that for nylon or rayon. Although it is impossible to determine the aspect ratio of bacterial cellulose based on the image, the reason that the DR value of bacterial cellulose is lower than those of asbestos fiber or biopolymers may be due to that the fibers and/or their assemblies in the test fluid are shorter.

Bacterial cellulose forms nata de coco when bacteria accumulate and stratify. Figure 8(b) is a micrograph of a suspension of uncompressed nata de coco that was agitated with a mixer. The fibers are closely associated and the assemblies are thick in comparison with those of bacterial cellulose. It is clear from the traditional experimental results that the thickness and aspect ratio of fibers have a large influence on drag reduction. Hence, the drag reduction mechanisms for the nata de coco suspension shown in Figure 8(b) differs from those of the bacterial cellulose suspension shown in Figure 8(a). Therefore, experiments with suspension made from agitated nata de coco were performed in order to investigate the influence of the bacterial cellulose fiber shape.

The results of the pressure drop measurements are shown in Figure 9. Although drag reduction is observed, similar to the case for the bacterial cellulose, the critical Reynolds numbers for the examined concentrations are smaller than that of water. The relationship between C_w and DR for the nata de coco suspension is shown in Figure 10. The DR value is seen to increase significantly with concentration, in comparison to the bacterial cellulose suspension (Figure 6). The higher drag reducing effect of the nata de coco suspension at lower concentrations may be

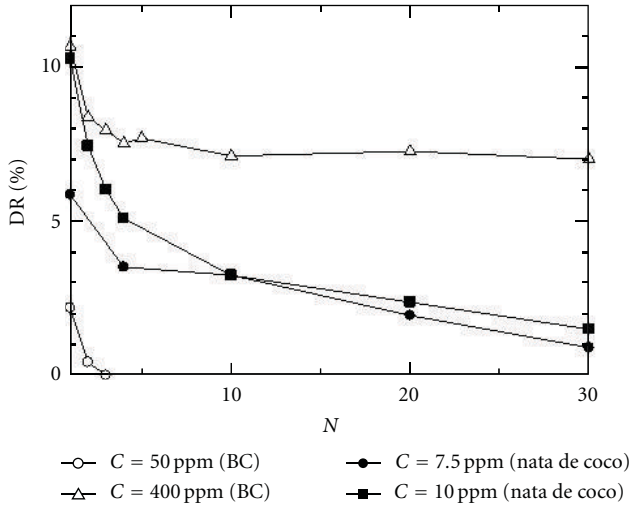

Figure 11: Experimental results for mechanical degradation: BC denotes bacterial cellulose suspensions, and nata de coco denotes nata de coco suspensions.

explained by the presence of thicker fiber assemblies (Figures 8(a) and 8(b)).

Figure 11 shows the results of a mechanical degradation experiment for suspensions of bacterial cellulose and nata de coco. For 400 ppm bacterial cellulose, the initial DR (N = 1, where N is the number of passages of the test fluid) was 11%, gradually decreased until N = 5, and thereafter maintained an almost constant value of about 5%. DR decreased immediately for the 50 ppm concentration. In contrast, for the nata de coco suspension, both the 7.5 and 10 ppm concentrations exhibited a decrease in DR with increasing N, and the drag reducing effect vanished for N = 30. These results suggest that bacterial cellulose suspensions are less susceptible to mechanical degradation.

Micrographs after the degradation experiment are shown in Figures 12(a) and 12(b). In comparison to the bacterial cellulose suspension (Figure 12(a)), the degree of breakup of fiber assemblies, which were closely associated before degradation, was greater for the nata de coco suspension (Figure 12(b)). Bacterial cellulose tends to contain gelled assemblies (liquid), and nata de coco is composed almost entirely of such ensembles. In addition, the degree of conglutination between bacterial cellulose fibers increases due to hydrogen bonding when the liquid in the gelled assemblies evaporates. This occurs even when the bacterial cellulose is in water. Since conglutination is weaker in nata de coco than in bacterial cellulose, and the fibers are fragile, the nata de coco suspension may suffer additional damage (mechanical degradation) when the fluid passes through an orifice or capillary.

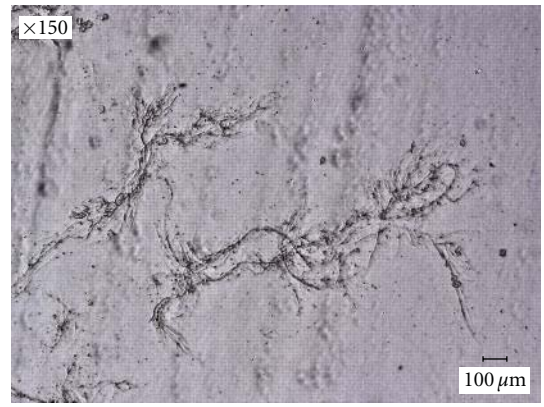

(a) Bacterial cellulose suspension (N = 30)

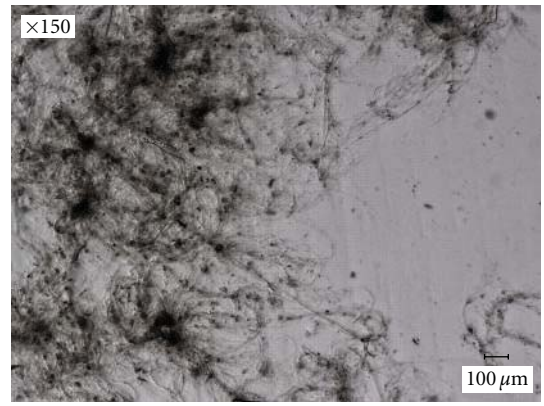

(b) Nata de coco (N = 30)

Figure 12: Micrographs of test fluid (after mechanical degradation).

4. Conclusions

Pressure drop measurements for bacterial cellulose suspensions flowing in a circular pipe were performed, and the following results were obtained.

(1) The drag reduction of bacterial cellulose increased with concentration and showed a maximum of 11%.

(2) The drag reduction decreased due to mechanical degradation, and finally became constant.

(3) Suspensions of nata de coco, which is a layered form of bacterial cellulose, showed a higher drag reduction at lower concentrations, although the effects of mechanical degradation were larger.

References

[1] K. Gasljevic and E. F. Matthys, "Field test of drag-reducing surfactant additives in a hydraulic cooling system," in *Proceedings of the ASME Fluids Engineering Division Summer Meeting(FED '96)*, vol. 237, pp. 249–260, San Diego, Calif, USA, 1996.

[2] B. A. Toms, "Some observations on the flow of linear polymer solutions through straight tubes at large reynolds numbers," in *Proceedings of the First International Congress on Rheology*, vol. 2, pp. 135–141, North-Holland Publishing, 1948.

[3] F.-C. Li, Y. Kawaguchi, K. Hishida, and M. Oshima, "Investigation of turbulence structures in a drag-reduced turbulent channel flow with surfactant additive by stereoscopic particle image velocimetry," *Experiments in Fluids*, vol. 40, no. 2, pp. 218–230, 2006.

[4] H. W. Bewersdorff, "Rheology of drag reducing surfactant solutions," in *Proceedings of the ASME Fluids Engineering Division Summer Meeting (FED '96)*, vol. 237, pp. 25–29, San Diego, Calif, USA, 1996.

[5] J. J. A Wei, Y. B. Kawaguchi, F.C.C Li et al., "Reduction and turbulence characteristics in sub-zero temperature range of cationic and zwitterionic surfactants in EG/water solvent," *Journal of Turbulence*, vol. 10, Article N10, 2009.

[6] J. W. Hoyt, "Drag reduction in polysaccharide solutions," *Trends in Biotechnology*, vol. 3, no. 1, pp. 17–21, 1985.

[7] J. Ramus, B. E. Kenney, and E. J. Shaughnessy, "Drag reducing properties of microalgal exopolymer," *Giotechnology and Bioengineering*, vol. 33, pp. 550–557, 1989.

[8] K. Gasljevic, K. Hall, D. Chapman, and E. F. Matthys, "Biotechnology-based drag reduction for naval applications: production of biopolymers from marine microalgae and scale-up for type-B reducers," in *Proceedings of the Proceedings of the 2nd International Symposium on Seawater Drag Reduction*, pp. 559–567, Busan, Korea, May 2005.

[9] P. S. Virk and R. H. Chen, "Type B drag reduction by aqueous and saline solutions of two biopolymers at high reynolds numbers," in *Proceedings of the 2nd International Symposium on Seawater Drag Reduction*, pp. 545–558, Busan, Korea, May 2005.

[10] A. A. Robertson and S. G. Mason, "The flow characteristics of dilute fiber suspensions," *TAPPI*, vol. 40, pp. 326–334, 1957.

[11] W. Mih and J. Parker, "Velocity profile measurements and phenomenological description of turbulent fiber suspension pipe flow," *TAPPI*, vol. 50, pp. 237–246, 1967.

Hindawi Publishing Corporation
Advances in Mechanical Engineering
Volume 2011, Article ID 879615, 8 pages
doi:10.1155/2011/879615

Research Article

Combined Effects of Temperature and Reynolds Number on Heat Transfer Characteristics of a Cationic Surfactant Solution

Ning Ma,[1,2] Jianfeng Wang,[1,2] and Jinjia Wei[1,2]

[1] *State Key laboratory of Multiphase Flow in Power Engineering, Xi'an Jiaotong University, Xi'an 710049, China*
[2] *Suzhou Academy, Xi'an Jiaotong University, Suzhou, Jiangsu 215021, China*

Correspondence should be addressed to Jinjia Wei, jjwei@mail.xjtu.edu.cn

Received 29 April 2011; Accepted 25 June 2011

Academic Editor: Bo Yu

The heat transfer characteristics of a dilute cationic surfactant solution, CTAC/NaSal aqueous solution, were experimentally investigated in a fully developed two-dimensional water channel flow at different temperatures ranging from 15°C to 60°C and at different mass concentrations, namely, 75, 100, and 200 ppm. The magnitudes of the maximum achievable heat transfer reduction (HTR) at the above three different surfactant concentrations are all about 90%. The cationic surfactant solution showed a great heat transfer reduction phenomenon, which was greatly affected by concentration, temperature, and Reynolds number. It was supposed that temperature and shear stress are two kinds of energy applied on the surfactant microstructure, which can be helpful to the surfactant network formation or dissociation depending on their values.

1. Introduction

Since the drag reduction phenomenon is discovered by Toms in 1948 [1], polymers and surfactants as two drag-reducing additives were studied by many researchers [2–4]. Polymer drag-reducing additives have been used extensively in crude oil pipelines of companies such as Shell and Conoco to increase the throughput and to save pumping energy [2]. However, due to the permanent decrease of drag reduction performance of polymer after passing through high shear stress sections of pipelines, they are not effective in closed circuit systems such as district heating and cooling (DHC) recirculation system. In contrast to polymers, the mechanical degradation of surfactants is only temporary [3].

In addition to the drag reduction effect, another noticeable effect of surfactant drag-reducing additives is the heat transfer reduction that occurs between a solid boundary and the flowing fluid [4–6]. Wei et al. [6] showed that heat transfer reduction is always a little larger than drag reduction. This reduced heat transfer behavior of drag-reducing surfactant solutions is an obstacle to their application in DHC systems since heat exchange in heating or cooling is essential.

Some research focused on the effect of the Reynolds number [7] and the concentration [8] on the drag reduction and heat transfer induction of the surfactant solutions. But there are few details, systematic investigations, and deep analyses of the concentration, the Reynolds number, and the temperature effects on the heat transfer reduction of the surfactant solution. In this paper, the combined effects of concentration, Reynolds, and temperature on the heat transfer behavior of CTAC/NaSal surfactant solution were experimentally investigated and analyzed from the viewpoint of thermal energy and shear stress energy in detail.

2. Experimental Apparatus and Procedure

2.1. Test Facility. The water channel test facility for heat transfer experiments was a closed loop shown schematically in Figure 1. The system consisted of a reservoir tank ($0.45\ m^3$), a stainless steel centrifugal pump, a settling chamber equipped with a nozzle, a two-dimensional channel, a diffuser, an electromagnetic flowmeter with a resolution of $\pm 0.01\ m^3/min$, the stainless steel tube, and some necessary components to connect the equipments. In order to get different fluid temperatures, a control system with a 4.4 kW heater was installed in the reservoir tank. The temperature of the fluid was controlled to ±0.1 K around the prescribed value.

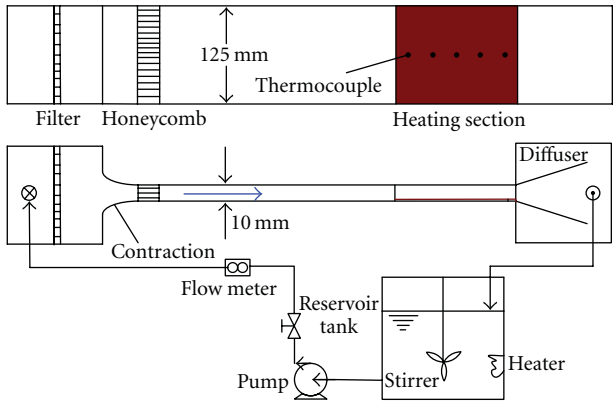

Figure 1: Schematic diagram of two-dimensional water channel.

The surfactant aqueous solution was circulated by the pump and supplied to the settling chamber. The chamber was equipped with a perforated pipe, stainless steel mesh, and 1/17 contraction nozzle. At the entrance of the test section, a 45 mm long honeycomb with $8 \times 8\,\text{mm}^2$ rectangular openings was used to remove large eddies.

The two-dimensional channel was 10 mm high, 125 mm wide, and 3 meters long (inside measurement), which was connected straightly by two sections of 1.5 meters each. The channel walls were of 20 mm thickness and made of transparent acrylic resin except for the heating wall. The heating wall consisted of a 2-mm thick stainless steel plate and five independent strips of electric heaters each of which was made by gluing a Nichrome heating wire (3 mm thick, 10 m long, 200°C resistance temperature, and 1000 W peak power) on the outer surface of the base plate by using an electrically insulating but highly conductive adhesive (Dow Corning Silicone, Dow Corning Co., Ltd., America). The five heaters having the same spanwise width as the channel width were total 1.40 meters in length located 1.60 meters downstream from the entrance of the channel, and thus all the five heaters were 280 mm long along the flow direction. Each heater was independently heated by an AC power supply. The voltage and electric resistance were measured to calculate the local wall heating power Q. On the midline of the channel span, five T-type thermocouples were embedded into the outer surface of the stainless steel plate with the positions corresponding to the centers of the heater patches for local wall temperature measurements. An independent heater-sensor circuit was designed for each heater to control the local wall temperature T_w. In the experiments, the local wall temperatures of all five parts of the stainless steel plate were set to the same value, making the heating plate serve as an isothermal heater. One thermocouple was set at the entrance of the heating section corresponding to the first part of the heating plate to measure the inlet bulk temperature T_0. The local bulk temperatures T_f corresponding to the other parts of the heating plate were estimated from the heat balance between the heating power and temperature increment of the flow. A data acquisition unit, PXI 6221 (National Instruments Co., America) having a high A/D resolution of ±20,000, was connected to a personal computer that automatically converted the thermocouples' output voltages into temperatures. Temperatures were monitored to ensure that data in the steady state was being acquired. All the temperature readings were obtained and averaged over about ten minutes.

2.2. Sample Material. In the experiments, the tested cationic surfactant was cetyl trimethyl ammonium chloride (CTAC) (Shandong Fusite Chemical Co., Ltd., China, 70% purity), with a molecular weight of 320.0 g/mol, which is less affected by calcium and sodium naturally existing in tap water. Sodium salicylate (NaSal) (Yixing City Shenguang Medicine Chemicals Co., Ltd., China, 99% purity), with molecular weight of 160.1 g/mol, was used as the counterion to stabilize the solution structure. The surfactant solution was prepared by adding the same mass concentrations of surfactant and counterion to the desired tap water for the heat transfer measurements. The surfactant solution is marked by the concentration of CTAC, and solutions of three mass concentrations (75, 100, and 200 ppm) were made for the heat transfer reduction (HTR) measurements.

2.3. Heat Transfer Reduction. The local Nusselt number was determined as

$$\text{Nu}_x = \frac{h_x H}{\lambda_s} = \frac{H}{\lambda_s} \cdot \frac{Q_x}{WL\left(T_w - T_f\right)}. \tag{1}$$

In this paper, we used the averaged Nusselt number which was determined as

$$\overline{\text{Nu}} = \frac{\overline{Q}H}{LW\lambda_s} = \frac{\left(\sum_{x=1}^{5} \text{Nu}_x\right)}{5}, \tag{2}$$

where Q_x is heating power, H the channel height, W the channel width, L the total length of the heaters along the flow direction, λ_s the thermal conductivity of the surfactant solution, T_w the local wall temperature, and T_f the local bulk fluid temperature. Here, the thermal conductivity of solvent was used instead of that of surfactant solution. One reason is that the surfactant concentrations involved in the experiments were so low that the thermal physical parameters were almost the same as those of solvent; another reason is that the comparison of the experimental results between pure solvent and surfactant solution becomes convenient. According to Ohlendorf et al. [9], the shear-reduced structure (SIS) made up of rod-like micelles exists as long as the solution is sheared and disappears at once after the shear is stopped. It is generally believed that SIS is essential for drag reduction and hear transfer reduction through suppressing the turbulence in the turbulent flow at high Reynolds number [10, 11]. For a given test facility, the local heat transfer coefficient h_x mainly depends on the heat convection; however the thermal conductivity λ_s is just decided by physical property and temperature of drag-reducing fluids. So using the thermal conductivity of water instead of that of surfactant solution can be convenient to understand the turbulence suppression degree of the surfactant additives. Furthermore, in the most application-oriented studies, such a treatment is convenient for comparing the heat transfer results of the solvent with the surfactant solution under the same situations of flow and heat flux [10]. The viscosity and thermal conductivity values

used in various nondimensional numbers are obtained at the temperature corresponding to specific experimental condition. For example, for the 15°C experimental condition of the bulk fluid, the viscosity and thermal conductivity are at 15°C.

The heat transfer reduction of the drag-reducing flow from that of solvent flow was defined as HTR:

$$\%\mathrm{HTR} = \frac{\mathrm{Nu}_s - \overline{\mathrm{Nu}}}{\mathrm{Nu}_s} \times 100, \quad (3)$$

where Nu_s is the Nusselt number of solvent.

In order to test the reliability of the experimental system, the test result of the tap water solvent was compared with the Gnielinski's formula [12] under the same experimental condition. The Gnielinski's formula is expressed as

$$\mathrm{Nu}_D = 0.012\left(\mathrm{Re}_D^{0.87} - 280\right)\mathrm{Pr}_f^{0.4}\left[1 + \left(\frac{D}{L}\right)^{2/3}\right]c_t, \quad (4)$$

where $c_t = (\mathrm{Pr}_f/\mathrm{Pr}_w)^{0.01}$, $\mathrm{Pr}_f/\mathrm{Pr}_w = 0.05\sim20$, D the hydraulic diameter, L the total length of the heaters along the flow direction, Re_D Reynolds number based on the hydraulic diameter D, Pr Prandtl number, the suffix f represents bulk temperature, and suffix w represents wall temperature.

3. Results and Discussion

Figure 3 shows the variation of averaged Nusselt numbers of 75, 100, and 200 ppm CTAC/NaSal surfactant solution flow with Reynolds number in the 2D channel at several different temperatures ranging from 15°C to 60°C. For comparison, the Gnielinski's equation for the heat transfer of Newtonian turbulent flow in the hydraulic fully developed and thermally developing region is also shown by a solid line in the same figure.

Figures 2(a)–2(c) show similar variation trends of Nusselt numbers with Reynolds number. The measured Nusselt numbers of water flow agree very well with the curve of Gnielinski's equation, validating the reliability of the experimental system. In a certain Reynolds number region, the Nusselt number of the surfactant solution is smaller than that of water, showing a great heat transfer reduction (HTR) phenomenon. It is also shown that the Nusselt numbers are very small in the lower Reynolds number region with a value about 2 and increase slowly before a certain Reynolds number, above which the Nusselt numbers increase rapidly up to higher values about 100 but still a little lower than the curve of Gnielinski's equation. It is suggested that the heat transfer performance is improved with increasing Reynolds number, and the improved level is high in the higher Reynolds number region. The Reynolds number above which the Nusselt number begins to increase rapidly, in other words, the HTR begins to decrease rapidly is so called the critical Reynolds number (Re_c). Heat transfer performances are different at different temperatures, indicating an obvious effect of temperature. For the same concentration, the critical Reynolds number increases as the temperature increases, and thus the heat transfer reduction range is enlarged. However, the critical Reynolds number starts to decrease with temperature when the temperature exceeds critical value depending on the corresponding concentration. The temperature above which the HTR begins to increase rapidly is defined as the critical temperature (T_c).

The relationship between the critical Reynolds number and temperature is shown in Figure 3 at different concentrations. We can see that at lower temperatures, the critical Reynolds number just shows little difference among the three different concentrations. As the temperature is increased, low-concentration solution will reach the maximum critical Reynolds number (corresponding to the critical temperature) very quickly, and then the critical Reynolds number at this concentration decreases rapidly with further increasing temperature. The increase in concentration increases the critical Reynolds number and also the critical temperature. For example, the critical temperatures for 75, 100, and 200 ppm surfactant solutions are 40, 45, and 50°C, respectively, and the critical Reynolds numbers corresponding to the critical temperatures increase from 13400 for 75 ppm to 18000 for 100 ppm, and then to 30900 for 200 ppm. This phenomenon has also been noticed by other researchers [6, 10, 13].

Figures 4(a)–4(c) show heat transfer reduction (HTR) measured at different temperatures, Reynolds numbers, and surfactant mass concentrations in a two-dimensional channel. It can been seen in Figure 4(a) that the HTR is higher in lower Reynolds number region, exceeding 90% and does not decrease until critical Reynolds numbers above which the HTR decreases very quickly to a very small value. At lower temperatures, the Reynolds number can reach the critical value easily and the heat transfer performance increases with further increasing Reynolds number above the critical value. The range of low heat transfer performance is enlarged as the temperature is increased up to the critical temperature above which the heat transfer performance is improved sharply. This phenomenon is so called temperature effect, as mentioned above.

Also, we can see in Figure 4(a) that for all temperatures not exceeding the critical value, the maximum HTRs are all about 92%. The same phenomenon can be seen in Figures 4(b) and 4(c). Comparing Figures 4(a), 4(b), and 4(c), we can find that at the same temperature below the critical temperature of the solution, the higher concentration solution has the wider range of low heat transfer performance: for instance, for 75 ppm surfactant solution at the temperature of 40°C, the Reynolds number range of low heat transfer is from 3000 to 15100; however, the Reynolds number ranged from 3000 to 21200 for solution at the concentration of 100 ppm and the temperature of 40°C and the Reynolds number ranged from 5000 to 31500 for 200 ppm surfactant solution at 40°C. Thus it can be seen that the heat transfer characteristic was greatly affected by the surfactant concentration. In a small range of Reynolds number, the HTR increases to, and keeps in the maximum value before and then decreases with further increasing Reynolds number above the critical value. The range of low heat transfer performance is enlarged as the temperature increases before a critical temperature above which the expansion

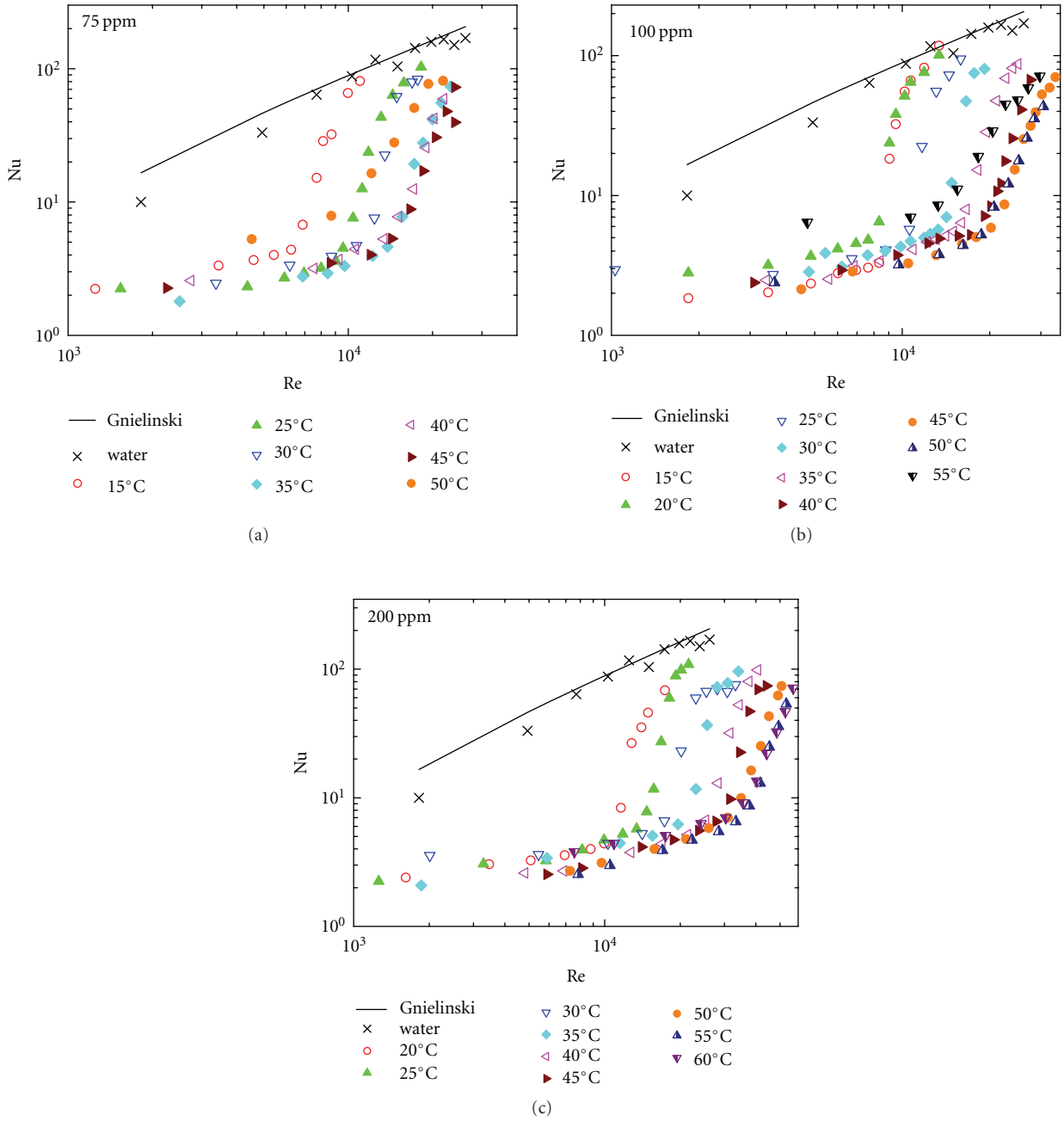

Figure 2: Averaged Nusselt numbers at 75, 100, and 200 ppm.

of low heat transfer performance has a setback with further increasing temperature.

Since the heat transfer reduction behavior is closely related to the micellar network in the surfactant solution, these phenomena may be explained by the effects of Reynolds number (shear stress) and temperature (thermal/Brownian motion) on the micellar network. We consider that the main energy applied to the solution consists of two parts, the thermal energy (H) and shear energy (S). For cationic surfactants, under the right conditions of surfactant/counterion chemical structures, ratios, concentrations, and temperatures, they form rod-like micelles [14]. The length of rod-like micelles is about dozens of times diameter of the micelles which is about several nanometers, and the length of rod-like micelles increases with increasing surfactant concentration [9]. Under a proper shear stress, the rod-like micelles form a network structure called shear-induced structure (SIS) [15] and align themselves along the flow direction to suppress turbulent flow near the wall [9], which is often stated to be responsible for the occurrence of heat transfer reduction [10, 16, 17]. Both the shear action and temperature can affect the formation and destruction of the shear-reduced structure (SIS). For dilute surfactant solutions, at a certain shear rate, the viscosity remains relatively constant for

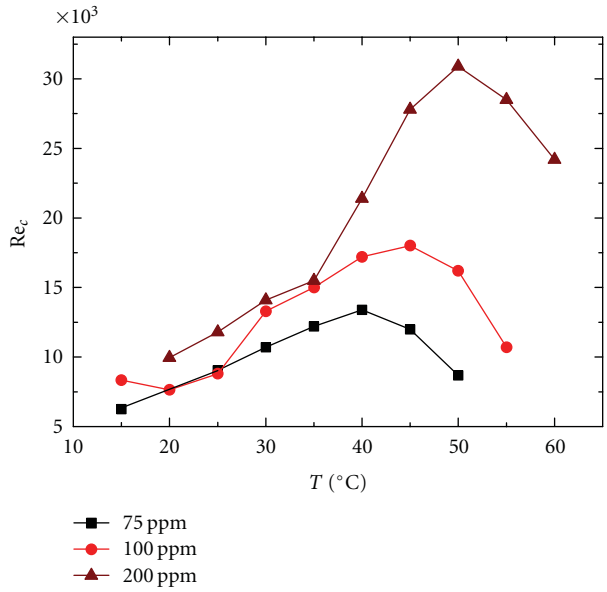

FIGURE 3: Critical Reynolds number versus solution temperature.

a period of induction time before beginning to increase due to the free rotation of the spherical micelles, then the shear thickening was observed by acquiring sufficient energy which is the combination of the shear rate and the flow duration [18, 19]. What is more, the induction time is approximately inversely proportional to the shear rate [20], and Zhang et al. [21] have pointed that the negative correlation between the induction time and the shear rate accords with power law mode with the exponent of −0.1. When the shear rate exceeds the second critical shear rate, the SIS is destroyed by mechanical breakdown [18, 19]. Similarly, at lower temperature below the critical temperature of the solutions, the increase of temperature can intensify the Brownian motion of micelles so that the micelles can get enough energy through the collision to overcome the mutual exclusion to aggregate, forming the supermolecular shear-reduced structure (SIS) which need more shear energy corresponding to bigger critical Reynolds number to be destroyed. When the temperature increases to a certain level, the SISs transform to spherical micelles, which has been proved by Lu et al. [11] using transmission electron microscopes (TMEs). This is the reason that when the temperature increases to a critical value, the critical Reynolds number decreases.

Through comparing Figures 3 and 3, we can find that the Nusselt number increases slowly and the HTR keeps in a considerable value before the critical Reynolds number, which can be explained by the theory that turbulent flow is suppressed to a state which is in between the laminar and turbulent flow states. Because the levels of suppression are almost the same for a given surfactant concentration with different temperatures below the corresponding values, the HTR is almost invariant before critical Reynolds number for different temperatures, as shown in Figure 3. With further increasing temperature above the critical value, some of the SISs fracture and transform to spherical micelles, which reduces the proportion of superorder rod-like micelle structures and enhances the turbulence intensity of the flow, so the heat transfer performance can be improved in lower Reynolds numberrange.

From Figure 3, we can see that the critical Reynolds number increases with increasing temperature whichis below the corresponding critical temperature for a given concentration surfactant solution. Considering the fact that the Brownian motion is enhanced with increasing temperature, we may conjecture that the shear-induced structure (SIS) is easily formed in the surfactant solution and the strength of these big structures are increased. Therefore, a larger Reynolds number is needed to improve the heat transfer performance; in other words, a larger shear stress is needed to disassociate micellar networks. However, when the temperature exceeds the critical value, the corresponding critical Reynolds number decreases with further increasing temperature above the critical value. The reason for this phenomenon is that the SISs transform to spherical micelles because of the larger thermal energy added to the solution. At the same time, we can see in Figure 3 that the critical temperature and critical Reynolds number increase as the concentration increases. It is suggested that the rod-like micelles are longer and stronger with increasing concentration and need more thermal energy to disrupt SISs to spherical micelles and more shear stress energy to destroy the net structure SISs adhered to the wall.

The heat transfer reduction of CTAC/NaSal solutions with the same proportion in terms of mass ratios has also been studied by Zhou et al. [22] and Zhang et al. [23] in the 50 × 500 mm and 20 × 250 mm two-dimensional channel, respectively. They found that the maximum HTRs for fully developed thermal boundary layer were 55% and 68%; however the HTR is 92% in the present experiment conducted in 10 × 125 mm two-dimensional channel. It suggests that the HTR increases with the decreases of the size of two-dimensional channel, according to the finding that DR increases with the decrease of the pipe diameters [24]. According to Zhou et al. [22], the reduction of heat transfer rate of surfactant solutions increases as the concentration is increased and then keeps a maximum value without further increasing with the concentration. This critical concentration is about 80 ppm; this agrees with the present experimental findings that all the maximum HTRs are about 92% for 75, 100, and 200 ppm surfactant reducing solution.

The same concentration, temperature, and Reynolds number can work together to impact on the heat transfer performance of the surfactant solution both positively and negatively: under the condition of the critical temperature (T_c) and the critical Reynolds number (Re_c), the two major energies constitute the critical energy of the solution for a given concentration of solution. Therefore, in practical engineering fields, the goal of energy savings can be achieved by controlling the temperature and Reynolds number of the flow. When the solution temperature is lower, the best heat transfer performance can be got by increasing Reynolds number to a value exceeding the critical Reynolds number.

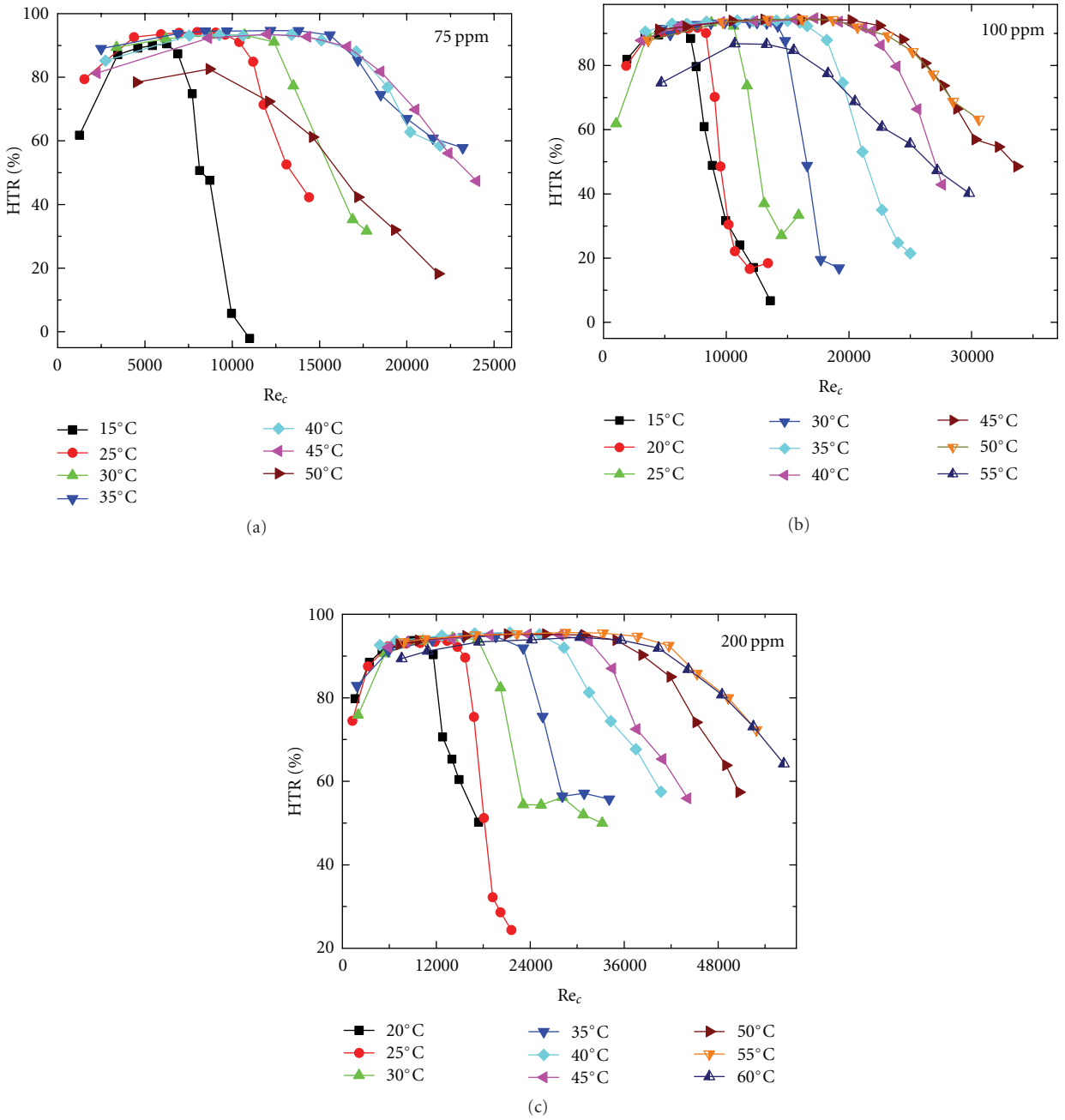

Figure 4: Heat transfer reduction characteristics of CTAC/NaSal solution.

Otherwise when the solution temperature is close to the critical temperature, in order to get the better heat transfer effect, the solution can be heated to a temperature just a little higher than the critical temperature. Of course, the study in this paper is just a qualitative analysis of the interesting heat transfer reduction phenomena; the relationship between the shear and thermal energy and their contribution to the heat transfer reduction remain to be further studied.

Such experimental data obtained in this experiment as temperatures in Figure 3 and Reynolds numbers in Figures 3 and 3 do not reach the same value on the right side of the abscissas; it is because the variation trend can be reflected by the obtained data and it is not necessary to get more data.

4. Conclusions

Turbulent heat transfer characteristics of CTAC/NaSal surfactant drag-reducing flow with concentrations of 75, 100, and 200 ppm in a two-dimensional channel at various

Reynolds numbers and temperatures were experimentally investigated. The main conclusions drawn from this study are as follows.

(1) There exists a critical temperature in each different concentration solution, below which the critical Re, the efficient rang of drag reduction, the drag-reducing characteristics of the solution increase with increasing temperature.

(2) For a surfactant solution with a given concentration, there exist two factors of temperature and Reynolds number affecting the heat transfer characteristic greatly. In order to get the quantitative analysis of influence exerted by these two factors, we defined critical Reynolds number (Re_c) and critical temperature (T_c) which increase with increasing concentration.

(3) For $\mathrm{Re} < \mathrm{Re}_c$, the HTR increases to a considerable maximum value about 92% quickly due to the shear-induced structure SIS formed at a suitable Reynolds number (shear stress) range. The micellar network can be destroyed by the higher shear stress corresponding to the critical Reynolds number, and the destruction is intensified with further increasing Reynolds number. Therefore, the heat transfer performance increases remarkably as the Reynolds number increases on the condition that Reynolds number exceeds the critical value at a given concentration and a given temperature.

(4) The temperature affects the heat transfer performance because of the thermal motion of surfactant micelles. For $T < T_c$, the Brownian motion of micelles gets intense with increasing temperature and the formation of SIS becomes more and more easy, resulting in wider and wider range of low heat transfer performance. When the temperature reaches the critical value, the heat transfer coefficient comes to the minimum value and then starts to increase with further increasing temperature. The reason is that when the temperature exceeds the critical one, the Brownian motion is so intense that the shear-induced network structure SISs transform to spherical micelles.

Acknowledgments

The authors gratefully acknowledge the financial support from the NSFC Fund (no. 51076124), the Specialized Research Fund for the Doctoral Program of Higher Education of China (no. 20090201110002), the Open Project of Institute of Rheological Mechanics and Material Engineering (Central South University of Forestry and Technology) (no. 10RM01), and Jiangsu Provincial Natural Science Foundation (BK2009145).

References

[1] B. A. Toms, "Some observations on the flow of liner polymer solutions through straight tubes at large Reynolds number," in *Proceedings of the 1st International Congress on Rheology*, vol. 2, pp. 135–141, North Holland, 1948.

[2] P. D. Manfield, C. J. Lawrence, and G. F. Hewitt, "Drag reduction with additives in multiphase flow: a literature survey," *multiphase Science and Technology*, vol. 11, no. 3, pp. 197–221, 1999.

[3] A. Gyr and H. W. Bewerslorff, *Drag Reduction of Turbulent Flows by Additives*, Kluwer Academic Publishers, Dodrecht, The Netherlands, 1995.

[4] J. L. Zakin, B. Lu, and H. W. Bewersdorff, "Surfactant drag reduction," *Reviews in Chemical Engineering*, vol. 14, no. 4-5, pp. 253–320, 1998.

[5] M. Poreh and U. Paz, "Turbulent heat transfer to dilute polymer solutions," *International Journal of Heat and Mass Transfer*, vol. 11, no. 5, pp. 805–818, 1968.

[6] J. J. Wei, Y. Kawaguchi, B. Yu, and Z. P. Feng, "Rheological characteristics and turbulent friction drag and heat transfer reductions of a very dilute cationic surfactant solution," *Journal of Heat Transfer*, vol. 128, no. 10, pp. 977–983, 2006.

[7] H. X. Zhang, D. Z. Wang, W. G. Gu, and Z. F. Dong, "Study on drag-reducing and heat transfer performances in heating water systems with CTAC additives," *HV&AC*, vol. 37, no. 9, pp. 45–49, 2007.

[8] J. Pollert, J. L. Zakin, J. Myska, and P. Kratochvil, "Use of friction reduction additives in district heating system field test at Kladno-Krocehlavy," in *Proceedings of the 85th International District Heating and Cooling Association*, pp. 141–156, Seattle, Wash, USA, 1994.

[9] D. Ohlendorf, W. Interthal, and H. Hoffmann, "Surfactant systems for drag reduction: physico-chemical properties and rheological behaviour," *Rheologica Acta*, vol. 25, no. 5, pp. 468–486, 1986.

[10] P. W. Li, Y. Kawaguchi, H. Daisaka, A. Yabe, K. Hishida, and M. Maeda, "Heat transfer enhancement to the drag-reducing flow of surfactant solution in two-dimensional channel with mesh-screen inserts at the inlet," *Journal of Heat Transfer*, vol. 123, no. 4, pp. 779–789, 2001.

[11] B. Lu, X. Li, J. L. Zakin, and Y. Talmon, "A non-viscoelastic drag reducing cationic surfactant system," *Journal of Non-Newtonian Fluid mechanics*, vol. 71, no. 1-2, pp. 59–72, 1997.

[12] S. M. Yang and W. Q. Tao, *Heat Transfer*, Higher Education Press, Beijing, China, 1998.

[13] J. J. Wei, Y. Kawaguchi, F. C. Li et al., "Drag-reducing and heat transfer characteristics of a novel zwitterionic surfactant solution," *International Journal of Heat and mass Transfer*, vol. 52, no. 15-16, pp. 3547–3554, 2009.

[14] J. L. Zakin, J. Myska, and Z. Chara, "New limiting drag reduction and velocity profile asymptotes for nonpolymeric additives systems," *AIChE Journal*, vol. 42, no. 12, pp. 3544–3546, 1996.

[15] B. Lu, X. Li, L. E. Scriven, H. T. Davis, Y. Talmon, and J. L. Zakin, "Effect of chemical structure on viscoelasticity and extensional viscosity of drag-reducing cationic surfactant solutions," *Langmuir*, vol. 14, no. 1, pp. 8–16, 1998.

[16] F. C. Li, Y. Kawaguchi, and K. Hishida, "Investigation on the characteristics of turbulence transport for momentum and heat in a drag-reducing surfactant solution flow," *Physics of Fluids*, vol. 16, no. 9, pp. 3281–3295, 2004.

[17] N. S. Berman and E. E. Cooper, "Stability studies in pipe flows using water and dilute polymer solutions," *AIChE Journal*, vol. 18, no. 2, pp. 312–320, 1972.

[18] J. Dehmoune, J. P. Decruppe, O. Greffier, and H. Xu, "Rheometric investigation on the temporal shear thickening of dilute micellar solutions of C_{14^-}, C_{16^-}, and C_{18} TABNaSal," *Journal of Rheology*, vol. 52, no. 4, pp. 923–940, 2008.

[19] Y. T. Hu, P. Boltenhagen, and D. J. Pine, "Shear thickening in low-concentration solutions of wormlike micelles. I. Direct visualization of transient behavior and phase transitions," *Journal of Rheology*, vol. 42, no. 5, pp. 1185–1208, 1998.

[20] Y. T. Hu, S. Q. Wang, and A. M. Jamieson, "Rheological and flow birefringence studies of a shear-thickening complex fluid-A surfactant model system," *Journal of Rheology*, vol. 18, no. 3, pp. 532–547, 1993.

[21] C. W. Zhang, J. J. Wei, B. Yu, and F. C. Feng, "The effects of shear action on the characteristics of surfactant solutions," in *Proceedings of the Engineering Thermophysics Congress on Multi-Phase Flow*, Xinjiang, China, 2009.

[22] T. Zhou, K. C. Leong, and K. H. Yeo, "Experimental study of heat transfer enhancement in a drag-reducing two-dimensional channel flow," *International Journal of Heat and mass Transfer*, vol. 49, no. 7-8, pp. 1462–1471, 2006.

[23] H. X. Zhang, D. Z. Wang, W. G. Gu, and Z. F. Dong, "Study on drag-reducing and heat transfer performances in heating water systems with CTAC additives," *Heating Ventilating and Air Conditioning*, vol. 37, no. 9, pp. 45–49, 2007.

[24] L. F. Jiao and F. C. Li, "Review of turbulent drag-reducing flow and heat transfer with additives," *Advances in Mechanics*, vol. 38, no. 3, pp. 339–357, 2008.

Hindawi Publishing Corporation
Advances in Mechanical Engineering
Volume 2011, Article ID 206219, 10 pages
doi:10.1155/2011/206219

Research Article

Flow Drag and Heat Transfer Reduction Characteristics of Organic Brine (Potassium Acetate) and Inorganic Brine (Calcium Chloride) Solutions with Nonionic Surfactant

Naoto Haruki and Akihiko Horibe

Graduate School of Natural Science and Technology, Okayama University, 1-1 Tsushima-Naka, 1-Chome, Kita-ku, Okayama 700-8530, Japan

Correspondence should be addressed to Naoto Haruki, haruki@mech.okayama-u.ac.jp

Received 4 March 2011; Revised 9 June 2011; Accepted 5 July 2011

Academic Editor: Yasuo Kawaguchi

Flow drag and heat transfer reduction effects are useful in heat energy transportation systems and can lead to lower pumping energy requirements. The purpose of this research is to describe the flow drag and heat transfer reduction characteristics of organic (potassium acetate) and inorganic (calcium chloride) brine solutions. The nonionic surfactant oleyl dihydroxyethyl amine oxide (ODEAO) is used as a drag-reducing additive. The pipe friction coefficient and heat transfer coefficient are investigated experimentally in a straight pipe for each type of solution with ODEAO. These coefficients are found to be lower than those of water in the turbulent flow range. However, the rod-like micelles of ODEAO, which are necessary to induce the flow drag reduction effect, are not readily formed in these solutions. Hence, the flow drag and heat transfer reduction effects are measured only under limited conditions and it is difficult to apply these solutions practically as heat transfer media.

1. Introduction

Recently, there has been some interest in flow drag and heat transfer reduction effects as a practical means of reducing energy consumption. Previous studies have verified the energy conservation capabilities of flow drag and heat transfer reduction effects [1]. If a surfactant used as a flow drag reduction fluid is capable of lowering the pipe friction coefficient by up to 78%, the energy consumption efficiency of the surfactant solution will decrease by 44% compared to water. The flow drag and heat transfer reduction effects of organic brine solution are particularly useful for transport energy conservation, since the high viscosity of organic brine solution requires high pumping power for transportation. The reduced heat transfer coefficient of the flow drag reduction fluid not only decreases the heat loss from the pipe, but also degrades the performance of the heat exchanger. Heat transfer enhancement methods have been proposed by Kawaguchi et al. [2], Sato et al. [3], and the present authors [4] to increase this reduced heat transfer coefficient.

When a surfactant is added to water, rod-like micelles can be formed by the functioning of the hydrophobic and hydrophilic groups of surfactant molecules [5]. In previous studies of the flow drag and heat transfer reduction effects of this phenomenon, suppression of the small-scale turbulent eddies of the solution caused the turbulent flow to laminarize [6]. Moreover, a surfactant was verified to be the most suitable additive, since its micelles are thermodynamically stable and self-assemble quickly after degradation [7]. Accordingly, there have been a number of reports on flow drag and heat transfer reduction effects.

In our previous research (e.g., [1, 8–11]), the nonionic surfactant oleyl dihydroxyethyl amine oxide (= ODEAO, $C_{16}H_{35}N$ $(C_2H_4OH)_2O$ = 371.6) was used as a flow drag reduction additive. ODEAO has less sterilization (acute oral toxicity: LD_{50} > 5,000 mg/kg [1]) and a low environmental load. Nakata et al. [1] used transmission electron microscopy (TEM) to confirm the shape of ODEAO micelles. Figure 1 shows an electron micrograph (photographic magnification:

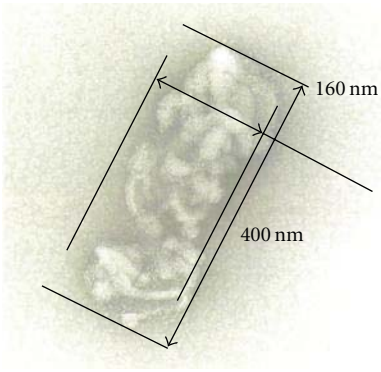

Figure 1: Rod-like micelles of ODEAO.

60,000) of the rod-like micelles of ODEAO. This specimen was prepared from an aqueous solution of ODEAO at a concentration of 5,000 ppm. The figure indicates rod-like or worm-like micelles (400 nm long and 160 nm wide) of ODEAO (or an entanglement network of rod-like micelles).

Our previous studies [8–11] have investigated the flow drag and heat transfer reduction effects of a surfactant (ODEAO) in organic brine (ethylene glycol (EG, $C_2H_4(OH)_2$ = 62.1)) and (propylene glycol (PG, $CH_3CH(OH)CH_2OH$ = 76.11)) solutions. Aggregation of the rod-like micelles of the surfactant was reinforced by a polar-nonpolar solubilization between the micelles and the EG or PG molecules. Therefore, the flow velocity range in which flow drag and heat transfer reduction effects occurred was much greater for EG or PG solution with surfactant than for an ODEAO water solution.

Inorganic brine (= calcium chloride (CC, $CaCl_2$ = 111.0) solution) has been used in actual heat energy transportation systems until recently, even though it presents some problems (including corrosion of steel and damage to equipment). CC solution is a strong acid and strong base solution. Potassium acetate (PA, CH_3COOK = 98.15) solution has been developed as a new type of brine for use in place of EG or PG solution, since its biodegradability is more rapid than that of glycol-based solutions and the environmental load is relatively small [12]. PA solution is a weak acid and strong base solution. However, there is very little quantitative data on the flow drag and heat transfer reduction effects of PA solution and CC solution. In order to apply flow drag and heat transfer reduction effects to these brine solutions, it is important to clarify the flow drag and heat transfer reduction characteristics of PA or CC solution with surfactant. In this paper, the pipe friction coefficient and mean forced convection heat transfer coefficient are investigated experimentally in a straight pipe for each of these solutions with surfactant, relative to the measurement parameters of brine concentration, surfactant concentration, and temperature of the brine solution.

2. Viscosity Measurement

It has been reported previously that EG and PG solutions with ODEAO are non-Newtonian fluids [5]. Thus, it is necessary to investigate the viscous characteristics of PA solution with ODEAO. In this study, the apparent viscosity of the solution was measured using a rotational (torsional) rheometer with a double gap cylinder sensor system (Viscotester VT550, Thermo Haake, Germany). This sensor system was able to measure low viscosity (0.5–10^4 mPa·s) of a small sample (4.5 cm^3) while a stepwise increase in the shear rate was imposed. The accuracy of the apparent viscosity measurements could be maintained within 6.0% by calibration with viscosity standards.

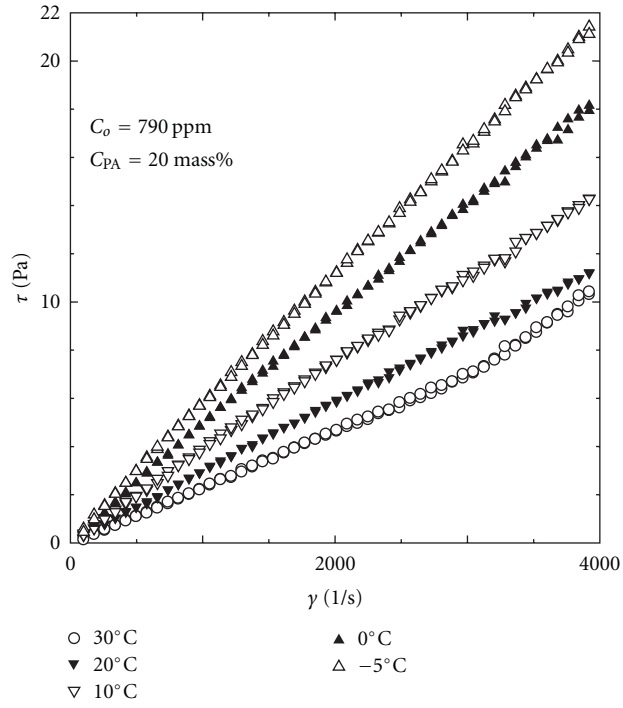

Figure 2: Relationship between γ and τ of PA solution with ODEAO.

Figure 2 shows the relationship between the shear rate γ (1/s) and the shear stress τ (Pa) of PA solution with ODEAO (ODEAO concentration: C_o = 790 ppm and PA concentration: C_{PA} = 20 mass%) for various solution temperatures (T_o = −5–30°C). The shear stress τ at T_o = 30°C indicated an increase in the high shear rate range (γ > 3000 1/s). This increase was caused by the generation of Taylor flow. With the double cylindrical rotor, Taylor flow was generated under low-viscosity and high-speed rotational conditions. However, the viscosity could not be measured under these conditions. Therefore, data indicative of Taylor flow was omitted from the viscosity measurements. As Figure 2 shows, the shear stress τ (Pa) at T_o = 30°C varied linearly with the shear rate γ (1/s). However, the shear stress τ (Pa) did not vary linearly with the shear rate γ (1/s) at lower solution temperatures (T_o < 20°C). This indicates that PA solution with ODEAO is a non-Newtonian fluid, except when T_o = 30°C.

In order to quantify the viscosity characteristics of PA solution with ODEAO, the relationship between the shear stress and shear rate was fitted to a power-law model ($\tau = K\gamma^n$, where K (Pa·s^n) is the pseudoplastic viscosity and n is the

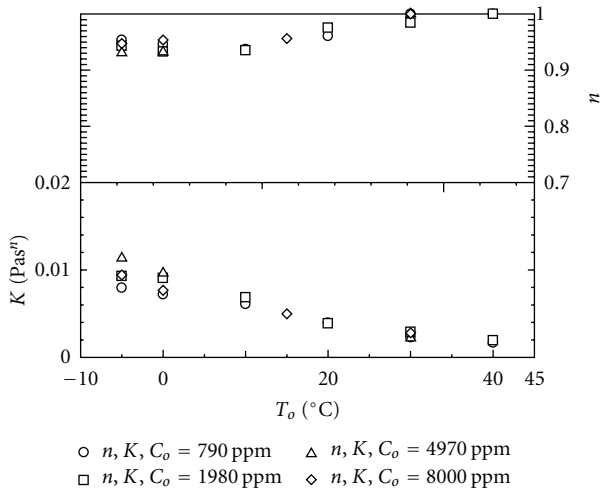

Figure 3: Relationship between T_o and K, n (C_{PA} = 20 mass%).

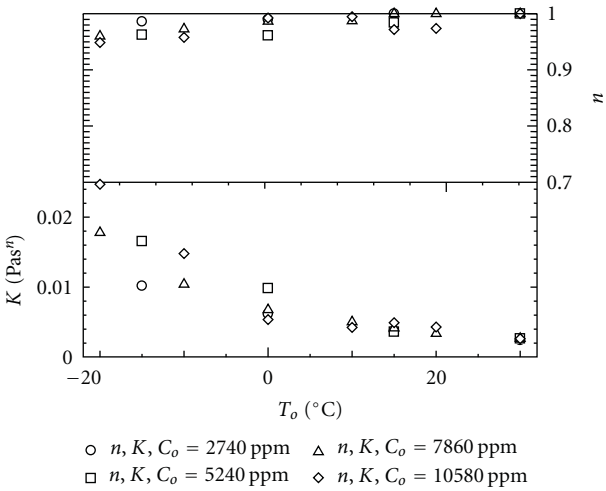

Figure 4: Relationship between T_o and K, n (C_{PA} = 30 mass%).

power-law exponent). Figures 3 and 4 show the relationship between K, n, and T_o for PA solutions with ODEAO and C_{PA} = 20 mass% and C_{PA} = 30 mass%, respectively. As these figures indicate, a decrease in the solution temperature led to a decrease in the power-law exponent n and an increase in the pseudoplastic viscosity K of the solution. These results show that a decrease in the solution temperature increased the non-Newtonian characteristics of PA solution with ODEAO. If the power-law exponent n was equal to 1 at higher solution temperatures, the solution became a Newtonian fluid under such conditions and the pseudoplastic viscosity K was equal to the viscosity μ.

The apparent viscosity of CC solution with ODEAO was not measured with the rotational rheometer. One reason for this was to avoid breakdown of the rheometer due to the corrosive effects of CC solution. Another reason was to verify that the apparent viscosity of CC solution with ODEAO was almost consistent with that of plain CC solution. From the nondimensional experimental result shown in Figure 14, the relationship between the pipe friction coefficient and the Reynolds number of CC solution with ODEAO without flow drag reduction effect was in agreement with the Blasius resistance formula in the turbulent flow range if the viscosity of CC solution was used as the apparent viscosity of CC solution with ODEAO.

3. Experimental Apparatus and Procedure

In order to examine the flow drag and heat transfer reduction characteristics of brine solutions with ODEAO, it is necessary to measure the pipe friction coefficients and mean heat transfer coefficients of these solutions. Figure 5 shows a schematic of the experimental apparatus used in this research. Since the apparatus was the same as that used in our previous work, only the main points are noted here. It was comprised of four units: a stainless steel test section (1.74 m length (L) × 0.016 m inside diameter (d_i)), a pump for circulating the test fluid, a low-temperature thermostatic water bath (with a minimum water temperature of −20°C), and an AC power supply unit for the heat input.

To determine the flow drag reduction effect, the pressure loss (ΔP) of the test fluid between the input and output of the test section was measured via a differential pressure gauge and manometer. The mean velocity (U_m) of the test fluid was measured with a magnetic flow meter. The pipe friction coefficient (λ) was then calculated from

$$\lambda = \frac{\Delta P}{L/d_i \cdot 1/2\rho U_m^2}, \tag{1}$$

where ρ is the density of the test fluid. The experimental uncertainty for the pipe friction coefficient (λ) was ±5.3%, allowing for other experimental uncertainties such as temperature ±0.1 K, pressure loss ±24 Pa, flow rate ±0.001 kg/s, and so forth.

The heat transfer characteristics were examined under constant heat flux conditions, provided by Joule heat. The mean heat transfer coefficient h_m (W/(m^2·K)) was calculated using the integrated equation (2). The local heat transfer coefficient ($h_x(x)$) in (2) was evaluated from the pipe wall temperature (T_{wx}) at the position (x) along the pipe, the bulk temperature of the test fluid (T_b), and the heat flux (Q/A, where Q is the input heat (W) and A is the heated area (m^2)). The wall temperatures were measured with 20 T thermocouples over the pipe length

$$h_m = \frac{1}{L}\int_0^L h_x dx = \frac{1}{L}\int_0^L \frac{Q}{A \cdot (T_{wx} - T_b)} dx. \tag{2}$$

The experimental uncertainty for the mean heat transfer coefficient (h_m) was ±7.5%, allowing for other experimental uncertainties (temperature ±0.1 K, heat flux ±0.8 W/m^2, flow rate ±0.001 kg/s, etc.).

In order to conduct non-dimensional analysis of the experimental results, the Reynolds number Re and Prandtl

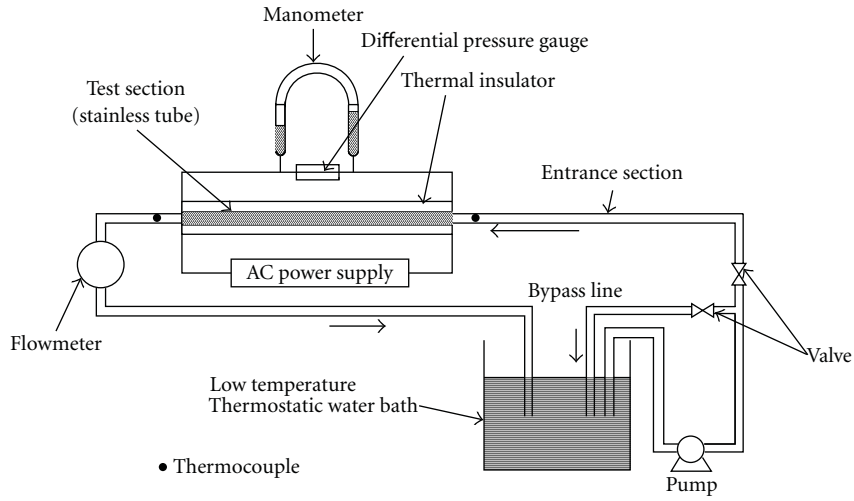

Figure 5: Schematic diagram of the experimental apparatus.

number Pr were determined from the following equations in the case of a Newtonian test fluid:

$$\mathrm{Re} = \frac{\rho \cdot U_m \cdot d_i}{\mu}, \qquad \mathrm{Pr} = \frac{\mu \cdot C_p}{\kappa}, \tag{3}$$

where μ is the viscosity, κ is the thermal conductivity, and C_p is the specific heat. When calculating Re and Pr for brine solutions with ODEAO, the values of the thermal conductivity κ, specific heat C_p, and density ρ of the brine solution (= solvent) were used, since the ODEAO concentrations were very low. The viscosities μ are shown as the pseudoplastic viscosity K in Figures 3 and 4, because the pseudoplastic viscosity K was equal to the viscosities μ in the case of a Newtonian test fluid.

In the case of a non-Newtonian fluid, the modified Reynolds number Re′ (4) and modified Prandtl number Pr′ (5) were calculated using the K and n values of the brine solutions with ODEAO:

$$\mathrm{Re}' = 8^{1-n}\left[\frac{3n+1}{4n}\right]^{-n}\left[\frac{\rho \cdot U_m^{2-n} \cdot d_i^n}{K}\right], \tag{4}$$

$$\mathrm{Pr}' = \frac{C_p \cdot [(3n+1)/4n]^n \cdot K \cdot [(8U_m)/d_i\ ]^{n-1}}{\kappa}. \tag{5}$$

If the test fluid was Newtonian ($n = 1$), the equations for Re′ and Pr′ reduced to the equations for Re and Pr.

Finally, the non-dimensional heat transfer coefficient (= Nusselt number) was defined by the following equation in these non-dimensional plots:

$$\mathrm{Nu} = \frac{h_m \cdot d_i}{\kappa}. \tag{6}$$

4. Experimental Results and Discussion

4.1. PA Solution with ODEAO (C_{PA} = 20 mass%). Figures 6 and 7 show the non-dimensional pipe friction coefficient (λ) and heat transfer coefficient ($\mathrm{Nu}/Pr'^{1/3}$), respectively, of a PA solution with ODEAO (ODEAO concentration C_o = 790 ppm and PA concentration C_{PA} = 20 mass%) for various solution temperatures (T_o). The solid lines represent the pipe friction coefficient and heat transfer coefficient of a Newtonian fluid in a laminar ((7) and (9)) and a turbulent flow ((8) and (10)):

$$\lambda = \frac{64}{\mathrm{Re}}, \tag{7}$$

$$\lambda = 0.3164 \cdot \mathrm{Re}^{-1/4}, \tag{8}$$

$$\mathrm{Nu} = 1.86 \cdot (\mathrm{Re} \cdot \mathrm{Pr})^{1/3} \cdot \left(\frac{d_i}{L}\right)^{1/3} \cdot \left(\frac{\mu}{\mu_w}\right)^{0.14}, \tag{9}$$

$$\mathrm{Nu} = 0.027 \cdot \mathrm{Re}^{0.8} \cdot \mathrm{Pr}^{1/3} \cdot \left(\frac{\mu}{\mu_w}\right)^{0.14}, \tag{10}$$

where μ_w is the apparent viscosity on the wall. As these figures indicate, the pipe friction coefficient (λ) and heat transfer ($\mathrm{Nu}/\mathrm{Pr}'^{1/3}$) at T_o = 20 and 30°C decreased according to (8) and (10) in the turbulent flow. These results imply that a PA solution with ODEAO at T_o = 20 and 30°C could show flow drag and heat transfer reduction effects. On the other hand, a PA solution with ODEAO at T_o = 0 and 10°C exhibited almost no drag reduction over the entire range of the modified Reynolds number.

Figure 8 shows the flow drag reduction rate (DR) and heat transfer reduction rate (HDR) of a PA solution with ODEAO, which could be used to evaluate the reduction rate

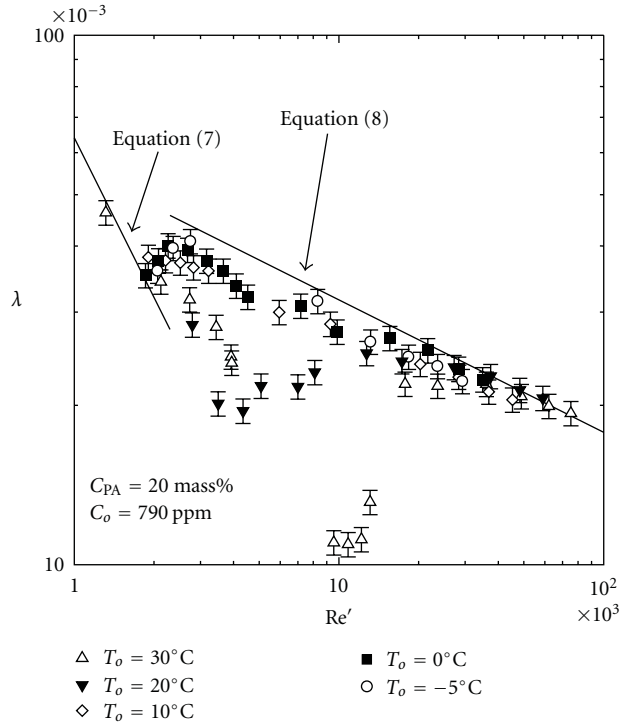

FIGURE 6: Relationship between Re′ and λ (C_{PA} = 20 mass%, C_o = 790 ppm).

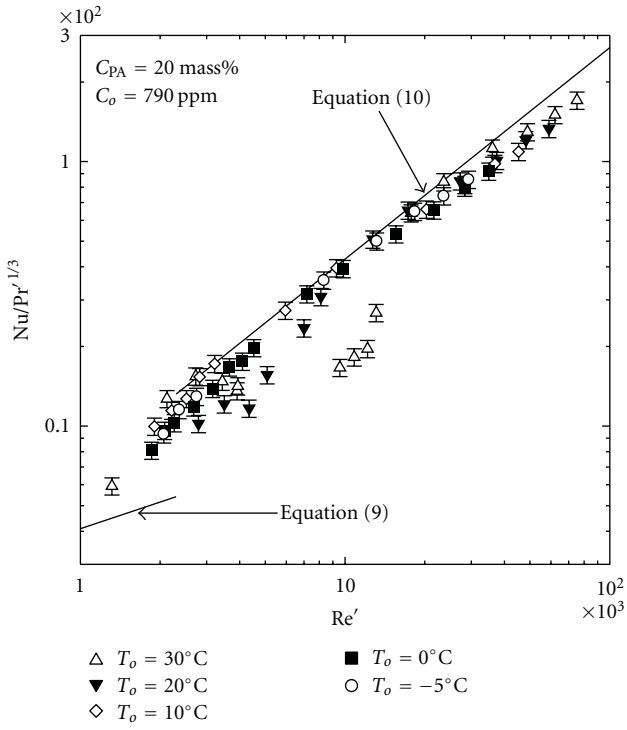

FIGURE 7: Relationship between Re′ and Nu/Pr′$^{1/3}$ (C_{PA} = 20 mass%, C_o = 790 ppm).

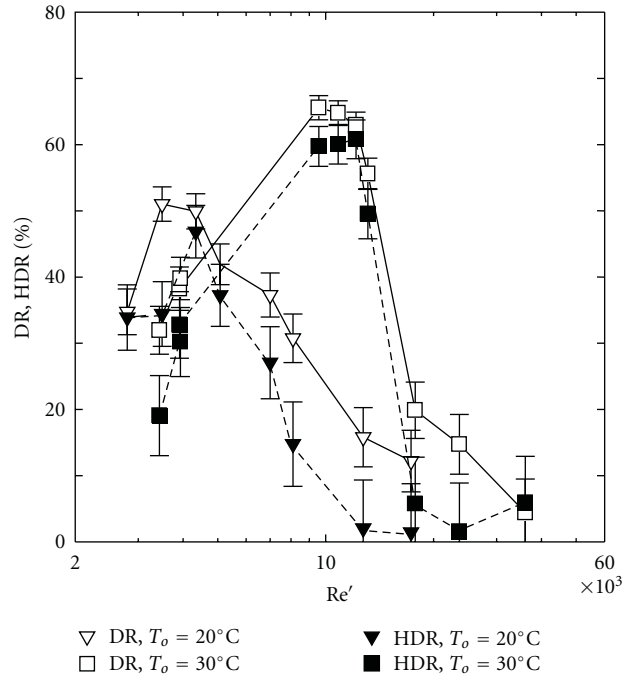

FIGURE 8: Relationship between Re′ and DR, HDR (C_{PA} = 20 mass%, C_o = 790 ppm).

of the pipe friction coefficient and the heat transfer. The DR and HDR values were defined by the following equations:

$$\begin{aligned} \mathrm{DR} &= \left(1 - \frac{\lambda}{\lambda_w}\right) \times 100, \\ \mathrm{HDR} &= \left(1 - \frac{\mathrm{Nu}}{\mathrm{Nu}_w}\right) \times 100, \end{aligned} \tag{11}$$

where λ_w and Nu_w are the pipe friction coefficient and heat transfer value of water under the same experimental conditions. Figure 8 indicates that DR at T_o = 30°C reached a maximum value of 65% at Re′ = 10000 and HDR at T_o = 30°C had almost the same value as DR. The range of Re′ in which the drag reduction effect existed was equal to the range of Re′ in which the heat transfer reduction effect appeared. In contrast, the maximum values of DR and HDR at T_o = 20°C were about 50% at Re′ = 4000, less than the value at T_o = 30°C and Re′ = 10000.

For quaternary ammonium salt cationic surfactants, the length of the rod-like micelles can be changed by increasing the solution temperature. When this type of solution contains aggregations above 40 nm in size, a large drag reduction effect is observed [13]. However, the effect suddenly disappears below an aggregate size of 30 nm. Assuming that the aggregation length changes with increasing solution temperature, aggregations of ODEAO rod-like micelles at only T_o = 20 or 30°C can result in an additional resistance against vortex stretching and turbulent eddy growth over the entire range of Re′. It can be inferred that the aggregation length of ODEAO rod-like micelles is more suitable for producing flow drag and heat transfer reduction effects at

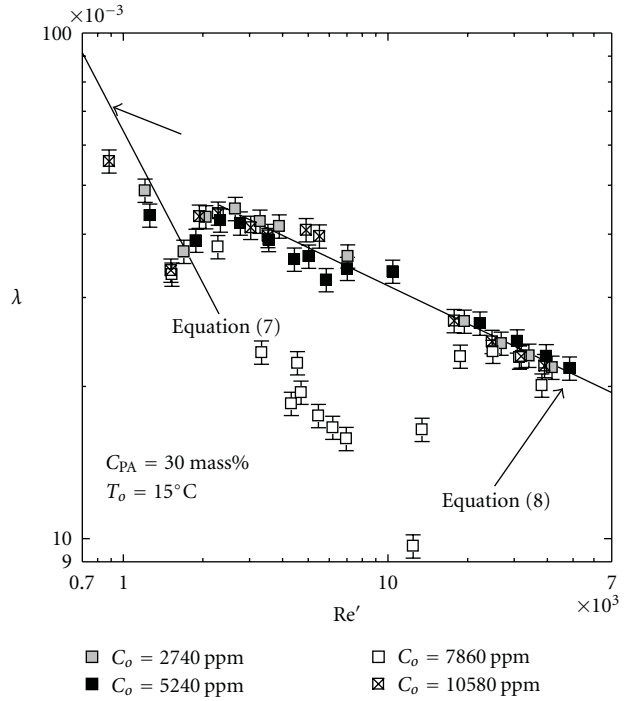

FIGURE 9: Relationship between Re′ and λ (T_o = 15°C, C_{PA} = 30 mass%).

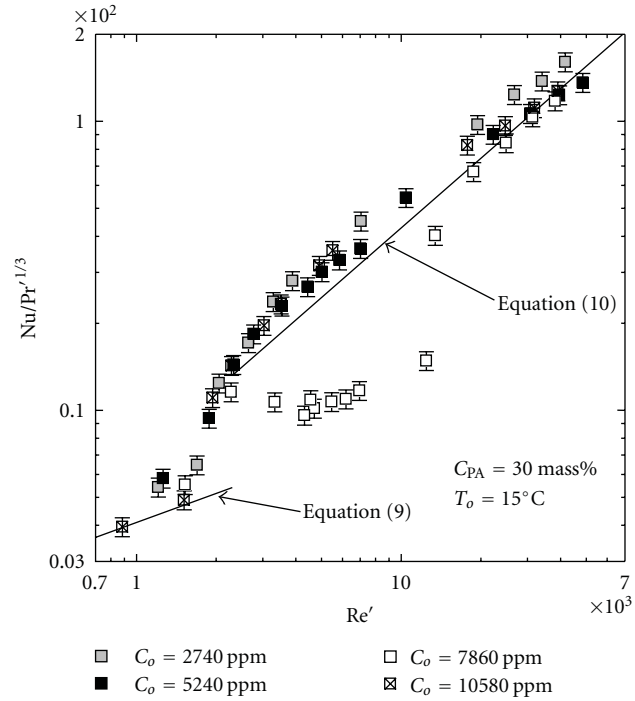

FIGURE 10: Relationship between Re′ and Nu/Pr′$^{1/3}$ (T_o = 15°C, C_{PA} = 30 mass%).

T_o = 30°C than at T_o = 20°C. When T_o = 0 or 10°C, the aggregation length is too long or too short to suppress vortex stretching and turbulent eddy growth, or else the micelles are not formed when the temperature decreases beyond a certain level.

In contrast, the flow drag and heat transfer reduction effects at C_{PA} = 20 mass% were refuted qualitatively at other ODEAO concentrations (C_o = 1980, 4970, and 8000 ppm). The reason for this seems to be that the rod-like micelles are transformed into lamellar or oblate micelles by increasing the ODEAO concentration and lamellar or oblate micelles cannot suppress vortex stretching and turbulent eddy growth.

4.2. PA Solution with ODEAO (C_{PA} = 30 mass%). Figures 9 and 10 show the variation of the flow drag and heat transfer reduction effects of a PA solution with ODEAO (T_o = 15°C and C_{PA} = 30 mass%) with respect to the ODEAO concentration (C_o). When C_{PA} = 30 mass%, the flow drag and heat transfer reduction effects were confirmed only for C_o = 7860 ppm, and there were no drag reduction effects under other experimental conditions (C_o = 2740, 5240, and 10580 ppm).

In a PA solution, potassium acetate molecules are hydrolyzed into potassium ions (K^+), hydroxide ions (OH^-) and acetic acid (CH_3COOH). Acetic acid is slightly ionized into acetate ions (CH_3COO^-) and hydrogen ions (H^+). Since the hydrophilic group (= hydroxyl group $-OH$) of an ODEAO molecule is hydrated by K^+ and CH_3COO^-, we inferred that ODEAO molecules could not form rod-like micelles at a low ODEAO concentration. Therefore, the flow drag and heat transfer reduction effects were lost at C_o = 2740 and 5240 ppm. In contrast, flow drag and heat transfer reduction effects could be observed at a high ODEAO concentration (C_o = 7860 ppm). This tendency was due to the formation of rod-like micelles of ODEAO after saturating the hydration reaction. However, the flow drag and heat transfer reduction effects were lost at C_o = 10580 ppm, because increasing the ODEAO concentration transforms the rod-like micelles to lamellar or oblate micelles [5].

When the ODEAO concentration was decreased (C_{PA} = 20 mass%), flow drag and heat transfer reduction effects of a PA solution with ODEAO were confirmed only at C_o = 790 ppm. This result indicates that rod-like micelles can be formed at a lower ODEAO concentration. This is because there is less K^+ and CH_3COO^- in the solution with C_{PA} = 20 mass% than in the solution with C_{PA} = 30 mass%, and hence the ODEAO concentration decreased when the hydration reaction was saturated.

Figures 11 and 12 show the relationship between the flow drag and heat transfer reduction effects of a PA solution with ODEAO (C_o = 7860 ppm and C_{PA} = 30 mass%) and the solution temperature (T_o). The flow drag and heat transfer reduction effects were measured in a range of solution temperatures from 15 to 20°C, due to the increasing length of the rod-like micelles with increasing solution temperature. However, the length transition of the micelles at C_{PA} = 30 mass% was different from that at C_{PA} = 20 mass%. Therefore, the drag reduction temperature ranges at C_{PA} = 30 mass% and C_{PA} = 20 mass% were different. The flow drag reduction

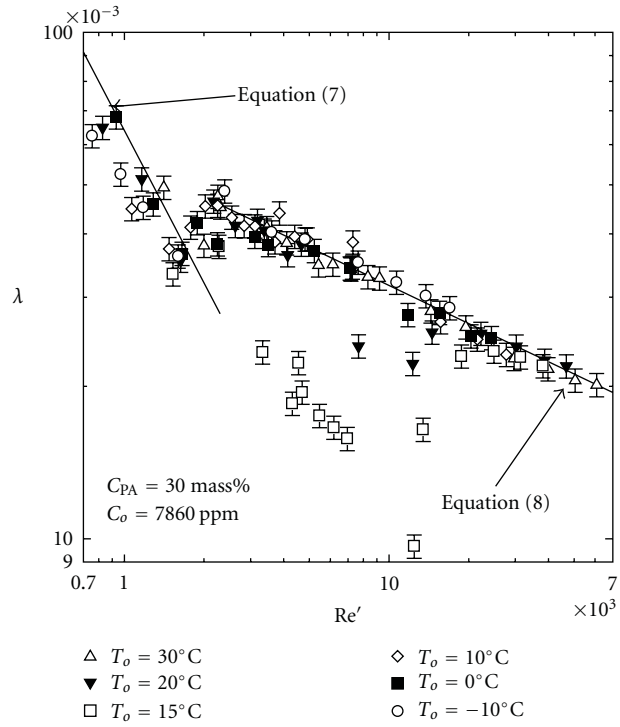

Figure 11: Relationship between Re′ and λ (C_{PA} = 30 mass%, C_o = 7860 ppm).

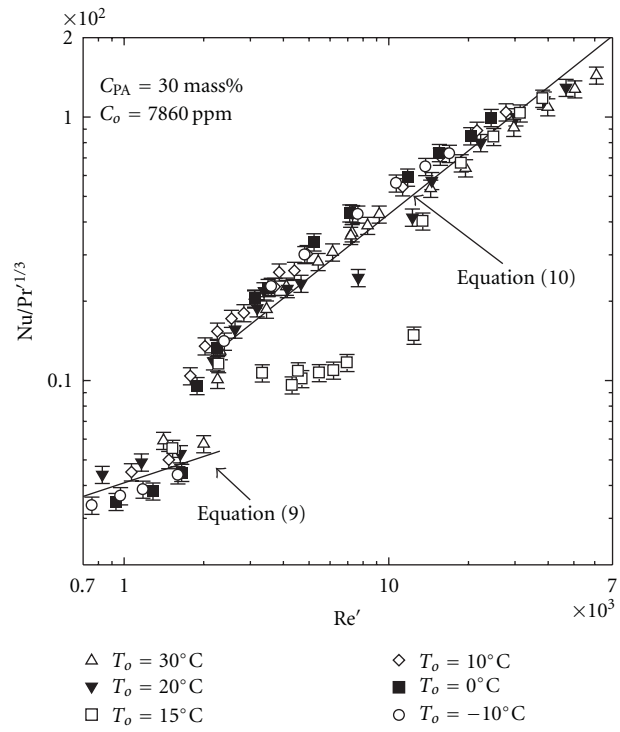

Figure 12: Relationship between Re′ and Nu/Pr′$^{1/3}$ (C_{PA} = 30 mass%, C_o = 7860 ppm).

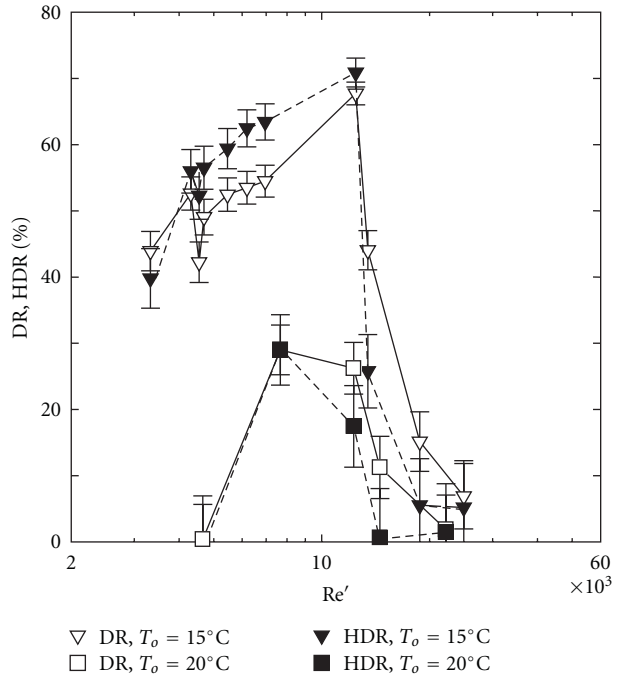

Figure 13: Relationship between Re′ and DR, HDR (C_{PA} = 30 mass%, C_o = 7860 ppm).

rate (DR) and heat transfer reduction rate (HDR) of a PA solution with ODEAO (C_o = 7860 ppm and C_{PA} = 30 mass%) are shown in Figure 13. The maximum values of DR and HDR were about 60% and were almost the same as those of Figure 8 (C_{PA} = 20 mass%). However, the maximum values of DR and HDR at C_{PA} = 30 mass% occurred at T_o = 15°C, which was different from the case of C_{PA} = 20 mass%. We hypothesized that this temperature difference was caused by a critical length change of the rod-like micelles with increasing PA concentration.

Taking these experimental results into account, we inferred that it would be difficult to use PA solution with ODEAO as an actual heat transfer medium. The reason is that flow drag and heat transfer reduction effects can only be exhibited under particular conditions.

4.3. CC Solution with ODEAO. Figures 14 and 15 show the experimental results for the pipe friction coefficient (λ) and heat transfer (Nu/$Pr^{1/3}$) of a CC solution with ODEAO (C_{CC} = 10 mass% and C_o = 3000, 6000, and 9000 ppm), and Figure 16 shows the relationship between Re and DR, HDR. Figures 14 and 15 indicate that flow drag and heat transfer reduction effects appeared at T_o = 20 and 30°C for C_o = 6000 and 9000 ppm. In particular, at around Re = 1.2×10^4, the pipe friction coefficient (λ) and heat transfer (Nu/$Pr^{1/3}$) increased markedly with slightly increasing Re (Re ranging from 1.25×10^4 to 1.26×10^4) in the case C_{CC} = 10 mass% and C_o = 9000 ppm. This is caused by breakage of the rod-like micelles due to wall shear stress. This result indicates that the wall shear stress at the minimum value of the pipe friction coefficient (λ) has been estimated precisely. Comparison of

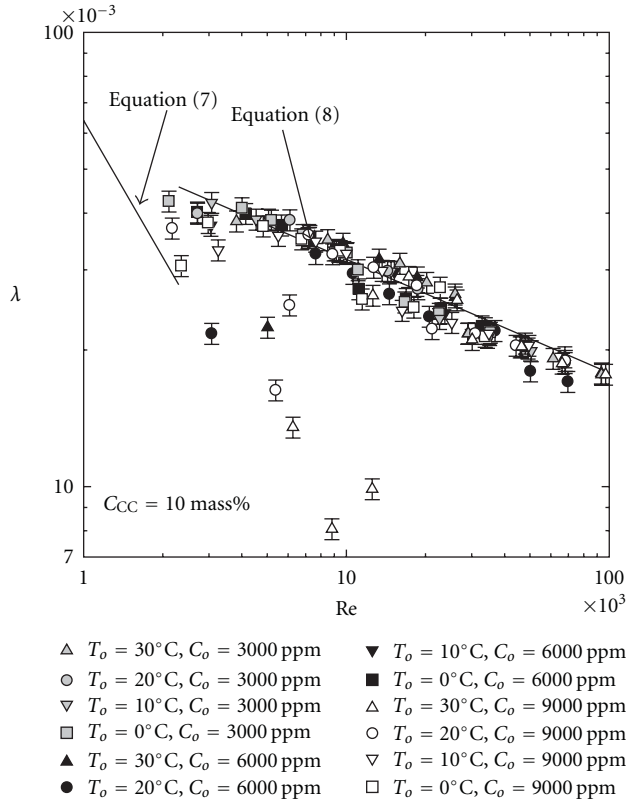

Figure 14: Relationship between Re and λ (C_{CC} = 10 mass%).

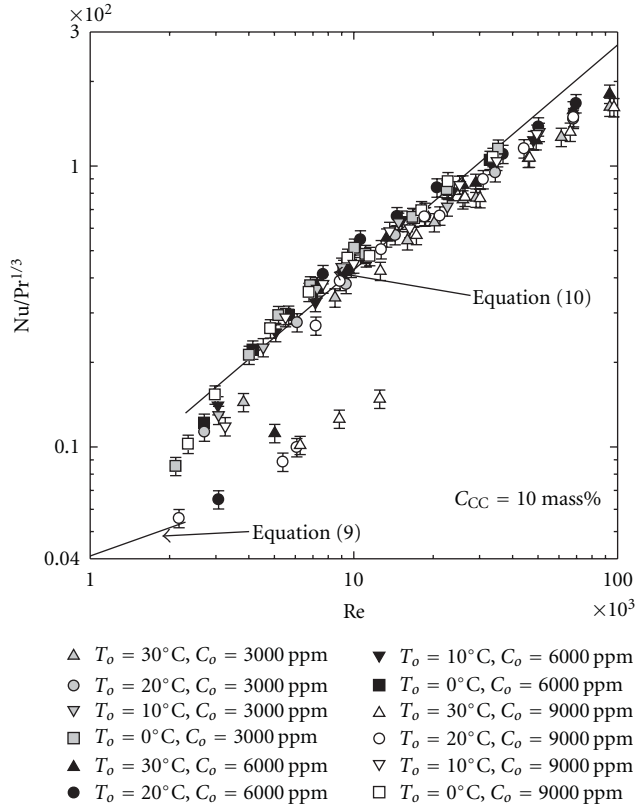

Figure 15: Relationship between Re and Nu/Pr $^{1/3}$ (C_{CC} = 10 mass%).

Figures 8 and 13 shows that the DR and HDR tendencies of the CC solution with ODEAO (C_{CC} = 10 mass% and C_o = 9000 ppm) were almost the same as those of the PA solution with ODEAO.

However, the Reynolds number range for flow drag and heat transfer reduction effects in a CC solution with ODEAO was smaller at C_o = 6000 ppm than at C_o = 9000 ppm. No flow drag and heat transfer reduction effects occurred at C_o = 3000 ppm. This tendency is probably due to the fact that the length or number of rod-like micelle aggregations increases with increasing ODEAO concentration and the length or number of rod-like micelle aggregations is most suitable for flow drag and heat transfer reduction effects at C_o = 9000 ppm.

In contrast, flow drag and heat transfer reduction effects in case of increasing CC concentration (C_{CC} = 20 mass%) were not confirmed. This is due to the decrease in the cloud point of the CC solution with increasing mineral salt (CC) concentration. If the solution temperature exceeds the cloud point, dissolved surfactants are no longer completely soluble and it is difficult to form surfactant micelles.

When CC is added to another nonionic surfactant solution [14], the cloud point at C_{CC} = 10 mass% is estimated to be about 30°C and the cloud point at C_{CC} = 20 mass% is estimated to be about −48°C. Therefore, a CC solution with ODEAO at C_{CC} = 10 mass% and temperatures of 20 or 30°C is capable of exhibiting flow drag and heat transfer reduction effects, since these experimental temperatures are

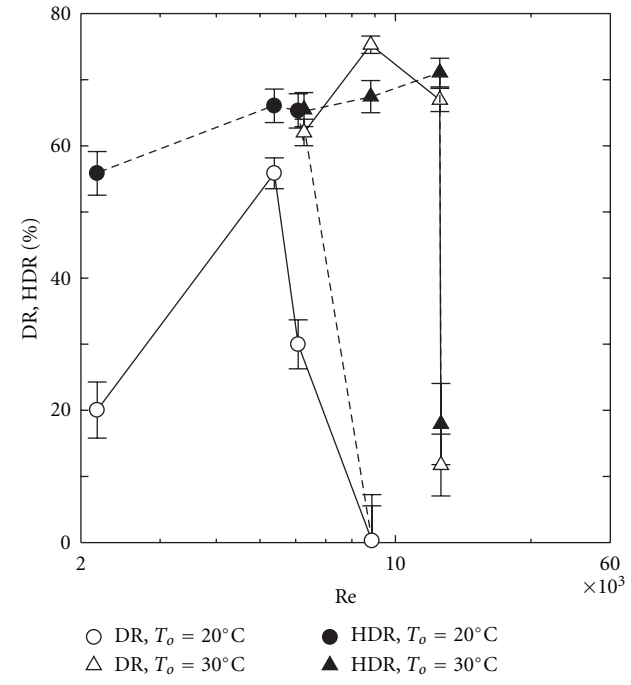

Figure 16: Relationship between Re and DR, HDR (C_{CC} = 10 mass%, C_o= 9000 ppm).

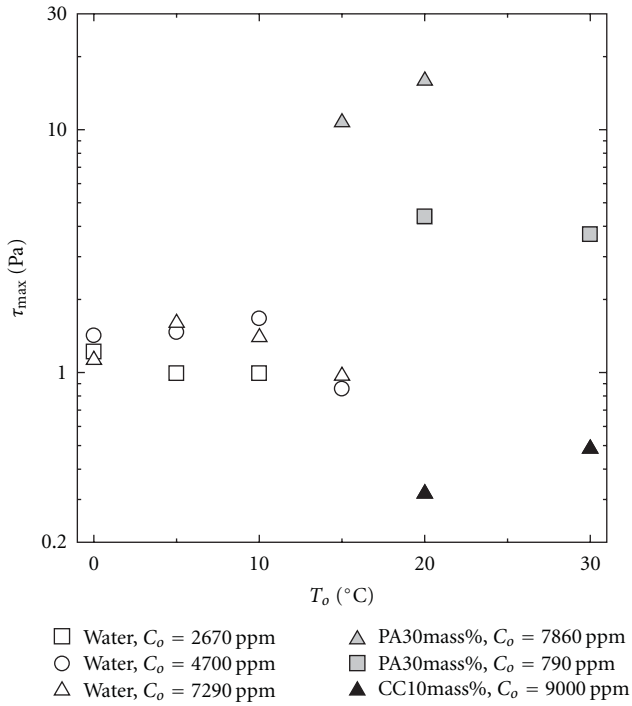

FIGURE 17: Relationship between T_o and τ_{max} of PA and CC solutions with ODEAO.

lower than the cloud point (30°C). On the other hand, at C_{CC} = 20 mass%, the experimental temperatures are higher than the cloud point (−48°C), and hence rod-like micelles cannot be formed in this case.

Finally, the experimental results indicate that flow drag and heat transfer reduction effects of a CC solution with ODEAO occurred only at C_{CC} = 10 mass% and C_o = 9000 ppm. This suggests that it would be difficult to use CC solution with ODEAO as a heat transfer medium.

4.4. Critical Wall Shear Stress. Previous research (e.g., [5]) has indicated that drag reduction disappears when the wall shear stress exceeds a critical value. In order to understand the flow drag reduction effect of a PA or CC solution with ODEAO, the critical wall shear stress (τ_{max}) at the minimum value of the pipe friction coefficient (λ) was investigated and compared with the critical wall shear stress (τ_{max}) of the ODEAO water solution. The wall shear stress (τ_{max}) in a fully developed pipe flow is related to the pressure drop (ΔP) by the following equation:

$$\tau_{max} = \frac{\Delta P d_i}{4L}. \quad (12)$$

Figure 17 shows the relationship between T_o and τ_{max} for a PA or CC solution with ODEAO, as well as for an ODEAO water solution. This graph indicates that the critical wall shear stress (τ_{max}) of the PA solution with ODEAO was higher than that of the ODEAO water solution. This increase in τ_{max} is probably due to solubilization between the PA molecules and the rod-like micelles of the ODEAO. As a result, the PA molecules are slightly mixed with the micelles and the micelles are reinforced by this mixture.

The critical wall shear stress (τ_{max}) of the CC solution with ODEAO was slightly less than that of the ODEAO water solution. This result suggests that there is no solubilization between the rod-like micelles of the ODEAO and the CC molecules and that the micelles become weak in a strongly acid brine solution such as CC solution. Hence, we hypothesized that the formation of rod-like micelles in an ODEAO is related to the ionic strength of the brine solution.

5. Conclusions

Pipe friction coefficients and mean heat transfer coefficients were measured to investigate the flow drag and heat transfer reduction effects of potassium acetate (PA) solution and calcium chloride (CC) solution with the surfactant ODEAO. The experimental parameters considered were PA concentration, CC concentration, ODEAO concentration, and solution temperature. The following conclusions may be drawn from the results and discussion.

(1) The flow drag and heat transfer reduction effects of PA solution with ODEAO and PA concentration = 20 mass% were confirmed only under particular conditions (ODEAO concentration of 790 ppm and solution temperatures of 20 and 30°C). The reason for this result is that the length of the rod-like micelles of ODEAO in the solution is not always suitable for producing a drag reduction effect, since the aggregation length of the micelles is dependent on the solution temperature and ODEAO concentration.

(2) When the PA concentration = 30 mass%, the ODEAO concentration that produces flow drag and heat transfer reduction effects (= 7860 ppm) was larger than in the case of 20 mass% concentration (= 790 ppm). This increase in PA concentration also increased the saturation concentration of the hydration reaction.

(3) CC solution with ODEAO at a CC concentration of 10 mass% could produce flow drag and heat transfer reduction effects, but there was no drag reduction at a CC concentration of 20 mass%. This is due to the decreasing cloud point of the CC solution with increasing CC concentration.

(4) The critical wall shear stress of a PA solution with ODEAO was larger than that of an ODEAO water solution, whereas the critical wall shear stress of a CC solution with ODEAO was slightly less than that of an ODEAO water solution. For a strongly acid brine solution such as CC solution, there was no solubilization between the rod-like micelles of ODEAO and the CC molecules and the micelles became weak. Therefore, it can be concluded that the formation of rod-like micelles in a nonionic surfactant is related to the ionic strength of the brine solution.

(5) In view of these findings, it would be difficult to put PA and CC solutions with ODEAO to practical

use as heat transfer media, since the flow drag and heat transfer reduction effects of these solutions only appear under limited conditions.

Acknowledgment

The authors would like to thank Mr. Kazuma Yamagata for his cooperation in this study.

References

[1] T. Nakata, H. Inaba, A. Horibe, N. Haruki, and K. Sato, "Surfactant development as a flow drag reduction agent in piping," *Japanese Journal of Tribology*, vol. 49, no. 1, pp. 1–10, 2004.

[2] Y. Kawaguchi, Y. Tawaraya, A. Yabe, K. Hishida, and M. Maeda, "Active control of turbulent drag reduction in surfactant solutions by wall heating," vol. 237, pp. 47–52.

[3] K. Sato, J. Mimatsu, and M. Kumada, "Turbulent characteristics and heat transfer augmentation of drag reduceing surfactant solution flow," *Thermal Science and Engineering*, vol. 7, no. 1, pp. 41–52, 1999.

[4] H. Inaba, N. Haruki, T. Nakata, A. Horibe, N. Furumoto, and K. Sato, "Heat transfer enhancement of water flow in a straight pipe with drag reduction surfactant by using wire coil," *Transactions of the Japan Society of Mechanical Engineers, Part B*, vol. 68, no. 666, pp. 481–488, 2002.

[5] J. L. Zakin, B. Lu, and H. W. Bewersdorff, "Surfactant drag reduction," *Reviews in Chemical Engineering*, vol. 14, no. 4-5, pp. 253–320, 1998.

[6] B. Lu, X. Li, J. L. Zakin, and Y. Talmon, "A non-viscoelastic drag reducing cationic surfactant system," *Journal of Non-Newtonian Fluid Mechanics*, vol. 71, no. 1-2, pp. 59–72, 1997.

[7] J. G. Savins, "A stress-controlled drag-reduction phenomenon," *Rheologica Acta*, vol. 6, no. 4, pp. 323–330, 1967.

[8] N. Haruki, H. Inaba, A. Horibe, and S. Tanaka, "Flow drag and heat transfer characteristics of organic brine with drag reduction surfactant in a straight pipe," *Transactions of the Japan Society of Mechanical Engineers, Part B*, vol. 23, no. 4, pp. 479–490, 2006.

[9] N. Haruki, H. Inaba, A. Horibe, and S. Tanaka, "Viscosity measurements of ethylene glycol solution with flow drag reduction additives," *Heat Transfer—Asian Research*, vol. 35, no. 8, pp. 553–567, 2006.

[10] N. Haruki, H. Inaba, A. Horibe, Y. Kodama, and K. Yamagata, "Flow drag and heat transfer characteristics of organic brine with drag reduction surfactant in a straight pipe (2nd report, influences of another kind of organic brine)," *Transactions of the Japan Society of Mechanical Engineers, Part B*, vol. 74, no. 12, pp. 2578–2587, 2008.

[11] N. Haruki, H. Inaba, A. Horibe, and Y. Kodama, "Flow resistance and heat transfer characteristics of organic brine (propylene glycol) solution by adding flow drag reduction additive," *Experimental Heat Transfer*, vol. 22, pp. 283–299, 2009.

[12] K. Tomita, H. Shirato, T. Sasaki et al., "Development of low environmental loading antifreeze solution for road heating," *Hokkaido Industrial Research Institute Report*, no. 304, pp. 33–40, 2005.

[13] T. Horiuchi, T. Majima, T. Yoshii, and T. Tamura, "Effect of alkyl chain length and number of 2-hydroxyethyl groups on drag reduction behaviors of quaternary ammonium salt-type cationic surfactant solutions," *Nippon Kagaku Kaishi*, no. 7, pp. 423–428, 2001.

[14] T. Kariyone, "Characteristics and application of surfactant," *Saiwaishobo, Tokyo*, pp. 47–55, 1988.

Hindawi Publishing Corporation
Advances in Mechanical Engineering
Volume 2011, Article ID 315943, 10 pages
doi:10.1155/2011/315943

Research Article

Enhancing Heat Transfer of Drag-Reducing Surfactant Solution by an HEV Static Mixer with Low Pressure Drop

Haifeng Shi,[1] Yi Wang,[2] Wu Ge,[3] Bo Fang,[4] Jacob T. Huggins,[1] Thaddaus R. Huber,[1] and Jacques L. Zakin[1]

[1] *Department of Chemical and Biomolecular Engineering, Ohio State University, 140 West 19th Avenue, Columbus, OH 43210, USA*
[2] *Beijing Key Laboratory of Urban Oil and Gas Distribution Technology, China University of Petroleum-Beijing, Beijing 102249, China*
[3] *Kraft Foods Global Research, Glenview, IL 60025, USA*
[4] *Research Center of Chemical Engineering, East China University of Science and Technology, 130 Meilong Road, Shanghai 200237, China*

Correspondence should be addressed to Jacques L. Zakin, zakin.1@osu.edu

Received 27 February 2011; Accepted 2 April 2011

Academic Editor: Bo Yu

A novel high-efficiency vortex (HEV) static mixer was used to locally enhance the heat transfer coefficient of a drag-reducing fluid, Ethoquad O/12 (EO12) (3 mM) with sodium salicylate (NaSal) (5 mM). Significant enhancement of heat transfer coefficients was observed. The Nusselt numbers were three to five times those of normal drag-reducing flow without mixer and were close to those of water at high Reynolds number with only modest energy penalty. In contrast, a Helix static mixer increased Nusselt number slightly with very high pressure loss. A performance number was used for comparisons among the HEV static mixer, the Helix static mixer, and water without mixer. The HEV static mixer had a performance number comparable to that of water. The enhanced heat transfer by the HEV static mixer resulted from streamwise vortices generated by the inclined tabs, which increased the convective heat transfer in the radial direction.

1. Introduction

Many solutions of polymers [1, 2] or surfactants [3] show reduced pressure loss compared with water at the same Reynolds number (based on water or solvent). This reduction in pressure loss, known as turbulent drag reduction (DR), can be utilized to reduce energy requirements for pumping the fluids. Polymer drag reducing agents (DRAs) have been utilized in the Trans-Alaska crude oil pipeline [4, 5] and in fire fighting [6] and have been studied for many other applications [7]. However, polymeric DRAs lose drag reducing effectiveness in pumping because their relatively long molecules are degraded in high shear stress regions of piping systems [8]. Therefore, to maintain their drag reduction effectiveness, polymeric DRAs have to be replenished after each pumping station. Surfactant drag reducing solutions, on the other hand, retain their drag reduction ability even in recirculation systems without the constant addition of surfactant DRAs, because the surfactant wormlike micelles, which are essential to induce drag reduction [3, 9–11] can reassemble after being temporarily broken up by high shear stress [3, 12]. Thus, surfactant DRAs are promising for use in recirculation systems such as district heating or cooling systems (DHCS) [3, 13, 14].

However, drag reduction is accompanied by heat transfer reduction for both polymeric [15–19] and surfactant [12, 20–23] DRAs. Heat transfer reduction is found to be always greater than drag reduction for a given Reynolds number [17, 24, 25]. Aguilar et al. [26] examined the coupling issue between drag reduction and heat transfer reduction (HTR) for both polymer and surfactant DRAs. They found the ratio between the heat transfer reduction and drag reduction was nearly constant from the onset of DR to the departure from the asymptotic regime. They [27] also determined the ratio of the maximum heat transfer reduction asymptote to the maximum drag reduction asymptote to be 1.06 for $\mathrm{Re} > 20,000$.

The mechanism of the reduced heat transfer has been investigated. Sellin et al. [28] found the viscous sublayer region in drag-reducing surfactant solutions was significantly thicker than that in Newtonian fluids. This thicker viscous sublayer provides greater thermal resistance between the bulk drag-reducing fluid and the wall of the heat exchanger, and therefore decreases the heat transfer ability of the solution [29]. At the same time, the velocity fluctuations in the radial direction in turbulent flow are also greatly suppressed [30, 31], resulting in reduced heat transfer in the radial direction [29]. A few other characteristics of Newtonian turbulent flow were observed to be different in drag reducing flow. With the aid of particle imaging velocimetry, the disappearance of strong vorticity fluctuation [32] and reduced strength and inhibited frequency of turbulent bursts [33, 34] were observed. And reduced wall-normal (radial) turbulence intensity was also observed by Laser Doppler velocimetry [35, 36]. In short, the reduced heat transfer is due to the thickened viscous sublayer and the inhibited radial turbulence, which are caused by wormlike micelles in surfactant drag reducing solutions.

This reduced heat transfer ability is a serious drawback in applying DR surfactant solutions to DHCS. So it is necessary to enhance the heat transfer ability locally in heat exchangers of DHCS without incurring a major energy penalty. Many devices have been studied to temporarily enhance the heat transfer ability of surfactant drag-reducing solutions either by destroying the wormlike micelles or by disturbing the flow to enhance turbulence. To break the wormlike micelle structures of surfactant solutions, ultrasonic energy [21] was used, and heat transfer was enhanced slightly, but this method was not economical in energy cost. Other methods such as fluted tube heat exchanger [20], wire meshes [37], static mixers [12], and impinging jets [38] were aimed to temporarily break the wormlike micelles; they actually also disturbed the flow, but their relative contributions to enhanced heat transfer are not clear. To disturb the flow, still other methods employed were contracted channel [39], grooved tubes [40], wire coils [41], helical pipes [42], and vortex generators [43].

However, the secondary flow and vortices generated by these methods are randomly directed, which means there exists mixing in the flow direction as well as in the direction normal to the flow. Since heat transfer in heat exchangers is essentially in the normal direction, the mixing in the flow direction does not help enhance heat transfer. Therefore, the brute and unorganized disturbance by the above devices costs unnecessary energy losses by inducing unnecessary mixing in the flow direction. A novel static mixer [44], commonly called a high-efficiency vortex (HEV) static mixer, has been designed to generate organized streamwise vortices, which promote mixing in the direction normal to the flow. This static mixer consists of arrays of tabs inclining from the conduit wall in the flow direction at a certain angle, so that streamwise and counter-rotating vortices interconnecting neighboring ones can be naturally generated at the tab tips. These special vortices are designed to enhance the mixing process and heat transfer between the conduit wall and the bulk fluid. The turbulent flow structure modified by an HEV static mixer has been studied. Both intensified and inhomogeneous or anisotropic turbulent structures were observed [45]. Counter-rotating vortices behind the tabs were shown both by experiments and simulations [46–48]. An HEV static mixer enhanced heat transfer and mixing in chemical reactions in integrated chemical reactor-heat exchangers [46, 49, 50].

Due to the organized streamwise vortices, which enhance radial convective transfer, HEV static mixers cost significantly lower pressure drop or energy loss than other conventional mixers to achieve equivalent performance in various applications [51]. Fasano [52] reported that an HEV static mixer required only one twelfth to one third of the pressure drop of other conventional mixers to achieve the equivalent blending performance and thermal mixing efficiency. In some emulsification processes, an HEV static mixer was 1000 times more energy efficient than other mixers [45, 53]. It was also energetically efficient in enhancing heat transfer between two immiscible liquid phases in turbulent flow [54].

Surprisingly, HEV has not received attention in enhancing heat transfer in drag reducing flows despite its energetically economical applications in mixing and heat transfer. In this paper, the effect of an HEV static mixer on the heat transfer of a drag reducing surfactant solution, namely, EO12/NaSal (3 mM/7.5 mM), was studied experimentally and compared with a common inline static mixer. The rheological properties and drag reduction ability of the surfactant solution were also measured.

2. Experimental

2.1. Materials. The surfactant studied, EO12 (Ethoquad O/12 PG, donated by AkzoNobel), is a mixture of oleyl bis(2-hydroxyethyl)methyl ammonium chlorides (75 wt%) and propylene glycol (25 wt%). NaSal (sodium salicylate, purity > 99.8%) was purchased from Fisher Scientific. Surfactant/counterion solutions were prepared for drag reduction and heat transfer experiments by stirring in a container for 8 hours at room temperature by a high shear disperser (Janke & Hunkel IKA Ultra-Turrax SD-45), followed by overnight storage at rest. Smaller solutions were prepared using magnetic stirrers in a beaker before rheological measurements.

The inner diameter of the tube-in-tube heat exchanger is 10.2 mm. Since the commercially available HEV static mixers from Chemineer, Inc. are 2 inches in diameter or larger, a small HEV static mixer was fabricated. Tabs were first shaped by cutting the wall of a stainless steel tube with a 10 mm outer diameter and 9 mm inner diameter (purchased from McMaster-Carr), and then were pushed inwards and they formed a 30° angle with the tube wall. As shown in Figure 1(a), the isosceles trapezoidal tabs are 5 mm high and 5 mm and 3 mm in the wall base and the end base, respectively. A group of three tabs are evenly distributed around the circle of one cross section of the tube. (Figure 1(b) is the cross section view of a tab group). 32 such groups are evenly spaced at 28 mm intervals along the tube.

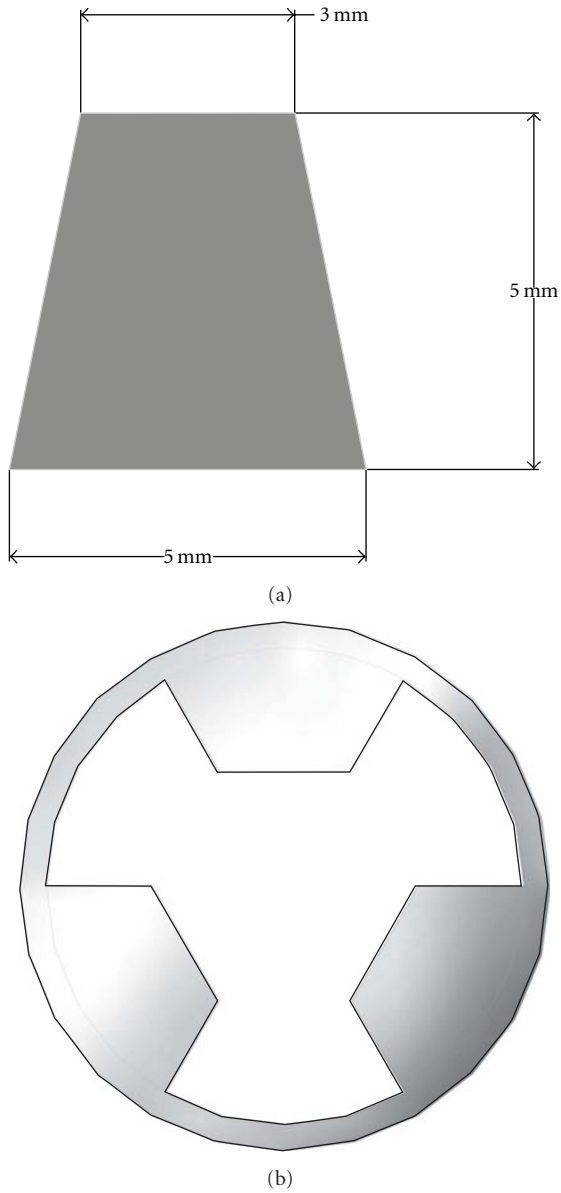

Figure 1: (a) Tab dimensions, (b) cross section view of a group of three tabs.

The distance between the wall base of the first tab group and the downstream end of the HEV tube is 868 mm, illustrated in Figure 2(a). Figure 2(b) is the overall view of the 1009 mm long HEV static mixer tube, which was inserted inside the tube-in-tube heat exchanger.

The plastic Helix static mixer, purchased from Cole-Parmer, had 10 helix elements, each element twisted in the opposite helical direction to the neighboring elements. Each element is 10 mm long and has an outer diameter of 10 mm (Figure 2(c)). This Helix static mixer was mounted inside the entrance of the tube-in-tube heat exchanger in some of the experiments.

2.2. Rheological Measurements. The first normal stress difference (N_1) and viscosity of the micellar solutions as functions of shear-rate were measured on an ARES rheometer

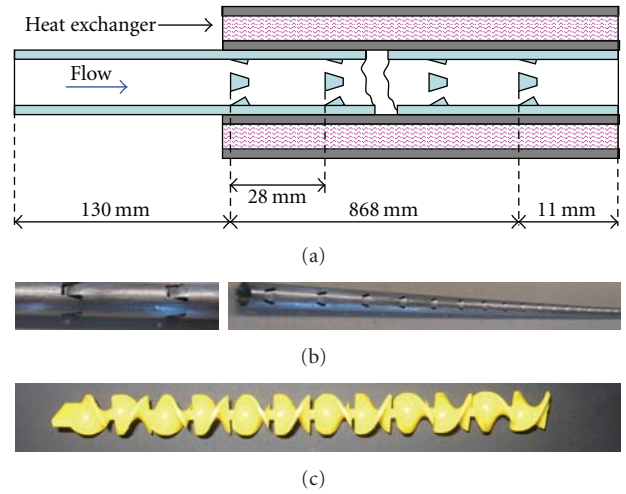

Figure 2: (a) HEV static mixer tab locations, (b) partial view (left) and overview (right) of the HEV static mixer tube, (c) an original 12-element Helix static mixer.

(TA instruments) using a 50 mm cone-and-plate geometry (0.02 rad cone angle). The measured N_1 readings were corrected for inertial effects according to the following relation [55]:

$$N_1^{\text{corrected}} = N_1^{\text{measured}} + 0.15\,\rho\omega^2 R^2, \tag{1}$$

where ρ is the density of the solution, ω is the angular velocity, and R is the radius of the cone.

2.3. Recirculation System. Figure 3 shows a schematic of the recirculation system for drag reduction and heat-transfer experiments. This recirculation loop consists of a centrifugal pump (PROCON), a reservoir tank, an electric heater (TrueHeat 1500 W), two heat exchangers, and a magnetic flow meter (TOSHIBA LF404) connected by smooth stainless steel tubes of 10.2 mm inner diameter (ID) and 12.7 mm outer diameter (OD). The recirculation loop has a total length of about 25 m and can hold up to 16 L of liquid. The reservoir tank has a volume of 14 L.

The pump rotation rate can be controlled in the range of 0 to 1969 rpm by a motor controller (BALDOR Adjustable Speed Drive). The flow rate (0.04 to 0.35 L/s) is monitored by the magnetic flow meter. The electric heater maintains the main loop temperature from room temperature up to ~60°C. A chiller (Bay Voltex) in the annulus loop of the fluted tube-in-tube heat exchanger (with a coolant of 50% ethylene glycol and 50% water) cools and maintains the temperature of the main loop as low as 0°C. The inner tube of the 0.914 m long tube-in-tube heat exchanger is 10.2 mm and 12.7 mm in ID and OD, respectively. The ID of the outer shell is 50 mm. Heat transfer measurements are taken on this tube-in-tube heat exchanger. The temperature of the shell side of this tube-in-tube heat exchanger is mediated by the circulators (NESLAB RTE-111 and VWR 1160) connected in series and can be varied from 0° to 90°C. The flow rate in the shell side of the tube-in-tube heat exchanger is preset for

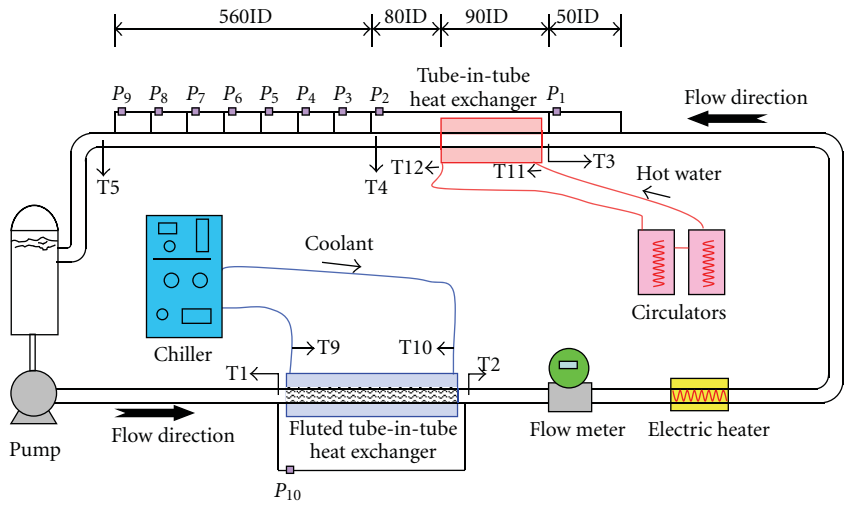

FIGURE 3: Schematic of apparatus for drag reduction and heat transfer experiments.

each experiment to keep the heat transfer resistance on the shell side constant.

All the tubes, pipes, and heat exchangers are insulated with Nomaco K-Flex polyolefin to minimize heat exchange with the environment. Temperatures at all locations are measured by T-type thermocouples (T1 through T4 and T9 through T12). The differential pressures of straight pipe sections are measured by the pressure transmitters (P_1 through P_{10}) (OMEGA PX2300 series). Transmitters P_1 through P_9 measure consecutive sections of straight pipe. P_1 measures the pressure difference across a section of 50 pipe diameters. P_2 measures the differential pressure across a pipe section of 180 diameters, including the tube-in-tube heat exchanger. P_3 through P_9 each measures differential pressures across 80 diameters length downstream of the tube-in-tube heat exchanger. All the thermocouples, pressure transmitters and flow meters are connected to the data acquisition system described by Ge [56].

2.4. Drag Reduction and Heat Transfer Measurement. To obtain %DR, pressure drops were measured in a range of flow rates at fixed temperatures. The friction factor was calculated according to the following equation:

$$f = \frac{\Delta P D}{2\rho L V^2}, \tag{2}$$

where f is the friction factor, ΔP is the pressure drop across the test section, D is the inner diameter of the pipe, ρ is the density of the solution, L is the length of the test section, and V is the mean flow velocity. Since ρ was essentially identical for the solutions and the solvent (water), the extent of DR (relative to water) could be calculated according to the following equation:

$$\%\mathrm{DR} = \frac{f_{\mathrm{water}} - f}{f_{\mathrm{water}}} \times 100\%, \tag{3}$$

where %DR is percent drag reduction and f_{water} is the friction factor of water. For direct comparison, f_{water} and f were taken at the same solvent Reynolds number (Re), based on the viscosity of water.

Heat loss per unit time in the annulus and heat gain per unit time in the inner tube were measured to ensure they were balanced. The difference was generally less than 5% and was mostly less than 3%. The average of these two quantities was used to calculate heat transfer coefficients. The inlet temperature (T3) was controlled at 10 ± 0.3°C, and the log-mean temperature difference between the annulus and tube was controlled at 25 ± 0.1°C. Thermocouple (T4) at the exit of the tube-in-tube heat exchanger was placed at the center of the flow to measure the mean temperature of the fluid. To avoid the radial temperature gradient established in the fluid once it got heated by the inner wall of the heat exchanger, a 6-element Helix static mixer was placed just upstream of T4 so that the fluid was well-mixed before reaching that point. This 6-element Helix static mixer was in position for all heat transfer measurements of drag-reducing solutions with and without any static mixer. Good heat balances could then be obtained under approximately steady-state conditions. The modified Wilson-plot method was used to calculate the heat transfer coefficient and Nusselt number (Nu) of the solution [29]. Heat-transfer reduction (relative to water) was then calculated by the following equation:

$$\%\mathrm{HTR} = \frac{\mathrm{Nu}_{\mathrm{water}} - \mathrm{Nu}}{\mathrm{Nu}_{\mathrm{water}}} \times 100\%, \tag{4}$$

where %HTR is percent heat transfer reduction and $\mathrm{Nu}_{\mathrm{water}}$ is the Nusselt number of water. $\mathrm{Nu}_{\mathrm{water}}$ and Nu were taken at the same solvent Re.

The physical properties of water were used to calculate Re and Nu values. For the calculation of Nu for the HEV static mixer, the sum of heat transfer resistances of the heat exchanger wall and the HEV tube was used. Since the HEV tube was tightly fitted against the inner wall of the heat exchanger, the total wall thickness was assumed to be 3.5 mm and the effect of holes that tabs left behind in the HEV tube and the wall-wall interface were ignored.

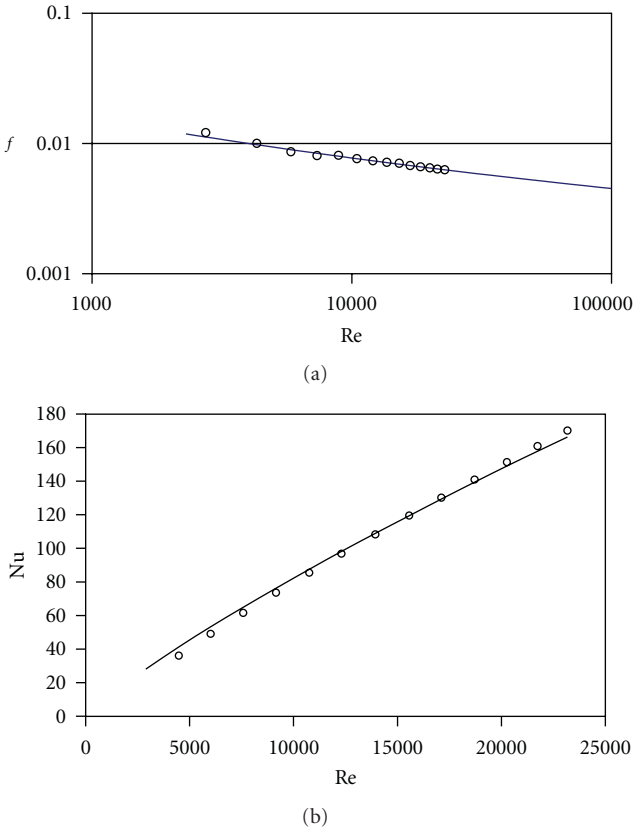

FIGURE 4: (a) Experimental Fanning friction factor (∘) compared with von Karman Equation (—). (b) Experimental Nusselt number (∘) compared with Dittus-Boelter Equation (—).

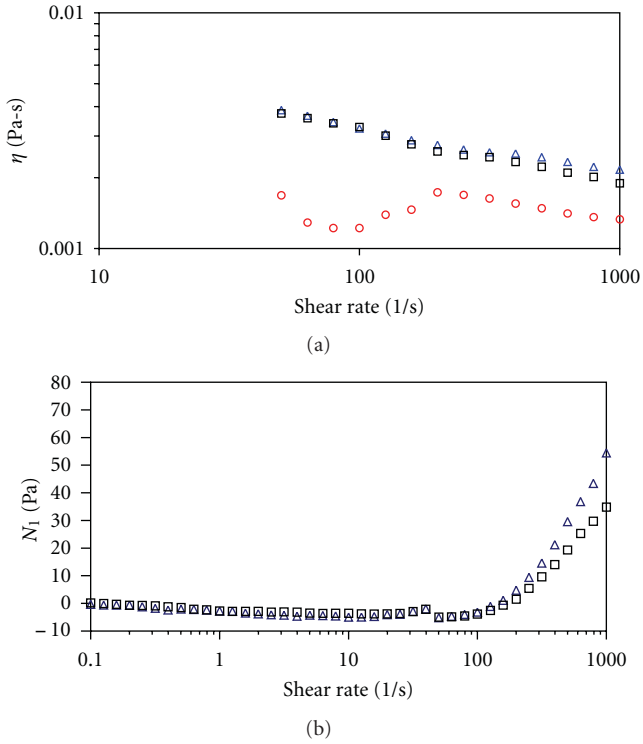

FIGURE 5: (a) Shear viscosity of EO12/NaSal (3 mM/7.5 mM) at 10°C (△), 20°C (□), and 30°C (∘). (b) N_1 of EO12/NaSal (3 mM/7.5 mM) at 10°C (△) and 20°C (□).

3. Results and Discussions

3.1. Water Baselines. To validate the drag reduction and heat transfer measurements, baselines of water were obtained and were compared with existing correlations. The f_{water} was measured and the data were in agreement with the von Karman Equation for water flowing in smooth circular pipes (5) at Re > 10,000 (Figure 4(a)). Therefore, this equation was used to calculate subsequent f_{water} and %DR,

$$\frac{1}{\sqrt{f_{water}}} = 4.0 \log\left(\mathrm{Re} \cdot \sqrt{f_{water}}\right) - 0.4. \quad (5)$$

Experimental results for Nu versus Re for water at 10°C for Re > 10,000 were also in good agreement with the Dittus-Boelter equation (6) for water heated in a smooth tube (Figure 4(b)). Therefore, this equation was used to calculate subsequent Nu_{water} and %HTR,

$$\mathrm{Nu} = 0.023\,\mathrm{Re}^{0.8}\mathrm{Pr}^{0.4}, \quad (6)$$

where Pr is the Prandtl number, defined as the ratio of viscous diffusion rate to thermal diffusion rate.

3.2. Viscoelasticity and Drag Reduction of EO12/NaSal (3 mM/7.5 mM). Drag-reducing surfactant solutions are usually shear thinning and show viscoelastic behavior [3] such as first normal stress differences (N_1). Figure 5(a) shows the shear viscosity, η, of EO12/NaSal (3 mM/7.5 mM). This solution showed shear thinning behavior in the shear rate range of 50 s^{-1} to 1000 s^{-1} for 10 and 20°C. η at 20°C was slightly lower than that at 10°C, but it was significantly lower at 30°C, where a shear-induced structure in viscosity was observed near 100 s^{-1}. The N_1 of EO12/NaSal (3 mM/7.5 mM) is shown in Figure 5(b). N_1 values at 10 and 20°C increased above 100 s^{-1} with higher values at 10°C. At 30°C N_1 was essentially zero (data not shown here), in the range of shear rates we could measure (0.1 to 1,000 s^{-1}), a surprising result in view of Qi et al.'s observation [57] that N_1 increased at shear rates near those at which shear-induced structure was observed.

Figure 6 shows the good drag reduction of EO12/NaSal (3 mM/7.5 mM) from 10°C to 60°C. Drag reduction increased rapidly at solvent Reynolds number of 20,000 for all temperatures and leveled off near 80%. Thus, this solution has a wide range of effective drag reducing temperatures.

3.3. Heat Transfer Reduction of EO12/NaSal (3 mM/7.5 mM). Figures 7(a) and 7(b) show the Nusselt number and %HTR of the EO12/NaSal (3 mM/7.5 mM) solution with no mixer, Helix static mixer, and HEV static mixer, and Figure 7(a) also shows water with and without HEV static mixer. In the tube-in-tube heat exchanger without any mixer, this solution had very low Nusselt numbers, ranging from 12.3 to 27.9 in the

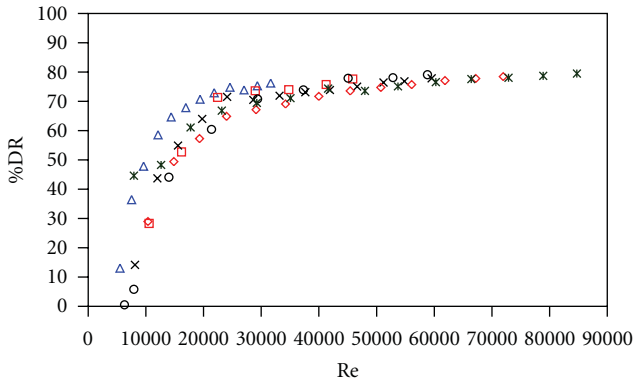

Figure 6: Drag reduction of EO12/NaSal (3 mM/7.5 mM) at 10°C (△), 20°C (□), 30°C (○), 40°C (×), 50°C (◊), and 60°C (∗).

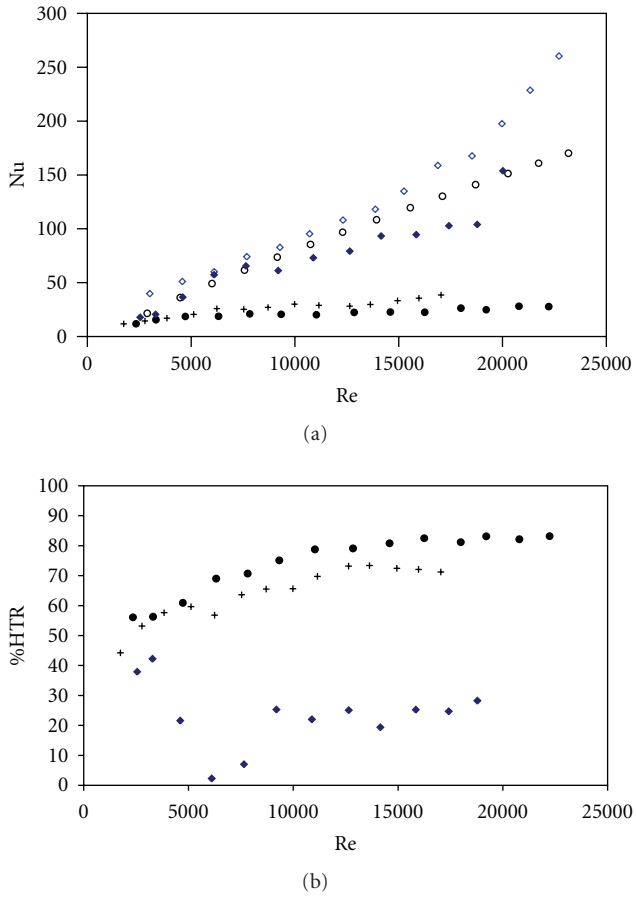

Figure 7: (a) Nusselt number of EO12/NaSal (3 mM/7.5 mM) with Helix mixer (+), no mixer (•), HEV (⧫) and water with no mixer (○) and HEV (◊). (b) %HTR of EO12/NaSal (3 mM/7.5 mM) with Helix mixer (+), no mixer (•) and HEV (⧫).

Reynolds number range of 2,300 to 22,000. Therefore, the heat transfer reduction for this solution was high, starting from 55% at Re=2,300 and increasing to 83% at Re = 22,000. Compared with %DR at 10°C, %HTR is slightly greater, confirming that the reduction in heat transfer is larger than that of drag.

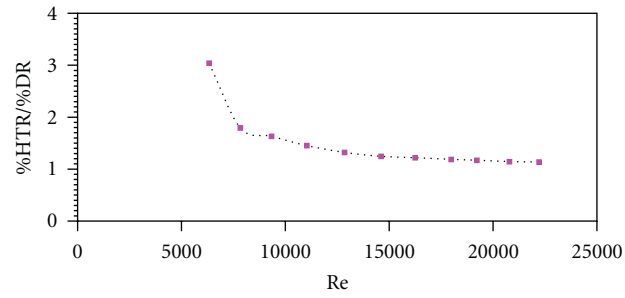

Figure 8: Ratio of %HTR to %DR of EO12/NaSal (3 mM/7.5 mM) at 10°C.

Figure 8 shows the ratio of %HTR to %DR of EO12/NaSal (3 mM/7.5 mM) at 10°C. Because heat transfer and drag reduction experiments were not carried out simultaneously, the %HTR and %DR were not at the same Reynolds number, so %DR was obtained by interpolation to calculate the ratio. This ratio decreased from 3.0 at Re = 6,300 and approached 1.1 as the Reynolds number increased to 22,000. This result is in agreement with the result reported by Aguilar et al. [27].

The Helix static mixer slightly increased the rate of heat transfer of the solution (Figure 7(a)). The maximum Nusselt number it reached was 39 at Re = 17,000, which was approximately 1.6 times that without any mixer. The %HTR was still high near 70% for Re > 12,600. This Helix static mixer had opposite helical elements. As the fluid passed by, it was first divided and followed the twist of the first element in one direction. When it came to the second element, the fluid was divided again and was forced to follow the twist in the opposite direction. The constant dividing and alternately changing of twisting direction generated disturbances and extra shear stress in the flow. The disturbances should enhance the momentum and mass transfer in the radial direction and thus enhance heat transfer. And, if the shear stress was high enough, the wormlike micelles would be broken, and the solution should become water like and have higher heat transfer ability. While the heat transfer in the Helix mixer region may be enhanced, the enhancement over the whole heat exchanger was not significant. Heat transfer reduction was apparently restored shortly downstream of this mixer. A Helix mixer as long as the tube-in-tube heat exchanger could be used to enhance the overall heat transfer throughout the heat exchanger but this would result in extremely high pressure drop across the long Helix static mixer. The pressure drop penalty of this Helix static mixer will be discussed in the following section.

The HEV static mixer with water enhanced the Nusselt numbers, compared with water without the HEV static mixer, especially at the Re > 15,000 (Figure 7(a)). The HEV static mixer with drag reducing solution had Nusselt numbers close to those of water at Re < 10,000. At Re = 20,000, it again approached the Nusselt number of water (Figure 7(a)). The Nusselt number with HEV static mixer with drag reducing solution ranged from three to five times that of the solution without mixer. This significant

enhancement of heat transfer was due to the HEV static mixer's disturbance to the drag reducing flow. As discussed in the introduction section, tabs in the HEV static mixer cause intensified turbulence and streamwise counter-rotating vortices behind the tabs near the wall [45–48]. The streamwise counter-rotating vortices bring the heated fluid near the wall to the axis of the flow, and at the same time, the wall region is replenished with cold fluid from the center of the bulk flow to receive heat from the wall. Thus, the radial mixing and heat transfer were significantly enhanced. In this HEV static mixer, there were three tabs in each group at one cross section. The three tabs generate three pairs of vortices, that is, three streams of fluid flowing from the bulk to the wall and three streams flowing from the wall to the bulk. As the fluid flows downstream, the streamwise vortices also move and become weaker. But when this portion of fluid hits the next group of tabs, new vortices are generated, enhancing radial mixing and heat transfer. This mechanism also explains the higher Nusselt number of water with HEV static mixer.

The high Nusselt number in the low Reynolds number range was unexpected. This might have resulted from the inaccuracy of temperature measurement because of the inhomogeneous temperature distribution of the viscoelastic solution flowing very slowly. The steep increase in the high Reynolds number range might be due in part to the breakup of wormlike micelles at high shear stress, as a high shear zone was observed at the top of HEV tab tips [45].

3.4. Pressure Drop Penalty. Pressure drops across the heat exchanger with mixers installed and an additional section downstream were measured by P_2 (refer to Figure 3). The total length of this section was 180ID (1836 mm). Figure 9 shows that the pressure drop for the 10-element Helix static mixer was three times that of the HEV static mixer, although this Helix mixer was only 100 mm long. If a Helix static mixer as long as the heat exchanger (914 mm) was used, the pressure drop would be extremely high. So the Helix static mixer was not energetically effective. In contrast, the HEV static mixer had a smaller pressure drop, while it enhanced the heat transfer much more. The pressure drop of the DR solution was also slightly lower than that of water with HEV static mixer. Without any mixer, both water and the solution had very low pressure drop. Figure 9 also shows that the maximum Reynolds number that water achieved at the maximum pump rate was 22,700 and 20,100 for no mixer and HEV static mixer, respectively. Although the pressure drop at P_2 for solution with HEV static mixer was higher than that of water without mixer, the solution could be pumped at a maximum flow rate of 0.26 L/s (Re = 25,000) compared with 0.24 L/s (Re = 22,700) for water.

To facilitate the comparison between the solution with HEV static mixer and water without mixer, a performance number, p, was defined by (7). It represents the heat transfer performance per unit pressure drop for a defined section of the heat exchanger region. Based on the same idea, a similar

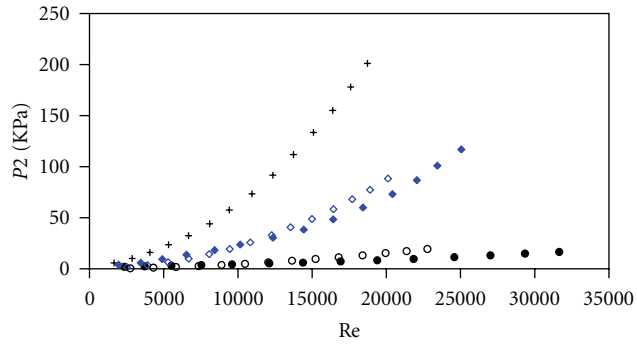

Figure 9: Pressure drops at P_2 for EO12/NaSal (3 mM/7.5 mM) with Helix mixer (+), no mixer (•), HEV (⧫) and water with no mixer (∘) and HEV (◇).

"Hydrodynamic Performance Ratio" was defined [58] to evaluate the combined thermo hydrodynamic performances,

$$p = \frac{\mathrm{Nu}}{2\sum_{i=3}^{8}\Delta P_i + \Delta P_2}, \tag{7}$$

where ΔP_2 is the pressure drop across the heat exchanger and $\sum_{i=3}^{8}\Delta P_i$ is the total pressure drop of the 400ID (4080 mm) section downstream of P_2. This pressure drop was doubled to include the pressure drop of the 400ID section upstream of the heat exchanger. Since the total length of the recirculation loop is more than 20 m, this estimation is conservative.

Figure 10 shows that as the Reynolds number increased, p for water without mixer decreased to $1.39 \times 10^{-3}\,\mathrm{Pa}^{-1}$, while p for solution with HEV is roughly constant at about $1.39 \times 10^{-3}\,\mathrm{Pa}^{-1}$. This means that for a tube-in-tube heat exchanger with 400ID sections upstream and downstream, the performance of the HEV static mixer was comparable to water without mixer for Re $> 20,000$. If the distance between neighboring tube-in-tube heat exchangers is larger than 800ID, the solution with HEV would have less energy consumption than water without the HEV static mixer to achieve the same Nusselt number for Re $> 20,000$ at 10°C Thus, in longer flow systems, the HEV static mixer with solution will have a larger p than water without mixers. In short, the HEV static mixer enhanced the heat transfer of the drag-reducing surfactant solution with a relatively lower energy penalty. The tabs of the HEV static mixer generate streamwise vortices, which enhance heat transfer in the radial direction. Few vortices in other directions, which would not be effective in enhancing heat transfer, are generated in the HEV static mixer and therefore, energy is not wasted in generating ineffective vortices, and the energy consumed is mainly used to generate streamwise vortices effective in enhancing heat transfer.

4. Conclusions

(1) The surfactant solution showed viscoelastic behavior at 10 and 20°C and had excellent drag-reducing ability, up to 80%, from 10°C to 60°C. The heat transfer ability of this solution was, however, reduced significantly. The ratio

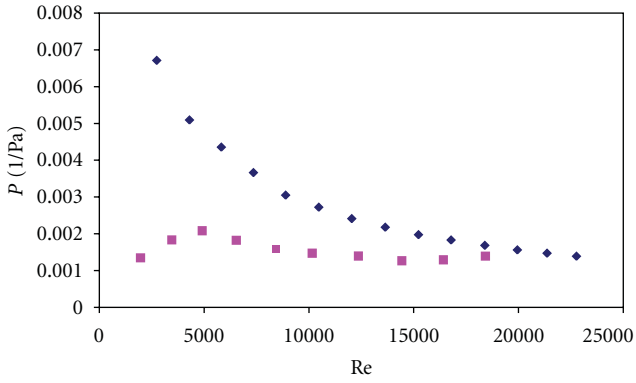

Figure 10: Performance number of solution with HEV static mixer (■) and water without mixer (♦).

of %HTR to %DR decreased with Reynolds number and approached 1.1.

(2) The HEV static mixer mounted in the tube-in-tube heat exchanger enhanced the heat transfer of EO12/NaSal (3 mM/7.5 mM) significantly throughout the range of Reynolds numbers tested. At high Reynolds number, the Nusselt number was close to that of water without any mixer. The heat transfer enhancement was due to the streamwise vortices generated by the HEV static mixer. The relatively low pressure drop was because the vortices were mainly streamwise. Pressure loss vortices in other directions, which could not enhance the radial heat transfer, were not generated. The HEV static mixer's ability to break up the micelles was not clear in our study, as it was not possible to observe the structures of the micelles in the turbulent flow in the heat exchanger. However, because of the relatively small pressure penalty, we believe micelle destruction was not the major contributor to improvement in heat transfer by the HEV static mixer.

(3) A Helix static mixer was also used to enhance the Nusselt number of EO12/NaSal (3 mM/7.5 mM) by destroying the wormlike micelle structures. This mixer may enhance the heat transfer in the mixer region, but did not enhance the overall heat transfer significantly. The extremely high pressure drop was due to the brutal disturbance to the flow and generation of vortices that did not improve heat transfer in the radial direction.

(4) A performance number was used to evaluate the heat transfer ability at the price of pressure loss. Under assumed conditions, the HEV static mixer performance number nearly matched that of water without mixer. If the neighboring tube-in-tube heat exchangers were spaced further apart than the assumed distance (800ID), the drag-reducing solution with HEV static mixer should have less energy consumption than water without mixer to achieve the same Nusselt number for $\mathrm{Re} > 20,000$ at 10°C.

(5) By adjusting the design parameters, such as the tab angle, the tab group distance, and the tab size, an even better performance number might be achieved.

Acknowledgments

The authors would like to thank Professor R. S. Brodkey in the Department of Chemical Engineering at The Ohio State University for discussion and advice. Thanks also go to Paul Green for his dedication and skill in making the HEV static mixer. The authors greatly appreciate Leigh Evrard's technical support and maintenance of the recirculation system.

References

[1] J. L. Lumley, "Drag reduction in turbulent flow by polymer additives," *Journal of Polymer Science: Macromolecular Reviews*, vol. 7, no. 1, pp. 263–290, 1973.

[2] R. H. Nadolink and W. W. Haigh, "Bibliography on skin friction reduction with polymers and other boundary-layer additives," *Applied Mechanics Reviews*, vol. 48, no. 7, pp. 351–460, 1995.

[3] J. L. Zakin, B. Lu, and H. W. Bewersdorff, "Surfactant drag reduction," *Reviews in Chemical Engineering*, vol. 14, no. 4-5, pp. 253–320, 1998.

[4] E. D. Burger, L. G. Chorn, and T. K. Perkins, "Studies of drag reduction conducted over a broad range of pipeline conditions when flowing prudhoe bay crude-oil," *Journal of Rheology*, vol. 24, no. 5, pp. 603–626, 1980.

[5] E. D. Burger, W. R. Munk, and H. A. Wahl, "Flow increase in the trans Alaska pipeline through use of a polymeric drag-reducing additive," *Journal of Petroleum Technology*, vol. 34, no. 2, pp. 377–386, 1982.

[6] A. G. Fabula, "Fire-fighting benefits of polymeric friction reduction," *Journal of Basic Engineering*, vol. 93, no. 3, pp. 453–455, 1971.

[7] R. H. J. Sellin, J. W. Hoyt, and J. Pollert, "The effect of drag reducing additives on fluid flows and their industrial applications. Part 2: present applications and future proposals," *Journal of Hydraulic Research*, vol. 20, no. 3, pp. 235–292, 1982.

[8] C. A. Kim, J. T. Kim, K. Lee, H. J. Choi, and M. S. Jhon, "Mechanical degradation of dilute polymer solutions under turbulent flow," *Polymer*, vol. 41, no. 21, pp. 7611–7615, 2000.

[9] D. Ohlendorf, W. Interthal, and H. Hoffmann, "Surfactant systems for drag reduction: physico-chemical properties and rheological behaviour," *Rheologica Acta*, vol. 25, no. 5, pp. 468–486, 1986.

[10] H. Rehage, I. Wunderlich, and H. Hoffmann, "Shear-induced phase transitions in dilute aqueous surfactant solutions," *Progress in Colloid & Polymer Science*, vol. 72, pp. 51–59, 1986.

[11] H. W. Bewersdorff and D. Ohlendorf, "The behaviour of drag-reducing cationic surfactant solutions," *Colloid & Polymer Science*, vol. 266, no. 10, pp. 941–953, 1988.

[12] Y. Qi, Y. Kawaguchi, R. N. Christensen, and J. L. Zakin, "Enhancing heat transfer ability of drag reducing surfactant solutions with static mixers and honeycombs," *International Journal of Heat and Mass Transfer*, vol. 46, no. 26, pp. 5161–5173, 2003.

[13] K. Gasljevic and E. F. Matthys, "On saving pumping power in hydronic thermal distribution systems through the use of drag-reducing additives," *Energy and Buildings*, vol. 20, no. 1, pp. 45–56, 1993.

[14] J. Yang, "Viscoelastic wormlike micelles and their applications," *Current Opinion in Colloid and Interface Science*, vol. 7, no. 5-6, pp. 276–281, 2002.

[15] K. A. Smith, G. H. Keuroghlian, and P. S. Virk, "Heat transfer to drag-reducing polymer solutions," *AICHE Journal*, vol. 15, no. 2, pp. 294–297, 1969.

[16] A. White, "Heat transfer characteristics of dilute polymer solutions in fully rough pipe flow," *Nature*, vol. 227, no. 5257, pp. 486–487, 1970.

[17] R. Monti, "Heat transfer in drag-reducing solutions," *Progress in Heat and Mass Transfer*, vol. 5, pp. 239–261, 1972.

[18] P. M. Debrule and R. H. Sabersky, "Heat transfer and friction coefficients in smooth and rough tubes with dilute polymer solutions," *International Journal of Heat and Mass Transfer*, vol. 17, no. 5, pp. 529–540, 1974.

[19] E. F. Matthys, "Heat transfer, drag reduction, and fluid characterization for turbulent flow of polymer solutions: recent results and research needs," *Journal of Non-Newtonian Fluid Mechanics*, vol. 38, no. 2-3, pp. 313–342, 1991.

[20] Y. Qi, Y. Kawaguchi, Z. Lin, M. Ewing, R. N. Christensen, and J. L. Zakin, "Enhanced heat transfer of drag reducing surfactant solutions with fluted tube-in-tube heat exchanger," *International Journal of Heat and Mass Transfer*, vol. 44, no. 8, pp. 1495–1505, 2001.

[21] Y. Qi, L. K. Weavers, and J. L. Zakin, "Enhancing heat-transfer ability of drag reducing surfactant solutions with ultrasonic energy," *Journal of Non-Newtonian Fluid Mechanics*, vol. 116, no. 1, pp. 71–93, 2003.

[22] J. Wei, Y. Kawaguchi, B. Yu, and Z. Feng, "Rheological characteristics and turbulent friction drag and heat transfer reductions of a very dilute cationic surfactant solution," *Journal of Heat Transfer*, vol. 128, no. 10, pp. 977–983, 2006.

[23] J. J. Wei, Y. Kawaguchi, F. C. Li et al., "Drag-reducing and heat transfer characteristics of a novel zwitterionic surfactant solution," *International Journal of Heat and Mass Transfer*, vol. 52, no. 15-16, pp. 3547–3554, 2009.

[24] C. S. Wells, "Turbulent heat transfer in drag reducing fluids," *AICHE Journal*, vol. 14, no. 3, pp. 406–410, 1968.

[25] M. Poreh and U. Paz, "Turbulent heat transfer to dilute polymer solutions," *International Journal of Heat and Mass Transfer*, vol. 11, no. 5, pp. 805–818, 1968.

[26] G. Aguilar, K. Gasljevic, and E. F. Matthys, "Coupling between heat and momentum transfer mechanisms for drag-reducing polymer and surfactant solutions," *Journal of Heat Transfer*, vol. 121, no. 4, pp. 796–802, 1999.

[27] G. Aguilar, K. Gasljevic, and E. F. Matthys, "Asymptotes of maximum friction and heat transfer reductions for drag-reducing surfactant solutions," *International Journal of Heat and Mass Transfer*, vol. 44, no. 15, pp. 2835–2843, 2001.

[28] R. H. J. Sellin, J. W. Hoyt, and O. Scrivener, "The effect of drag-reducing additives on fluid flows and their industrial applications part 1: basic aspects," *Journal of Hydraulic Research*, vol. 20, no. 1, pp. 29–68, 1982.

[29] Y. Qi, *Investigation of relationships among microstructure, rheology, drag reduction and heat transfer of drag reducing surfactant solutions*, Ph.D. dissertation, The Ohio State University, Columbus, Ohio, USA, 2002.

[30] J. Myska, J. L. Zakin, and Z. Chara, "Viscoelasticity of a surfactant and its drag-reducing ability," *Applied Scientific Research*, vol. 55, no. 4, pp. 297–310, 1995.

[31] A. Gyr and J. Bühler, "Secondary flows in turbulent surfactant solutions at maximum drag reduction," *Journal of Non-Newtonian Fluid Mechanics*, vol. 165, no. 11-12, pp. 672–675, 2010.

[32] Y. Kawaguchi, T. Segawa, Z. Feng, and P. Li, "Experimental study on drag-reducing channel flow with surfactant additives—spatial structure of turbulence investigated by PIV system," *International Journal of Heat and Fluid Flow*, vol. 23, no. 5, pp. 700–709, 2002.

[33] F. C. Li, Y. Kawaguchi, B. Yu, J. J. Wei, and K. Hishida, "Experimental study of drag-reduction mechanism for a dilute surfactant solution flow," *International Journal of Heat and Mass Transfer*, vol. 51, no. 3-4, pp. 835–843, 2008.

[34] W. H. Cai, F. C. Li, H. N. Zhang et al., "Study on the characteristics of turbulent drag-reducing channel flow by particle image velocimetry combining with proper orthogonal decomposition analysis," *Physics of Fluids*, vol. 21, no. 11, Article ID 021911PHF, pp. 1–12, 2009.

[35] S. Tamano, M. Itoh, T. Inoue, K. Kato, and K. Yokota, "Turbulence statistics and structures of drag-reducing turbulent boundary layer in homogeneous aqueous surfactant solutions," *Physics of Fluids*, vol. 21, no. 4, Article ID 045101, 2009.

[36] S. Tamano, M. Itoh, K. Kato, and K. Yokota, "Turbulent drag reduction in nonionic surfactant solutions," *Physics of Fluids*, vol. 22, no. 5, Article ID 055102, 12 pages, 2010.

[37] P. Li, Y. Kawaguchi, H. Daisaka, A. Yabe, K. Hishida, and M. Maeda, "Heat transfer enhancement to the drag-reducing flow of surfactant solution in two-dimensional channel with mesh-screen inserts at the inlet," *Journal of Heat Transfer*, vol. 123, no. 4, pp. 779–789, 2001.

[38] H. Mizunuma, T. Kobayashi, and S. Tominaga, "Drag reduction and heat transfer in surfactant solutions with excess counterion," *Journal of Non-Newtonian Fluid Mechanics*, vol. 165, no. 5-6, pp. 292–298, 2010.

[39] P. W. Li, Y. Kawaguchi, and A. Yabe, "Transitional heat transfer and turbulent characteristics of drag-reducing flow through a contracted channel," *Journal of Enhanced Heat Transfer*, vol. 8, no. 1, pp. 23–40, 2001.

[40] A. Kishimoto, H. Suzuki, and H. Usui, "Influences of the inner-surface conditions of circular tubes on the heat transfer in a surfactant drag-reduction system," *Kagaku Kogaku Ronbunshu*, vol. 27, no. 3, pp. 350–351, 2001.

[41] H. Inaba, N. Haruki, T. Nakata, A. Horibe, N. Furumoto, and K. Sato, "Heat transfer enhancement of water flow in a straight pipe with drag reduction surfactant by using wire coil," *Nippon Kikai Gakkai Ronbunshu, B Hen*, vol. 68, no. 666, pp. 481–488, 2002.

[42] W. I. A. Aly, H. Inaba, N. Haruki, and A. Horibe, "Drag and heat transfer reduction phenomena of drag-reducing surfactant solutions in straight and helical pipes," *Journal of Heat Transfer*, vol. 128, no. 8, pp. 800–810, 2006.

[43] T. Zhou, K. C. Leong, and K. H. Yeo, "Experimental study of heat transfer enhancement in a drag-reducing two-dimensional channel flow," *International Journal of Heat and Mass Transfer*, vol. 49, no. 7-8, pp. 1462–1471, 2006.

[44] C. R. Smith, "Static fluid flow mixing method," US patent 88-224690, 1991.

[45] T. Lemenand, P. Dupont, D. Della Valle, and H. Peerhossaini, "Turbulent mixing of two immiscible fluids," *Journal of Fluids Engineering*, vol. 127, no. 6, pp. 1132–1139, 2005.

[46] C. H. Phillips, G. Lauschke, and H. Peerhossaini, "Intensification of batch chemical processes by using integrated chemical reactor-heat exchangers," *Applied Thermal Engineering*, vol. 17, no. 8-10, pp. 809–824, 1997.

[47] H. Mohand Kaci, T. Lemenand, D. Della Valle, and H. Peerhossaini, "Effects of embedded streamwise vorticity on turbulent mixing," *Chemical Engineering and Processing: Process Intensification*, vol. 48, no. 10, pp. 1459–1476, 2009.

[48] A. Mokrani, C. Castelain, and H. Peerhossaini, "Experimental study of the influence of the rows of vortex generators on turbulence structure in a tube," *Chemical Engineering and Processing: Process Intensification*, vol. 48, no. 2, pp. 659–671, 2009.

[49] S. Ferrouillat, P. Tochon, C. Garnier, and H. Peerhossaini, "Intensification of heat-transfer and mixing in multifunctional heat exchangers by artificially generated streamwise vorticity," *Applied Thermal Engineering*, vol. 26, no. 16, pp. 1820–1829, 2006.

[50] C. Habchi, T. Lemenand, D. D. Valle, and H. Peerhossaini, "Alternating mixing tabs in multifunctional heat exchanger-reactor," *Chemical Engineering and Processing*, vol. 49, no. 7, pp. 653–661, 2010.

[51] H. Mohand Kaci, C. Habchi, T. Lemenand, D. Della Valle, and H. Peerhossaini, "Flow structure and heat transfer induced by embedded vorticity," *International Journal of Heat and Mass Transfer*, vol. 53, no. 17-18, pp. 3575–3584, 2010.

[52] J. B. Fasano, "Kenics HEV mixer sets a new standard for turbulent mixing efficiency," in *Mixing XIII Conference*, Banff, Alberta, Canada, June 1991.

[53] T. Lemenand, D. Della Valle, Y. Zellouf, and H. Peerhossaini, "Droplets formation in turbulent mixing of two immiscible fluids in a new type of static mixer," *International Journal of Multiphase Flow*, vol. 29, no. 5, pp. 813–840, 2003.

[54] T. Lemenand, C. Durandal, D. Della Valle, and H. Peerhossaini, "Turbulent direct-contact heat transfer between two immiscible fluids," *International Journal of Thermal Sciences*, vol. 49, no. 10, pp. 1886–1898, 2010.

[55] C. W. Macosko, *Rheology: Principles, Measurements, and Applications*, VCH, New York, NY, USA, 1994.

[56] W. Ge, *Studies on the nanostructure, rheology and drag reduction characteristics of drag reducing cationic surfactant solutions*, Ph.D. dissertation, The Ohio State University, Columbus, Ohio, USA, 2008.

[57] Y. Qi, E. Kesselman, D. J. Hart, Y. Talmon, A. Mateo, and J. L. Zakin, "Comparison of oleyl and elaidyl isomer surfactant-counterion systems in drag reduction, rheological properties and nanostructure," *Journal of Colloid and Interface Science*, vol. 354, no. 2, pp. 691–699, 2011.

[58] B. V. N. R. Rama Kumar and B. V. S. S. S. Prasad, "Experimental investigation of flow and heat transfer for single and multiple rows of circular jets impinging on a concave surface," in *Proceedings of ASME Turbo Expo: Power for Land, Sea, and Air. Volume 4: Heat Transfer, Parts A and B*, pp. 921–929, Berlin, Germany, June 2008.

Hindawi Publishing Corporation
Advances in Mechanical Engineering
Volume 2011, Article ID 345328, 5 pages
doi:10.1155/2011/345328

Research Article

On Relationships among the Aggregation Number, Rheological Property, and Turbulent Drag-Reducing Effect of Surfactant Solutions

Ying-Bo Zhou,[1] Na Xu,[2] Ning Ma,[2] Feng-Chen Li,[1] Jin-Jia Wei,[2] and Bo Yu[3]

[1] *School of Energy Science and Engineering, Harbin Institute of Technology, Harbin 150001, China*
[2] *State Key Laboratory of Multiphase Flow in Power Engineering, Xi'an Jiaotong University, Xi'an 710049, China*
[3] *Beijing Key Laboratory of Urban Oil and Gas Distribution Technology, China University of Petroleum-Beijing, Beijing 102249, China*

Correspondence should be addressed to Feng-Chen Li, lifch@hit.edu.cn

Received 31 May 2011; Accepted 29 June 2011

Academic Editor: Yasuo Kawaguchi

In this study, turbulent drag-reducing effect, rheological characteristics and micelle aggregation number of aqueous solutions of anionic surfactant, sodium dodecyl sulfate (SDS), and cationic surfactant cetyltrimethylammonium chloride (CTAC) aided with sodium salicylate (NaSal). SDS solution was experimentally investigated at various concentrations in CMCs (critical micelle concentration) with and without sodium chloride. 200 ppm (ppm means part per million) CTAC/NaSal (mass ratio 1 : 1) solution was tested within temperature range from 20°C to 80°C. We were aiming at gaining insights into relationships among turbulent drag reduction rate, rheological properties and micelle microstructures of drag-reducing surfactant solution. Experiments on aggregation number, turbulent drag reduction and shear-rate dependent shear viscosity were performed for solution of SDS and 200 ppm CTAC/NaSal, respectively. The relationships among these three parameters were analyzed and discussed. The results are of importance from both theoretical and practical viewpoints for micellar transitions of surfactant solution.

1. Introduction

By dissolving a minute amount of additives such us polymers and surfactants in water, the frictional drag of turbulent flow through pipes and channels can be reduced dramatically [1–3]. This phenomenon is called turbulent drag reduction. For drag-reducing surfactant solutions, it is proposed that the transition of large aggregates into rod-like micelles is responsible for the onset of drag reduction behavior of these systems [4, 5]. The drag-reducing effect is determined by many factors, such as the chemical structure of surfactants, counterions, the concentration, and the ratio of counterions to surfactants. The number of surfactant monomers forming a micelle is a structurally relevant parameter that contains indirect information on the micelle geometries. Most surfactant drag-reducing systems form rod-like micelles in the quiescent state and have distinctive rheological properties such as high zero-shear viscosities, shear thinning behavior with increasing shear rate, and shear-induced structure represented by a local increase in both shear viscosity and the first normal stress difference at a certain shear rate range [6, 7].

In order to clarify the factors influencing on the turbulent drag-reducing ability of surfactant additives, we measured the aggregation number, drag reduction rate of turbulent pipe flow, and shear-rate-dependent shear viscosity of aqueous solutions of anionic surfactant sodium dodecyl sulfate (SDS) with/without addition of NaCl and cationic surfactant cetyltrimethylammonium chloride (CTAC) aided with sodium salicylate (NaSal). This study focuses on investigating the inherent relationships among the aggregation number, rheological property, and turbulent drag-reducing effect of surfactant additives.

2. Experimental Setup and Procedures

2.1. Working Fluids. Aqueous solution of anionic surfactant SDS (Chengxin Ltd.) with/without addition of sodium

chloride (NaCl, Sigma Chemical Company) and 200 ppm (ppm means part per million) CTAC/NaSal (mass ratio 1 : 1) was tested in the present study. The SDS and CTAC were used after repeated recrystallization from an ethanol-water mixture. No minimum in surface tension versus concentration plot was observed in the purified surfactant. Pyrene 99.0% pure, benzophenone 99.0% pure (Aldrich, USA), and triple-distilled water were used for preparation of solutions in which benzophenone was used as the quencher and pyrene for probing. The temperature of working fluid was controlled to be 40°C for SDS solution measurements and be from 15°C to 60°C for CTAC/NaSal solution measurements.

2.2. Test Facility

2.2.1. Aggregation Number Measurement. Steady-state fluorescent quenching method was utilized for measurement of aggregation number, N_m, of surfactant. The steady-state fluorescent quenching technique belongs to fluorescence probing methods, which uses a fluorescent probe, commonly pyrene in the case of aqueous solution. N_m of surfactant, that is, the number of surfactant monomers forming a micelle, is a structurally relevant parameter that contains indirect information on the micelle geometries [8].

Steady-state fluorescence quenching experiments of anionic surfactant SDS and CTAC/NaSal were performed with a spectrofluorometer (Tianjin Gangdong Company, China), which is usually equipped in most chemistry laboratories. The excitation source was successive xenon light. Take SDS for example, there exist five emission wave crests at wavelengths of 373 nm, 379 nm, 384 nm, 390 nm, and 393 nm [8, 9], among which 393 nm was chosen to be emission wavelength. Fluorescence emission spectra were recorded using an excitation wavelength of 335 nm. The aggregation number, N_m, is determined from the slope obtained from the plot of $\ln(I_0/I)$ versus C_Q according to some mathematical assumptions, where I_0 and I are the fluorescence intensities in the absence and presence of a quencher, respectively, and C_Q is the quencher concentration [9].

2.2.2. Measurement of Turbulent Drag Reduction. Drag reduction was measured in two closed loop fluid flow facilities. The test sections are acrylic resin tube with inner diameter of 0.025 m and length of 1.4 m and channel with height of 0.01 m, width of 0.125 m, and length of 3.0 m, respectively [10]. The pressure drop was measured with a differential pressure transducer, and flow rate was measured with an electromagnetic flow meter. The system was temperature controlled, which allows for the experiments being carried out at a temperature range of 5°C to 90°C. The turbulent drag reduction rate is defined as $\mathrm{DR}\% = ((f_s - f)/f_s) \times 100\%$, where f_s is the pressure drop of solvent flow and f is the pressure drop of solution flow at the same flow rate [4]. Before experiments, the reliability of this loop has been verified: the measured friction factor for water flow agrees very well with commonly accepted correlation for turbulent pipe flow ($C_f = 0.0791\ \mathrm{Re}^{-0.25}$) or channel flow of the Newtonian fluids ($C_f = 0.073\ \mathrm{Re}^{-0.25}$).

2.2.3. Shear Viscosity Measurement. The shear-rate-dependent shear viscosity of SDS and CTAC/NaSal solutions was measured with a stress-controlled rheometer AR-G2 (TA Instruments). Parallel plate and cone-and-plate geometries offered by TA Instruments are available for AR-G2. The cone-and-plate measuring system has the best advantage of the shear rate across the entire surface being uniform. In this paper, we choose the cone-and-plate geometry with 60 mm cone diameter, 2° cone angle, 58 μm gap for the rheological measurements. The sample is loaded between the cone-and-plate discs. The upper cone is driven by an oscillatory force on the axis normal to the plate surface.

3. Results and Discussions

3.1. Aggregation Number. Figure 1 shows the variation of aggregation numbers of SDS solution with addition of NaCl, in which aggregation numbers are plotted against concentrations at 40°C. The concentration range within which the solution has a fluctuation in a narrow range is called "stabilized zone" in this study. At each stabilized zone the tested aggregation numbers increase by small degree. Between stabilized zones there exist some concentration ranges where aggregation numbers have a sharp increase. Contrasting to other researcher's cryo-TEM results [11], in salt-free system, micelle shapes transform from spherical to rodlike, then to hexagonal, till lamellar [4]. Every stabilized zone corresponds to one micelle configuration, that is, concentrations less than 15 CMCs stand for spherical, bigger than 17 CMCs but less than 47 CMCs stand for rodlike and hexagonal, and bigger than 60 CMCs stand for lamellar shapes, respectively. When the concentration goes on increasing, transmittance of the solution decreased too much to determine aggregation numbers.

Figure 2 shows the variation of aggregation numbers of SDS in water without addition of NaCl, in which aggregation numbers are plotted against concentrations at 40°C. Salt-free systems have similar stabilized zones with salt systems. Generally, without counterions, cationic surfactants would not form rod-like micelles which are necessary for drag reduction at low concentration. In most cases organic salts play a role of counterions in cationic surfactant solution, and inorganic salts play a role of counterions in anionic surfactant solution. Therefore, the addition of NaCl has great effects on micelle aggregation ability of surfactant SDS. For instance, in salt-free system rod-like micelles appear at 75 CMCs (94 mM) in SDS solution, while in salt system they turn out to be 17 CMCs (64 mM). Inorganic salts make less powerful effects than organic salts in bonding surfactant monomers. For the same concentration, salt system has larger aggregation number than that of salt-free system, that is to say, micelles in salt system may be stronger and get more powerful shearing ability [4]. As the concentration increases to 360 CMCs, phase separation happens so that aggregation number increases suddenly.

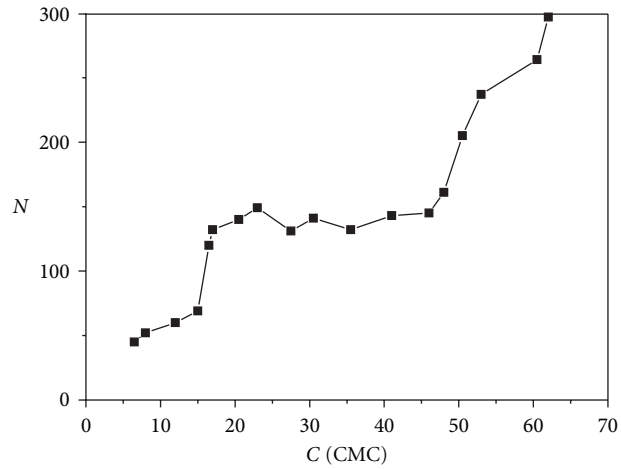

Figure 1: Steady-state fluorescent quenching method for SDS solution N_m measurement with NaCl.

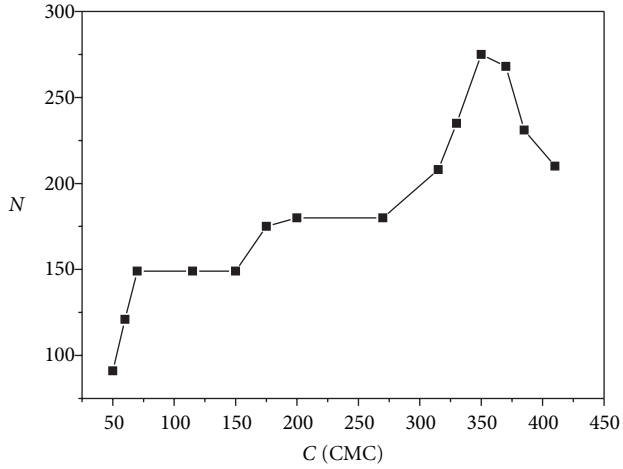

Figure 2: Steady-state fluorescent quenching method for SDS solution N_m measurement without NaCl.

Figure 3 shows the variation of aggregation numbers of 200 ppm CTAC/NaSal solution, in which aggregation numbers are plotted against temperature. When temperature is varied from 15 to 30°C, aggregation number increases slowly in a stabilized zone (lager than 95 but smaller than 100). As temperature goes on rising to 50°C, micellar aggregation number enters into another stage (average size 120) in a narrow temperature range. This maybe presents two different kinds of micellar structures.

3.2. Shear Viscosity. Figure 4 shows the measured zero-shear viscosity for the case of SDS solution without NaCl (the aggregation number replotted together with viscosity for comparison). It can be seen that in every stabilized zone shear viscosity has an increase-then-decrease tendency. When aggregation number rises towards the local maximum values, shear viscosity in those stabilized zones turns to be larger. In the first half of each stabilized zone representing micelle

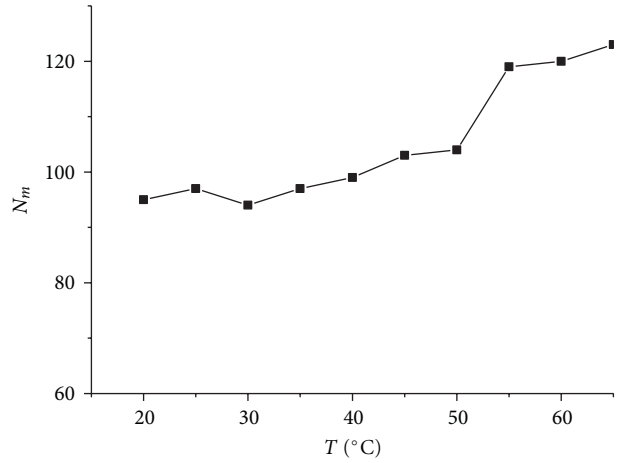

Figure 3: Steady-state fluorescent quenching method for 200 ppm CTAC/NaSal solution N_m measurement.

shape formation, the corresponding viscosity increases obviously, which might be caused by more monomers arranging in order. In the last half of shape-changing stage, the corresponding viscosity decreases, which is probably due to more monomers being arranged disorderedly.

Figure 5 shows the measured shear viscosity versus shear rate of 200 ppm CTAC/NaSal solution at different temperatures. We can see that the shear viscosity first increases sharply and then decreases gradually with increasing shear rate at 20°C and 30°C in the present measurement. The increase of viscosity at very low shear rate might be due to the system error of the rheometer during operation, since from zero-shear rate, there should be a plateau range characterizing the zero-shear viscosity. The effect of shear rate becomes small, and the measured shear viscosity is close to that of water when temperature is increased up to 40°C and 50°C. Generally speaking there exists a critical temperature exceeding which rheological properties of 200 ppm CTAC/NaSal solution are the same as those of water.

3.3. Drag Reduction in Surfactant Solution Flows. Measurement of drag reduction characteristics was performed for flows of SDS solution at a concentration from 17 CMCs to 60 CMCs with NaCl and from 75 CMCs to 300 CMCs without NaCl within a temperature range from 10°C to 50°C, and 200 ppm CTAC/NaSal solution at a Reynolds number range from 20000 to 120000 at 20°C in pipe and at a Reynolds number range from around 2600 to 50000 and within a temperature range from 15°C to 55°C in channel.

It is concluded that no obvious drag reduction phenomenon occurs in SDS solution flows. Most researchers argued rod-like micelles were responsible for drag reduction behavior. In this experiment, however, rod-like micelles are found [4], but no turbulent drag reducing effect is observed, which implies that the formation of rod-like micelles only is not enough for the occurrence of turbulent drag reduction.

Obvious drag reduction phenomenon is observed for 200 ppm CTAC/NaSal solution cases. Figure 6 shows the drag

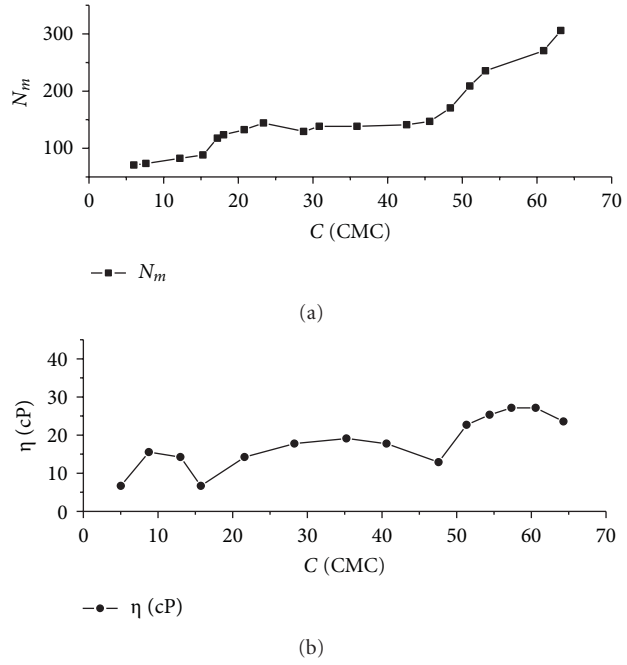

Figure 4: Relationships between aggregation number and shear viscosity of SDS solution without NaCl.

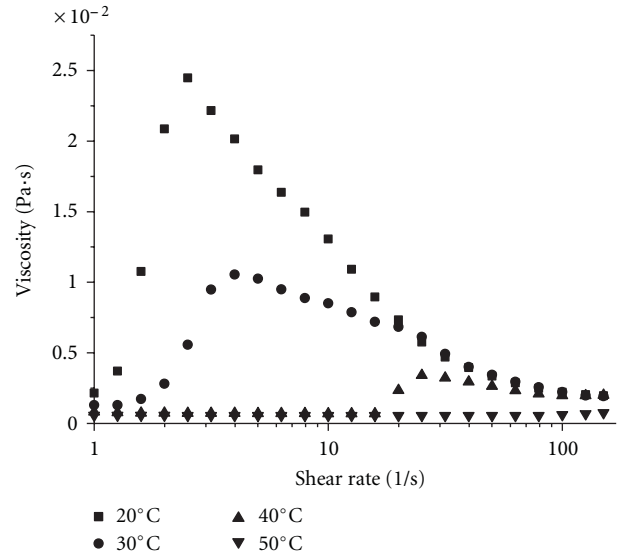

Figure 5: Shear viscosity of 200 ppm CTAC/NaSal at temperature from 20°C to 50°C.

reduction measurement results for 200 ppm CTAC/NaSal solution flow at 20°C in pipe. Due to the limitation of this pipe-flow facility, lower Reynolds number was not realized (as shown in Figure 6(a)). All the measured Reynolds numbers have been in the range over the optimum drag-reducing state for 200 ppm CTAC/NaSal solution. However, obvious turbulent drag-reducing effect still exists for all the measured runs, which can be used for comparative analysis with the shear viscosity.

As shown in Figure 6(b), the abscissa is changed to be average shear rate (mean velocity divided by the diameter

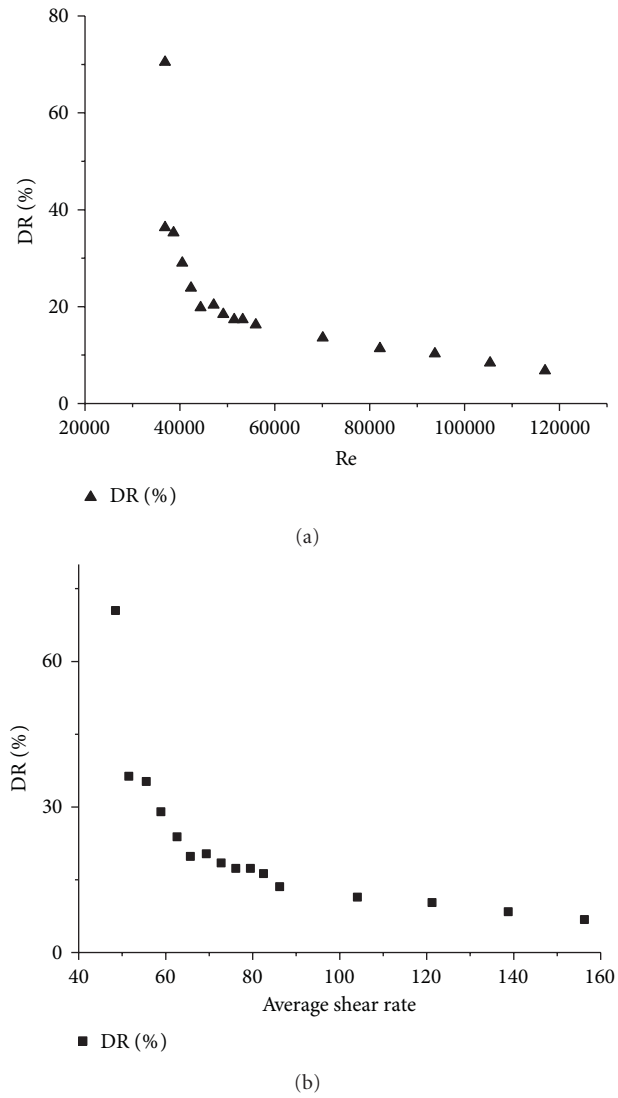

Figure 6: Drag reduction effectiveness of 200 ppm CTAC/NaSal solution at 20°C in a pipe flow.

of pipe) corresponding to each measured Reynolds number. It can be seen that the average shear rates for all the measurements are all in the range at which shear thinning becomes serious as shown in Figure 5. The phenomena of both the decrease of turbulent drag-reducing ability and the serious shear thinning appearing in the shear viscosity within the measured shear rate are closely relevant to each other.

Figure 7 shows the results of drag reduction measurement versus the Reynolds number for 200 ppm CTAC/NaSal solution flows within a temperature range from 15°C to 55°C in a channel flow [10]. It can be seen that, for the two cases at temperatures of 50°C and 55°C, the turbulent drag-reducing effect of 200 ppm CTAC/NaSal solution is significant in a much broader range of the Reynolds number. In the aggregation number measurement, as shown in Figure 3, it has been demonstrated that from 50°C N_m begins to increase and reaches to a local maximum plateau value (120) from around 55°C. The above-mentioned two phenomena

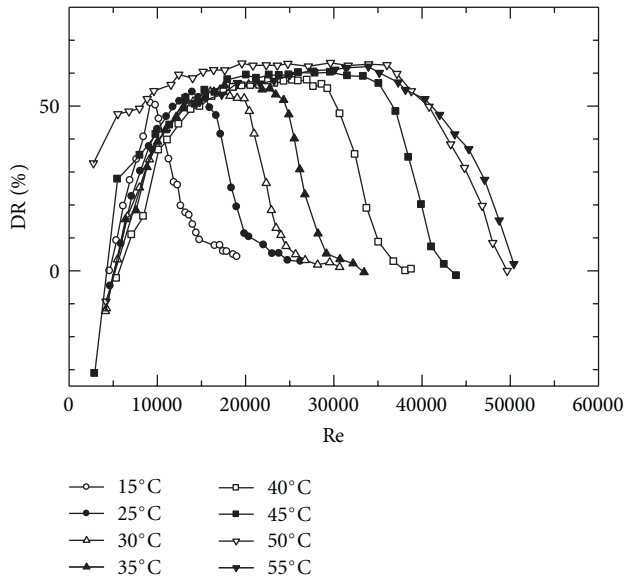

Figure 7: Drag reduction rate versus the Reynolds number for 200 ppm CTAC/NaSal solution at different temperature in a channel flow [10].

appearing in drag reducing ability and aggregation number, again, are closely relevant to each other, that is, a larger aggregation number corresponds to stronger microstructures in the surfactant solution flow that shows significant turbulent drag-reducing effect in a broader Reynolds number, or in other words, a higher shear stress is needed to destroy the microstructures in a surfactant solution with larger aggregation number.

4. Conclusion

Aggregation number, turbulent frictional drag, and shear viscosity characteristics of SDS solution with and without NaCl and of 200 ppm CTAC/NaSal solution at various temperatures were experimentally investigated. The relationships among the shear viscosity, turbulent drag reduction, and aggregation number that can indirectly characterizes the micellar microstructures in surfactant solution have been analyzed. The main conclusions are as follows.

(1) There exist stabilized zones according to the changing of aggregation numbers, which corresponds to the micelle shape change process. In every stabilized zone, shear viscosity has an increase-then-decrease tendency. This phenomenon is probably caused by formation and breakdown of the micelle network structures.

(2) The pipe flow test of 200 ppm CTAC/NaSal solution at 20°C indicates that the shear-rate-dependent shear viscosity and drag reduction efficiency exhibited a close relevance. Experiments on SDS solution flows imply that the formation of rod-like micelles only is not enough for the occurrence of turbulent drag reduction.

(3) The channel flow test of 200 ppm CTAC/NaSal solution at different temperatures shows that the aggregation number and drag-reducing ability of a surfactant solution flow have close relevance, that is, larger aggregation number corresponds to a larger range of effective Reynolds number for drag reduction.

Acknowledgments

The authors acknowledge the support from the National Natural Science Foundation of China (no. 51076036, no. 50876114, no. 51076124) and the Fundamental Research Funds for the Central Universities (HIT.BRET1.2010008).

References

[1] Y. Y. Qi and L. K. Weavers, "Enhancing heat-transfer ability of drag reducing surfactant solutions with ultrasonic energy," *Journal of Non-Newtonian Fluid Mechanics*, vol. 116, no. 1, pp. 71–93, 2003.

[2] F. C. Li, Y. Kawaguchi, and K. Hishida, "Structural analysis of turbulent transport in a heated drag-reducing channel flow with surfactant additives," *International Journal of Heat and Mass Transfer*, vol. 48, no. 5, pp. 965–973, 2005.

[3] J. L. Zakin, B. Lu, and H. W. Bewersdorff, "Surfactant drag reduction," *Reviews in Chemical Engineering*, vol. 14, no. 4-5, pp. 253–318, 1998.

[4] Y. Zhang, J. Schmidt, Y. Talmon, and J. L. Zakin, "Co-solvent effects on drag reduction, rheological properties and micelle microstructures of cationic surfactants," *Journal of Colloid and Interface Science*, vol. 286, no. 2, pp. 696–709, 2005.

[5] H.-X. Zhang and D.-Z. Wang, "Experimental study on the effects of shear induced structure in a drag-reducing surfactant solution flow," *Archive of Applied Mechanics*, vol. 79, no. 8, pp. 773–778, 2009.

[6] Y. Zhang, J. Schmidt, Y. Talmon, D. J. Hart, and J. L. Zakin, "Drag reduction and rheological properties of a novel zwitterionic surfactant compared with cationic surfactant/counterion systems," in *Proceedings of the Society of Rheology*, Seoul, Republic of Korea, August 2004.

[7] J. J. Wei, Y. Kawaguchi, F. C. Li et al., "Drag-reducing and heat transfer characteristics of a novel zwitterionic surfactant solution," *International Journal of Heat and Mass Transfer*, vol. 52, no. 15-16, pp. 3547–3554, 2009.

[8] K. Kuperkar, K. Prasad, L. Abezgauz, and P. Bahadur, "Formation and growth of micelles in dilute aqueous CTAB solutions in the presence of $NaNO_3$ and $NaClO_3$," *Journal of Surfactants and Detergents*, vol. 13, no. 3, pp. 293–303, 2010.

[9] X. Cai, S. C. Wang, J. F. He, X. Liu, J. F. Peng, and T. Y. Kuang, "Steady state fluorescence spectroscopy of the photosystem II core complex," *Journal of Plant Physiology and Molecular Biology*, vol. 32, no. 2, pp. 169–174, 2006.

[10] J.-F. Wang, *Experimental study of comprehensive effect of temperature and reynolds number on drag reducing and heat transfer characteristics of a cationic surfactants solution*, M.S. thesis, Xi'an Jiaotong University, Xi'an, 2010.

[11] Y. Zhang, *Correlations among surfactant drag reduction, additive chemical structures, rheological properties and microstructures in water and water/co-solvent systems*, Ph.D. thesis, Ohio State University, Columbus, Ohio,USA, 2005.

Hindawi Publishing Corporation
Advances in Mechanical Engineering
Volume 2011, Article ID 120438, 12 pages
doi:10.1155/2011/120438

Research Article

Experimental Investigation on Zonal Structure in Drag-Reducing Channel Flow with Surfactant Additives

Masaaki Motozawa,[1] Takahiro Watanabe,[1] Weiguo Gu,[2] and Yasuo Kawaguchi[1]

[1] *Department of Mechanical Engineering, Tokyo University of Science, 2641 Yamazaki, Noda-shi, Chiba 278-8510, Japan*
[2] *School of Mechanical Engineering, Shanghai Jiao Tong University, Shanghai 200230, China*

Correspondence should be addressed to Masaaki Motozawa, motozawa@rs.noda.tus.ac.jp

Received 9 June 2011; Accepted 18 July 2011

Academic Editor: Jinjia Wei

The spatial structure of a drag-reducing channel flow with surfactant additives in a two-dimensional channel was investigated experimentally. We carried out detailed measurements of the instantaneous velocity in the streamwise wall-normal plane and streamwise spanwise plane by using particle image velocimetry (PIV). The surfactant used in this experiment is a kind of cationic surfactant CTAC. The weight concentrations of the CTAC solution were 25 and 40 ppm on the flow. We considered the effects of Reynolds number ranging from 10000 to 25000 and the weight concentration of CTAC. The results of this paper showed that in the drag-reducing flow, there appeared an area where the root mean square of streamwise velocity fluctuation and the vorticity fluctuation sharply decreased. This indicated that two layers with different turbulent structure coexisted on the boundary of this area. Moreover, these layers had characteristic flow structures, as confirmed by observation of the instantaneous vorticity fluctuation map.

1. Introduction

It is well known that adding a small amount of polymer or surfactant additives to water flow causes a dramatic reduction in turbulent drag. This phenomenon is called the Toms effect [1]. If we could apply this phenomenon to industrial applications, it would have the great benefit of saving fuel and mitigating environmental problems. For instance, drag-reduction using a polymer solution has been applied to the oil pipeline system [2]. By adding a certain amount of polymer solution to the crude oil in the pipeline, the desired discharge of two million barrels per day could be achieved without constructing additional pumping stations. However, with drag-reduction by a polymer solution, the network structure of the polymer solution which causes the drag-reduction is broken easily due to mechanical shear stress of the pump, and the drag-reducing effect is lost [3]. Therefore, the polymer is not effective for an application with a closed circuit system. On the other hand, some kinds of surfactant additives have a self-repairing ability and can keep the drag-reducing effect through mechanical shear stress. In the surfactant solution, rod-like micelles are formed under moderate conditions of fluid temperature and concentrations of surfactant. Moreover, suitable shear stress assists the formation of a micellar network, and this network expresses the viscoelasticity of the surfactant solution [4]. This state is known as a shear induced structure (SIS). There have been several studies on the rheological characteristics and chemical structure of viscoelastic fluid, which is believed to cause drag-reduction [5, 6]. Hu and Matthys [7] investigated the formation and the relaxation of the SIS under conditions of shear and normal stress. They revealed that the buildup times of the SIS were inversely proportional to the shear rate. Moreover, the buildup times and final state depended on flow geometry.

The micellar network which is formed in the surfactant solution leads to a large drag-reduction. Moreover, even if this micellar network is broken by the large shear stress, this network structure is repaired quickly and the drag-reducing effect can be sustained. Thus, surfactant additives are very useful for applications having a closed-circuit system, such as air-conditioning systems or district heating/cooling (DHC)

systems [8]. For instance, Takeuchi et al. [9] applied surfactant additives to a central heating/cooling system and reported that pumping energy consumption was reduced by 65% in winter heating and by 47% in summer cooling.

Because of this background, there has been intense research on drag-reduction with surfactant additives since the discovery of the Toms effect. In particular, the spatial structure of the drag-reducing flow has been extensively investigated in many studies. The slight viscoelasticity of the surfactant solution affects the energy dissipation process of the flow, and drag-reduction occurs. Therefore, it seems that the drag-reducing flow has a unique structure which is different from the turbulent structure or the laminar structure of Newtonian fluid. However, there is not enough knowledge about this, and the actual mechanism of drag-reduction has yet to be fully explained. Therefore, it is worth investigating in more detail the structure of the drag-reducing flow of the viscoelastic fluid experimentally.

Recently, many studies on drag-reducing flow with surfactant additives and polymer have been conducted [10–13]. In the drag-reducing flow of the polymer solution, White and Mungal [14] investigated experimentally the detail of dynamic interactions between polymer and turbulence in the drag-reducing wall-bounded shear flow of a diluted polymer solution. In their research, polymer was found to disrupt the near-wall turbulence regeneration cycle and reduce the turbulent friction drag. Therefore, it was concluded that vortex suppression leads to drag-reduction except in the case of low Reynolds number.

On the other hand, regarding the drag-reducing flow of the surfactant solution, Kawaguchi et al. [15] investigated the turbulent statistics in a two-dimensional channel flow with surfactant additives by using two-component laser-doppler velocimetry (LDV) and particle image velocimetry (PIV). They found that two components of velocity fluctuation were suppressed and Reynolds shear stress almost disappeared in the surfactant drag-reducing flow. Yu et al. [16] and Wu et al. [17] investigated turbulent characteristics in a drag-reducing flow with surfactant additives by direct numerical simulation (DNS). They obtained instantaneous flow structures near the wall, which are difficult to measure precisely in experiments. Thus, various characteristics including turbulent statistics and coherent structures in the drag-reducing flow have been revealed. Li et al. [18] analyzed the Reynolds number dependence of the turbulent structures in a drag-reducing flow by PIV. They measured precisely the velocity of streamwise components u, and wall-normal components v, in the x-y plane at different Reynolds numbers. This revealed the relationship between the dynamic process of the SIS in the solution and turbulence. They also categorized Reynolds number dependence on the drag-reduction into four flow regimes considering that the drag-reduction rate and turbulent statistics were different in each regime, despite similar drag-reduction rates. Itoh and Tamano [19] and Tamano et al. [20] investigated the influence of the drag-reducing flow with surfactant additives on the velocity fields of the turbulent boundary layer using a two-component LDV and PIV. They found the existence of the additional maximum of the streamwise turbulent intensity near the center of the boundary layer. They also proposed a bilayered structure model. The near-wall region has an SIS and viscoelasticity, but the region away from the wall does not have these due to mixing potential and turbulent flow. Therefore, an additional maximum of the streamwise turbulent intensity may appear.

As mentioned above, several studies on the spatial structure of the drag-reducing flow with surfactant additives have been conducted by using PIV. However, there have been few studies of PIV measurement in the x-z plane because of the difficulty. To discuss the spatial structure of the drag-reducing flow of the viscoelastic fluid in more detail, it is important to measure precisely the turbulent statistics in the x-z plane in addition to the x-y plane. Therefore, in this study, we carried out detailed measurements of the instantaneous velocity in the x-y plane and x-z planes by using PIV. In order to analyze the flow pattern in both planes, turbulent statistics including mean velocity profiles, spatial distribution of RMS of velocity fluctuation components u, v and w, Reynolds shear stress, and vorticity fluctuation were calculated. Based on these measurements, the three-dimensional spatial structure in the drag-reducing flow of the viscoelastic fluid was discussed.

2. Experiment

2.1. Experimental Facility and PIV Procedure. Figure 1 shows the flow system of our experimental facility, and Figure 2 shows the PIV system arrangement for measurements (a) in the x-y plane and (b) in the x-z plane. The experiments were performed with a closed-circuit water loop as shown in Figure 1. The test section was a two-dimensional channel made of transparent acrylic resin, which was 6000 mm in length, 500 mm in width, and 40 mm in height (2δ). A honeycomb rectifier was set at the channel entrance to remove large eddies. In order to measure the flow rate Q, an electromagnetic flowmeter with an accuracy of $\pm 0.01\,\mathrm{m}^3/\mathrm{min}$ was installed in the flow path. The bulk mean velocity U_b was estimated from Q/A, and A was the cross-sectional area in the channel. The storage tank in the flow path contained a heater and an agitator in order to adjust the temperature of the fluid, which was maintained at 25°C with an accuracy of ±0.1°C. The PIV measurement was carried out at a position located 5000 mm downstream from the entrance of the test section. In this position, the channel was equipped with two circular glass windows which were 150 mm in diameter on both side walls and with two rectangle glass windows on the top and bottom of the channel. As shown in Figure 2(b), two pressure taps were attached on one side of the channel wall at a distance of 1650 mm. The static pressure gradient between these two taps was measured in order to estimate the drag-reduction rate. Wall shear stress and friction velocity were calculated from this pressure gradient.

The PIV system consisted of a double-pulse laser, laser sheet optics, CCD camera, synchronizer, and a computer with image-processing software (Dantec, Dynamics Studio version 2.30). The double-pulse laser (New Wave Research Co. Ltd., MiniLase-II/30 Hz) was a combination of a pair

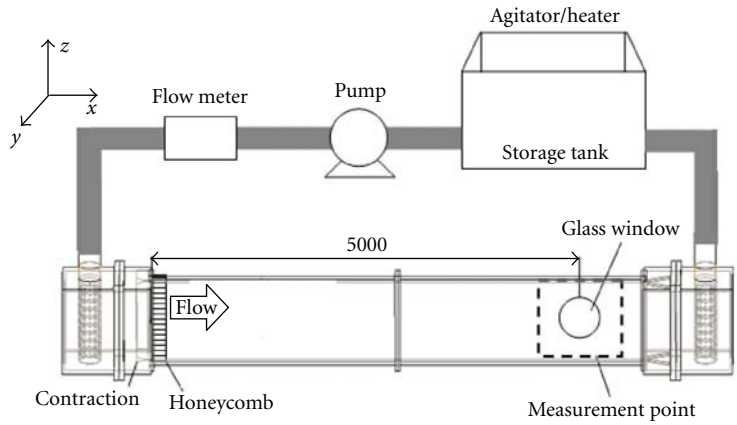

Figure 1: Flow system.

of Nd : YAG lasers, each having an output of 30 mJ/pulse and wavelength of 532 nm. The pulse interval was set to range from 300 μs to 500 μs considering the displacement of particles while measuring flow velocity. The laser sheet thickness and spread angle were set to 0.6 mm and 20°, respectively. The synchronization device communicated with the CCD camera and the computer, and generated pulses to control the double-pulse laser. The CCD camera had a resolution of 2048 × 2048 pixels and pixel pitch of 7.4 × 7.4 μm. The camera lens had a focal length of 60 mm and an aperture of 2.8. The flow was seeded with acrylic colloids to act as tracer particles. These particles were 0.1–1 μm in mean diameter. The particle concentration was adjusted so that more than 10 particles were observed on average in the interrogation area for each experiment. The interrogation area was 64 × 64 pixels with a cross-correlation with each interrogation area overlapping by 75%.

In this study, we measured the instantaneous velocity u-v in the x-y plane and u-w in the x-z plane by using PIV. For the measurements in the x-y plane, the measurement field was set to 70 mm (streamwise direction) × 40 mm (channel height). We obtained 125 × 65 vectors for each direction in the instantaneous velocity fields. Turbulence statistics were calculated from 500 velocity vector fields. On the other hand, for the measurements in the x-z plane, the instantaneous velocity was measured at 40 positions in the y direction, 0.5 mm to 20 mm from the wall at intervals of 0.5 mm, presuming the flow was symmetrical. The measurement field was set to 80 mm (streamwise direction) × 80 mm f(spanwise direction). There were 125 × 125 vectors in the x-z plane in each measurement field. Turbulent statistics were calculated from 100 velocity fields at each y position.

The Reynolds number was defined by the following equation based on the channel height and ranged from 10000 to 25000:

$$\mathrm{Re} = \frac{U_b H}{\nu}, \tag{1}$$

where H is the channel height and ν is the kinematic viscosity of water. Because we used a dilute surfactant solution in our experiment, the kinematic viscosity of the surfactant solutions was not so different from that of water [21].

2.2. Surfactant Solution. The surfactant used in this experiment was a cationic surfactant, cetyltrimethyl ammonium chloride (CTAC: $C_{16}H_{33}N(CH_3)_3Cl$), which had a molecular weight of 320.0 g/mol. Local tap water was used as a solvent because CTAC is hardly affected by the metallic ions of calcium and sodium which naturally exist in tap water. Sodium salicylate (NaSal), with a molecular weight of 160.1 g/mol, was added to this surfactant solution in the same weight concentration in order to provide counter ions. A diluted surfactant solution can produce drag-reduction due to counter ions being in a lower concentration than the critical micelle concentration (CMC). The concentration of the surfactant solution was 25 ppm or 40 ppm.

3. Results and Discussion

3.1. Drag-Reduction Rate. Table 1 shows the drag-reduction rate in each experimental condition. We performed PIV measurement in the x-y plane with different Reynolds numbers, but the Reynolds number was fixed at 20000 for the measurement in the x-z plane. In this paper, the experimental results for each condition are shown by the code name listed in this table.

The drag-reduction rate is defined by the following equation:

$$\mathrm{DR} = \frac{C_{f,w} - C_{f,s}}{C_{f,w}} \times 100\ (\%), \tag{2}$$

where C_f is the friction coefficient, and the subscripts w and s represent water and surfactant solution, respectively. The friction coefficient was calculated by

$$C_f = \frac{\tau_w}{1/2\rho U_b^2}, \tag{3}$$

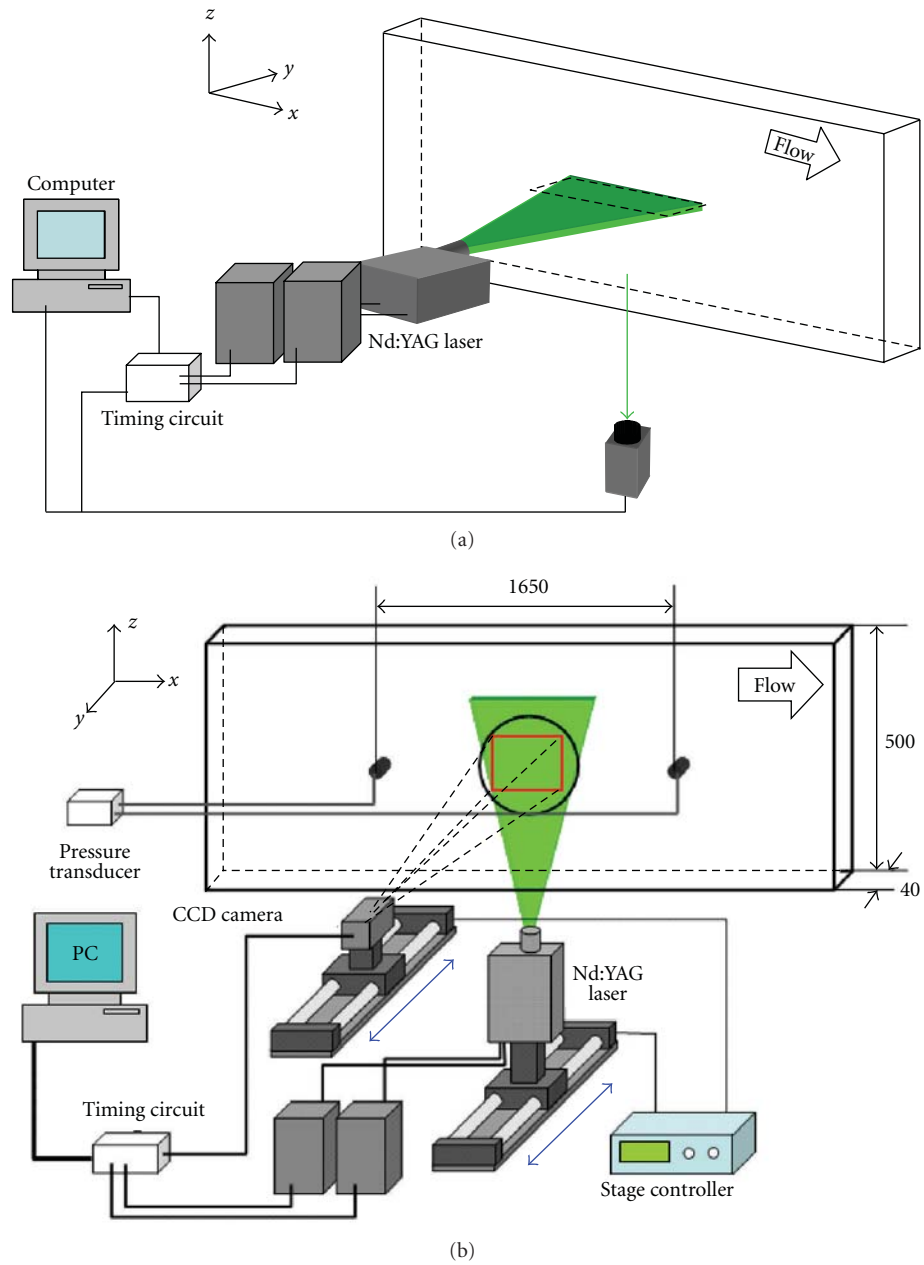

Figure 2: PIV system arrangement for measurements (a) in the x-y plane and (b) in the x-z plane.

where τ_w is the wall shear stress obtained from the static pressure gradient of the channel, and ρ is the density of the water.

The drag-reduction rate increases with increasing Reynolds number, and a 62% maximum drag-reduction rate was obtained. Generally speaking, drag-reduction is related to the existence of a thread-like micelle network in the surfactant solution. Wunderlich and Brunn [22] reported that long thread-like micelles form under high shear rate in the surfactant solution and a shear induced state (SIS) occurs. These thread-like micelles are formed under suitable conditions of steady shear, surfactant concentration, and temperature. It is well known that there is a critical Reynolds number which has a maximum drag-reduction rate in surfactant drag-reducing flow as shown in Figure 3. Li et al. [18] categorized the relationship between Reynolds number and friction coefficient in the case of CTAC 25 ppm at 30°C into the following four regimes: (i) laminar, (ii) increase of drag-reduction rate, (iii) decrease of drag-reduction rate, and (iv) loss of drag-reduction rate as shown in Figure 3. In regime (ii), the drag-reduction rate increases with increasing Reynolds number because moderate shear assists the formation of the micellar network. However, in regime (iii), the micellar network cannot be formed because of the large shear stress. Therefore, the drag-reduction rate decreases in this regime. Moreover, they concluded that a

Table 1: Drag-reduction rate.

Code	Measurement	Fluid	Re	DR(%)
W-10	*x-y*	Water	10000	—
W-15		Water	15000	—
W-20		Water	20000	—
W-25		Water	25000	—
C25-10	*x-y*	CTAC 25 ppm	10000	33
C25-15		CTAC 25 ppm	15000	48
C25-20		CTAC 25 ppm	20000	59
C25-25		CTAC 25 ppm	25000	62
C40-10	*x-y*	CTAC 40 ppm	10000	32
C40-15		CTAC 40 ppm	15000	34
C40-20		CTAC 40 ppm	20000	52
C40-25		CTAC 40 ppm	25000	59
W-20-z	*x-z*	Water	20000	—
C25-20-z		CTAC 25 ppm	20000	59
C40-20-z		CTAC 40 ppm	20000	57

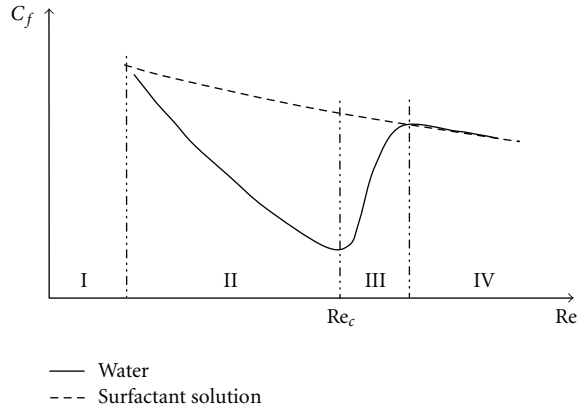

Figure 3: Schematic relationship between friction coefficient and Reynolds number.

critical Reynolds number with a maximum drag-reduction rate exists between regime (ii) and regime (iii). The value of the critical Reynolds number is affected by the surfactant concentrations and temperatures.

Figure 4 shows the result of detailed measurement of the friction coefficient for each concentration of CTAC solution at 25°C. In this figure, the solid line represents the friction coefficient of the two-dimensional rectangular duct flow obtained by Dean [23]:

$$C_f = 0.073\mathrm{Re}^{-1/4}. \quad (4)$$

The critical Reynolds number shifts to a large value with increasing surfactant concentrations. In our experiment, the critical Reynolds number does not agree with the results obtained by Li et al. [18], but the trend corresponds to their results. Because the critical Reynolds number is over 25000 in both concentrations, the drag-reduction rate increases with increasing Reynolds number in both concentrations, and this trend corresponds to the regime (ii).

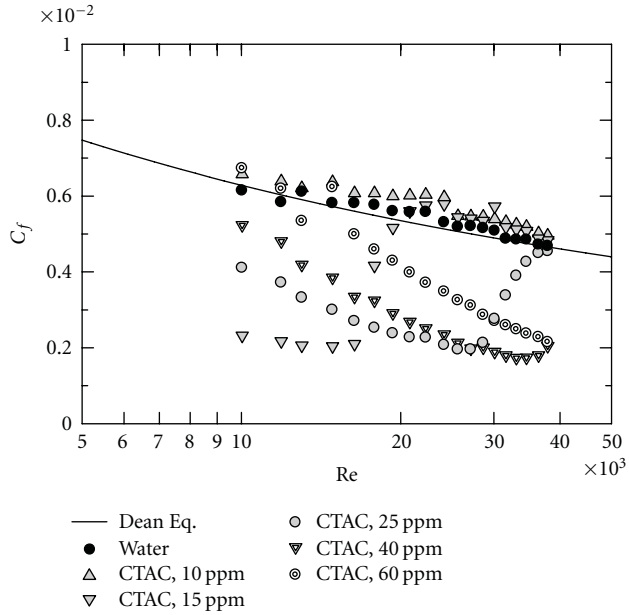

Figure 4: Reynolds number dependence on the friction coefficient.

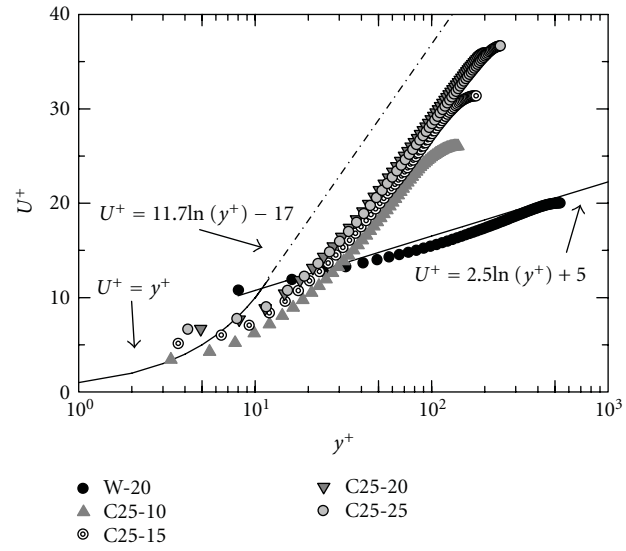

Figure 5: Mean streamwise velocity profiles of the water flow and the drag-reducing flow.

3.2. Mean Streamwise Velocity. Figure 5 shows the mean streamwise velocity profiles in the water flow at Re = 25000 and in CTAC solution for each Reynolds number. U^+ is defined as the mean velocity $\overline{U}$ normalized by friction velocity u_τ and y^+ is defined as position y normalized by ν/u_τ.

The solid line in this figure represents the linear profile and log-law profile of streamwise velocity for Newtonian turbulent flow. The viscous sublayer is expressed by the following equation:

$$U^+ = y^+. \quad (5)$$

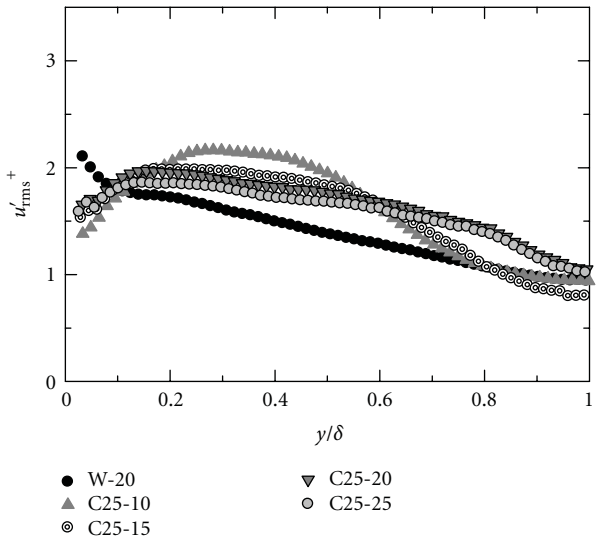

Figure 6: Distribution of RMS of streamwise velocity fluctuation for the 25 ppm surfactant solution.

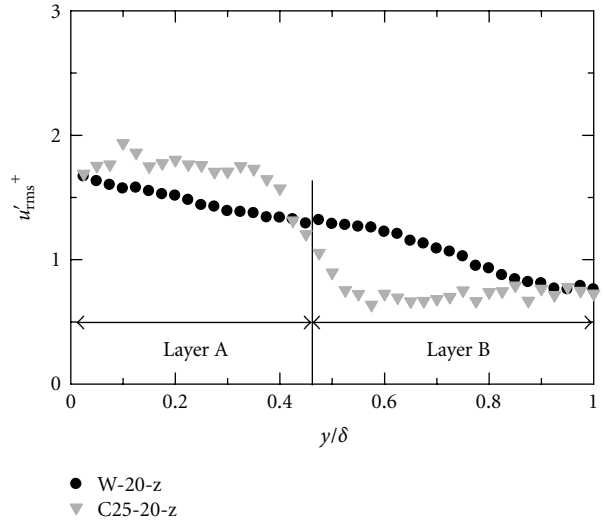

Figure 7: Same as Figure 6 for C25-20 obtained by the measurement in x-z plane.

In addition, the buffer layer and the logarithmic layer are expressed by

$$U^+ = 2.4 \ln y^+ + 5.5. \tag{6}$$

For comparison with our experiment, Virk's ultimate profile in the polymer drag-reducing flow, which was obtained by Virk et al. [24], is plotted using a dashed line in Figure 5. This line represents the following equation:

$$U^+ = 11.7 \ln y^+ - 17. \tag{7}$$

In the water flow, the measured velocity profile is in good agreement with the log-law profile of the turbulent flow of Newtonian fluid. In the drag-reducing flow, the mean velocity profiles are upshifted in the log-law layer with a larger gradient compared with that in the water flow. Of particular significance is that the profile has the same gradient as Virk's ultimate profile at the high drag-reduction rate. According to Warholic et al. [25], if the drag-reduction rate is more than 35% (large drag-reduction), the velocity profile is displaced upward and the gradient increases with increasing drag-reduction rate. Therefore, our result with the homogeneous surfactant solution corresponds to the experimental results with the homogeneous polymer solution obtained by Warholic et al.

3.3. Turbulent Intensity. Figure 6 shows the effect of the Reynolds number on the distribution of the RMS of the streamwise velocity fluctuation u_{rms} normalized by the friction velocity u_τ for 25 ppm surfactant solution. The horizontal axis is normalized by half of the channel height δ. In the water flow, the streamwise velocity fluctuation monotonously decreases from the near-wall to the center of the channel. On the other hand, in the drag-reducing flow, the streamwise velocity fluctuation has a larger value than that of the water flow. Notably, an area appeared where the streamwise velocity fluctuation sharply decreased toward the center of the channel in the drag-reducing flow. For example, in the case of C25-10 (i.e., Re = 10000 and CTAC 25 ppm), this area exists in the range of y/δ from 0.4 to 0.8. This indicates that two different layers coexist on the boundary of this area.

Figure 7 shows the same as Figure 6 obtained by the measurement in the x-z plane. Although the value of the velocity fluctuation is slightly different from the results by the measurements in the x-y plane, the trend corresponds to Figure 6. This figure represents more clearly the structure of the two layers as mentioned in Figure 6.

In this paper, we define these two layers as "Layer A" and "Layer B" as shown in Figure 7. Moreover, h_A is defined as the thickness of Layer A. Comparing Layer A with Layer B, the value of the streamwise velocity fluctuation of Layer A is larger than that of Layer B. As shown in Figure 6, Layer A seems to expand to the center of the channel as the drag-reduction rate increases. A similar tendency was observed with a CTAC of 40 ppm. Therefore, the thickness of the two layers depends on the drag-reduction rate. A detailed discussion of this bilayer structure will be given in another section. In the case of turbulent boundary flow, a characteristic distribution of the streamwise velocity fluctuation was also observed in the drag-reducing flow [19, 20]. However, the detailed structure of these peaks has not been discussed.

The distribution of RMS of wall-normal velocity fluctuation v_{rms} normalized by the friction velocity for the 25 ppm surfactant solution is shown in Figure 8. In the drag-reducing flow, the wall normal velocity fluctuation is much smaller than that of the water flow throughout the channel height. In addition, the decrease level of the wall normal fluctuation is much higher than the increase level of the streamwise velocity fluctuation. This fact suggests that the turbulent energy transport between the different directional

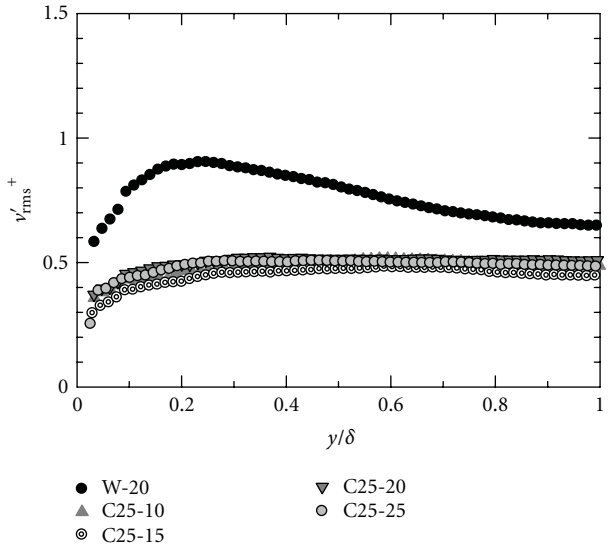

Figure 8: Distribution of RMS of wall-normal velocity fluctuation for 25 ppm surfactant solution.

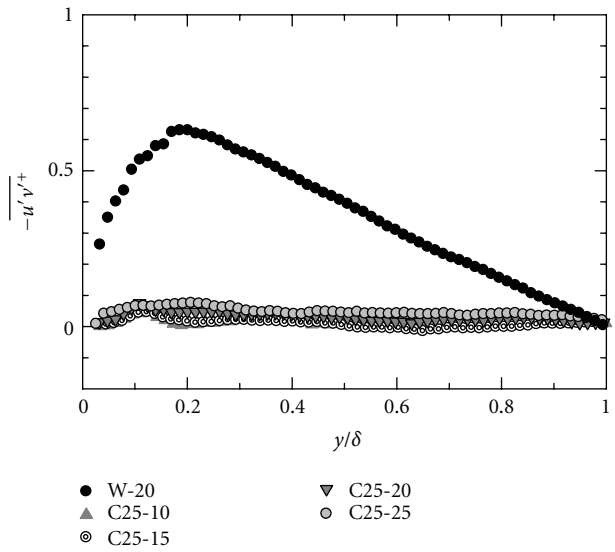

Figure 9: Distribution of Reynolds shear stress for the 25 ppm surfactant solution.

components is inhibited by the effect of additives. Therefore, the directional components become anisotropic in the drag-reducing flow.

Moreover, we observed a slight peak in the wall normal velocity fluctuation at $y/\delta = 0.2$ in the water flow. This peak almost disappeared and the wall normal velocity fluctuation slightly increased toward the center of the channel. This seemed to indicate that the buffer layer expands to the center of the channel in the drag-reducing flow. Yu and Kawaguchi [26] investigated the drag-reducing channel flow by DNS and reported that adding surfactant additives to the water flow altered the energy redistribution. Surfactant additives inhibit the input energy transfer from mean flow to turbulent production, and inhibit energy transfer from the streamwise velocity component to the wall-normal and spanwise velocity components because of the large extensional viscosity. A similar result seems to have been obtained in our experiment.

3.4. Reynolds Shear Stress. Figure 9 shows the distribution of the Reynolds shear stress of the water flow and the drag-reducing flow of the 25 ppm surfactant solution, normalized by the friction velocity. In the drag-reducing flow, Reynolds shear stress is almost zero throughout the channel. This indicates that the momentum transport mechanism of the drag-reducing flow is quite different from that of the Newtonian fluid flow. A similar tendency was also found for the 40 ppm surfactant solution.

The viscoelastic effect of the surfactant solution also appears to increase the velocity fluctuation. Actually, in the drag-reducing channel flow with surfactant solution, the correlation between the streamwise velocity fluctuation and the wall-normal velocity fluctuation decreases, as does the Reynolds shear stress due to the effect of the surfactant solution. A similar result of an increase in fluctuation was reported in turbulent boundary layer experiments with a surfactant solution conducted by Tamano et al. [20]. In addition, an increase in the Reynolds number corresponded to an increase of the Weissenberg number defined by relaxation time and friction velocity. Tsukahara et al. [27] and Yu and Kawaguchi [28] carried out a DNS study of the drag-reducing flow using the Giesekus model for surfactant solutions and investigated the relation between the Weissenberg number and drag-reduction. According to their calculations, high drag-reduction can be achieved by suppressing the production of turbulence for a high Weissenberg number. Therefore, our experimental results match those of their DNS study.

3.5. Vorticity Intensity. We calculated turbulent statistics of vorticity fluctuation ω'_y. ω_y is defined in the following equation:

$$\omega_y = \frac{\partial w}{\partial x} - \frac{\partial u}{\partial z}. \tag{8}$$

In this study, the calculational procedure of ω_y is based on the circulating volume of the surrounding 8 velocity values as shown in Figure 10. Therefore, ω_y in the position (i, j) is expressed with the following equation:

$$\left(\overline{\omega}_y\right)_{i,j} = \frac{1}{A}\Gamma_{i,j} = \frac{1}{A}\oint_{l(X,Z)} (U, W) \cdot dl, \tag{9}$$

where A represents the circulation pathway.

Figure 11 shows the effect of the surfactant concentration on the distribution of the vorticity fluctuation ω^*_{yrms} for Re = 20000. ω^*_{yrms} is normalized by the following equation:

$$\omega^*_{\text{yrms}} = \frac{\omega'_{\text{yrms}} \cdot (H/2)}{U_b}. \tag{10}$$

This figure indicates that the vorticity fluctuation monotonously decreases from the near-wall to the center of

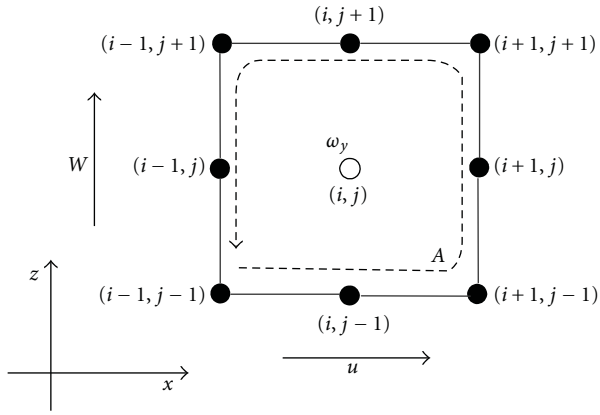

Figure 10: Calculation route of vorticity in the position (i, j).

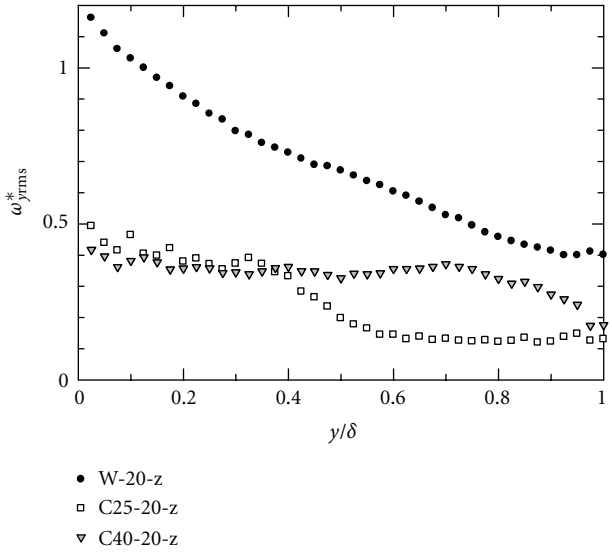

Figure 11: Effect of surfactant concentration on the distribution of the vorticity fluctuation at Re = 20000.

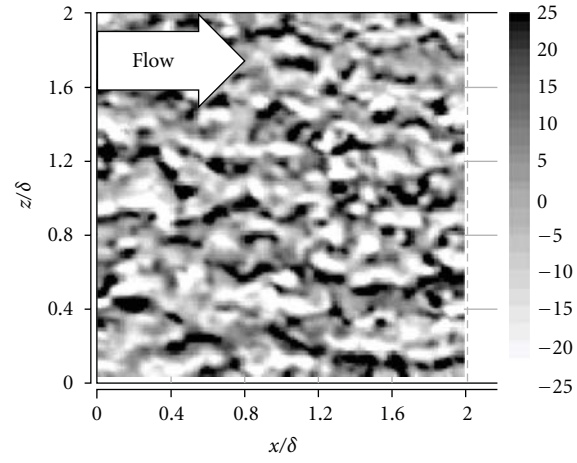

(a) $y/\delta = 0.025$

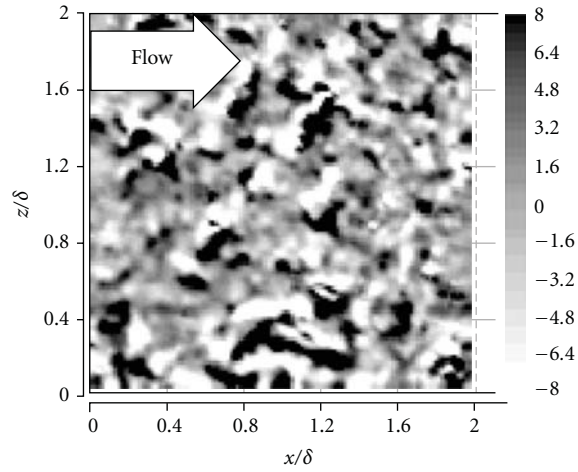

(b) $y/\delta = 1.0$

Figure 12: Instantaneous vorticity fluctuation map of the water flow at Re = 20000; (a) $y/\delta = 0.025$ and (b) $y/\delta = 1.0$.

the channel in the water flow. On the other hand, the vorticity fluctuation in the drag-reducing flow is much smaller than that in water flow throughout the channel height. This suggests that the turbulent vortex is suppressed in the drag-reducing flow, and drag-reduction occurs. Similar to the distribution of the streamwise velocity fluctuation, Layer A and Layer B can be observed in the same area. In addition, the value of the vorticity fluctuation of Layer A is larger than that of Layer B.

Figure 12 shows the instantaneous vorticity fluctuation map in the water flow obtained by the measurement in the x-z plane. In this figure, (a) and (b) show the structure in the near-wall region ($y/\delta = 0.025$) and at the center of the channel ($y/\delta = 1.0$), respectively. The contour is determined from the value of the vorticity fluctuation at each position, and a positive value indicates a clockwise rotation. In the case of the water flow, although the value of the vorticity fluctuation is different, the flow patterns are similar to each position. In addition, similar patterns were also observed at all other positions in the water flow.

On the other hand, Figure 13 shows an instantaneous vorticity fluctuation map in the drag-reducing flow at the position (a) $y/\delta = 0.025$ (i.e., the near-wall region), (b) $y/\delta = 0.4$ (i.e., edge of Layer A), (c) $y/\delta = 0.6$ (i.e., edge of Layer B) and (d) $y/\delta = 1.0$ (i.e. center of the channel), respectively. In Layer A (see Figures 13(a) and 13(b)), the distribution of the vorticity fluctuation pattern shows a striped structure. In contrast, quite a different structure was observed in Layer B (see Figures 13(c) and 13(d)). It had a grained structure and this structure was similar to the pattern of the water flow but the spatial structure scale was much smaller (see Figure 12). In Layer A, the striped structure seemed to stretch along streamwise, and streaks with a variety of lengths were observed. The pattern was not very different from that for other Reynolds numbers or concentrations.

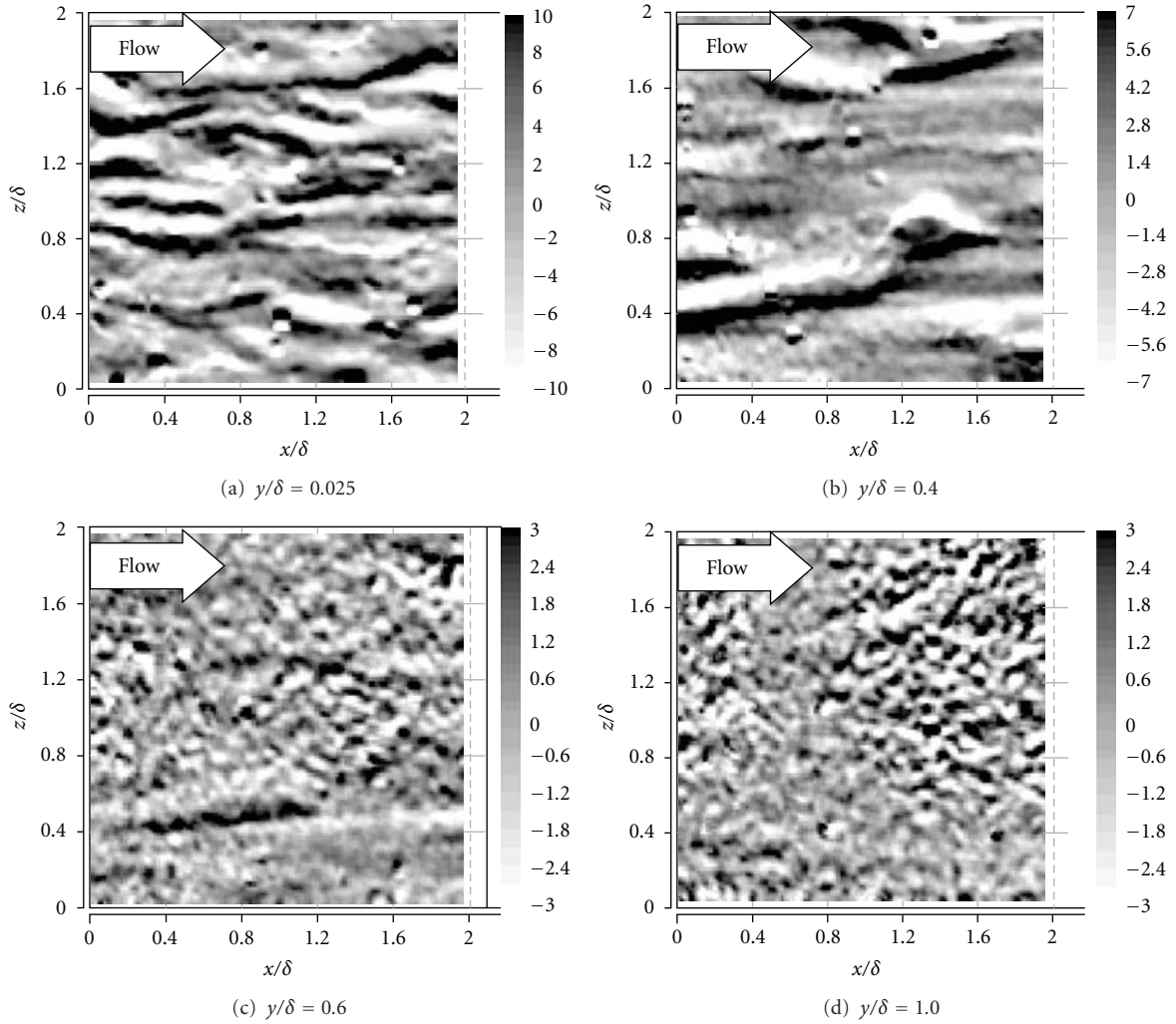

Figure 13: Instantaneous vorticity fluctuation map of the drag-reducing flow for Re = 20000; (a) $y/\delta = 0.025$, (b) $y/\delta = 0.4$, (c) $y/\delta = 0.6$, and (d) $y/\delta = 1.0$.

In our previous study [29], we measured the instantaneous velocity of the drag-reducing channel flow in the x-y plane by using a PIV system with a large measurement field. As a result, in the drag-reducing flow, there were large-scale fluid lumps in the near wall region. These structures extended toward the streamwise direction and were inclined at approximately 10 degrees to the channel wall. These characteristic structures were only observed in the case of high drag-reduction rate, and the tendency of these structures did not change with varying Reynolds number. The striped structure which stretches to the streamwise direction corresponds to this large-scale structure.

3.6. Discussion of the Bilayer Structure. Figure 14 shows the schematic interpretation of the relation between the thickness of two layers and the drag-reduction rate. When the drag-reduction rate increases, the thickness of Layer A spreads to the center of the channel. On the other hand, in the case of a low drag-reduction rate, Layer A is thin. This characteristic difference of structure seems to be attributed to SIS, which is characteristic of viscoelastic fluid. In Layer A, SIS occurs and contributes to the drag-reduction. In contrast, Layer B does not contribute to the drag-reduction and SIS does not occur because the instantaneous vorticity fluctuation map is similar to the water flow in this layer.

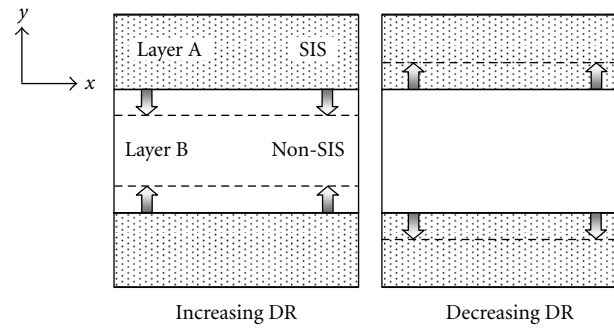

Figure 14: Schematic interpretation of relation between thickness of two layers and the drag-reduction rate.

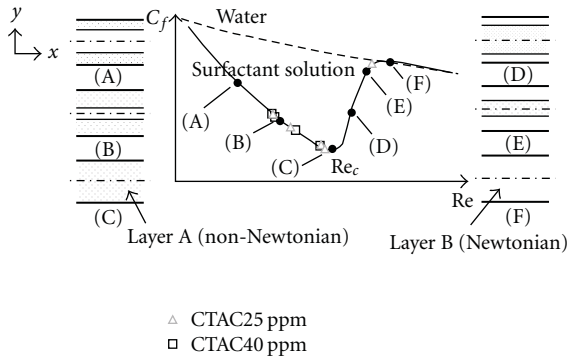

Figure 15: Detailed discussion of the relation between the bilayer structure and drag-reduction.

Yu and Kawaguchi [30] and Wu et al. [17] investigated drag-reducing channel flow using the Giesekus model by DNS. They applied a bilayer model, in which Newtonian and non-Newtonian fluids coexist. In their calculation, the interface between two layers sets to parallel to the wall and normal stress balance equation was satisfied. If the network structure (non-Newtonian fluids) exists in the near-wall region, the thickness of this layer spreads with increasing drag-reduction rate. Comparing the distribution of turbulent intensity between our experiment and their DNS results, they found that the distribution of the streamwise velocity fluctuation had the same or a larger value compared to the water one, but the distribution of the wall normal velocity distribution was smaller than the water one. Similar results were obtained in our experiment except for the area where the streamwise velocity fluctuation sharply decreased toward the center of the channel in the drag-reducing flow.

Figure 15 shows a schematic interpretation of the relation between the thickness of the two layers and the friction coefficient (i.e., drag-reduction rate). When the drag-reduction rate increased (i.e., a friction coefficient decreased) before the critical Reynolds number, the Non-Newtonian fluid (SIS) which contributed to drag-reduction existed in the near-wall region due to moderate shear stress, and the thickness of this layer spread to the center of the channel like (A) and (B) as shown in Figure 15, and in the region away from the wall (i.e., Newtonian fluid), shear stress was not enough for SIS to occur. Then, as the Reynolds number reached a critical point, the Non-Newtonian fluid spread all over the channel represented as (C) and the drag-reduction rate reached the maximum. Beyond the critical Reynolds number, drag-reduction rate decreased and non-Newtonian fluid existed in a region away from the wall, like (D) and (E). This was because the shear rate near the wall was so large it could not form a network structure in the near-wall region. Finally, as the Reynolds number increased more, drag-reduction vanished due to the high shear rate all over the channel and the non-Newtonian fluid disappeared as shown (F).

In our experiment, because a large drag-reduction occurred, the flow structure seemed to be like (B) or (C). In addition, we observed that the flow pattern of Layer B was similar to the water flow. Although there is no conclusive evidence that Layer A has similar characteristics to the non-Newtonian fluids, the bilayer structure observed in our experiment corresponds to these DNS results. More detailed experiments will be performed to clarify the flow structures of the two layers in the drag-reducing surfactant flow in the future.

3.7. Summary of the Zonal Structure. Finally, we describe briefly the zonal structure of the drag-reducing channel flow observed in this study and previous studies [29]. As shown in Figure 7, there appeared an area where the streamwise velocity fluctuation sharply decreased toward the center of the channel in the drag-reducing flow. Therefore, two layers having different structures appear to coexist on the boundary of this area in the drag-reducing channel flow. The structure near the center of the channel (Layer B) has a grained pattern, which is similar to the pattern of the water flow. On the other hand, the structure in the near-wall region (Layer A) has a striped pattern which extends in the streamwise direction. The pattern is not so different at other Reynolds numbers or concentrations but the thickness of Layer A spreads to the channel center as the drag-reduction rate increases. According to our previous study [29], sweep and ejection are greatly suppressed and large-scale inclined fluid lumps appear alternately in Layer A. In contrast, these fluid lumps do not appear in the center of the channel (Layer B). For the same CTAC concentration, the scale and inclination angle of these large-scale structures did not depend on Reynolds number and rheological parameters.

4. Conclusions

Characteristic zonal structures of the drag-reducing channel flow with surfactant additives were investigated experimentally. We performed PIV measurement of the instantaneous velocity in the *x-y* plane and in the *x-z* plane with changing Reynolds number and the weight concentration of CTAC. The following conclusions on the drag-reducing flow were obtained.

(1) The distribution of the wall normal velocity fluctuation in the drag-reducing flow was much smaller than that of the water flow and Reynolds shear stress in the drag-reducing flow was almost zero throughout the channel.

(2) The streamwise velocity fluctuation monotonously decreased from the near-wall to the center of the channel in the water flow, but an area appeared where the streamwise velocity fluctuation sharply decreased toward the center of the channel in the drag-reducing channel flow. This indicated that two layers having different structures appeared to coexist on the boundary of this area. The distribution of the vorticity fluctuation also sharply decreased in the same area.

(3) The layer in the near-wall region had a striped structure, and the layer in the center of the channel had a grained structure. This grained structure was similar

to the flow structure of the water flow. The thickness of the layer in the near-wall region expanded toward the center of the channel as the drag-reduction rate increased. These characteristic differences seem to be attributed to the SIS and viscoelasticity of the fluid.

Acknowledgments

The authors would like to thank Mr. A. Saito of Mitsubishi Heavy Industries, Ltd., and Mr. D. Tsurumi of the Tokyo University of Science for their collaboration in this study.

References

[1] B. A. Toms, "Some observations on the flow of linear polymer solutions through straight tubes at large Reynolds numbers," in *Proceedings of the 1st International Congress on Rheology*, pp. 135–141, Amsterdam, The Netherlands, 1978.

[2] E. D. Burger, W. R. Munk, and H. A. Wahl, "Flow increase in the Trans Alaska Pipeline through use of a polymeric drag-reducing additive," *Journal of Petroleum Technology*, vol. 34, no. 2, pp. 377–386, 1982.

[3] L. R. Cox, E. H. Dunlop, and A. M. North, "Role of molecular aggregates in liquid drag reduction by polymers," *Nature*, vol. 249, no. 5454, pp. 243–245, 1974.

[4] I. A. Kadoma, C. Ylitalo, and J. W. Van Egmond, "Structural transitions in wormlike micelles," *Rheologica Acta*, vol. 36, no. 1, pp. 1–12, 1997.

[5] B. Lu, X. Li, L. E. Scriven, H. T. Davis, Y. Talmon, and J. L. Zakin, "Effect of chemical structure on viscoelasticity and extensional viscosity of drag-reducing cationic surfactant solutions," *Langmuir*, vol. 14, no. 1, pp. 8–16, 1998.

[6] Y. Hu and E. F. Matthys, "Rheological and rheo-optical characterization of shear-induced structure formation in a nonionic drag-reducing surfactant solution," *Journal of Rheology*, vol. 41, no. 1, pp. 151–166, 1997.

[7] Y. Hu and E. F. Matthys, "Characterization of micellar structure dynamics for a drag-reducing surfactant solution under shear: normal stress studies and flow geometry effects," *Rheologica Acta*, vol. 34, no. 5, pp. 450–460, 1995.

[8] K. Gasljevic and E. F. Matthys, "Field test of a drag-reducing surfactant additive in a hydronic cooling system," in *Proceedings of the ASME Fluids Engineering Division Summer Meeting*, vol. 237, pp. 249–260, 1996.

[9] H. Takeuchi et al., "Actual proof test of energy conservation in central heating/cooling system adapting surfactant drag reduction," in *Proceedings of the 8th International Conference on Sustainable Energy Technologies*, Aachen, Germany, 2009.

[10] M. D. Warholic, D. K. Heist, M. Katcher, and T. J. Hanratty, "A study with particle-image velocimetry of the influence of drag-reducing polymers on the structure of turbulence," *Experiments in Fluids*, vol. 31, no. 5, pp. 474–483, 2001.

[11] C. D. Dimitropoulos, R. Sureshkumar, A. N. Beris, and R. A. Handler, "Budgets of Reynolds stress, kinetic energy and streamwise enstrophy in viscoelastic turbulent channel flow," *Physics of Fluids*, vol. 13, no. 4, pp. 1016–1027, 2001.

[12] V. S. R. Somandepalli, X. Y. Hou, and M. G. Mungal, "Turbulent schmidt number measurements in a polymer drag-reduced turbulent boundary layer," in *Proceedings of the 6th International Symposium on Turbulence and Shear Flow Phenomena*, Seoul, Korea, 2009.

[13] Y. Wang, B. Yu, J. J. Wei, F. C. Li, and Y. Kawaguchi, "Direct numerical simulation on drag-reducing flow by poly-mer additives using a spring-dumbbell model," *Progress in Computational Fluid Dynamics*, vol. 9, no. 3–5, pp. 217–224, 2009.

[14] C. M. White and M. G. Mungal, "Mechanics and prediction of turbulent drag reduction with polymer additives," *Annual Review of Fluid Mechanics*, vol. 40, pp. 235–256, 2008.

[15] Y. Kawaguchi et al., "Turbulent transport mechanism in a drag-reducing flow with surfactant additive investigated by two component LDV," in *Proceedings of the 8th International Symposium on Applications of Laser Techniques to Fluid Mechanics*, pp. 4.1–4.7, Lisbon, Portugal, 1996.

[16] B. Yu, F. Li, and Y. Kawaguchi, "Numerical and experimental investigation of turbulent characteristics in a drag-reducing flow with surfactant additives," *International Journal of Heat and Fluid Flow*, vol. 25, no. 6, pp. 961–974, 2004.

[17] X. Wu et al., "DNS study on heat transfer reduction of drag-reducing channel flow induced by surfactant additives with a bilayer mode," in *Proceedings of the 2nd Asian Symposium on Computational Heat Transfer and Fluid Flow*, pp. 175–181, Jeju, Korea, 2009.

[18] F.-C. Li, Y. Kawaguchi, T. Segawa, and K. Hishida, "Reynolds-number dependence of turbulence structures in a drag-reducing surfactant solution channel flow investigated by particle image velocimetry," *Physics of Fluids*, vol. 17, no. 7, pp. 1–13, 2005.

[19] M. Itoh and S. Tamano, "Drag reduction of turbulent flows of surfactant solutions," in *Proceedings of the 7th JSME-KSME Thermal and Fluids Engineering Conference*, Sapporo, Japan, 2008.

[20] S. Tamano, M. Itoh, T. Inoue, K. Kato, and K. Yokota, "Turbulence statistics and structures of drag-reducing turbulent boundary layer in homogeneous aqueous surfactant solutions," *Physics of Fluids*, vol. 21, no. 4, Article ID 045101, 2009.

[21] Y. Kawaguchi, B. Yu, J. Wei, and Z. Feng, "Rheological characterization of drag-reducing cationic surfactant solution -shear and elongational viscosities of dilute solutions," in *Proceedings of the 4th ASME/JSME Joint Fluids Engineering Conference*, pp. 721–728, Honolulu, Hawaii, USA, July 2003.

[22] A. M. Wunderlich and P. O. Brunn, "The complex rheological behavior of an aqueous cationic surfactant solution investigated in a Couette-type viscometer," *Colloid & Polymer Science*, vol. 267, no. 7, pp. 627–636, 1989.

[23] R. B. Dean, "Reynolds number dependence of skin friction and other bulk flow variables in two-dimensional rectangular duct flow," *Journal of Fluids Engineering*, vol. 100, no. 2, pp. 215–223, 1978.

[24] P. Virk et al., "The ultimate asymptote and mean flow structure in Toms phenomenon," *Journal of Applied Mechanics*, vol. 37, no. 2, pp. 488–493, 1970.

[25] M. D. Warholic, H. Massah, and T. J. Hanratty, "Influence of drag-reducing polymers on turbulence: effects of Reynolds number, concentration and mixing," *Experiments in Fluids*, vol. 27, no. 5, pp. 461–472, 1999.

[26] B. Yu and Y. Kawaguchi, "Direct numerical simulation of viscoelastic drag-reducing flow: a faithful finite difference method," *Journal of Non-Newtonian Fluid Mechanics*, vol. 116, no. 2-3, pp. 431–466, 2004.

[27] T. Tsukahara et al., "DNS study on viscoelastic effect in drag-reduced turbulent channel flow," *Journal of Turbulence*, vol. 12, pp. 1–25, 2010.

[28] B. Yu and Y. Kawaguchi, "Effect of Weissenberg number on the flow structure: DNS study of drag-reducing flow with

surfactant additives," *International Journal of Heat and Fluid Flow*, vol. 24, no. 4, pp. 491–499, 2003.

[29] M. Motozawa, T. Watanabe, and Y. Kawaguchi, "PIV measurements of large-scale structures in a drag-reducing channel flow with surfactant additives," *Nihon Reoroji Gakkaishi*, vol. 39, no. 3, pp. 99–104, 2011.

[30] B. Yu and Y. Kawaguchi, "DNS of drag-reducing turbulent channel flow with coexisting Newtonian and non-Newtonian fluid," *Journal of Fluids Engineering*, vol. 127, no. 5, pp. 929–935, 2005.

Hindawi Publishing Corporation
Advances in Mechanical Engineering
Volume 2011, Article ID 367042, 9 pages
doi:10.1155/2011/367042

Research Article

Analysis of Zero Reynolds Shear Stress Appearing in Dilute Surfactant Drag-Reducing Flow

Weiguo Gu,[1] Dezhong Wang,[1] and Yasuo Kawaguchi[2]

[1] *School of Mechanical Engineering, Shanghai Jiao Tong University, Shanghai 200240, China*
[2] *Department of Mechanical Engineering, Faculty of Science and Technology, Tokyo University of Science, 278-8510, Japan*

Correspondence should be addressed to Weiguo Gu, guweiguo@sjtu.edu.cn

Received 3 June 2011; Accepted 18 July 2011

Academic Editor: Jinjia Wei

Dilute surfactant solution of 25 ppm in the two-dimensional channel is investigated experimentally compared with water flow. Particle image velocimetry (PIV) system is used to take 2D velocity frames in the streamwise and wall-normal plane. Based on the frames of instantaneous vectors and statistical results, the phenomenon of zero Reynolds shear stress appearing in the drag-reducing flow is discussed. It is found that 25 ppm CTAC solution exhibits the highest drag reduction at Re = 25000 and loses drag reduction completely at Re = 40000. When drag reduction lies in the highest, Reynolds shear stress disappears and reaches zero although the RMS of the velocity fluctuations is not zero. By the categorization in four quadrants, the fluctuations of 25 ppm CTAC solution are distributed in all four quadrants equally at Re = 25000, which indicates that turnaround transportation happens in drag-reducing flow besides Reynolds shear stress transportation. Moreover, the contour distribution of streamwise velocity and the fluctuations suggests that turbulence transportation is depressed in drag-reducing flow. The viscoelasticity is possible to decrease the turbulence transportation and cause the turnaround transportation.

1. Introduction

If small amounts of polymer or surfactant are added into the water, the friction will decrease in a large degree in turbulent flow. This phenomenon of drag reduction is named "Toms effect" because it was firstly reported by Toms in 1948 [1]. Li et al. reported that ultimate 80% frictions were reduced in the very dilute aqueous solution of cetyltrimethylammonium-chloride (CTAC) while the concentration was only 30 ppm [2, 3]. For the energy conservation purpose, surfactant solution has increasingly received the significant attention during the past some decades studying by experiments and simulations in order to clarify the mechanism of drag reduction [4, 5]. Gyr and Tsinober summarized the dynamic characteristics of drag-reducing flow, and concluded that the small scale part of the flow (both in time and space) was suppressed, and the streamwise velocity fluctuations remained approximately the same whereas the transverse one was strongly reduced [6].

Reynolds shear stress is important to the turbulence transportation in wall-bounded flow [7], but it was strongly reduced in drag-reducing flow and some researchers ascribed the phenomenon to the less correlation between the two velocity fluctuations. Moreover, surfactant solution flow exhibited that the cyclic turbulent bursts were inhibited and the vortex structures were modified [8]. Kawaguchi et al. found that the penetration of the fluid from the low-speed fluid region into the high-speed region almost disappeared, and the strong fluctuations of spanwise vorticity near the wall also disappeared in surfactant solution channel flow [9, 10]. Li et al. found that the inclination angle of the low-momentum region below the hairpin vortices decreased and the frequency of bursts was reduced, which indicated the inhibition of bursting events by surfactant additives [11, 12]. However, all these studies have not given the reasonable explanation to the appearance of zero Reynolds shear stress.

Rheology of the solution, such as the viscoelasticity, was always considered to modify the turbulent structures and lead to the phenomenon of drag reduction [13], because surfactant additives added into the water would form the cross-linked micellar networks under a proper shear stress [14, 15]. The investigation by Cryo-TEM proved that the solution

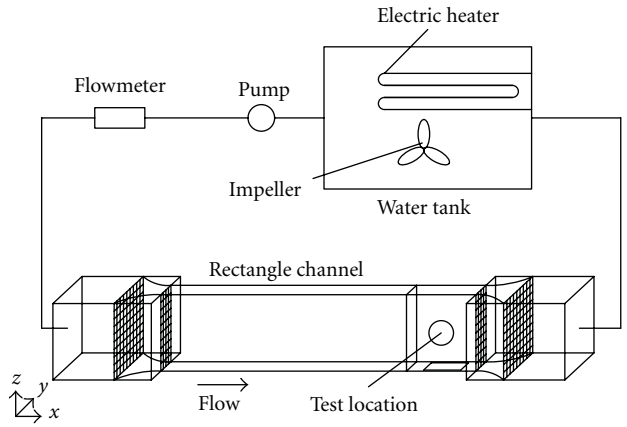

Figure 1: Schematic diagram of solution circulation system in experiment.

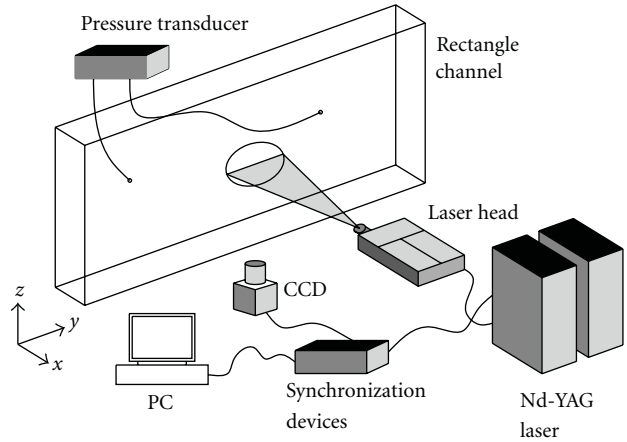

Figure 2: Optical configuration of PIV system.

with wormlike micella displayed rich rheological behaviors such as drag-reducing agents and viscosity enhancers [16]. But the micella have not been tested dynamically because of the shortage of present measure method.

This paper will aim at the modification of turbulence transportation in the drag-reducing channel flow and analyze the disappearance of Reynolds shear stress. PIV is used to measure the velocity field in streamwise-wall-normal plane. The dynamic characteristics of the surfactant solution flow are studied based on the statistic results and instantaneous velocity distribution.

2. Experimental Facility

Experiments are performed on a closed-circuit water loop as shown in Figure 1. The tested fluid is through a two-dimensional channel made of transparent acrylic resin with the length (L) of 10 m, height (H) of 0.04 m, and width (W) of 0.5 m. A honeycomb rectifier with length of 0.15 m is set at the channel entrance for removing large eddies. The test segment lies 6 m downstream from the entrance of the channel. An electromagnetic flow meter with uncertainty of $\pm 0.01\,\mathrm{m}^3/\mathrm{min}$ is installed upstream of the channel for flow measurement. The water tank in the flow loop contains an electrical heater for heating the circulating solution with uncertainty of $\pm 0.1^\circ$C when the fluid temperature is below 25°C. The wall shear stress was estimated from the static pressure gradient which is tested between two pressure tabs which are located on the vertical side wall of the channel with 1.5 m distance and the uncertainty of ± 0.1 Pa.

The surfactant added to the water in this experiment is one kind of cationic surfactant, cetyltrimethylammonium-chloride (CTAC). Sodium salicylate (NaSal) is added to the solution with the same weight concentration with CTAC for providing counterions. The CTAC concentration of 25 ppm is selected in this experiment.

PIV system consists of a double-pulsed laser, laser sheet optics, charge-coupled device (CCD) camera, timing circuit, image-sampling computer, and image-processing software. The double-pulsed laser isa combination of a pair of Nd-YAG lasers. The timing circuit communicates with the CCD camera and computer and generates pulses to control the double-pulse laser. The CCD camera used in the experiment has a resolution of 2048×2048 pixels. Figure 2 shows a schematic of the optical configuration of PIV to measure the flow on the streamwise and wall-normal (x-y) plane. Cartesian coordinates are also shown in the diagram. The laser sheets are aligned at $z = 250$ mm, where $z = 0$ represents the plane at the bottom of the channel. The tracers seeded in the flow are white water-based synthetic resins coatings with a diameter of 0.1–1 μm. When adding tracers to the solution, particle density is adjusted and on average at least 10 particle pairs will be observed in an interrogation window.

In the experiments, five hundred of PIV image pairs are taken for one condition case. The photograph acquisition rate is 4 Hz. The picture frames cover the full width of the channel with the size of about $x \times y = 58 \times 42\,\mathrm{mm}^2$. The interrogation area is set as 32×32 pixels with 75% overlap in each direction. As a result, the vector numbers are about 127×90, respectively, in x and y direction. The spacing between adjacent vectors in both directions is about 0.45 mm.

3. Results and Discussion

This section will analyze the instantaneous velocity images and the statistic results based on five hundred of 2D frames of velocity vectors in streamwise-wall-normal (x-y) plane. Water and CTAC solution with the weight concentration of 25 ppm are compared under the Reynolds number from 10000 to 40000. Reynolds number is defined as $\mathrm{Re} = U_b W/\mu$, where U_b is the bulk velocity of the flow, W is the width of the channel in y direction, and μ is the dynamic viscosity of the solution. However, the CTAC solution of 25 ppm is very dilute, so the dynamic viscosity of the solution is selected as same as the water.

3.1. Frictional Drag Factor and Drag Reduction Rate. Fanning friction factor and drag reduction (DR) are defined as

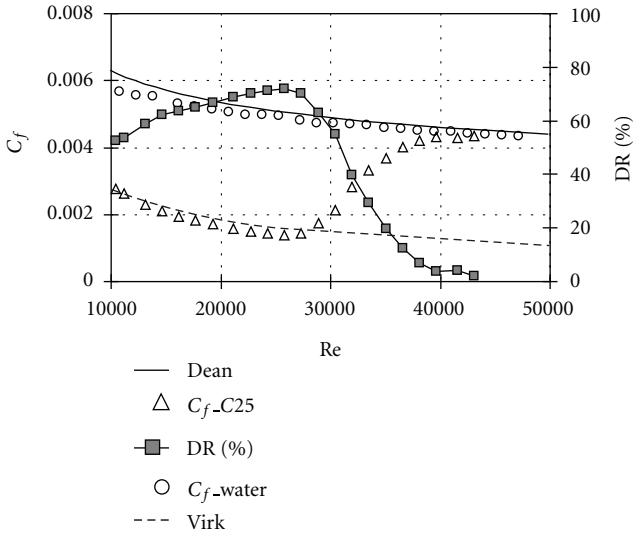

Figure 3: Distributed profiles of drag coefficient (C_f) and drag reduction (DR).

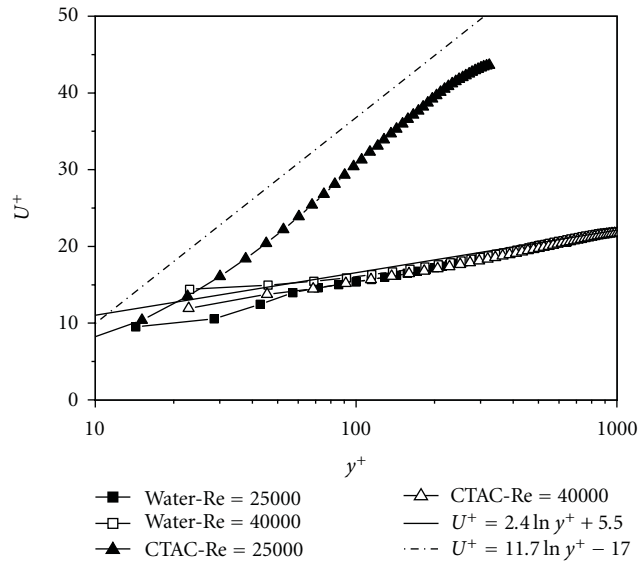

Figure 4: Distributed profiles of U^+ across the channel.

following equations where the subscripts of "W" and "C" represent water and CTAC solution, respectively,

$$C_f = \frac{\tau_w}{\left(1/2\rho U_b^2\right)},$$
$$\text{DR} = \frac{\left(C_{f,W} - C_{f,C}\right)}{C_{f,W}} \times 100\%. \tag{1}$$

The profiles of friction factor and DR are presented in Figure 3. At the same time, Dean's correlation of friction factor for a Newtonian fluid in a two-dimensional channel [17]

$$C_f = 0.073\text{Re}^{-0.25} \tag{2}$$

and Virk's ultimate correlation of friction factor for polymers solution flow [18]

$$C_f = 0.58\text{Re}^{-0.58} \tag{3}$$

are also included in Figure 3 for comparison.

The figure exhibits that the friction factors of water obey Dean's equation well especially during the high Reynolds numbers. The friction factors of CTAC solution are markedly smaller than the water and reach the profile of Virk's ultimate friction factor before Re = 27000. According to the division of DR state [19], the Reynolds number at which DR reaches the maximum is called the 1st critical Reynolds number and at which DR disappears completely is called the 2nd critical Reynolds number. As a result, Re = 25000 where DR reaches the maximum nearly 80% is the 1st critical Reynolds number for 25 ppm CTAC solution at the temperature of 25°C in this experiment. When the Reynolds number is larger than the 1st critical Reynolds number, the friction becomes large and DR decreases quickly while Re increases which indicates the degradation of drag reduction. DR almost disappears at Re = 40000.

3.2. Mean Velocity and Fluctuations. At the same Reynolds number, five hundred of velocity frames are used to do statistical average. Then ensemble average is performed along streamwise direction based on about fifty thousand of vectors at one identical y coordinate.

Figure 4 presents the profiles of mean streamwise velocities handled dimensionlessly with friction velocity (u_τ) which is marked as the superscript "+". Because the CTAC solution of 25 ppm exhibits the maximal DR at Re = 25000 and drag reduction degradation at Re = 40000, these two Reynolds numbers are selected for comparison with Newtonian.

The log law equation of mean velocity for Newtonian turbulent flow

$$U^+ = 2.4 \ln y^+ + 5.5 \tag{4}$$

and the ultimate velocity profile of polymeric solution flow suggested by Virk

$$U^+ = 11.7 \ln y^+ - 17.0 \tag{5}$$

are included in Figure 4, where $y^+ = y\rho u_\tau/\mu$.

Figure 4 shows that mean streamwise velocities of water are distributed in close agreement with the profile of (4) for Newtonian turbulent channel flow. This phenomenon also appears in the case of 25 ppm CTAC solution at Re = 40000 because drag reduction disappears completely. At Re = 25000, the mean streamwise velocities of 25 ppm CTAC solution are distributed upward and close to the line of (5).

Root mean square (RMS) is defined as (6), where N represents the number of the vectors. RMS is usually regarded as the representation of turbulence intensity.

$$\text{RMS} = \sqrt{\frac{1}{N}\sum_i^N \left(u_i^+ - U^+\right)^2}. \tag{6}$$

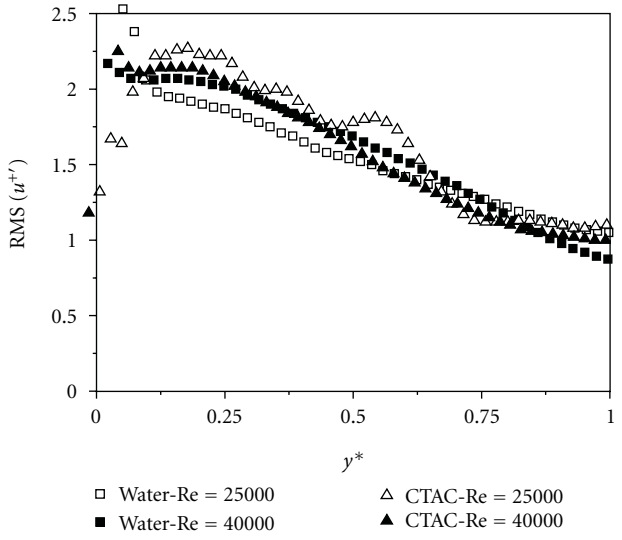

(a) RMS of $u^{+\prime}$

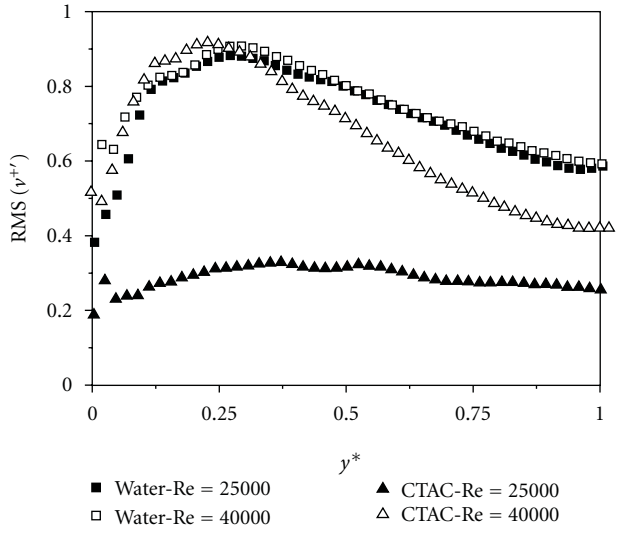

(b) RMS of $v^{+\prime}$

Figure 5: Profiles of RMS of velocity fluctuations across the channel.

Figures 5(a) and 5(b) exhibit the RMS-distributed profiles, respectively, of streamwise velocity fluctuations ($u^{+\prime}$) and wall-normal velocity fluctuations ($v^{+\prime}$). The abscissa of the figure is the wall-normal coordinate (y^*) in the channel where the superscript "$*$" represents the dimensionless of geometry by the half of channel width ($y^* = 2y/W$).

Small difference appears in the distribution of streamwise velocity fluctuations of the two fluids at two Reynolds numbers in Figure 5(a), whereas the wall-normal velocity fluctuations decrease in a large degree for 25 ppm CTAC solution at Re = 25000. This phenomenon indicates that the wall-normal fluctuations are depressed in drag reducing flow. As mentioned above, some references suppose that

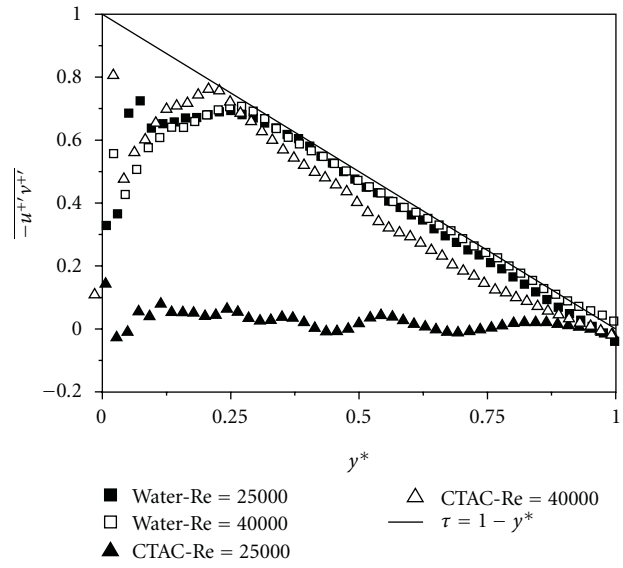

Figure 6: Distributed profiles of Reynolds shear stress ($-\overline{u^{+\prime}v^{+\prime}}$) across the channel.

the viscoelasticity of the micella in the solution suppresses the turbulent fluctuations toward the bulk flow when drag reduction appears. The decrease of wall-normal velocity fluctuations in 25 ppm CTAC solution at Re = 25000 will confirm this assumption. Although 25 ppm CTAC solution at Re = 40000 almost loses DR, the wall-normal velocity fluctuations are also smaller than the water in the centre of the channel, which indicates that the suppression also happens in CTAC solution and the micella degrade only near the wall because of the high shear rate.

Figure 6 shows the statistical correlation coefficients between streamwise and wall-normal velocity fluctuations which represents the Reynolds shear stress in turbulence. As we know, the sum of Reynolds shear stress and viscous shear stress obeys the equation of $\tau = 1 - y^*$, and Reynolds shear stress dominates in the main flow because the shear rate and viscous shear stress decrease quickly. The water agrees well with the law, but the Reynolds shear stress of 25 ppm CTAC solution at Re = 25000 is diminished and surprisingly approaches zero. This phenomenon is called "zero Reynolds shear stress." In Figure 5, the auto-correlations of both streamwise and wall-normal velocity fluctuations are not zero, but the cross-correlation of the two fluctuations almost becomes zero. Some researches explained this phenomenon with the reason of correlation degradation. In fact, this phenomenon relates to special fluid motions of the solution.

3.3. Distribution of Velocity Fluctuations. In turbulent flow, the distribution of velocity fluctuations is categorized in four quadrants according to the plus-minus of fluctuations as shown in Figure 7. The abscissa of the figure is

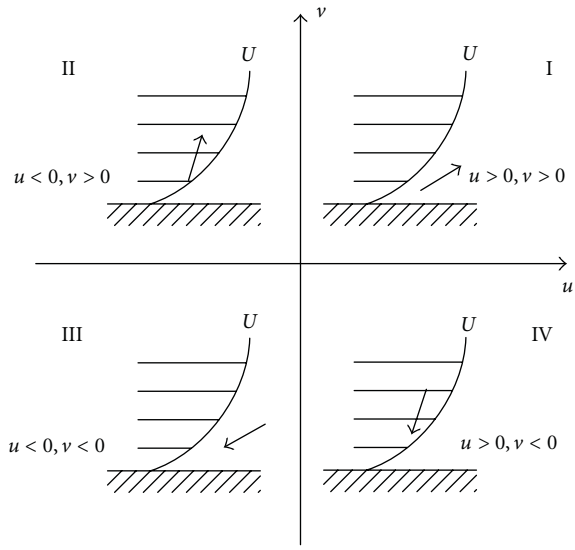

Figure 7: Schematic diagram of the categorization of turbulent fluid motions.

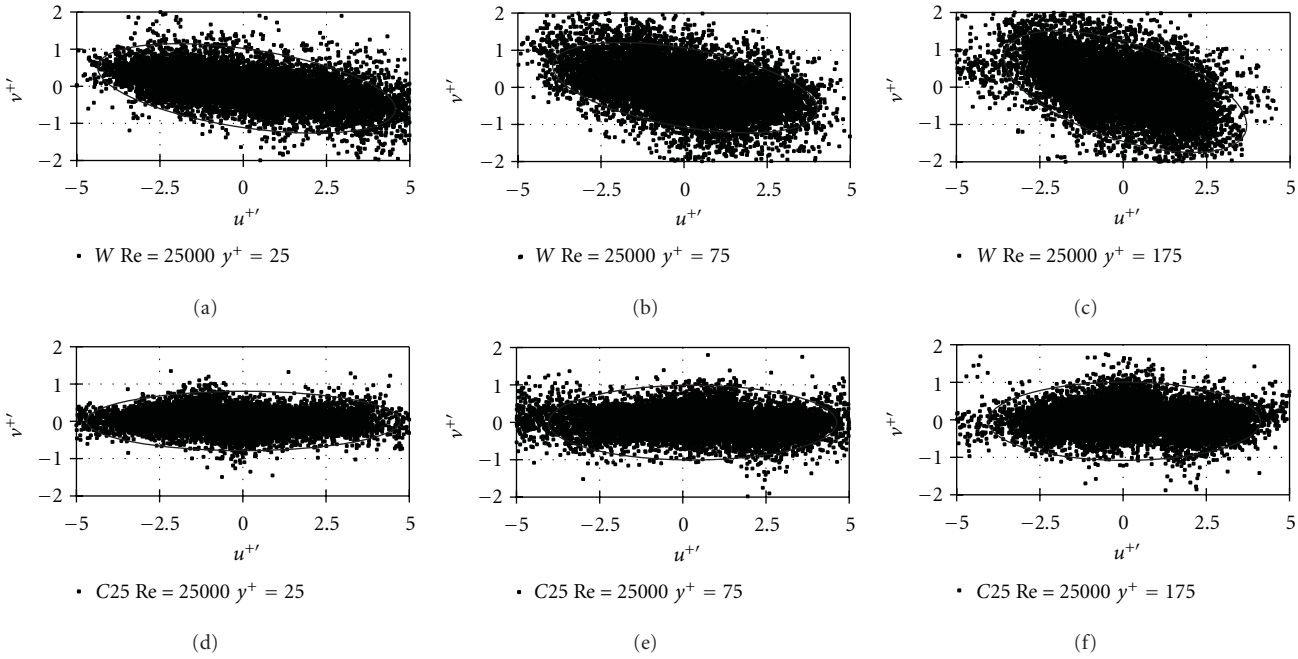

Figure 8: Distribution of velocity fluctuations ($u^{+\prime}$-$v^{+\prime}$) at Re = 25000.

the streamwise velocity fluctuations ($u^{+\prime}$), and the ordinate is the wall-normal velocity fluctuations ($v^{+\prime}$). The plus or minus of velocity fluctuations in two direction is dependent on the fluid motions in the flow.

Figures 8 and 9 show the statistical categorization of velocity fluctuations based on one group of 2D velocity frames, about ten thousand of vectors in one identical y position. Three positions in y direction within the channel flow are selected for comparison. In water flow, the fluctuations are distributed mainly in the second and fourth quadrants with elliptical shape. And with the increase of y position, the horizontal angle of ellipse also increases because the streamwise velocity fluctuations ($u^{+\prime}$) become weak. However, the fluctuations of 25 ppm CTAC solution at Re = 25000 are equally distributed in all quadrants. Moreover, the characteristics are almost not changed versus different y positions.

It should be pointed out that the products of the two fluctuations are both minus in second quadrant ($u < 0$ and $v > 0$) and fourth quadrant ($u > 0$ and $v < 0$). As a result, the Reynolds shear stress of water channel flow will be larger than zero based on this definition. At the

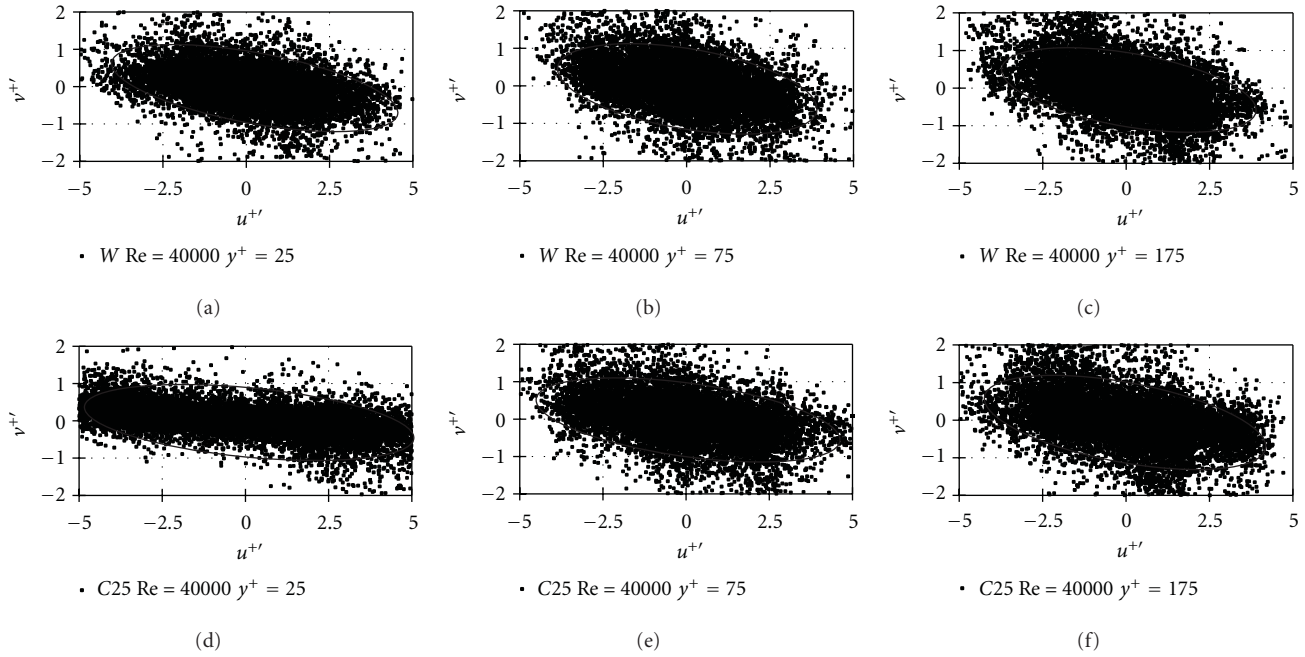

Figure 9: Distribution of velocity fluctuations ($u^{+\prime}$-$v^{+\prime}$) at Re = 40000.

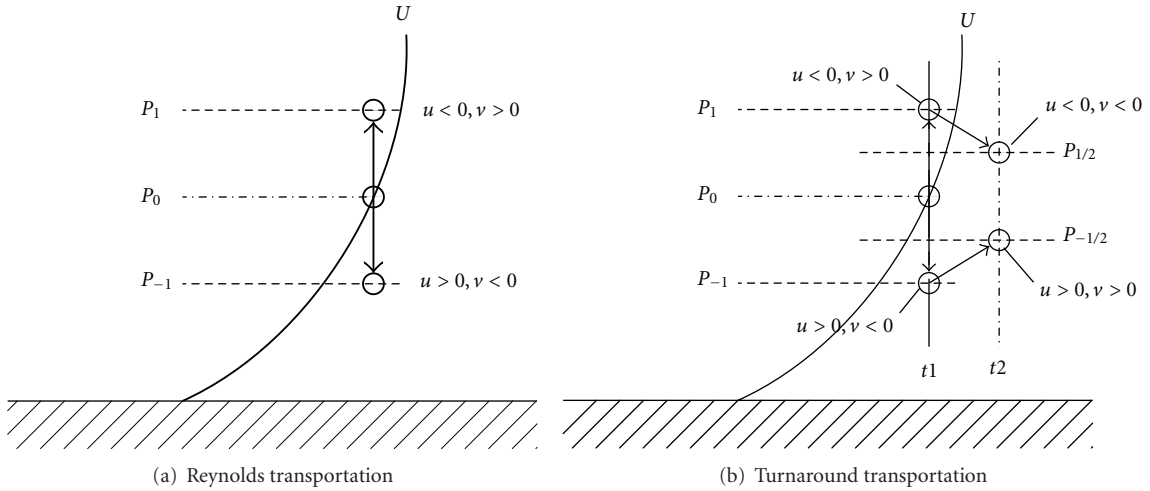

(a) Reynolds transportation (b) Turnaround transportation

Figure 10: Schematic diagram of turbulence transportation.

same time because the fluctuations of drag-reducing flow are equally distributed in all quadrants, the products of the tow fluctuations will be minus in second and fourth quadrant, plus in first and third quadrant, then the sum will probably be zero.

In Reynolds turbulence transportation as shown in Figure 10(a), if the fluid jumps from the location P_0 to P_1 ($v' > 0$) and mixes with the local fluid, the streamwise velocity fluctuation is minus ($u' < 0$). This case will lie in the second quadrant. In contrast, if the fluid jumps from the location P_0 to P_{-1} ($v' < 0$) and mixes with the local fluid, the streamwise velocity fluctuation is plus ($u' > 0$). This case will lie in the fourth quadrant. Consequently, the fluctuations of water are mainly distributed in the second and fourth quadrants as shown in Figures 8 and 9 because Reynolds transportation as shown in Figure 10(a) dominates the turbulence transportation in the water flow.

In 25 ppm CTAC solution flow at Re = 25000, the fluctuations are distributed not only in the second and fourth quadrants but also in the first and third quadrants, which indicates that there is another type of turbulence transportation besides Reynolds transportation. Figure 10(b) exhibits the assumption of the new turbulence transportation. When the fluid jumps from the location P_0 to P_1 and does not mix enough with the local fluid then turns back to

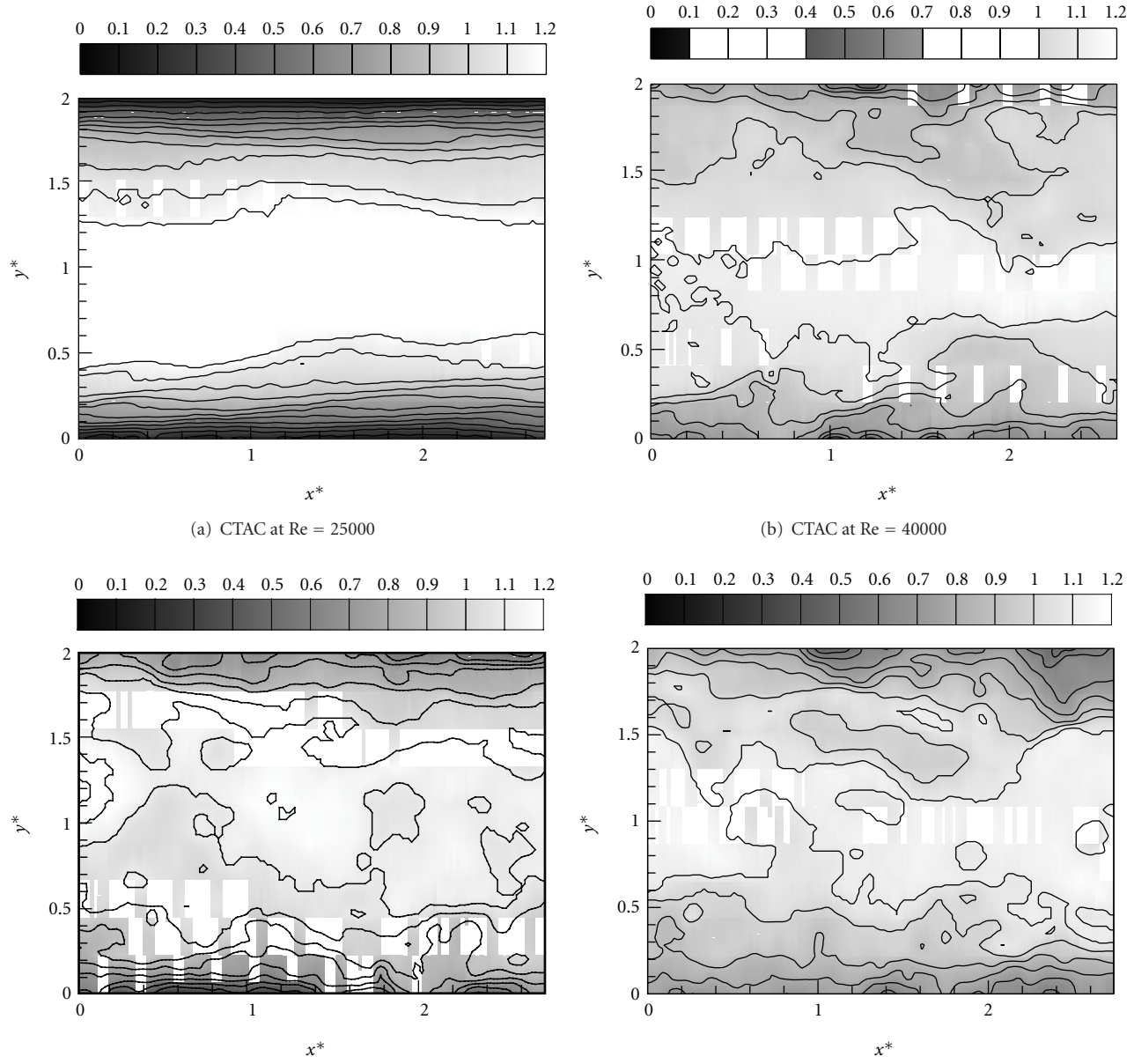

(a) CTAC at Re = 25000

(b) CTAC at Re = 40000

(c) Water at Re = 25000

(d) Water at Re = 40000

Figure 11: 2D distribution of streamwise velocity (u/u_b) in x-y plane.

the location $P_{1/2}$ at once, the fluctuations will show $u' < 0$ and $v' < 0$ in location $P_{1/2}$ which lies in the third quadrant. At the same time, the fluid jumps from the location P_0 to P_{-1} and does not mix enough with the local fluid then turns back to the location $P_{-1/2}$ at once, consequently $u' > 0$ and $v' > 0$ which lies in the first quadrant. So two important events occur in drag-reducing flow that the mixture process of fluids is delayed and turnaround transportation happens by some stress driving. In other words, the fluids in drag-reducing flow are vibrating during its flowing toward. Because the wall-normal fluctuations are small, vibration is slight. It is supposed that turnaround transportation in drag-reducing flow possibly relates to the viscoelasticity of the solution.

3.4. Instantaneous 2D Velocity Distribution. Figure 11 shows the instantaneous 2D contour of streamwise velocity (u/u_b), where u_b is the bulk velocity. Large difference appears between drag-reducing flow and water flow. The contour lines of the velocity in 25 ppm CTAC solution flow at Re = 25000 are regular and almost parallel to the wall surface, whereas the contour lines in water flow are irregular. Because 25 ppm CTAC solution flow at Re = 40000 loses drag reduction, the contour lines are also irregular as same as the water.

The regular and parallel contour lines indicate that turbulence transportation is depressed in drag-reducing flow. But it does not imply that there is no turbulence transportation which causes the zero Reynolds shear stress.

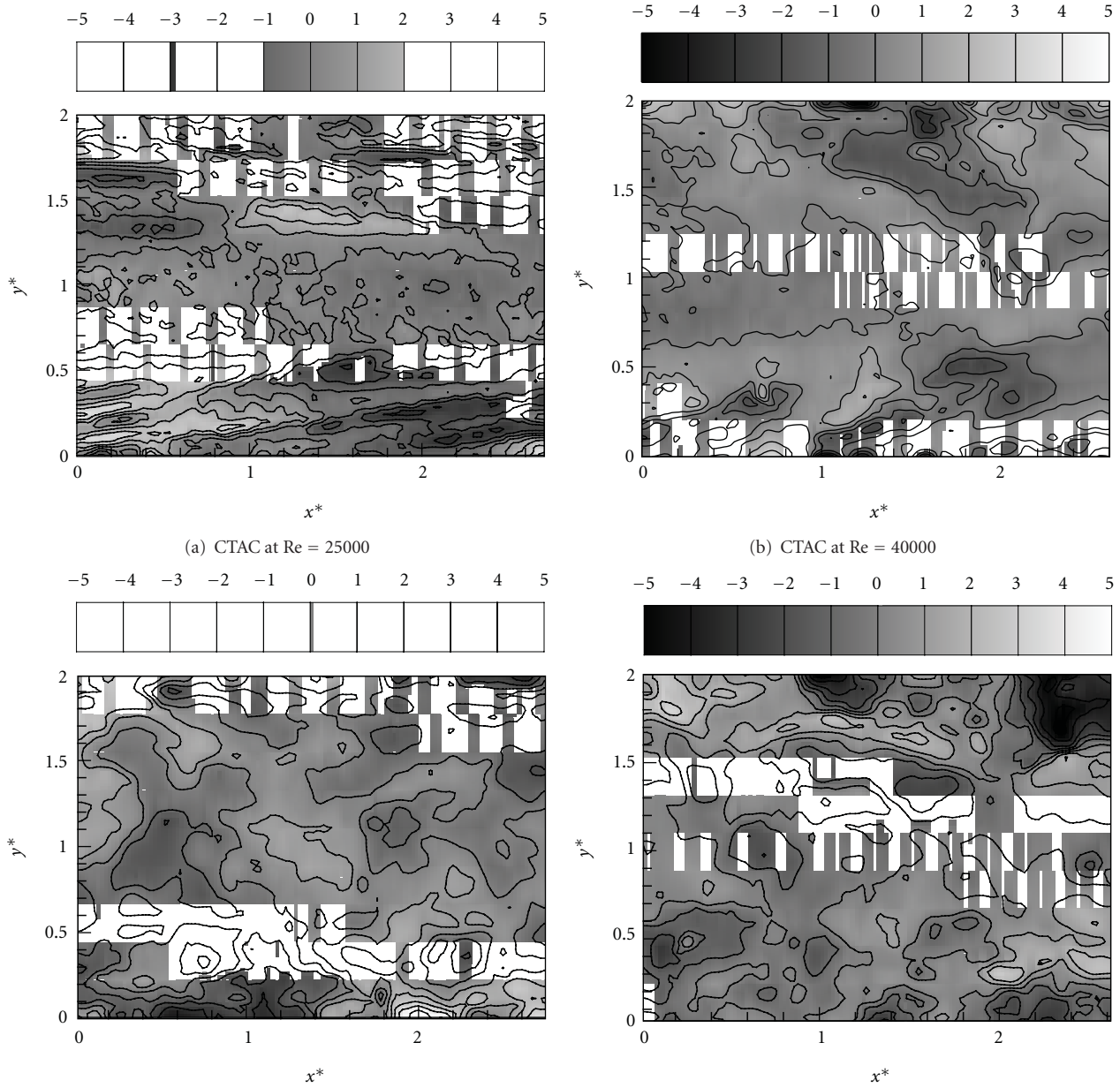

(a) CTAC at Re = 25000

(b) CTAC at Re = 40000

(c) Water at Re = 25000

(d) Water at Re = 40000

Figure 12: 2D distribution of streamwise velocity fluctuations ($u^{+\prime}$) in x-y plane.

On the other hand, the regular and parallel contour lines also indicate the possibility of the above-mentioned vibration.

Figure 12 shows the contour lines of streamwise velocity fluctuations. It clearly exhibits that the contours of streamwise velocity fluctuations are band-like in drag-reducing flow, but block-like in water flow. Moreover, the bands as shown in Figure 12(a) are developed toward streamwise direction with small declined angle. This phenomenon indicates that turbulence transportation is prevented from the wall toward the main flow by the viscoelasticity of the solution. During this progress, the micella will produce deformation, and the counter elastic force will drive the fluids turning back and then vibrating.

But when the Reynolds numbers is high enough, the micella cannot sustain the large deformation and then break. In this case, the contour of fluctuations exhibits the large declined angle, and high turbulence transportation occurs as shown in Figure 12(b), which is the degradation of DR at Re = 40000.

4. Conclusions

The velocity fluctuations of water and dilute CTAC surfactant solution flow in a two-dimensional channel are studied experimentally by using a PIV system. The phenomenon of "zero Reynolds shear stress" is analyzed by the categorization

in four quadrants. The following conclusions are drawn from the present study.

(1) The dilute CTAC surfactant solution with the concentration of 25 ppm exhibits the high drag reduction when Reynolds number is below 25000, and then DR degrades quickly and disappears completely at Re = 40000. When DR reaches the highest at Re = 25000, the Reynolds shear stress of the solution decreases and reaches zero at the same time, but the RMS of both two velocity fluctuations is not zero.

(2) The fluctuations are analyzed by the categorization in four quadrants. The fluctuations are distributed in all four quadrants equally for 25 ppm CTAC solution at Re = 25000, but distributed mainly in the second and fourth quadrants for water. It is indicated that Reynolds transportation dominates the water flow during the turbulence transportation, whereas turnaround transportation also happens besides Reynolds transportation in drag-reducing flow.

(3) Turbulence transportation is depressed in drag-reducing flow, which leads to the regular and parallel contour lines of the streamwise velocity. Band-like contour lines with small declined angle of streamwise velocity fluctuations are found in drag-reducing flow. The phenomenon and turnaround transportation are supposed to depend on the viscoelasticity of the solution.

Acknowledgment

This research is supported by National Natural Science Foundation of China and China Scholarship Council.

References

[1] B. A. Toms, "Some observations on the flow of linear polymer solutions through straight tubes at large Reynolds numbers," in *Proceedings of 2nd the International Congress on Rheology*, pp. 135–138, 1948.

[2] P. W. Li, Y. Kawaguchi, and A. Yabe, "Transitional heat transfer and turbulent characteristics of drag-reducing flow through a contracted channel," *Journal of Enhanced Heat Transfer*, vol. 8, no. 1, pp. 23–40, 2001.

[3] P. Li, Y. Kawaguchi, H. Daisaka, A. Yabe, K. Hishida, and M. Maeda, "Heat transfer enhancement to the drag-reducing flow of surfactant solution in two-dimensional channel with mesh-screen inserts at the inlet," *Journal of Heat Transfer*, vol. 123, no. 4, pp. 779–789, 2001.

[4] D. O. A. Cruz and F. T. Pinho, "Turbulent pipe flow predictions with a low Reynolds number k-ε model for drag reducing fluids," *Journal of Non-Newtonian Fluid Mechanics*, vol. 114, no. 2-3, pp. 109–148, 2003.

[5] B. Yu and Y. Kawaguchi, "DNS of drag-reducing turbulent channel flow with coexisting Newtonian and non-Newtonian fluid," *Journal of Fluids Engineering, Transactions of the ASME*, vol. 127, no. 5, pp. 929–935, 2005.

[6] A. Gyr and A. Tsinober, "On the rheological nature of drag reduction phenomena," *Journal of Non-Newtonian Fluid Mechanics*, vol. 73, no. 1-2, pp. 153–162, 1997.

[7] K. Fukagata, K. Iwamoto, and N. Kasagi, "Contribution of Reynolds stress distribution to the skin friction in wall-bounded flows," *Physics of Fluids*, vol. 14, no. 11, pp. L73–L76, 2002.

[8] G. Hetsroni, J. L. Zakin, and A. Mosyak, "Low-speed streaks in drag-reduced turbulent flow," *Physics of Fluids*, vol. 9, no. 8, pp. 2397–2404, 1997.

[9] Y. Kawaguchi, T. Segawa, Z. Feng, and P. Li, "Experimental study on drag-reducing channel flow with surfactant additives-Spatial structure of turbulence investigated by PIV system," *International Journal of Heat and Fluid Flow*, vol. 23, no. 5, pp. 700–709, 2002.

[10] F. C. Li, Y. Kawaguchi, T. Segawa, and K. Hishida, "Reynolds-number dependence of turbulence structures in a drag-reducing surfactant solution channel flow investigated by particle image velocimetry," *Physics of Fluids*, vol. 17, no. 7, pp. 1–13, 2005.

[11] F. C. Li, Y. Kawaguchi, K. Hishida, and M. Oshima, "Investigation of turbulence structures in a drag-reduced turbulent channel flow with surfactant additive by stereoscopic particle image velocimetry," *Experiments in Fluids*, vol. 40, no. 2, pp. 218–230, 2006.

[12] F. C. Li, Y. Kawaguchi, B. Yu, J. J. Wei, and K. Hishida, "Experimental study of drag-reduction mechanism for a dilute surfactant solution flow," *International Journal of Heat and Mass Transfer*, vol. 51, no. 3-4, pp. 835–843, 2008.

[13] W. Gu, Y. Kawaguchi, D. Wang, and S. Akihiro, "Experimental study of turbulence transport in a dilute surfactant solution flow investigated by PIV," *Journal of Fluids Engineering, Transactions of the ASME*, vol. 132, no. 5, Article ID 051204, pp. 1–7, 2010.

[14] T. M. Clausen, P. K. Vinson, J. R. Minter, H. T. Davis, Y. Talmon, and W. G. Miller, "Viscoelastic micellar solutions: microscopy and rheology," *Journal of Physical Chemistry*, vol. 96, no. 1, pp. 474–484, 1992.

[15] B. Lu, X. Li, L. E. Scriven, H. T. Davis, Y. Talmon, and J. L. Zakin, "Effect of chemical structure on viscoelasticity and extensional viscosity of drag-reducing cationic surfactant solutions," *Langmuir*, vol. 14, no. 1, pp. 8–16, 1998.

[16] Y. I. González and E. W. Kaler, "Cryo-TEM studies of worm-like micellar solutions," *Current Opinion in Colloid and Interface Science*, vol. 10, no. 5-6, pp. 256–260, 2005.

[17] R. B. Dean, "Reynolds number dependence of skin friction and other bulk flow variables in two-dimensional rectangular duct," *Journal of Fluids Engineering, Transactions of the ASME*, vol. 100, no. 2, pp. 215–223, 1978.

[18] P. S. Virk, E. W. Mickley et al., "The ultimate asymptote and mean flow structure in Tom's phenomenon," *Transactions of ASME, Journal of Applied Mechanics*, vol. 37, pp. 480–493, 1970.

[19] Y. Kawaguchi, H. Daisaka, and A. Yabe, "Turbulent characteristics in transition region of dilute surfactant drag reducing flow," in *Proceedings of the 11th Symposium on Turbulent Shear Flows*, vol. 9, pp. 49–54, 1997.

Hindawi Publishing Corporation
Advances in Mechanical Engineering
Volume 2011, Article ID 947179, 7 pages
doi:10.1155/2011/947179

Research Article

Evaluation of Surfactant Drag Reduction Effect in a District Heating System

Ning Ma,[1,2] Jinjia Wei,[1,2] and Jianfeng Wang[1,2]

[1] *State Key laboratory of Multiphase Flow in Power Engineering, Xi'an Jiaotong University, Xi'an 710049, China*
[2] *Suzhou Academy, Xi'an Jiaotong University, Suzhou, Jiangsu 215021, China*

Correspondence should be addressed to Jinjia Wei, jjwei@mail.xjtu.edu.cn

Received 15 April 2011; Accepted 25 May 2011

Academic Editor: Bo Yu

A scale-up method proposed by Hoyt was used to evaluate the flow resistance of working fluid in a district heating system (DHS) after a surfactant drag reducer, CTAC/NaSal, was added. The measured drag reduction data of 100 ppm surfactant solution obtained from an 18.5 mm diameter pipe in the laboratory were used for the evaluation. The results show that the reduction of the pressure drop in the system reaches 23.28% by the addition of surfactants, indicating a very good energy saving effect and application prospective. Comparing with the effect of 100 ppm solution, it is found that the drag reduction will not be further improved obviously in the system with increasing concentration. It was also found that the local pressure drop takes a large proportion in the total pressure drop of the DHS, which could not be reduced by adding the surfactants.

1. Introduction

District heating systems (DHSs) are widely used in engineering fields. The energy consumption of DHS is a main branch of the whole world energy consumption, so the study on the energy-saving method of DHS is quite necessary. The application of the drag reducer to the district heating system can reduce turbulent flow friction drag, increase flow rate, and save energy [1–4]. Jiao et al. [5] pointed out that the drag reduction effect of the whole pipe system should be obtained in the specific DHS with drag reducers.

As is well known, the drag reduction data are usually obtained in small diameter pipes in laboratory, which cannot be directly used to evaluate the drag reduction performance of fluid flow in large diameter pipes of the district heating system due to the pipe diameter effect of surfactant drag-reducing flow. Therefore, the scale-up method is needed to calculate the drag reduction performance of larger diameter pipe in the industrial fields based on the data measured from the smaller pipe diameters in the laboratory. In the present study, we evaluate the drag reduction performance of the CTAC/NaSal surfactant flow in the DHS by using scale-up method.

2. Experimental

2.1. Surfactant Solution. The cationic surfactant used in the present study was cetyltrimethylammonium chloride (CTAC) (Shandong Fusite Chemical Co., Ltd., China, 70% purity), with a molecular weight of 320.0 g/mol, which is less affected by calcium and sodium naturally existing in tap water. Sodium salicylate (NaSal) (Yixing City Shenguang Medicine Chemicals Co., Ltd., China, 99% purity), with molecular weight of 160.1 g/mol, was added to the solution with the same weight concentration as that of CTAC to provide counterions. The surfactant solution is marked by CTAC concentration. Two mass concentrations of 100 and 200 ppm of the surfactant solution were used in the experiment by dissolved CTAC and NaSal in tap water.

2.2. Test Facility. Figure 1 schematically shows the closed loop flow facility used in the present experiment, in which the steel centrifugal pump derived fluids through the reservoir tank (0.45 m^3), the stainless steel tube, the settling chamber equipped with a nozzle, the two-dimensional test, channel and the diffuser. In order to get different fluid temperatures, a control system with a 4.4 kW heater was

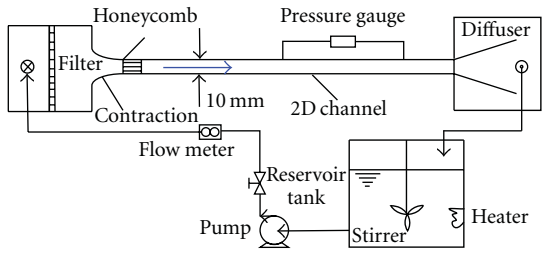

Figure 1: Schematic diagram of two-dimensional water channel.

installed in the reservoir tank. The temperature of the fluid was controlled to ±0.1 K around the prescribed value.

The two-dimensional channel was 10 mm high, 125 mm wide, and 3 meters long (inside measurement), which was connected straightly by two sections of 1.5 meters each. Most of the test section was made of transparent acrylic resin having thickness of 20 mm. To remove large eddies, a honeycomb of 45 mm length was employed at the entrance of the test section. The flow rate and pressure drops were measured by an electromagnetic flowmeter with a resolution of $\pm 0.01\,\mathrm{m}^3/\mathrm{min}$ and a precise pressure gauge with an uncertainty of ±0.1 Pa. The distance of two pressure tabs was 1.10 meters in length located 1.65 meters downstream from the entrance of the channel.

3. Pipe Diameter Effect and Scale-Up Method

3.1. Pipe Diameter Effect. For turbulent flow of Newtonian fluid through a smooth pipe, the friction resistance coefficient is only a function of Reynolds number and is expressed as

$$\frac{1}{\sqrt{\lambda}} = 0.873 \ln\left[\mathrm{Re}\sqrt{\lambda}\right] - 0.8. \tag{1}$$

The above equation is the Karman-Prandtl resistance formula which is suited to fully developed turbulent flow through smooth circular tubes, where λ is friction resistance coefficient and Re is Reynolds number.

However, for drag-reducing fluids in the nonasymptotic region, this is not the case, even for the same drag reducer, the effects of friction reduction are different for different pipe diameters. This is the so-called "diameter effect" for drag-reducing fluids [6]. This effect indicates that the friction resistance coefficient is not only dependent on Reynolds number but also dependent on the pipe diameter. The friction resistance coefficient or Fanning friction factor C_f can be expressed as

$$C_f = \frac{\lambda}{4} = f(\mathrm{Re}, D). \tag{2}$$

This effect is a vexing issue from the practical point of view. It is not very difficult to measure the drag-reduction level (DR) for a given fluid in tubes with diameters from 10 to 60 mm in the laboratory, but it is not easy for much larger pipes. In a hydronic system of a building, the pipe diameters vary from 40 mm to 350 mm, so it is better to predict DR in such a building system by using scale-up method [7].

3.2. Scale-Up Method. To solve the problem of "diameter effect" existing in the drag-reducing flows, some scale-up models and mathematical derivation methods have been developed in order to reduce or eliminate the "diameter effect" of the fluids. In 1968, Whitsitt et al. [8] proposed a method that correlates DR with the solution friction velocity (u_p^*), based on the assumption that the wall being shear stress is the mechanism that controls DR, where the friction velocity is defined as $u_p^* = (\tau_w/\rho)^{0.5}$, with τ_w and u_p^* the wall shear stress and friction velocity, respectively, then plotted the drag-reduction level DR as a function of the solution friction velocity (u_p^*). This is the so-called "correlate model of DR and u_p^*." This procedure has the drawback that both variables (DR and u_p^*) contain the unknown parameter (τ_w), and an iterative procedure is therefore necessary to predict the DR of the solution. A number of other researchers, for example, Astarita et al. [9], Lee et al. [10], and Savins and Seyer [11], then simplified Whitsitt's procedure by using the solvent friction velocity (u_w^*) instead of the solution friction velocity (u_p^*) and proposed "correlate model of DR and u_w^*." After that, Schmitt et al. [12] proposed two different empirical correlations for surfactants depending upon the shear stress level: DR versus τ_w for high stresses and τ_w versus V (bulk velocity) for low stresses. Gasljevic and Matthys [13] proposed a new correlation model on the diameter effect of drag-reducing flow by correlating drag-reduction level (DR) with bulk velocity.

All the methods discussed above except for Schmitt's were developed for, and tested with, polymer solutions data. All these four models have very similar characteristics: there exists no theoretical or empirical formula; therefore, the specific analysis of these models can only be done after getting corresponding experimental data. Gasljevic et al. [6] proved that Schmitt's procedure was not universal; in other words, the fitting results have great distinctions for different surfactant solutions. Hoyt [14, 15] proposed a scale-up method for polymer additives pipes by introducing an additional term (ΔB) in the nondimensional pipe velocity profile. He simplified his scaling procedure by using the idea of negative roughness. ΔB is a function of the type of drag-reducing polymer, polymer concentration, pipe roughness, and so forth. The core equation and finally scale-up equation of this scaling procedure are as follows.

The core equation of this method is

$$\frac{1}{\sqrt{\lambda_{\mathrm{large}}}} = \frac{1}{\sqrt{\lambda_{\mathrm{small}}}} + 2\log\frac{D_{\mathrm{large}}}{D_{\mathrm{small}}}. \tag{3}$$

The scale-up equation is

$$\mathrm{Re}_{\mathrm{large}} = \mathrm{Re}_{\mathrm{small}}\left(\frac{\sqrt{\lambda_{\mathrm{small}}}}{\sqrt{\lambda_{\mathrm{large}}}}\right)\left(\frac{D_{\mathrm{large}}}{D_{\mathrm{small}}}\right). \tag{4}$$

This scaling procedure appears to have an excellent accuracy based on a series of experimental data obtained by Hoyt. By using this scaling procedure, the predictions are almost consistent with each other and consistent with the experimental results. This behavior is illustrated in Figure 2,

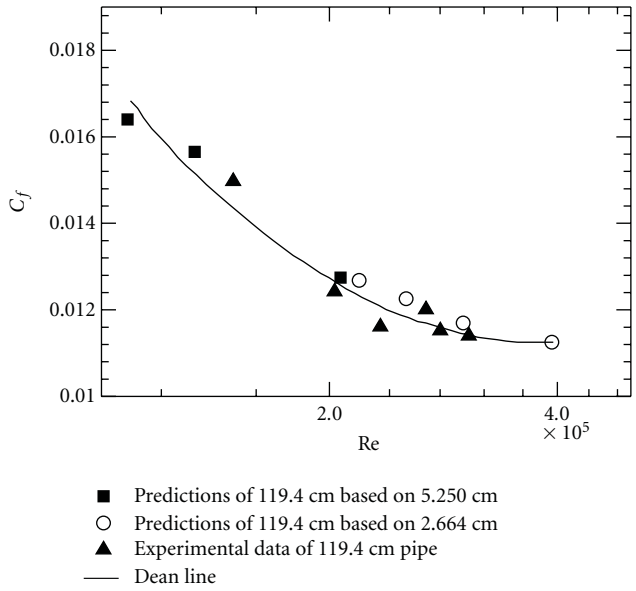

Figure 2: Fanning friction factors versus Reynolds number. Solid triangles are the measured data of 119.4 cm diameter pipe. Solid squares are predictions of the 119.4 cm diameter pipe based on the 2.664 cm diameter pipe data, and solid circles are predictions of the 119.4 cm diameter pipe based on the 5.250 cm diameter pipe data. The solid line is the Dean line.

where the Fanning friction factor C_f is plotted as a function of Reynolds number, Re.

4. Test of the Scale-Up Method Proposed by Hoyt

Through the above discussion we can know that the scaling procedure proposed by Hoyt has great advantage compared with others. Therefore, in this study, we try to use this scale-up method to analyze and process the size effect of the CTAC/NaSal (Hexadecyl Trimethyl Ammonium Chloride/Sodium salicylate) surfactant flow. The ratio of CTAC to NaSal is 1 : 1 by weight. At the same temperature of 30°C and the same concentration of 100 ppm, the friction coefficient of CTAC surfactant solution shows great differences for different pipe diameters, which indicates that the CTAC surfactant solution has a strong size effect. The data for $D_1 = 18.5$ mm (the equivalent diameter of 10×125 mm^2 rectangular cross-section of a channel) obtained in the laboratory and the data for $D_2 = 74.1$ mm (the equivalent diameter of 40×500 mm^2 rectangular cross-section of a channel) got from the literature [16] are shown in Figure 3. The "Dean line" [17] for Newton fluid turbulent flow is also shown for comparison.

Figure 4 shows the prediction of friction factors of CTAC/NaSal surfactant flow in 74.1 mm diameter pipe from the measured data of $D_1 = 18.5$ mm pipe at 100 ppm and 30°C, and the predicted values are compared with the actual test data for the larger pipe of $D_2 = 74.1$ mm. At the beginning, the predicted values have some difference from the experimental values, but the difference becomes smaller and smaller with the increase of Reynolds number.

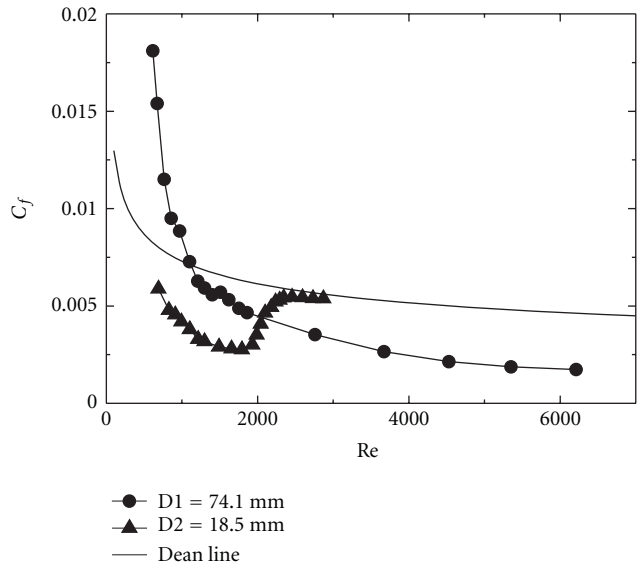

Figure 3: Measured friction factors for 100 ppm surfactant solutions in pipes of 18.5 mm and 74.1 mm diameters.

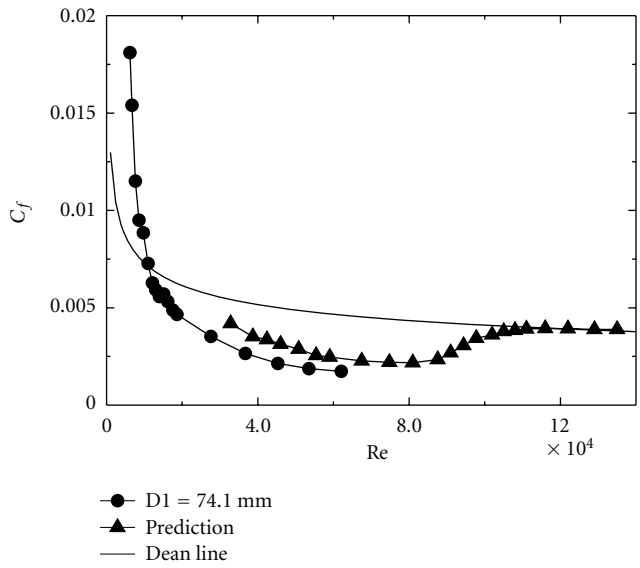

Figure 4: Comparison of measured friction factors of 74.1 mm diameter pipe with scale-up prediction based on the measured friction factors of 18.5 mm diameter pipe.

The prediction agrees well with the measured data generally. Therefore, this scale-up method can be used in an actual districting heating system.

5. Prediction of Drag Reduction Performance of a District Heating System with Surfactant Additives

In consideration of the good applicability of the scale-up method proposed by Hoyt, we apply this method to predict the drag reduction performance of an actual district heating

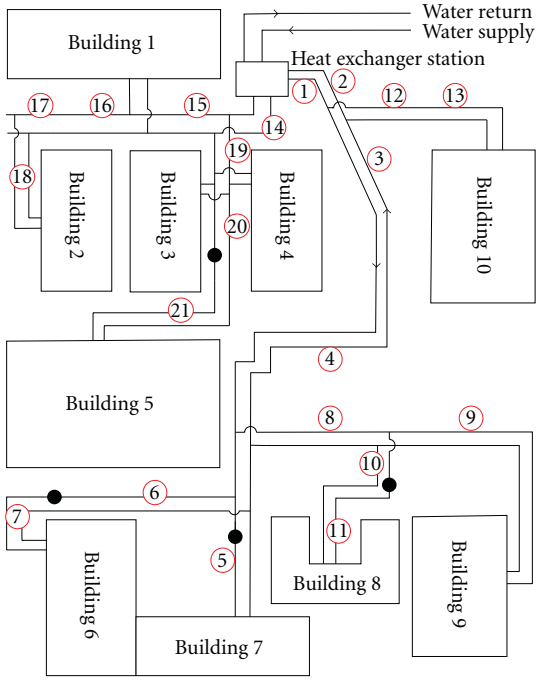

FIGURE 5: Schematic diagram of the DHS in a community.

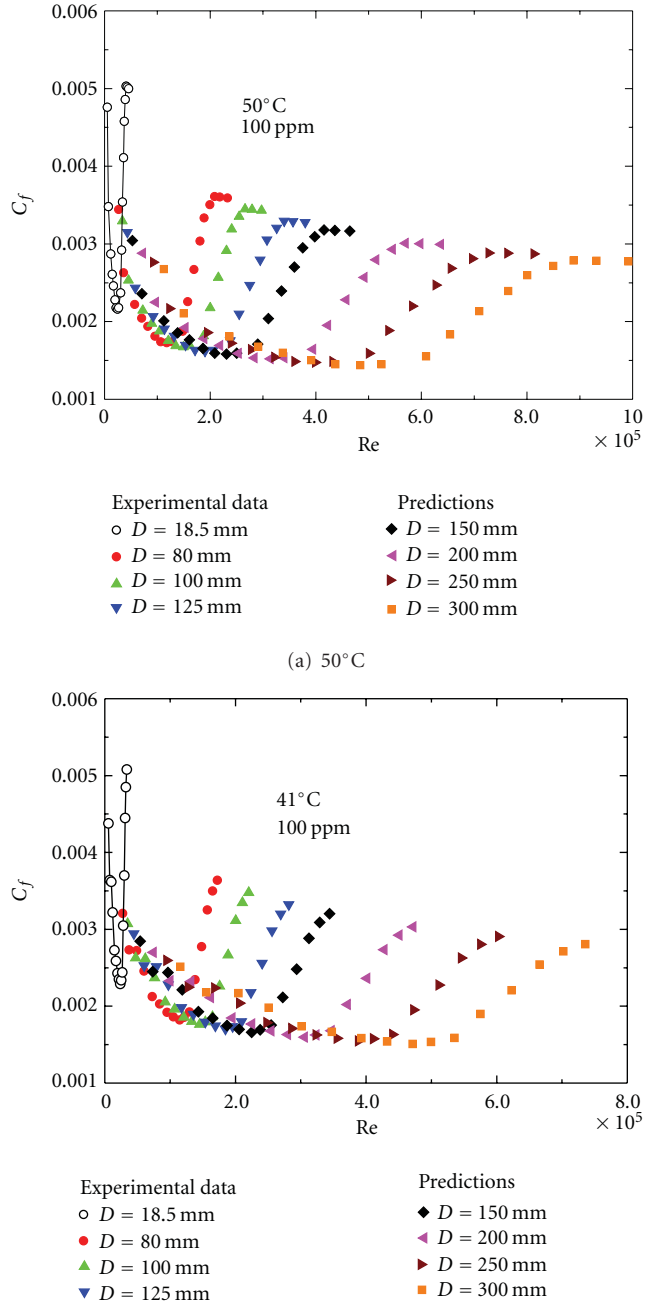

FIGURE 6: Fanning friction factors of seven different diameters in the DHS predicted from the experimental data of the 18.5 mm diameter channel.

system with surfactant additives of CTAC/NaSal and thus evaluate the energy saving effect of the DHS by adding surfactant to the working fluid in the system.

The schematic of the district heating system in a community located in Qingdao City, Shandong Province, China, is shown in Figure 5, and the solid circles the connection points of different pipe diameters. The lengths, diameters, and flow parameters are shown in Table 1. Since the layouts of pipe networks in houses of users are not clear, we do not consider the branch pipes (shown as the thinner lines connecting buildings and comparative thicker lines in Figure 5) leading into specific houses. For example, the flowrate of pipe no. 15 is not equal to the flowrates in pipes no. 16, no. 17, and 18; it is because some of the fluid coming from pipe no.15 flows into building 1 which is not considered. The steam coming from the boiler enters the heat-exchanging station where the working fluid (water) gets heat from the steam to become hot water and then is supplied to the community users.

The hot water pipes which are connected to the heat-exchanging station are divided into two branches: one branch is to the buildings in a comparative intensive residential area, and the other is to some worker dormitories. Temperatures of the supply and return water are 50°C and 41°C, respectively. The pipes used in this district heating system have several different diameters of 300 mm, 250 mm, 200 mm, 150 mm, 125 mm, 100 mm, and 80 mm. The diameter and length of the pipes and the corresponding flowrate are shown in Table 1.

Figure 6 shows the plot of the measured Fanning friction factors (C_f) as a function of Reynolds number (Re) for a 100 ppm CTAC/NaSal surfactant solution in the channel with the hydraulic diameter of 18.5 mm, and the corresponding predictions of friction factors by using (3) and (4) for seven different pipe diameters are also shown in Figure 6. The predicted curves shown in Figures 6(a) and 6(b) are based on the experimental data obtained in the 18.5 mm diameter channel at 50°C and 41°C, respectively.

For both Newtonian fluid and non-Newtonian flow in the fully developed turbulent flow region, the wall shear

Table 1: Parameters of the pipes in the DHS.

No.	Flowrate (m^3/h)	Diameter (mm)	Length (m)	No.	Flowrate (m^3/h)	Diameter (mm)	Length (m)
1	77.91	300	4.80	12	17.50	250	60
2	77.91	300	14.40	13	17.50	250	24
3	60.41	300	7.20	14	167.41	300	27.60
4	60.41	250	151.80	15	71.05	200	12
5	1.41	125	60	16	32.46	200	13.20
6	29.88	125	36	17	32.46	200	37.20
7	29.88	100	35	18	32.46	100	31.80
8	29.12	200	54	19	96.36	200	32.40
9	21.7	150	63.60	20	52	200	4.20
10	7.42	200	6.60	21	52	150	69
11	7.42	80	42				

stress (τ_w) and Fanning friction factor (C_f) are defined as follows:

$$\tau_w = \frac{\Delta PD}{4L}, \tag{5}$$

$$C_f = \frac{\Delta PD}{2\rho u_b^2 L}, \tag{6}$$

where ΔP is pressure drop, D is equivalent diameter, L is distance between pressure taps, ρ is the fluid density, and u_b is bulk velocity. In the engineering field, however, the commonly used parameter is friction resistance coefficient (λ) which is defined as

$$\lambda = \frac{2\Delta PD}{\rho u_b^2 L}. \tag{7}$$

Comparing (7) with (6), we see that $\lambda = 4C_f$. We have two empirical formulas for the friction resistance coefficient, (1) and (2). Equation (1) is an implicit function of λ. In order to make λ a function of Re, Nikuladse proposed an empirical equation which is fitted in the region of $10^5 < \mathrm{Re} < 3 \times 10^6$ as follows [18]:

$$\lambda = 0.0032 + \frac{0.221}{\mathrm{Re}^{0.237}}. \tag{8}$$

For $\mathrm{Re} < 10^5$, we use the Blasius equation, thus

$$\lambda = 0.3164\,\mathrm{Re}^{-0.25}. \tag{9}$$

Before adding surfactant, we can calculate the pressure drop of pure water in a pipe by using the following equation:

$$\Delta P = \lambda \frac{\rho u_b^2 L}{2D}. \tag{10}$$

The results show that the pressure drops of water in the supply and return pipes are 13209.12 Pa and 13667.51 Pa, respectively, and the total pressure drop is 26876.63 Pa.

After adding surfactant, the Fanning friction factor (C_f) for different pipe diameters can be obtained from Figure 6 and can be transformed to friction resistance coefficient (λ) according to (2). The pressure drop for the surfactant flow in the pipes can also be calculated by using (10). For the 100 ppm CTAC/NaSal surfactant solution, the pressure drops in the supply pipes and return pipes are 6758.30 Pa and 6842.10 Pa, respectively, and the total pressure drop is 13600.40 Pa. For the 200 ppm CTAC/NaSal surfactant solution, the pressure drops in the supply pipes and return pipes are 7498.54 Pa and 7164.89 Pa, respectively, and the total pressure drop is 14663.44 Pa.

All the above calculations are carried out only in straight pipes. In addition, there are two methods to calculate the local flow resistance of the district heating system: resistance coefficient method and equivalent length method [14]. We adopt the equivalent length method in the present study. The equation of this method is

$$\Delta P = \lambda \frac{\rho u_b^2 L_e}{2D}, \tag{11}$$

where L_e is equivalent length of local fittings such as elbows, tee shape fittings, and valves. This method transfers local fittings to straight pipes which are L_e long and have the same diameters with fittings, and then (11) is used to calculate the flow resistance. The equivalent lengths of different local fittings in the district heating system can be obtained in a relevant literature [14]. The calculated results of local fittings show that the pressure drops in the supply and return pipes are 5596.70 Pa and 24550.90 Pa, respectively, and the total pressure drop is 30147.60 Pa.

The analysis of the drag reduction of local fittings through the laboratory experimental study was given in detail in [19]. The results showed that the drag reduction effects of local fittings were not only affected by all factors affecting the drag reduction of straight pipe but also affected by two other factors: dimensionless local resistance coefficient and own structures of local fittings; what more, the increase in local resistance decreased the drag reduction effect until the drag reduction effect disappeared. Considering the average effects of all the local fittings on the drag reduction of surfactant solutions, Jiao [19] proposed that the drag-reducing behavior of CTAC/NaSal surfactant solution flow is observed just in the straight section of pipes rather than in local fittings. Therefore, we can calculate the rates

of drag reduction for the 100 ppm and 200 ppm surfactant solutions as follows:

(i) for 100 ppm

$$\begin{aligned} \mathrm{DR}\% &= \frac{(\Delta P_w - \Delta P_c)}{(\Delta P_w + \Delta P_e)} \times 100\% \\ &= \frac{(26876.63\,\mathrm{Pa} - 13600.37\,\mathrm{Pa})}{(26876.63\,\mathrm{Pa} + 30147.56\,\mathrm{Pa})} \times 100\% \\ &= 23.28\%, \end{aligned} \tag{12}$$

(ii) for 200 ppm

$$\begin{aligned} \mathrm{DR}\% &= \frac{(\Delta P_w - \Delta P_c)}{(\Delta P_w + \Delta P_e)} \times 100\% \\ &= \frac{(26876.63\,\mathrm{Pa} - 14663.44\,\mathrm{Pa})}{(26876.63\,\mathrm{Pa} + 30147.56\,\mathrm{Pa})} \times 100\% \\ &= 21.42\%, \end{aligned} \tag{13}$$

where ΔP_w is the total pressure drop of straight pipes before adding surfactant, ΔP_c is the total pressure drop of straight pipes after adding surfactant, and ΔP_e is the total pressure drop of local fittings.

The drag reduction rates of both 100 ppm and 200 ppm are approximately 20%. Furthermore, the drag reduction effect of the 100 ppm CTAC/NaSal surfactant solution is a little larger than that of 200 ppm. The actual pressure drop in the district heating system in Figure 5 had been measured by Jiao et al. [5]. The results showed that with the same running frequency of the circulation pump, the water circulation flow rate in the tested system is increased by 11.7% and, with a constant flow rate, the pumping power (electricity consumption) could be reduced by 28.4%. These data are corresponding to a drag reduction of 24.7%, which agree well with our prediction.

In addition, the above analysis shows that the pressure drops of local fittings are considerable, but the drag reduction effects are extremely weak. Therefore, the designer should try to avoid using local fittings when designing the district heating system in order to improve drag reduction performance of the system by adding surfactant.

6. Conclusions

The drag reduction effects of CTAC/NaSal surfactant in a community district heating system was evaluated by using the scale-up method proposed by Hoyt, and the main conclusions are as follows.

(1) The scale-up method of Hoyt is applicable to the CTAC/NaSal surfactant solution, and the data obtained in our setup confirms that the pressure drop in the system is reduced after adding surfactant in this system.

(2) The drag reduction rates of the 100 ppm and 200 ppm CTAC/NaSal surfactants in the DHS are 23.28% and 21.42%, respectively, which are much lower than the drag reduction rates measured in the laboratory. This is due to the existence of local fittings in the DHS in which the flow resistance takes a very large proportion in the whole system but cannot be reduced by surfactant additives.

Acknowledgments

The authors gratefully acknowledge the financial support from the NSFC Fund (no. 51076124), the Specialized Research Fund for the Doctoral Program of Higher Education of China (no. 20090201110002), and Jiangsu Provincial Natural Science Foundation (BK2009145).

References

[1] S. Ezrahi, E. Tuval, and A. Aserin, "Properties, main applications and perspectives of worm micelles," *Advances in Colloid and Interface Science*, vol. 128–130, pp. 77–102, 2006.

[2] M. Bannai, K. Kuwabara, and H. Itasaka, "Energy-saving in chilled-water supply system for clean room of semiconductor manufacturing plant: variable flow control of chilled-water and addition of drag reduction," *Transactions of the Japan Society of Refrigerating and Air Conditioning Engineers*, vol. 23, no. 2, pp. 133–143, 2006.

[3] J. Pollert, J. L. Zakin, J. Myska, and K. Kratochvil, "Use of friction reducing additives in district heating system field test at Kladno-Krocehlavy," in *Proceedings of the International District Heating and Cooling Conference*, vol. 85, pp. 141–156, Czech Republic, 1994.

[4] J. Myska and V. Mik, "Application of a drag reducing surfactant in the heating circuit," *Energy and Buildings*, vol. 35, no. 8, pp. 813–819, 2003.

[5] L. F. Jiao, F. C. Li, W. T. Su et al., "Experimental study on surfactant drag-reducer applying to district heating system," *Energy Conservation Technology*, vol. 26, no. 3, pp. 195–201, 2008.

[6] K. Gasljevic, G. Aguilar, and E. F. Matthys, "An improved diameter scaling correlation for turbulent flow of drag-reducing polymer solutions," *Journal of Non-Newtonian Fluid Mechanics*, vol. 84, no. 2-3, pp. 131–148, 1999.

[7] H. Usui, T. Itoh, and T. Saeki, "On pipe diameter effects in surfactant drag-reducing pipe flows," *Rheologica Acta*, vol. 37, no. 2, pp. 122–128, 1998.

[8] N. F. Whitsitt, L. G. Harrington, and H. R. Crawford, "Effect of wall shear stress on drag reduction of viscoelastic fluids," Tech. Rep. no. DTMB-3, Western Company, Dallas, Tex, USA, 1968.

[9] G. Astarita, G. G. Jr, and L. Nicodemo, "A phenomenological interpretation and correlation of drag reduction," *AIChE Journal*, vol. 15, no. 4, pp. 564–567, 1969.

[10] W. K. Lee, R. C. Vaseleski, and A. B. Metzner, "Turbulent drag reduction in polymeric solutions containing suspended fibers," *AIChE Journal*, vol. 20, no. 1, pp. 128–133, 1974.

[11] J. G. Savins and F. A. Seyer, "Drag reduction scale-up criteria," *Physics of Fluids*, vol. 20, no. 10, pp. S78–S84, 1977.

[12] K. Schmitt, P. O. Brunn, and F. Durst, "Scaling-up correlations for drag reducing surfactants," *Progress and Trends in Rheology II*, vol. 2, no. 2, pp. 249–252, 1988.

[13] K. Gasljevic and E. F. Matthys, "Developments and applications of non-Newtonian flows," *ASME MD*, vol. 231, no. 66, pp. 237–243, 1995.

[14] J. W. Hoyt, "Scale-up from laboratory pipe-flow data to large flows," in *Proceedings of the ASME/JSME 4th Joint Fluids Summer Engineering Conference (FEDSM '03)*, vol. 1, pp. 745–749, Honolulu, Hawaii, USA, July 2003.

[15] J. W. Hoyt, ""Negative roughness" and polymer drag reduction," *Experiments in Fluids*, vol. 11, no. 2-3, pp. 142–146, 1991.

[16] Y. Kawaguchi, Y. Kawaraya, and A. Yabe, "Turbulent transport mechanism in a drag reducing flow with surfactant additives investigated by two component LDV," in *Proceedings of the 8th International Symposium on Application of Laser Techniques to Fluid Mechanics*, Lisbon, Portugal, August 1996, 2941-2947.

[17] R. B. Dean, "Reynolds number dependence of skin friction and other bulk flow variables in two-dimensional rectangular duct flow," *ASME Journal of Fluids Engineering*, vol. 100, no. 2, pp. 215–223, 1978.

[18] W. X. Huang and W. M. Chen, *Engineering Fluid Mechanics*, Chemical Industry Press, Beijing, China, 2001.

[19] L. F. Jiao, *Application of additive drag reducing technology in district heating system*, M.S. thesis, School of Energy Science and Engineering, Harbin Institute of Technology, Harbin, China, 2008.